SEARCHING FOR THE MISSING LINKS:
CONNECTING POLEROVIRUS STRUCTURAL BIOLOGY TO FUNCTION

A Dissertation

Presented to the Faculty of the Graduate School

of Cornell University

In Partial Fulfillment of the Requirements for the Degree of

Doctor of Philosophy

by

Mariko Matsuda Alexander

May 2019

SEARCHING FOR THE MISSING LINKS:
CONNECTING POLEROVIRUS STRUCTURAL BIOLOGY TO FUNCTION

Mariko Matsuda Alexander, Ph. D.

Cornell University 2019

The genus *Polerovirus* contains numerous economically important pathogens of crop plants worldwide, with more species discovered every year. Although poleroviruses have been the subject of active research for decades, relatively little is known about the ways they interact with host plants on a direct, molecular level. Here, we expand on previous work probing polerovirus structural biology and host-virus interactions using Protein Interaction Reporter (PIR) technology, a type of cross-linking proteomics. We demonstrate for the first time that this technology can be successfully applied to *Turnip yellows virus*, a model polerovirus pathogen of brassicas; discover new interactions between polerovirus structural proteins and host proteins; and show through experiments *in planta* that PIR identifies biologically relevant interactions. These data provide not only proof-of-concept for PIR in plant virology, but also generate new insight about polerovirus biology that would have been prohibitively time- and resource-intensive to obtain by conventional means.

BIOGRAPHICAL SKETCH

Mariko Matsuda Alexander is originally from Castle Rock, Colorado. She received her Bachelor of Science degree from Colorado State University in Soil and Crop Science with a concentration in Plant Biotechnology, Genetics, and Breeding in 2011. During her undergraduate studies, Mariko worked in the laboratories of Dr. June Medford, Dr. Nora Lapitan, and Dr. Jan Leach. Her undergraduate Honors thesis investigated plant defense responses to *Rhopalosiphum padi* and *Diuraphis noxia*. After graduation, Mariko received a Fulbright Research Grant, which allowed her to spend a year working on molybdenum cofactor biosynthesis in the laboratory of Dr. Ralf Mendel at the Technical University of Braunschweig, Germany. Mariko came to Cornell University in 2013 to pursue her Ph.D. in Plant-Microbe Biology with Dr. Michelle (Cilia) Heck, working on interactions between host plants and pathogenic viruses in the family *Luteoviridae*. While at Cornell, Mariko has been active in student government, serving one term as the Treasurer and Appropriations Committee Chair for the Cornell Graduate and Professional Student Association, and in science communication, participating in outreach events and writing press releases for the Boyce Thompson Institute.

To

Dave, my heart and lifeline, who makes my life joyful,

Midori, who taught me to keep swimming, and that one torch can light many others,

and my parents, Dale and Gretchen, who told me I could be anything I wanted to be.

ACKNOWLEDGMENTS

I would like to thank my advisor, Michelle Heck, for her guidance and support, and for not giving up on me when everything seemed lost. I'd also like to thank all the current and former members of the Heck lab. In particular, I'd like to thank Stacy DeBlasio, who has been an invaluable resource, tireless ally, and constant friend since the moment I stepped into the lab; Ana Rita Rebelo, the best technician in the world; Angela Kruse, who has picked me up so many times when I have fallen; and Jackie Mahoney, Laura Fleites, Jenny Wilson, and Jared Mohr, for hours of moral and technical support, laughter, and friendship. You are all brilliant scientists and amazing people, and I am so glad to know you.

I would like to thank Jim Bruce, who has been a patient mentor and teacher, even from the other side of the country, as well as Juan Chavez and Jared Mohr, who have been the best collaborators a person could ask for. I would also like to thank Adam Bogdanove, Magdalen Lindeberg, Josh Chappie, and Alan Collmer, who I am honored to have had as mentors. Special thanks to Stewart Gray, Jason Ingram, and other members of the Gray lab for their support, collaboration, and tolerance of the many hours I spent camped out in their lab.

I'd like to thank Veronique Ziegler-Graff and Veronique Brault, who have not only been stellar collaborators, but who also took me under their wings during one of the most stressful weeks of my life, though they hardly knew me.

Thank you to Michael Bereman, Bill Fry, Mary McKellar, and Kathie Hodge for helping me to become a better teacher and science communicator.

My thanks to Lori Dempsey and Mary Westlake for their support on grant applications and reports, and to Keith Hannon for the opportunity to build my writing portfolio. Special thanks to Paul Chomet, whose gentle encouragement and guidance gave me the courage to step onto a new career path.

Finally, I'd like to thank my friends and family, whose support brought me here and shaped me into the scientist and person I am today. I would especially like to thank my parents, who have always encouraged me to chase my dreams, even when doing so meant buying a llama, moving to Germany, or trying to get a PhD; my sister and best friend, Midori, who I look up to more than I can describe; and my partner, Dave, whose love, encouragement, strength, and light have saved me so many times.

Funding for my research was provided by a Cornell Presidential Life Science Fellowship, the Cornell School of Integrative Plant Science, the National Science Foundation (NSF grant number 1354309), and the United States Department of Agriculture – National Institute of Food and Agriculture (USDA-NIFA grant numbers 2016-67011-24683 and 1907-22000-021-20).

TABLE OF CONTENTS

LIST OF FIGURES

LIST OF TABLES

CHAPTER 1

A MOLECULAR TUG-OF-WAR: GLOBAL PLANT PROTEOME CHANGES DURING VIRAL INFECTION[1]

Abstract

Plant pathogenic viruses cause economically important diseases in food, fuel, and fiber crops worldwide. As obligate parasites with highly reduced genomes, viruses rely heavily on their hosts for replication, assembly, intra- and intercellular movement, and attraction of vectors for dispersal. Therefore, viruses must influence or directly utilize many host proteins and processes. While many general effects of virus infection have long been known (e.g., reduction in photosynthesis, alterations in carbon metabolism and partitioning, increased expression of pathogenesis-related proteins), the precise underlying mechanisms and functions in the viral life cycle are largely a mystery. Proteomic studies, including studies of differential protein regulation during infection as well as studies of host–viral protein–protein interactions, can help shed light on the complex and varied molecular interactions between viruses and plant hosts. In this review, we summarize current literature in plant-virus proteomics and speculate on why viruses have been selected to manipulate these diverse biochemical pathways in their plant hosts. We also discuss in greater detail the biology of viruses in the family *Luteoviridae*, and their interactions with their hosts and vectors.

[1]This chapter has been modified from its original publication as: Alexander, M.M and Cilia, M. A molecular tug-of-war: Global plant proteome changes during virus infection. Current Plant Biology 5 (2016): 13-24. doi: 10.1016/j.cpb.2015.10.003

1. Introduction

Plant diseases caused by viruses incur enormous costs to growers each year, both directly, in the form of yield and quality loss, and indirectly, in the forms of time and funds spent on scouting and disease management. Compared to even the smallest known bacterial genome, the genomes of plant viruses are tiny, sometimes encoding fewer than ten proteins. Therefore, they are masterful at co-opting host cell components to complete their life cycle. Many aspects of the life cycles of plant pathogenic viruses remain a mystery.

When infecting a new cell, a virus must first uncoat and transit to its replication site, which may be the nucleus (for viruses with DNA genomes) or cytoplasmic membranes (for viruses with RNA genomes). With assistance from host proteins, viral proteins and new viral genomes are produced. Progeny virions and ribonucleoprotein complexes (RNPs; complexes of viral nucleic acid and proteins, which are different from transmissible virions) are assembled and translocated to plasmodesmata. For viruses with single-stranded RNA genomes, formation of replication sites near plasmodesmata is facilitated by interactions between viral movement proteins (MPs) and plant synaptotagmin-family proteins, which create contact sites between the ER and plasma membranes (Levy et al., 2015). Viral MPs promote callose degradation in plasmodesmata to facilitate passage of virions or RNPs into a neighboring cell (Levy et al., 2007a), where the process starts again. Viruses use the phloem to travel to distal regions of the plant to achieve a systemic infection. The majority of circulative viruses infect only the phloem tissue during a natural infection. Phloem tropism may facilitate plant-to-plant transmission by phloem-feeding insect vectors (Peter et al., 2009). Viruses must also evade host defenses and ensure an environment conducive to their replication. Often, infection results in the production of symptoms in plants, including chlorosis, necrosis, tissue proliferation, phyllody,

leaf curling, and other physiological changes, although the selection pressures and underlying molecular mechanisms for these symptoms remain largely uncharacterized.

Host responses to viral infection can be broadly categorized in two ways: compatible versus incompatible, or susceptible versus resistant. A compatible response results in successful virus infection, replication, and spread to other cells. An incompatible response occurs when the virus is recognized by the host, resulting in the hypersensitive response (HR; localized programmed cell death), preventing virus spread (Dangl et al., 1996; Greenberg and Yao, 2004; Lam et al., 2001; Pennell and Lamb, 1997). Susceptibility and resistance, in contrast, are defined in terms of the ability of the virus to cause disease in a given host. A susceptible reaction to a virus results in disease—replication of the virus and production of symptoms by the host. A resistant reaction does not result in the production of symptoms, but may still permit viral replication if the host exhibits tolerance to the virus. In some cases, a host may be said to be partially resistant if the virus is able to cause a reduced level of disease as compared to susceptible hosts of the virus. This review considers proteomic studies from the full spectrum of host responses: tolerant, partially resistant, and resistant.

Most publications in plant-virus proteomics use 2-dimensional electrophoresis or 2D difference in gel electrophoresis (2D DIGE) to look for proteins or protein isoforms which are differentially regulated during virus infection, although shotgun proteomic studies are becoming more popular. New advances include characterization of virus–plant protein interactions using co-immunoprecipitation coupled to LC–MS/MS. Structural proteomics using chemical cross-linking has also been used to identify regions in the viral capsid that regulate host–virus interactions (Chavez et al., 2012).

Among plant pathogenic viruses, species in the family *Luteoviridae* can be

particularly challenging both to control and to study. Luteovirids (members of the *Luteoviridae*) are transmitted exclusively by aphids in a circulative, non-propagative manner, and are restricted to phloem tissues in natural infections (Day, 1955; Esau and Hoefert, 1972a, b). Due to their transmission mode, insecticide applications to control aphid vectors are often not effective at preventing disease spread within a field (Gibson et al., 1951).

The best-studied members of the *Luteoviridae* are the classic pathogens *Potato leafroll virus* (PLRV; discovered in 1916), several species of cereal/*Barley yellow dwarf virus*es (B/CYDVs; first described in the 1950s), *Pea enation mosaic virus-1* (PEMV-1; discovered in 1935), and *Beet western yellows virus* (BWYV; discovered in 1960) (Duffus, 1960; Osborn, 1935; Oswald and Houston, 1951; Quanjer et al., 1916). In addition to their economic importance as pathogens in their own right, these classic luteovirid species serve as useful models for the study of luteovirid biology. Decades of research have generated infectious clones, virion purification protocols, antibodies, and other key tools for studying these species. Advancements made in model luteovirids are critical for understanding the biology of the many newly emerging luteovirid species, for which these tools are not yet available.

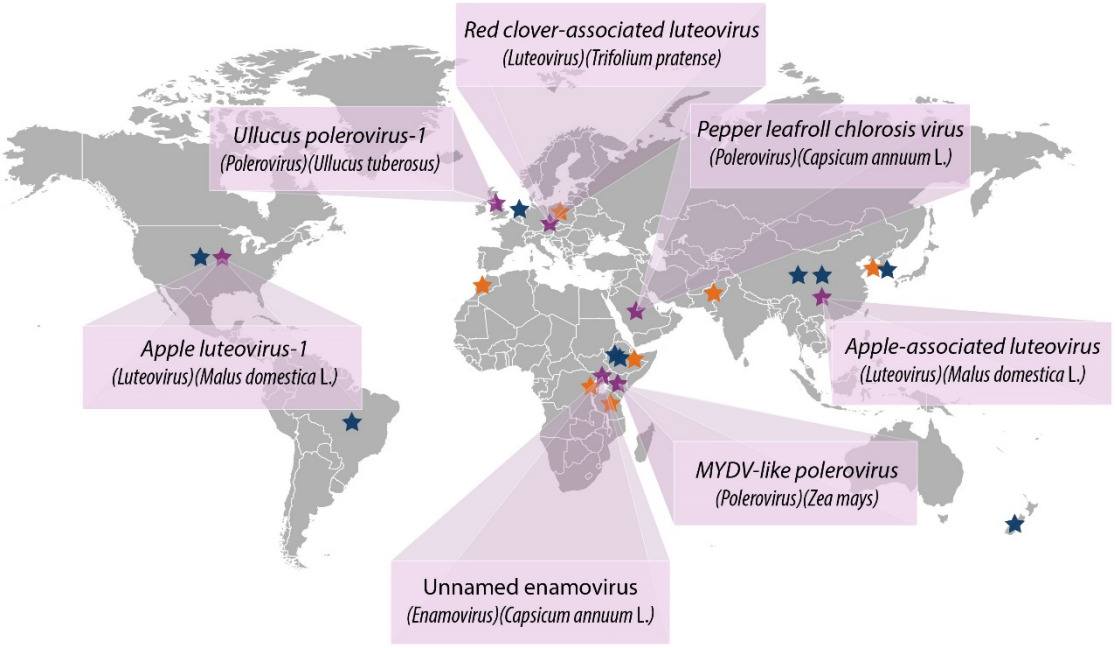

Figure 1.1: Worldwide distribution of new and emerging luteovirid species in 2018. Purple stars mark countries in which a new luteovirid species was discovered; pop-out boxes list species name (top row), and genus and host species (bottom row). Orange stars mark first reports of a luteovirid species in a country. Blue stars mark first reports of a luteovirid species on a new host plant. Refs: (Aarabe et al., 2018; Ahmad et al., 2018; Bekele et al., 2018; Buzkan et al., 2018; Eicholtz et al., 2018; Fox et al., 2018; Guadie et al., 2018; Ilbagi et al., 2018; Kamran et al., 2018; Kumar et al., 2018; Lenz et al., 2018; Lim et al., 2018a; Lim et al., 2018b; Liu et al., 2018; Ma et al., 2018; Massawe et al., 2018; Shen et al., 2018; Skelton et al., 2018; Vidal et al., 2018; Zarzyńska-Nowak et al., 2019; Zheng et al., 2018)

In 2018 alone, seven new luteovirid species were described on diverse hosts around the world (Figure 1.1). Of these, three have been classified as poleroviruses, three as luteoviruses, and one as an enamovirus (Fox et al., 2018; Kamran et al., 2018; Lenz et al., 2018; Liu et al., 2018; Massawe et al., 2018; Shen et al., 2018; Skelton et al., 2018). Additionally, expansion of host and geographic ranges were described for multiple known luteovirids (Figure 1.1). These trends are not unique to 2018 - over fifty papers have been published in the last five years describing new luteovirids or host/geographic range expansions for existing species. It has become clear that luteovirids are both ubiquitous and spreading. While not every report is associated with clear symptoms, asymptomatic infections may still represent important reservoirs that may be pathogenic on other crops or cultivars. Additionally, several of the newest luteovirid species were identified in plants also co-infected with other viruses (Carvajal-Yepes et al., 2014; Villamor et al., 2016; Yoo et al., 2017). The interaction between plant pathogenic viruses in co-infections, other than in cases where co-infection is strictly required (e.g. for enamoviruses and umbraviruses), remains an understudied area of plant virology.

To better understand luteovirid biology, we first focus broadly on proteomics studies from diverse virus species, including non-luteovirids, to discuss impacts on plant health during virus infection and speculate on how selection has favored viruses to tap into these host pathways. For a review of common techniques in plant proteomics, their limitations, and a summary of some previous literature in plant–virus proteomic studies, see: (Di Carli et al., 2012). Following our survey of proteomics studies in plant virology, we delve more deeply into the biology of viruses in the *Luteoviridae*, on which the remainder of this dissertation will be focused.

2. Manipulation of host intracellular trafficking

Plant viruses associate with a variety of subcellular structures for replication and movement, including the endomembrane system and the cytoskeleton. It is sometimes difficult to separate associations important for inter- and intra-cellular movement of plant viruses from associations important for replication, as noted by several recent reviews on the subject (Heinlein, 2015; Tilsner et al., 2013). It is possible that these two important aspects of the viral lifecycle are inextricably linked in plant infections.

2.1 Endomembrane systems

RNA viruses, which make up the majority of plant pathogenic viruses, replicate in the cytoplasm in concert with ER, vacuole, chloroplast, peroxisome, or other membranes, which may be recruited or remodeled to form inclusion bodies or complex structures (Grangeon et al., 2012; Patarroyo et al., 2012; Sanfaçon, 2005). Endomembrane systems are also important for transport of some viruses and viral proteins.

Plant viral MPs enable plant viruses to move from cell to cell through specialized, ER-lined intercellular channels called plasmodesmata. Understanding how plant viral MPs function has been a major focus of the plant virology field for the past two decades. A synaptotagmin-family protein (AtSYTA) was found by yeast two-hybrid to interact with the movement proteins of *Cabbage leaf curl virus* (CaLCuV; *Geminiviridae*: *Begomovirus*), *Squash leaf curl virus* (SqLCV; *Geminiviridae*: *Begomovirus*), and *Tobacco mosaic virus* (TMV; *Virgaviridae*: *Tobamovirus*), and to be important for cell-to-cell movement of CaLCuV and TMV MPs (Lewis and

Lazarowitz, 2010). The native functions of AtSYTA are regulation of endocytosis and formation of ER-plasma membrane contact sites which support ER structure. Interestingly, a Rab GTPase (also involved in membrane trafficking) was found in a separate study to be upregulated during TMV infection (Lee et al., 2006). Further studies with *Turnip vein clearing virus* (TVCV; *Virgaviridae*: *Tobamovirus*) led to a paradigm-shifting model for MP function linking viral replication, intercellular movement, and endomembrane transport: TVCV MP hijacks AtSYTA to remodel membrane contact sites near plasmodesmata, where the virus forms replication complexes and moves from cell-to-cell (Levy et al., 2015).

A recent publication by DeBlasio et al. (DeBlasio et al., 2015a) identified a number of proteins involved in clathrin-mediated endocytosis as co-immunoprecipitating with the aphid-transmitted *Potato leafroll virus* (PLRV; *Luteoviridae*: *Polerovirus*), and PLRV also directly interacts with golgin and a dymeclin-like protein (DeBlasio et al., 2016a). PLRV has been previously observed by transmission electron microscopy in cytoplasmic vesicles, which fuse with the nucleus, mitochondria, vacuoles, and sites in the ER near plasmodesmata (Golinowski et al., 1987; Shepardson et al., 1980). Although the function of these vesicles is unknown, clathrin-mediated endocytosis is also thought to be used by PLRV to traffic across tissue barriers in aphids (Gray and Gildow, 2003) and may use these pathways in their plant hosts as well. This possibility is supported by the fact that the same viral capsid protein, a translational readthrough product from the coat protein open reading frame called the readthrough protein (RTP), is required for movement in both plant hosts and aphid vectors.

Aside from the aforementioned, endomembrane and related proteins tend to be identified only rarely in proteomic studies. This may be due to experimental bias—

membrane proteins are often poorly soluble and difficult to extract with conventional protocols, and may be low in abundance to begin with—or simply because viruses are able to hijack these pathways without altering the levels or post-translational modifications of the relevant proteins. Such proteins would not be easily identified in quantitative proteomics studies looking at differential expression.

2.2 Cytoskeleton: Microtubules

The cell cytoskeleton is a dynamic network of microtubules and microfilaments. Use of the cytoskeleton by viruses has been established for a number of animal viruses; both directly, by interaction of viral proteins with microtubules or microfilaments as they polymerize, or indirectly, by interaction with motor proteins that traffic various cargo along the cytoskeleton (Greber and Way, 2006; Ward, 2011). The best-studied example of a similar association in a plant virus exists for TMV (for review: (Liu and Nelson, 2013)). TMV forms replication complexes of genomic RNA, MP, and replication-associated proteins at ER-plasma membrane contact sites as discussed in Section 2.1 (Levy et al., 2015; Lewis and Lazarowitz, 2010). Multiple lines of evidence show an association between the TMV MP and microtubules (Heinlein et al., 1995; Heinlein et al., 1998; McLean et al., 1995), and a region of the TMV MP shows sequence similarity to tubulin (Boyko et al., 2000). However, the function of this association is uncertain. Although some evidence suggests that the MP-microtubule association is important for intracellular movement of the replication complex (Boyko et al., 2000; Boyko et al., 2007; Más and Beachy, 1999), pharmacological disruption of microtubules does not inhibit TMV movement (Gillespie, 2002; Kawakami et al., 2004). To wit, an MP mutant which does not bind microtubules still localizes strongly to plasmodesmata (Gillespie, 2002), suggesting

that MP function at PD is not dependent on the microtubule network. It has been suggested that microtubules actually function to promote degradation of MP by the proteasome (Gillespie, 2002; Más and Beachy, 1999; Padgett et al., 1996; Reichel and Beachy, 1998); however, further studies are necessary to confirm this hypothesis. In addition to the TMV MP, some evidence suggests that the MPs of *Tomato mosaic virus Ob* (ToMV; *Virgaviridae*: *Tobamovirus*) and *Potato mop-top virus* (PMTV; *Virgaviridae*: *Pomovirus*) also interact with microtubules (Padgett et al., 1996; Wright et al., 2010), and *Grapevine fanleaf virus* (GFLV; *Secoviridae*: *Nepovirus*) requires intact microtubules for cell–cell movement in some hosts (Laporte, 2003). Microtubule interactions are also important for transmission of *Cauliflower mosaic virus* (CaMV; *Caulimoviridae*: *Caulimovirus*), which forms inclusion bodies key for aphid acquisition in a microtubule-dependent manner (Blanc et al., 1996; Martinière et al., 2009).

Several proteomic studies have found a link between other virus species and microtubules: PLRV was recently reported to co-immunoprecipitate with tubulin (DeBlasio et al., 2016a), and β-tubulin was shown to be upregulated in papaya leaves during infection with *Papaya meleira virus* (PMeV; *unclassified*), as well as in grape berries during mixed infection with *Grapevine leafroll-associated virus 1* (GLRaV-1; *Closteroviridae*: *Ampelovirus*), *Grapevine virus A* (GVA; *Betaflexiviridae*: *Vitivirus*), and *Rupestris stem pitting-associated virus* (RSPaV; *Betaflexiviridae*: *Foveavirus*) (Giribaldi et al., 2011; Rodrigues et al., 2011). Although the role of microtubules in infection with these viruses is yet unknown, their identification is unsurprising given their importance for other diverse virus species.

2.3 Cytoskeleton: Microfilaments

Ample evidence also exists for involvement of the other component of the cytoskeleton—actin microfilaments—in plant virus movement. The replication complexes of TMV and *Turnip mosaic virus* (TuMV; *Potyviridae*: *Potyvirus*) traffic along microfilaments (Harries et al., 2009; Liu et al., 2005), TMV MP binds to microfilaments in vitro (McLean et al., 1995), and some evidence suggests that intact microfilaments are required for cell–cell movement of TMV and *Potato virus X* (PVX; *Potyviridae*: *Potyvirus*)(Harries et al., 2009; Kawakami et al., 2004). Several other diverse viruses, including CaMV, PMTV, and *Tobacco etch virus* (TEV; *Potyviridae*: *Potyvirus*) form granules or other small structures which traffic along microfilaments (Cotton et al., 2009; Haupt et al., 2005; Ju et al., 2005). Interestingly, impairing the ability of the MPs of both TMV and CaMV to sever microfilaments also prevents these proteins from affecting plasmodesmata pore size (Su et al., 2010), suggesting that some viral MPs may utilize the cytoskeleton for manipulation of plasmodesmata. Although the mechanism by which this may occur is unknown, we can hypothesize that microfilaments may be important for MP targeting of plasmodesmata, or that interfering with the ability of MPs to sever microfilaments also impairs the ability of these proteins to recruit callose-degrading enzymes. Motor proteins that traffic along microfilaments have also been shown to be important for movement of some plant viruses. Silencing of certain myosins inhibits the intercellular movement of TMV, and movement-associated tubule formation in GFLV (Amari et al., 2011; Harries et al., 2009).

The frequency with which actin and related motor proteins have been identified in plant virus proteomic studies underscores their importance in viral movement. Levels of actin are increased in both resistant and susceptible sugar beets six weeks after germination in soils inoculated with *Beet necrotic yellow vein virus* (BNYVV; *Benyviridae*: *Benyvirus*) (Larson et al., 2008). Infection of papaya with

PMeV induces an increase in one isoform of actin, but a decrease in another, as well as a decrease in actin polymerizing factor (Rodrigues et al., 2011). Grapevines co-infected with GLRaV-1, GVA, and RSPaV also show a decrease in fimbrin, a microfilament cross-linking protein, but an increase in alpha actin (Giribaldi et al., 2011), suggesting that cross-linked and free microfilaments may play opposing roles in infection with these viruses. Specific functions of fimbrim have been understudied in plants, but include formation of intestinal microvilli in vertebrates and cytokinesis in yeast, among other functions (Glenney et al., 1981; Mooseker, 1983; Wu et al., 2001). PLRV was found to co-immunoprecipitate with multiple actin and myosin homologs in *N. benthamiana* (DeBlasio et al., 2016a), and a direct interaction with the PLRV CP/RTP has been shown (DeBlasio et al., 2016a). Although the decrease in some actin isoforms and/or related proteins seen in the infected papaya and grapevines may seem counterintuitive if microfilaments are used for virus transport, these plants were in relatively late stages of infection, unlike many other proteomic studies reviewed here. The decrease in actin and related proteins in these plants may have been related to decreased cell health rather than a targeted effect of the viruses. It is also possible, given the increase in tubulin in these plants, that viral trafficking by these species or during late infection uses primarily microtubules, rather than microfilaments.

3. Manipulation of photosynthesis and host primary metabolism

3.1 Photosynthesis and carbon fixation

Chlorosis and net reduction in photosynthesis are among the most commonly observed symptoms of virus infection in plants. It is unknown whether viruses directly manipulate the photosynthetic machinery to promote a successful infection or whether

the impact on photosynthesis during infection is an indirect effect of the virus. As several studies have also found photosynthetic proteins in complex with viral particles, it is possible that virus proteins themselves may regulate photosynthesis, either directly or as part of a complex of interacting proteins. It is also possible that downregulation of photosynthesis is partially an effect of damage done to chloroplasts, directly or indirectly, by the virus, as infection with a number of diverse viruses has been observed to alter chloroplast structure, size, or number (Gao and Nassuth, 1993; Magyarosy et al., 1973; Mochizuki and Ohki, 2011; Técsi et al., 1994). Notably, a recent study showed that disrupting chloroplast function by virus-induced gene silencing (VIGS) of phytoene desaturase, an enzyme important for chlorophyll, carotenoid, and gibberellic acid biosynthesis, resulted in a significant increase in PLRV titer (DeBlasio et al., 2018a).

Photosynthesis is also tightly linked to the production of reactive oxygen species (ROS), as chloroplasts are the primary site of ROS production in plants (for review: see Refs. (Asada, 2006; Gill and Tuteja, 2010)). During photosynthesis, oxygen produced can be reduced by electrons passing through the electron transport chain, forming superoxide. Under normal conditions, superoxide and other ROS byproducts of photosynthesis are detoxified by ROS-scavenging enzymes; however, under conditions of biotic or abiotic stress, or when photosynthesis is perturbed, ROS may be allowed to build up. These accumulated ROS are important for defense and stress responses (see Section 5.1), but may also damage organelles and cellular components. In cases where HR is triggered, ROS are a key component of cell death signaling pathways.

The interplay between viruses and the photosynthetic machinery, including ROS signaling, during infection is complex. During infection with some viruses, the

decrease in net photosynthetic capacity is due not to a decrease in proteins involved in light capture, but rather an increase in amount or activity of proteins involved in carbon fixation (Lehrer and Komor, 2008; Shalitin and Wolf, 2000), which may contribute to chlorosis by buildup of assimilates (Gonçalves et al., 2005). In other cases, however, carbon fixation acts as the rate-limiting step that inhibits photosynthesis during virus infection (Lehrer and Komor, 2008; Sampol et al., 2003). There is also evidence to support the involvement of relative levels of the different proteins in the oxygen evolving complex as important in determining photosynthetic rates during infection (Rahoutei et al., 2000), which is supported by the frequency with which these proteins have been found in proteomic studies (Brizard et al., 2006; Carmo et al., 2013; Casado-Vela et al., 2006; DeBlasio et al., 2016a; DeBlasio et al., 2015a; Di Carli et al., 2010; Lai et al., 2013; Larson et al., 2008; Novakova et al., 2015; Obrepalska-Steplowska et al., 2013; Perez-Bueno et al., 2004; Pineda et al., 2010; Rodrigues et al., 2011; Wang et al., 2015; Wu et al., 2013a). Alterations in ferredoxin levels, also found in several proteomic studies reviewed here (Brizard et al., 2006; Cilia et al., 2012; DeBlasio et al., 2015a; Pineda et al., 2010; Wu et al., 2013a; Wu et al., 2013b), have been shown to be associated with symptom development in TMV-infected plants (Ma et al., 2008).

Substantiating the ample literature linking viral infection to photosynthesis, photosynthetic proteins make up a major category of virus-interacting or differentially regulated proteins in most plant-virus proteomic studies. This is likely due both to photosynthesis being commonly exploited (or altered) by plant pathogenic viruses and to the relatively high abundance of photosynthetic proteins in green tissues. Two subunits of photosystem II were found to be down-regulated during PVY infection of transgenic potato depleted for salicylic acid accumulation (Stare et al., 2015). Many photosynthetic proteins co-purify with NIa from TEV (Martinez et al., 2016). A

number of photosynthetic proteins have been identified as co-purifying with *Rice yellow mottle virus* (RYMV; Unclassified: *Sobemovirus*), including: phosphoenolpyruvate carboxylase, a RuBisCO binding protein, the RuBisCO large subunit, PsbQ, PsbP, and subunits of ATP synthase (Brizard et al., 2006). Photosynthetic enzymes, including a putative transketolase, components of ATP synthase, and ferredoxin NADP(H) oxidoreductase were also found to co-purify with the RPV strain of *Cereal yellow dwarf virus* (CYDV-RPV; *Luteoviridae*: *Luteovirus*) (Cilia et al., 2012). PLRV was recently shown to co-immunoprecipitate with a number of proteins involved in photosynthesis and gluconeogenesis, including the oxygen-evolving enhancer proteins PsbP and PsbQ, proteins from both photosystem I and II, subunits of ATP synthase, multiple chlorophyll-binding proteins, and transketolase (DeBlasio et al., 2015a), and a direct interaction with the CP/RTP could be demonstrated for PsbQ (DeBlasio et al., 2016a). A number of photosynthetic proteins were found exclusively or were significantly enriched in co-immunopurifications of wild-type PLRV compared to a mutant form of PLRV lacking the readthrough domain of the RTP (the minor structural protein), showing that the readthrough domain mediates protein interactions with the photosynthetic machinery. These interactions may lead to the development of chlorosis during infection or suppression of host immune responses (DeBlasio et al., 2015a). Finally, ORSV co-immunoprecipitates with RuBisCO and related proteins, three subunits of photosystem I, and several proteins involved in photorespiration (Lin et al., 2015).

CMV infection has been shown to downregulate a subunit of photosystem II, PsbO, the large subunit of RuBisCO, RuBisCO activase, and carbonic anhydrase, as well as four proteins involved in photorespiration, and a plastidic aldolase (Di Carli et al., 2010). PsbO and carbonic anhydrase were undetectable in yellow mosaic diseased soybean, but present in healthy leaves (Pavan Kumar et al., 2016). Unexpectedly,

grape berries co-infected with GLRaV-1, GVA, and RSPaV show an increase in a subunit of ATP synthase, although it is unknown if this trend holds for leaves and other photosynthetically-active tissue (Giribaldi et al., 2011). Similarly Larson and colleagues (Larson et al., 2008) reported a relative increase in levels of several members of the oxygen-evolving complex in susceptible sugar beet roots, as well as an increase in the RuBisCO large subunit in both resistant and susceptible roots, during BNYVV infection. Mixed regulation of proteins related to photosynthesis and carbon fixation was found in maize leaves infected with *Rice black-streaked dwarf virus* (RBSDV; *Reoviridae*: *Fijivirus*) (Li et al., 2011; Xu et al., 2013). Infection of *Nicotiana benthamiana* with *Pepper mild mottle virus* (PMMoV; *Virgaviridae*: *Tobamovirus*) caused a decrease in PsbP, but not PsbO (Perez-Bueno et al., 2004). Changes specifically in chloroplastic protein levels during infection of *N. benthamiana* with PMMoV were assessed by Pineda et al. (Pineda et al., 2010), who identified 16 down-regulated polypeptides, including cytochrome F, ATP synthase, RuBisCO, and phosphoglycerate kinase. Infection of papaya with PMeV decreases levels of the small chain of RuBisCO, RuBisCO activase, a member of the oxygen-evolving complex, and beta hydroxyacyl ACP dehydratase (Rodrigues et al., 2011). Analysis of proteins responsive to *Peanut stunt virus* (PSV; *Bromoviridae*: *Cucumovirus*) infection found multiple proteins involved in photosynthesis and gluconeogenesis to be differentially regulated by the virus, its satellite RNA, or both (Obrepalska-Steplowska et al., 2013), and the Calvin cycle enzyme ribose-5-phosphate isomerase was found to be downregulated during infection of tomato with TMV (Casado-Vela et al., 2006). Transketolase, a Calvin cycle enzyme, was found to be upregulated during SCMV infection of susceptible maize (Wu et al., 2013a), and all but one isoform was also upregulated during infection of maize with RBSDV (Li et al., 2011). Differential regulation of ferredoxins, ATP synthase, Psb proteins,

RuBisCO, and other photosynthetic proteins was also shown during SCMV infection of maize (Wu et al., 2013a). Several photosynthetic and carbon fixation proteins are differentially regulated during *Cymbidium mosaic virus* (CymMV; *Alphaflexiviridae*: *Potexvirus*) and *Ondontoglossum ringspot virus* (ORSV; *Virgaviridae*: *Tobamovirus*) infection of *Phalaenopsis amabilis* orchids, both in single and double infections (Lai et al., 2013). Mixed regulation of proteins important for photosynthesis, carbon fixation, and chlorophyll biosysnthesis was shown during *Zucchini yellow mosaic virus* (ZYMV; *Potyviridae*: *Potyvirus*) infection of partially resistant zucchini (Novakova et al., 2015). Proteins involved in photosynthesis and chlorophyll biosynthesis were generally found to be downregulated in RSV-infected rice (Wang et al., 2015). Proteins important for carbon fixation, including ATP synthase and RuBisCO, were found to be upregulated in a resistant cultivar of soybean during infection with *Soybean mosaic virus* (SMV; *Potyviridae*: *Potyvirus*), although one homolog of RuBisCO appeared downregulated (Yang et al., 2011). A Psb protein, subunits of ATP synthase, and a Calvin cycle enzyme are differentially regulated during transient expression of the AC2 protein from *Tomato chlorotic mottle virus* (ToCMoV; *Geminiviridae*: *Begomovirus*) in *N. benthamiana* (Carmo et al., 2013). Photosynthetic and carbon fixation proteins are also differentially regulated during *Mungbean yellow mosaic India virus* (MYMIV; *Geminiviridae*: *Begomovirus*) infection of *Vigna mungo* (Kundu et al., 2011). Proteins involved in photosynthesis and carbon fixation were found to be generally downregulated in tobacco infected with TMV (Wang et al., 2016). Upregulation of PsbA was found to be associated with a tolerant response to TMV.

3.2 Carbon partitioning and metabolism

Proteomic studies show that the alteration of primary metabolism in virus-infected plants is widespread and complex, a finding substantiated by enzyme activity studies in CMV-infected *Cucurbita pepo* L. two decades ago (Tecsi et al., 1994; Tecsi et al., 1996). Multiple enzymes involved in carbon metabolism were found to co-immunoprecipitate with PLRV (DeBlasio et al., 2015a), and to co-purify with CYDV-RPV and RYMV (Brizard et al., 2006; Cilia et al., 2012). One or more enzymes important for carbon metabolism were found to be upregulated during infection with TMV, RSV, and ORSV (Casado-Vela et al., 2006; Lai et al., 2013; Wang et al., 2015), but downregulated during infection with CMV, PMMoV, PMeV, and CymMV (Di Carli et al., 2010; Lai et al., 2013; Pineda et al., 2010; Rodrigues et al., 2009). Differential regulation of carbon metabolic enzymes was observed during infection with RBSDV, RYMV, SCMV, SMV, PSV, ZYMV, MYMIV, RSV, PVY, and during triple infection of grapes with GLRaV-1, GVA, and RSPaV (Giribaldi et al., 2011; Kundu et al., 2013; Li et al., 2011; Novakova et al., 2015; Obrepalska-Steplowska et al., 2013; Stare et al., 2015; Ventelon-Debout et al., 2004; Wang et al., 2015; Wu et al., 2013a; Wu et al., 2013b; Xu et al., 2013; Yang et al., 2011). All differentially regulated carbon metabolic enzymes were decreased during infection with RBSDV, except for glyceraldehyde-3-phosphate (GAPDH), which was increased (Li et al., 2011). Phosphoglycerate kinase was downregulated in skin of grape berries co-infected with GLRaV-1, GVA, and RSPaV, but upregulated in in infected fruit pulp (Giribaldi et al., 2011). These data highlight the importance of tissue choice when performing and interpreting proteomic studies, as virus infection may have different effects even in tissues in proximity to one another. Such differences may also be observed in resistant vs. susceptible hosts: GAPDH levels were increased during RYMV infection of resistant rice, but unchanged in susceptible rice; whereas aldolase levels were increased in susceptible rice but unchanged in resistant (Ventelon-Debout

et al., 2004). Most differentially regulated carbon metabolic enzymes in SCMV-infected maize were downregulated during infection of a susceptible cultivar, although GAPDH was increased in the resistant cultivar (Wu et al., 2013a). GAPDH levels were decreased during infection of a resistant soybean cultivar with SMV, while NADPH-specific isocitrate dehydrogenase levels were increased (Yang et al., 2011). Changes in several carbon metabolic enzymes are induced by transient expression of the ToCMoV AC2 protein in *N. benthamiana* (Carmo et al., 2013). It is important to note here that many carbon metabolic enzymes are common to glycolysis and carbon fixation/gluconeogenesis; without further information it is not possible to say which process is being targeted by viral infection. Viral targets in these pathways may vary by virus species, host species and cultivar, infection time point, and plant age. These variables likely account for some of the proteome variation observed in carbon metabolic enzymes during infection. However, these proteome data paint a compelling picture that carbon metabolism is a key hub for viral manipulation during infection.

A number of plant-pathogenic viruses are known to also have an effect on carbon partitioning and allocation or phloem biology/physiology. Some plant pathogenic viruses cause damage to or blockage of phloem (Ashraf et al., 1999). Many plant pathogenic viruses have been observed to cause an alteration in starch content of infected leaves (Arias et al., 2003; Ashraf and Zafar, 2000; Ashraf et al., 1999; Shalitin and Wolf, 2000; Técsi et al., 1994) or roots (Ephraim et al., 2015). Transgenic expression of the TMV MP has been shown to increase sugar and starch content in source leaves by preventing export to phloem, and decreases plant biomass allocated to roots (Lucas et al., 1993; Olesinski et al., 1995). Interestingly, the effect of the MP on biomass partitioning has been shown by mutational studies to be independent of the ability of the MP to affect plasmodesmata pore size (Balachandran et al., 1995; Olesinski et al., 1995). The starch biosynthetic enzymes ADP/UDP-glucose

pyrophosphorylase have been found by proteomic studies to be upregulated during infection of maize with RBSDV (Li et al., 2011; Xu et al., 2013) and infection of tomato with TMV (Casado-Vela et al., 2006), and RYMV from both resistant and infected rice plants co-purifies with a putative 4-alpha glucanotransferase (an enzyme involved in starch and sucrose metabolism) (Brizard et al., 2006).

Manipulation of carbon metabolism, partitioning, and allocation may occur due to direct manipulation of involved proteins by viruses, or indirect effects of virus infection. In the case of insect-vectored viruses, we can hypothesize that alterations in carbon content may increase attractiveness of infected plants to insect vectors, encourage them to feed for a longer or shorter amount of time (depending on the vectoring strategy), or improve vector fitness. Changes to carbon partitioning may also have effects on photosynthesis if photoassimilates are allowed to build up. Similar to insect-vectored human diseases, plant viruses are known to manipulate the behavior of their vectors to their advantage, both by affecting the biology of diseased hosts and by altering the behavior of viruliferous insects (Gray et al., 2014; Holmes and Bethel, 1972; Ingwell et al., 2012).

4. Manipulation of host amino acid metabolism

Metabolic changes during virus infection are not limited to carbon metabolism. Multiple studies point to an increase in amino acid metabolism in virus-infected plants. During infection of squash with *Squash mosaic virus* (SqMV; *Secoviridae*: *Comovirus*), chloroplastic amino acid biosynthesis has been shown to be increased (Magyarosy et al., 1973), and TRV infection was shown to cause an increase in leaf amino acid content (Fernandez-Calvino et al., 2014). Analysis of combined microarray data revealed that amine biosynthetic processes and processes related to aromatic

amino acid metabolism are overrepresented in the upregulated category during infection of plants with compatible viruses (Postnikova and Nemchinov, 2012).

Amino acid biosynthetic enzymes and proteins involved in protein transport were found as part of a major network of proteins, centering around the 14-3-3 protein GRF2, found co-immunoprecipitating with PLRV (DeBlasio et al., 2015a). Multiple members of the glycine cleavage system, a group of four proteins which degrade excess glycine, co-immunoprecipitate or co-purify with PLRV, RYMV, and CYDV-RPV (Brizard et al., 2006; Cilia et al., 2012; DeBlasio et al., 2015a), and glycine dehydrogenase is upregulated during PMeV infection (Rodrigues et al., 2011). Aminotransferases also co-immunoprecipitate or co-purify with PLRV, RYMV, and ORSV (Brizard et al., 2006; DeBlasio et al., 2015a; Lin et al., 2015), and a subunit of isopropyl malate isomerase (part of the leucine biosynthesis pathway) co-immunoprecipitates with ORSV coat protein (Lin et al., 2015). Phosphoglycerate dehydrogenase, another amino acid biosynthetic enzyme, was found to be upregulated in a susceptible rice cultivar during infection with RYMV (Ventelon-Debout et al., 2004), as well as in a resistant maize cultivar during SCMV infection (Wu et al., 2013a); and methionine synthase and ornithine carbamoyltransferase levels are increased during papaya infection with PMeV (Rodrigues et al., 2011). Serine hydroxymethyltransferase was found to be upregulated during MNSV-1 infection, and fumarylacetoacetate hydrolase, an enzyme important for tyrosine degradation, was downregulated (Serra-Soriano et al., 2015). Three enzymes involved in amino acid biosynthesis are upregulated during RBSDV infection (Xu et al., 2013). In contrast to data showing an increase in amino acid content during virus infection, amino acid biosynthetic enzymes are also sometimes found to be downregulated in proteomic studies: Aminotransferases are downregulated during infection of maize with RBSDV or SCMV (susceptible cultivar only) (Li et al., 2011; Wu et al., 2013a). Glutamine

synthase is downregulated during PMeV infection, and cysteine synthase is downregulated during both PMeV and RBSDV infection (Li et al., 2011; Rodrigues et al., 2011). This seemingly contradictory finding may be unique to these particular virus-host combinations or infection stages. Additionally, the RBSDV and PMeV studies were both performed on infected plants from field trials. Although both studies used uninfected plants from the same field as controls, it is still possible that unseen biotic or abiotic stresses may have had different effects on infected versus uninfected plants.

Increased amino acid biosynthesis may serve simply to provide amino acids for synthesis of viral proteins during replication. Alternatively, there is significant emerging evidence for modulation of defense responses to a broad spectrum of plant pathogens by amino acid homeostasis (for review: see Ref. (Zeier, 2013)). Although most related studies focus on resistance to bacterial, fungal, and oomycete pathogens, many of the demonstrated downstream effects of perturbing amino acid homeostasis could certainly function in defense against viruses. For viruses transmitted by insects, it is also possible that manipulation of amino acid metabolism is related to host manipulation to improve attractiveness, nutrition, or palatability for insect vectors.

5. Manipulation of host stress-responsive proteins

5.1 Reactive oxygen species

ROS and ROS-scavenging enzymes are an important part of plant response to both biotic and abiotic stress. ROS can participate in defensive signaling, act as a local microbicide, or assist in strengthening of cell walls. The most common enzymes implicated in generation of ROS during pathogen defense are peroxidases (Bauer, 2000). However, the highly reactive nature of ROS means that they can also be

harmful to host cell molecules, membranes, and proteins. Chlorotic symptoms of virus infection have been proposed to be due, in full or part, to damage done to chlorophyll and/or chloroplasts by ROS (Rodriguez et al., 2010). To control ROS levels, ROS-scavenging enzymes, such as superoxide dismutases (SODs), catalases, peroxidases, and thioredoxins, detoxify hydrogen peroxide and superoxide anions.

Direct or indirect interactions of virions with ROS-scavenging and related enzymes have been shown for multiple species. Brizard et al. (Brizard et al., 2006) found that SOD and four peroxidases co-purify with viruses from both RYMV resistant and susceptible rice, whereas a peroxidase co-purifies only with virus from resistant plants, and a peroxiredoxin purifies only with virus from susceptible plants. PLRV co-immunoprecipitates with at least one member of each major class of ROS-scavenging enzymes (DeBlasio et al., 2015a), and directly interacts with a peroxidase (DeBlasio et al., 2016a), and the related *Cucurbit aphid-borne yellows virus* (CABYV; *Luteoviridae*: *Polerovirus*) was shown to bind to a peroxidase by far western (Bencharki et al., 2010). Infection with SMV, RYMV, RBSDV, RSV, or CMV, causes an increase in one or more ROS-scavenging enzymes (Di Carli et al., 2010; Li et al., 2011; Ventelon-Debout et al., 2004; Wang et al., 2015; Yang et al., 2011), although a second study instead found mixed differential regulation of ROS-scavenging enzymes during RBSDV infection (Xu et al., 2013). Levels of two catalase isozymes are altered during ZYMV infection (Novakova et al., 2015). A peroxidase was found to be present at greater levels in leaves infected with an HR-causing strain of PMMoV than leaves infected with a non-HR-causing strain, and was absent in uninfected plants (Elvira et al., 2008). A comparison of the proteome in resistant versus susceptible maize cultivars infected with SCMV found a SOD to be downregulated in the susceptible cultivar, but a peroxiredoxin and a peroxidase to be upregulated in the resistant cultivar (Wu et al., 2013a). A similar study in BNYVV-infected beets found a

SOD to be upregulated in the susceptible cultivar, and a peroxidase to be upregulated in both resistant and susceptible cultivars, as compared to the uninfected controls (Larson et al., 2008); and, two peroxiredoxins were found to be upregulated during MYMIV infection of a resistant *V. mungo* cultivar, but not a susceptible (Kundu et al., 2013). A comparison of infected, but asymptomatic tomato fruits to uninfected tomato fruits showed mixed changes in regulation of four peroxidases (Casado-Vela et al., 2006). During ZYMV infection of a resistant zucchini cultivar, peroxiredoxin levels are increased, but thioredoxin and superoxide dismutase levels are decreased (Wu et al., 2013a). During PMeV infection of papaya, catalase levels are decreased in leaves, but levels of a peroxidase and a peroxiredoxin are increased (Rodrigues et al., 2011). MNSV-1 infection causes an alteration in levels of two isoforms of phospholipid hydroperoxide glutathione peroxidase in phloem sap (Serra-Soriano et al., 2015).

5.2 Chaperones and related proteins

Heat shock proteins (HSPs), are a class of chaperone proteins which aid in proper folding of other proteins, either after they are synthesized, or during stress conditions which promote protein misfolding (Xu et al., 2011). Chaperones are broadly important for cell function under normal conditions as well as conditions of biotic and abiotic stress, and many are conserved across eukaryotes and prokaryotes. HSPs are classified into five major families: the Hsp70, or DnaK, family; the Hsp60, or chaperonin/GroEL family; the Hsp100, or Clp, family; the Hsp90 family; and the small Hsp (sHsp) family (for review: see Ref. (Tecsi et al., 1994)). In addition to their role in protein folding, chaperonins are also important for intercellular trafficking of transcription factors in plants (Xu et al., 2011). Although not always classified as chaperones, some other proteins also perform functions in protein folding, including

protein disulfide isomerases, calreticulins, calnexins, and lectins (Williams, 2005). In recent years, the importance of HSPs and their co-chaperones in plant innate immunity has come to light (for review: see Refs. (Chen and Shimamoto, 2010; O'Brien et al., 2012; Shirasu, 2009)). However, HSPs serve additional roles in plant-virus interactions. Host cell HSPs have been shown to be important factors in virus movement, folding of viral proteins, assembly of RNA replication complexes, and other functions in viral infection (for review: see Ref. (Verchot, 2012)). Additionally, *Beet yellows virus* (BYV; *Closteroviridae*: *Closterovirus*) encodes a 65 kDa protein which is homologous to Hsp70, which seems to function in assembly, intracellular movement, and interactions with the cytoskeleton (Agranovsky et al., 1991; Alzhanova et al., 2007; Avisar et al., 2008; Karasev et al., 1992; Napuli et al., 2000; Prokhnevsky et al., 2005; Prokhnevsky et al., 2002).

Chaperones and related proteins are frequently identified in plant-virus proteomic studies. Four Hsp70 homologs were found to co-purify with RYMV, and four were also found to co-immunoprecipitate with PLRV (Brizard et al., 2006; DeBlasio et al., 2015a). Levels of an Hsp70 homolog are increased during infection of a susceptible rice cultivar with RYMV (Ventelon-Debout et al., 2004) and RSV (Wang et al., 2015), decreased during infection of papaya with PMeV (Rodrigues et al., 2011), and are detectable in CMV-infected (but not control) melon phloem sap (Malter and Wolf, 2011). An Hsp90 homolog was found to co-purify with RYMV from both resistant and susceptible rice (Brizard et al., 2006). Direct interaction was shown between PLRV CP/RTP and a luminal binding protein HSP (DeBlasio et al., 2016a), and two Hsp90s were found to co-immunoprecipitate with PLRV (DeBlasio et al., 2015a). Small heat-shock proteins (sHsps) also co-immunoprecipitate with PLRV (DeBlasio et al., 2015a), and two sHsps are upregulated in resistant rice during RYMV infection (Ventelon-Debout et al., 2004). Calreticulin was found to co-purify with

RYMV from resistant rice (Brizard et al., 2006) and to co-immunoprecipitate with PLRV (DeBlasio et al., 2015a), and is upregulated during infection with SMV (Yang et al., 2011) and infection with PMeV (Rodrigues et al., 2011). Three HSPs and a heat shock factor have been shown to interact with PVX stem loop 1 RNAs, indicating that PVX may have one or more HSP-responsive elements in its promoter(s) (Cho et al., 2012). Other chaperonins were found to co-purify with RYMV (Brizard et al., 2006) or co-immunoprecipitate with PLRV (DeBlasio et al., 2015a). A TCP-1/cpn60 family chaperonin and two other chaperonins were found to be upregulated during SCMV infection of maize (Wu et al., 2013a). A 20 kDa chaperonin was upregulated during TMV infection of a partially tolerant cultivar (Casado-Vela et al., 2006) and was upregulated during transient expression of the AC2 protein from ToCMoV (Carmo et al., 2013), and a chaperonin 60 is differentially regulated during MYMIV infection of resistant and susceptible cultivars of V. mungo (Kundu et al., 2013). Unusually, most differentially regulated chaperonins and related proteins were found to be down-regulated during RSV infection in rice (Wang et al., 2015); however, this study was performed during later stages of infection when plants were becoming necrotic.

5.3 Stress response and pathogen defense

Viruses, like other pathogens, trigger a number of inducible basal defense responses when recognized by plants, including the upregulation of a number of common defensive proteins. These proteins have broad functions, including beta-1,3-glucanases, chitinases, peroxidases (discussed above), defensins, and a number of proteins with poorly-understood functions. Some defensive proteins have been classified as pathogenesis-response (PR) proteins, which are typically small, protease-resistant proteins that are induced during pathogen attack (for review: see Refs.

(Edreva, 2005; van Loon et al., 2006)). Defensive proteins, including PR proteins, have been shown to contribute to resistance against many diverse plant pathogens, including viruses.

Beta-1,3-glucanases/PR-2 proteins hydrolyze callose, and are hypothesized to function in pathogen defense primarily by regulating the size of plasmodesmal openings (Levy et al., 2007b). A beta-1,3-glucanase was found to co-immunoprecipitate with PLRV from *N. benthamiana* (DeBlasio et al., 2015a). In a survey of PR proteins during compatible and incompatible interactions of PMMoV with hot pepper, two beta-1,3-glucanases were shown to be upregulated during both compatible and incompatible infections, while a third was only detectable during the incompatible reaction (Elvira et al., 2008). Beta-1,3-glucanase was also upregulated during CMV infection of both susceptible and transgenic resistant tomato (Di Carli et al., 2010), in asymptomatic tomato fruits during TMV infection (Casado-Vela et al., 2006), and during RBSDV infection of rice (Xu et al., 2013).

Chitinases, enzymes which break down chitin, are also classified as defensive proteins. The PR-3, 4, 8, and 11 classes all contain proteins with chitinase activity. Although chitinases function in defense against fungi and insects, proteomic studies revealed they are also differentially regulated during viral infection. In the aforementioned study by Elvira et al. (Elvira et al., 2008), four chitinases were upregulated during both compatible and incompatible PMMoV infection, of which two were upregulated to a greater degree in the incompatible reaction. Infection of papaya with PMeV upregulated one chitinase but downregulated another (Rodrigues et al., 2011). A chitinase was found to downregulated in the bark of *Citrus sudden death-associated virus* (CSDaV; *Tymoviridae*: *Marafivirus*) -infected citrus of a susceptible cultivar, but not a tolerant cultivar (Cantú et al., 2008), and a chitinase was

also downregulated in asymptomatic TMV-infected tomato fruits (Casado-Vela et al., 2006) and in RSV-infected rice (Wang et al., 2015). Chitinases are upregulated during RBSDV infection of rice (Xu et al., 2013) and a chitinase is upregulated during transient expression of the ToCMoV AC2 protein (Carmo et al., 2013). While differential regulation of chitinases during viral infection could be due to triggering of non-specific defense responses, a class III chitinase co-purified with RYMV from a susceptible rice cultivar, and a different putative chitinase co-purified with RYMV when a resistant cultivar was used instead (Brizard et al., 2006). Simple induction of basal defense does not explain why different chitinases would be induced during resistant versus susceptible responses, indicating that a more nuanced explanation is needed.

The PR-5 class of proteins contains thaumatins, a class of proteins with antifungal properties (Vigers et al., 1992) which are also associated with osmotic stress. Although no role for these proteins in viral infection has yet been identified, it is possible that an undiscovered function exists, or that there is overlap between antiviral and antifungal signaling or defense pathways in plants. Two thaumatins were found to co-immunoprecipitate with PLRV (DeBlasio et al., 2015a), and a thaumatin was found to be upregulated in the apoplast of *Plum pox virus* (PPV; *Potyviridae*: *Potyvirus*) -infected peach cells (Diaz-Vivancos et al., 2006). A thaumatin was also found to be upregulated during infection of *Capsicum chinense* with an incompatible, but not a compatible, strain of PMMoV (Elvira et al., 2008), and during RBSDV infection of rice (Ju et al., 2005; Xu et al., 2013).

Oxalate oxidase (PR-15) and germin-like proteins (GLPs; PR-16) have well-established roles in defense against a spectrum of plant pathogens. Both classes are part of the cupin superfamily of proteins, and bear homology to one another; however,

oxalate oxidase is believed to be cereal-specific and catalyzes the degradation of oxalate to hydrogen peroxide, whereas GLPs are ubiquitous in plants and perform other functions, many of which are poorly understood (Dunwell et al., 2008). Although no oxalate oxidases have been confirmed outside of cereal species, Rodrigues et al. (Rodrigues et al., 2011) reports a putative oxalate oxidase in papaya which is downregulated during infection with PMeV, a finding which is supported by the observation of calcium oxalate crystals correlating with ROS production in latex (Rodrigues et al., 2009). A GLP was found to be upregulated in the roots of a resistant variety of sugar beet during BNYVV infection (Larson et al., 2008), and GLPs were downregulated during PMMoV, CMV, and SCMV infection (Di Carli et al., 2010; Elvira et al., 2008; Wu et al., 2013a). A 24k GLP was also found to co-immunoprecipitate with PLRV (DeBlasio et al., 2015a), showing that these proteins may function in complex with viruses.

Other PR proteins were found less frequently in proteomic studies, a trend which could be due to low abundance of these proteins rather than diminished importance in viral pathosystems. A PR-10 ribonuclease was found to be upregulated in a susceptible, but not a resistant, rice cultivar during RYMV infection (Ventelon-Debout et al., 2004), and was also upregulated in RSV-infected rice (Wang et al., 2015). Defensin/PR-12 was found co-immunoprecipitating with PLRV (DeBlasio et al., 2015a), and is upregulated in a resistant cultivar during SCMV infection (Wu et al., 2013a). The functions of proteins in the PR-1 and PR-17 families are yet unknown, but a PR-1 was found to be upregulated during infection of *C. chinense* with an incompatible strain of PMMoV, as well as during infection of rice with RSV(Elvira et al., 2008; Wang et al., 2015). A PR-17 protein was shown to be enriched during infection with both the compatible and incompatible strain (Elvira et al., 2008). The PR-6 and PR-7 classes encode proteinase inhibitors and endoproteinases, respectively,

and will be covered in section 7, below.

Although not strictly defensive, 14-3-3-like proteins were also found in a significant number of proteomic studies. 14-3-3 proteins are ubiquitous in eukaryotes and are involved in signal transduction pathways related to environmental response, defense, response to light, brassinosteroid signaling, legume nodulation, and many others ((Gampala et al., 2007; Oh et al., 2009) and for review: see Refs. (Denison et al., 2011; Lozano-Duran and Robatzek, 2015)). Many 14-3-3 proteins regulate enzymes important for carbon and nitrogen metabolism, making them prime targets for manipulation of host primary metabolism (Huber et al., 2002). Six 14-3-3 proteins form protein complexes with PLRV from *N. benthamiana* (DeBlasio et al., 2015a). A putative 14-3-3 protein co-purifies with RYMV in a susceptible cultivar (Brizard et al., 2006), and a 14-3-3 protein interacts with PVX stem loop 1 RNAs (Cho et al., 2012). In a study of differential regulation of nuclear proteins during TMV infection of *Capsicum annuum* L., a 14-3-3 protein was shown to be upregulated during infection (Lee et al., 2006), suggesting a role for 14-3-3 proteins in transcriptional responses that occur during viral infection. 14-3-3 proteins were also found to be differentially regulated in response to TMV infection in tobacco, and were particularly upregulated in a tolerant variety (Wang et al., 2016).

Glutathione-S-transferases (GSTs) are stress-responsive proteins that perform a number of functions, including sequestration of toxins, mitigation of oxidative stress, and possibly hormone response (Sappl et al., 2009). A GST was found to co-immunoprecipitate with PLRV (DeBlasio et al., 2015a), and to co-purify with RYMV from resistant rice (Brizard et al., 2006). At least one GST was found to be upregulated during infection with TMV, PMeV, and a yellow mosaic virus (Casado-Vela et al., 2006; Pavan Kumar et al., 2016; Rodrigues et al., 2011), as well as during

infection of resistant sugar beet roots with BNYVV (Larson et al., 2008) and during infection of susceptible maize seedlings with SCMV (Wu et al., 2013a). In older maize plants, different GST isoforms were downregulated in resistant and susceptible maize cultivars (Wu et al., 2013b), and long-term RBSDV infection of rice induced an increase in a GST (Xu et al., 2013).

A number of other defense-related or stress-responsive proteins were also found to be targeted during virus infection, including dehydrin (Ventelon-Debout et al., 2004), unknown salt-stress induced proteins (Brizard et al., 2006; Ventelon-Debout et al., 2004), the R-protein RPS2 (Li et al., 2011), cinnamoyl CoA reductase CCR2 (Lai et al., 2013), and cystatin (Larson et al., 2008). This is by no means an exhaustive list, as there are a staggering number of defense-related proteins in plants, but a sample to provide an idea of the diversity of defense responses triggered or manipulated during viral infection.

6. Manipulation of host cell wall biogenesis and metabolism

Proteome studies show that the cell wall is a target of plant viruses during infection. Callase and callose synthase were found to be upregulated during transient expression of the ToCMoV AC2 protein (Carmo et al., 2013). Xyloglucan endo-transglycosylase, an enzyme involved in xyloglucan (a type of hemicellulose) metabolism, was found to be upregulated during infection of papaya with PMeV (Rodrigues et al., 2011), and two putative xyloglucan endo-transglycosylases co-immunoprecipitate with PLRV (DeBlasio et al., 2015a). Xyloglucan endo-transglycosylases are important for degradation of hemicellulose associated with loosening of the cell wall during growth, and are also believed to be important for fruit ripening and abscission (for review: see Ref. (Braam and Campbell, 1999)). Despite

these findings, enzymes involved in cell wall biogenesis, metabolism, and modification represent a minor category in plant-virus proteomic studies. This is likely due in large part to experimental bias, as apoplastic proteins are difficult to extract even using specialized techniques (for review: Ref. (Lee et al., 2004); examples: see Refs. (Printz et al., 2015; Ruiz-May and Rose, 2013)), and are therefore likely to be undersampled. That this category of enzymes is also found infrequently in proteomic studies of bacterial pathogens of plants further substantiates this theory (Afroz et al., 2013). Additionally, the overwhelming majority of proteomic studies reviewed here are performed in leaf tissue. It is possible that cell wall modification is generally less important for viral pathogenesis in leaves than it is in fruits, roots, or other tissues. As per the details in Section 5.3, beta-1,3-glucanases, which hydrolyze callose, are commonly found to be differentially regulated during virus infection. Unlike most other cell-wall modifying proteins, beta-1,3-glucanases are often cytoplasmic, exempting them from the aforementioned difficulties (Levy et al., 2007b). Callase and callose synthase were also found to be upregulated during transient expression of the ToCMoV AC2 protein (Carmo et al., 2013).

Lignin is actually the name for any of the many aromatic polymers which are important for cell wall rigidity and resistance against degradation by pathogens (Vanholme et al., 2010). Several enzymes involved in lignin biosynthesis are highlighted in plant-virus proteomic studies: larreatricin hydroxylase was found to be downregulated, then upregulated at a later time point, during infection of beet roots with BNYVV (Larson et al., 2008); cinnamyl alcohol dehydrogenase is upregulated during SCMV infection of a resistant maize cultivar (Wu et al., 2013a), as well as during RBSDV infection of maize (Li et al., 2011); and caffeic acid 3-O-methyltransferase is also upregulated during RBSDV infection.

Pectin forms a gel-like polysaccharide matrix in cell walls, and has been shown to be important for plant growth and development, defense, cell–cell adhesion, wall porosity, and a variety of other functions. Its structure is highly complex, and its biosynthesis involves a multitude of enzymes, mainly transferases (for review: see Ref. (Mohnen, 2008)), making it difficult to pinpoint whether its biosynthesis is affected by virus infection. However, pectin methylesterases, which catalyze the demethylesterification of pectin, have been found in two proteomic studies: pectin methylesterase co-immunopurifies with PLRV (DeBlasio et al., 2015a); and was found to be upregulated during GLRaV-1/GVA/RSPaV triple infection of grape berries (Giribaldi et al., 2011). Pectin methylesterases are involved in cell wall remodeling, and their expression has been shown to be correlated with a variety of biotic and abiotic stresses. Additionally, the interaction of pectin methylesterases with the TMV MP is required for cell–cell movement of TMV (Chen et al., 2000).

Several other proteins involved in cell wall metabolism or modification have been found more rarely in proteomic studies. A putative exoglucanase precursor (a cellulase) co-purifies with RYMV from both resistant and susceptible rice cultivars (Brizard et al., 2006), and an expansin co-immunoprecipitates with PLRV (DeBlasio et al., 2015a).

An understanding of the impact of viral infection on the cell wall is important not only in agricultural systems, but in biofuel crops as well. In particular, biofuel crop breeders aim to reduce lignin content, increase biomass, and increase growth rate. However, evidence in switchgrass suggests that these changes may also result in an increased susceptibility to insect-vectored viruses (Schrotenboer et al., 2011). Highly-selected modern switchgrass cultivars were more susceptible to Barley and *Cereal yellow dwarf virus*es than near-wild cultivars, both in greenhouse and field studies.

This study highlights the need for future research in to consider cell wall proteome effects on disease susceptibility when breeding crops for biofuel, particularly as many of these species are perennial and could act as long-term reservoirs for viruses.

7. Manipulation of host translation, protein processing, and protein degradation

The final category of interacting or differentially regulated proteins to be discussed in this review is that of peptide metabolism. One or more ribosomal proteins co-purify with RYMV (Brizard et al., 2006) and CYDV-RPV (Cilia et al., 2012), or co-immunoprecipitate or directly interact with PLRV (DeBlasio et al., 2016a; DeBlasio et al., 2015a). One or more ribosomal proteins are also differentially regulated during infection with SMV, SCMV, RYMV, PMeV, PMMoV, RBSDV, BNYVV, RSV, and MYMIV, TMV, and during transient expression of the ToCMoV AC2 protein (Kundu et al., 2013; Larson et al., 2008; Li et al., 2011; Pineda et al., 2010; Rodrigues et al., 2011; Ventelon-Debout et al., 2004; Wang et al., 2015; Wang et al., 2016; Wu et al., 2013a; Wu et al., 2013b; Yang et al., 2011). Translation initiation and elongation factors, which are also co-opted by viruses for production of viral proteins, are differentially regulated during infection with SCMV, RYMV, PMeV, RBSDV, RSV, and MYMIV (Kundu et al., 2011; Li et al., 2011; Rodrigues et al., 2011; Ventelon-Debout et al., 2004; Wang et al., 2015; Wu et al., 2013a; Xu et al., 2013). An elongation factor and a ribosomal protein were shown to interact with stem loop 1 RNAs from PVX (Cho et al., 2012). One translation elongation factor co-purifies with RYMV from a resistant rice cultivar (Brizard et al., 2006), and nearly 20 elongation or initiation factors co-immunoprecipitate with PLRV (DeBlasio et al., 2015a), at least one of which directly interacts with the CP/RTP (DeBlasio et al., 2016a). Given the importance of protein synthesis for viral replication, and the strict

dependence of viruses on host machinery for this process, it is unsurprising that related proteins are so frequently differentially regulated.

The abundant differential regulation of proteases and related proteins and protease inhibitors during viral infection highlights the molecular tug-of-war between host and virus that occurs during infection. A ubiquitin-like protein was found to be upregulated during RYMV infection of a susceptible rice cultivar, while another was downregulated during infection of a resistant cultivar (Ventelon-Debout et al., 2004). Ubiquitin fusion protein is upregulated in resistant beet roots during BNYVV infection (Larson et al., 2008), in tomato during TMV infection (Lee et al., 2006), and in rice during long-term RBSDV infection (Xu et al., 2013). A ubiquitin fusion protein was also found to co-immunoprecipitate with PLRV, as did an E3 ubiquitin ligase (DeBlasio et al., 2015a), which interacts directly with the PLRV CP/RTP (DeBlasio et al., 2016a). An E1 ubiquitin-activating enzyme was found to bind to bind in vitro to RYMV (Brizard et al., 2006). One or more subunits of the proteasome co-immunoprecipitate or co-purify with RYMV or PLRV, respectively (Brizard et al., 2006; DeBlasio et al., 2015a), and are differentially regulated during infection with SMV, PMeV, RBSDV, TMV, GLRaV-1/GVA/RSPaV, ZYMV, RSV, and MNSV-1 (Giribaldi et al., 2011; Lee et al., 2006; Li et al., 2011; Novakova et al., 2015; Rodrigues et al., 2011; Serra-Soriano et al., 2015; Wang et al., 2015; Yang et al., 2011). A proteasome subunit was found to be more abundant in soybean with yellow mosaic disease than in healthy soybean (Pavan Kumar et al., 2016). Assorted proteases are differentially regulated during infection with SMV, PMeV, RBSDV, CMV, TMV, RSV, and in latex of PMeV-infected papaya (Casado-Vela et al., 2006; Di Carli et al., 2010; Li et al., 2011; Rodrigues et al., 2011; Rodrigues et al., 2012; Wang et al., 2015; Xu et al., 2013; Yang et al., 2011); co-purify with RYMV, CYDV-RPV, and ORMV(Cilia et al., 2012; Rodrigues et al., 2012); and co-immunoprecipitate with

PLRV (DeBlasio et al., 2015a). A serine protease is down-regulated during PVY infection of salicylic acid-depleted potato(Stare et al., 2015). Finally, putative protease inhibitors co-purify with RYMV (Brizard et al., 2006), and are upregulated in leaves during PMeV infection (Rodrigues et al., 2011). A serine protease inhibitor is downregulated in latex sap of papaya during PMeV infection (Rodrigues et al., 2012), but upregulated in phloem sap of melon during MNSV-1 infection (Serra-Soriano et al., 2015). A cystatin is upregulated in resistant sugar beet roots during BNYVV infection (Larson et al., 2008), and a trypsin inhibitor co-immunoprecipitates with ORSV CP (Lin et al., 2015).

8. Suppression of host RNA silencing

The primary plant defense against viruses is RNA silencing, which is triggered by the presence of double-stranded RNA (dsRNA) in the cytoplasm, typically produced during replication of viruses with RNA genomes. dsRNA is recognized and cleaved by Dicer-like (DCL) proteins. Short, single-stranded small interfering RNAs (siRNAs) produced by cleavage can be loaded into the RNA-Induced Silencing Complex (RISC). The exact composition of the completed RISC varies, but always includes an siRNA and an Argonaute- (AGO-) family protein. The loaded siRNA (also called the guide RNA) targets the RISC to homologous RNA, which is then silenced by cleavage or translation inhibition. siRNAs can also be replicated by host RNA-dependent RNA polymerases, amplifying the silencing signal.

To combat this defense, most plant viruses encode one or more proteins with silencing suppressor activity. Viral silencing suppressors are highly diverse in both sequence and mechanism of action, and are poorly understood for many species. Known silencing suppressor mechanisms include: binding to dsRNA; sequestration of

siRNA; inhibition of RISC formation; inhibition or destabilization of AGO proteins; downregulation or inhibition of RNA-dependent RNA polymerases; and a variety of others, which are discussed in greater detail in a recent review: (Csorba et al., 2015).

Proteins involved in RNA silencing have occasionally been identified as directly or indirectly interacting with plant virus proteins (Baumberger et al., 2007; Csorba et al., 2010; DeBlasio et al., 2015a; DeBlasio et al., 2015b; Derrien et al., 2018; Garcia-Ruiz et al., 2015; Kenesi et al., 2017; Li et al., 2019; Pazhouhandeh et al., 2006; Zhang et al., 2006) but are rarely identified in the type of large-scale proteomics studies reviewed here (DeBlasio et al., 2015a). This may be due to low abundance of these proteins, an absence of differential regulation of these proteins during virus infection, or a combination of both. RNA silencing and viral silencing suppression in luteovirids is discussed in greater detail in Chapter 3.

9.'Omics studies in virus-vector interactions

Due to the barrier of the cell wall, plant pathogenic viruses require outside assistance to infect a new host. Mechanically transmissible viruses are carried on tools, equipment and herbivores to infect a new host through contact with wounds. Other viruses require a vector for transmission. The most prolific vectors are sap-feeding insects, such as aphids, whiteflies, and leafhoppers, although some viruses are transmitted by beetles, nematodes, mites, or plasmodiophorids. Insect-transmitted plant viruses can be broadly categorized by the length of time they remain associated with their vector. Stylet- and foregut-borne viruses associate transiently with the cuticle lining the stylet or foregut, and may be transmissible for only hours or days after acquisition, respectively. In contrast, circulative viruses are acquired into the insect hemolymph, where they circulate until they reach salivary tissues. Once

acquired, circulative viruses remain associated with their vector for the remainder of the insect's life. Unlike stylet- and foregut-borne viruses, an extended feeding period is required for both the acquisition of circulative viruses from infected plant hosts and the inoculation of healthy hosts. Evidence shows that some plant pathogenic viruses manipulate their host and/or vector to promote vector behavior conducive to their transmission (Gray et al., 2014; Holmes and Bethel, 1972; Ingwell et al., 2012).

Many plant-pathogenic viruses are transmitted by insects in the orders Hemiptera and Thysanoptera. Transmission is a complex process involving interaction with and manipulation of insect proteins and processes, and is still poorly understood for most plant virus species. However, reviewing the knowledge obtained through proteomic, transcriptomic, genomic, and metabolomic (broadly, 'omics) studies can help identify common targets.

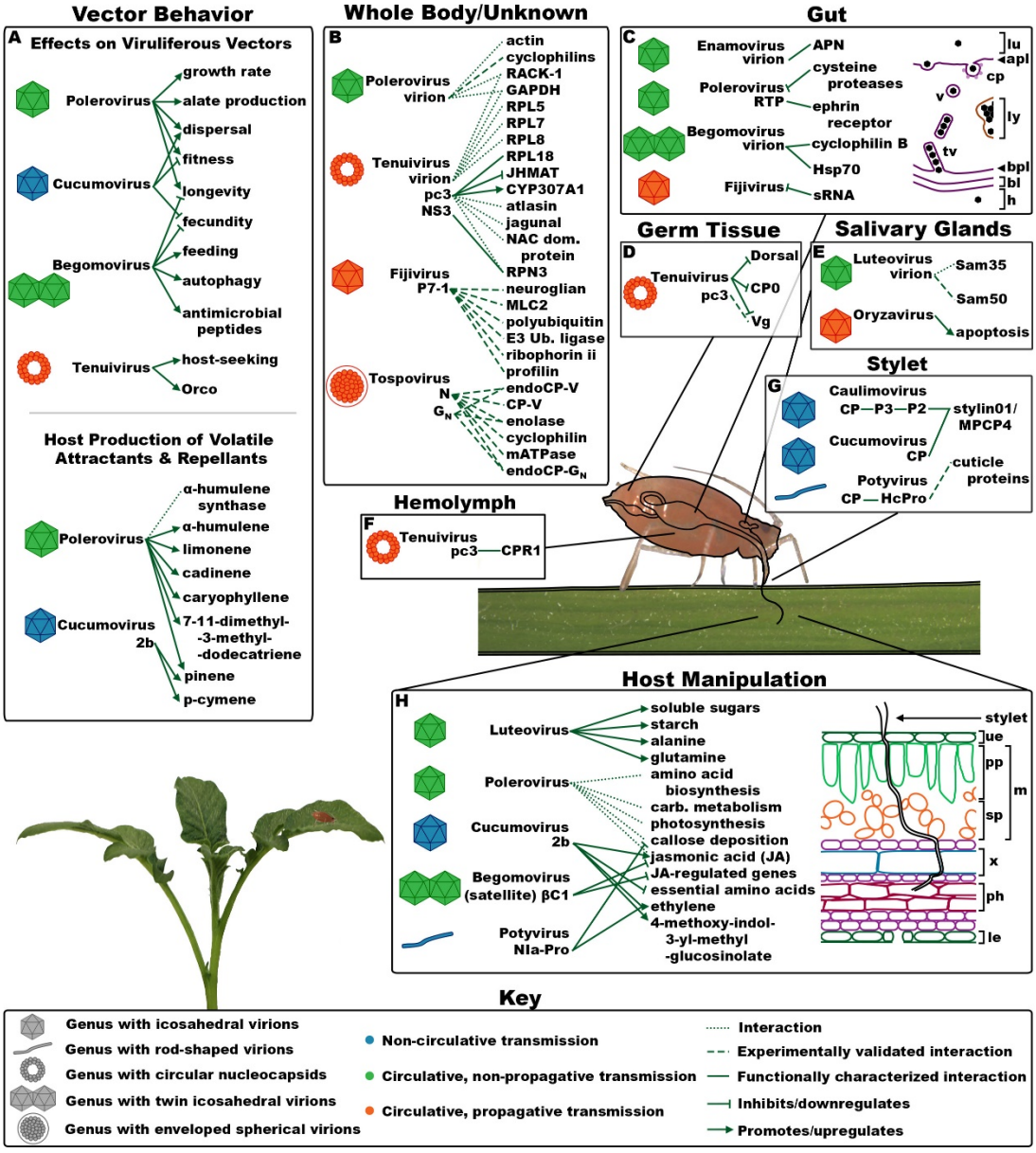

Figure 1.2*: Overview of interactions between virus, vector and host involved in the transmission of plant viruses, as determined using 'omics technologies. (A) Interactions affecting vector behavior, including the production of volatile attractants. (B) Interactions between virus and vector proteins with unknown or undetermined localization. (C) Interactions between virus and vector proteins and processes

occurring in the insect gut. Diagram at right shows a model for virion movement across the gut. apl, apical plasmalemma; bl, basal lamina; bpl, basal plasmalemma; cp, coated pit; h, hemolymph; lu, lumen; ly, lysosome; tv, tubular vesicle; v, vesicle. (D) Interactions between virus and vector proteins occurring in the germ tissue. (E) Interactions between virus and vector proteins and processes occurring in the salivary glands. (F) Interactions between virus and vector proteins occurring in the hemolymph. (G) Interactions between viruses and vector proteins occurring in the stylet. (H) Interactions between virus and plant host factors affecting vector transmission. Diagram at right shows a cross-section of a hemipteran feeding on a leaf; le, lower epidermis; m, mesophyll; ph, phloem; pp, palisade parenchyma; sp, spongy parenchyma; ue, upper epidermis; x, xylem. Key for colour and symbol codes; left column: symbol for virion structure; centre column: transmission mode indicated by virion symbol colour; right column: edge types denoting different types of virus–host or virus–vector interactions.

**Figure originally created for and published in: Wilson, J.R., DeBlasio, S.L., Alexander, M.M., Heck, M. 2019. "Chapter 6: Looking through the lens of 'omics technologies: Insights into the transmission of insect vector-borne plant viruses" Insect Molecular Virology: Advances and Emerging Trends. Caister Academic Press. In Press.*

A graphical summary of the virus-vector-host interactions known from 'omics studies is shown in Figure 1.2. Vector interactions are a complex topic, worthy of their own review, and will not be discussed in detail for most plant pathogens here. The vector biology of viruses in the *Luteoviridae* is discussed further below, in Section 11.3. An in-depth review of 'omics studies in vector biology of plant pathogens can be found in: Wilson J.R., DeBlasio S.L., Alexander M.M., and Heck, M.L. 2019. "Chapter 6: Looking through the lens of 'omics technologies: Insights into the transmission of insect vector-borne plant viruses" Insect Molecular Virology: Advances and Emerging Trends. Caister Academic Press. *In Press*.

10. Problems, pitfalls, and future directions for proteomics studies in plant virology

Differential regulation of proteins during viral infection is complex, and likely varies according to virus species and strain, host species and cultivar, infection stage, plant age, tissue, cellular compartment, and environmental conditions. In many cases, two homologs of the same protein will be regulated in different directions during infection with different viruses, in different hosts, or at different time points, and it is not unusual for two homologous proteins to be found to be regulated in opposite directions even in the same study at the same time point. This makes it extremely difficult to establish specific directional trends in proteins, protein classes, or pathways which are altered or exploited—for example, while we can certainly say that peroxidases are often differentially regulated during virus infection, it is much harder to make a generalization about the direction of their regulation, or even to identify the general set of conditions under which they are up- or down-regulated.

It is nonetheless clear that virus infection generally has large effects on core plant metabolism, including photosynthesis and carbon and amino acid metabolism.

Some of these effects may be collateral damage as a result of general stress and defense responses during infection; however, as multiple virus species have been shown to interact directly or indirectly with metabolic proteins, it is likely that this regulation has been selected due to benefits obtained by the virus during infection or by the plant during the anti-viral defense response, to at least some extent. As viruses are entirely dependent on their hosts for replication, it is likely advantageous for the virus to utilize vital enzymes for its own life cycle whenever possible, as these host proteins cannot be easily deleted or mutated during the host-pathogen arms race. Additionally, the manipulation of core metabolism by insect-vectored viruses may occur as part of the host manipulation hypothesis (Gray et al., 2014; Holmes and Bethel, 1972), to enhance virus transmission to new hosts. Although plant anti-viral defense pathways only overlap with defense pathways against other pathogens to a limited extent, viral infection nonetheless has an influence on many proteins involved in biotic and abiotic stress responses. It is likely that a portion of these effects can be attributed to a basal defense response; however, some PR proteins, including HSPs and beta-1,3-glucanases, have well-studied roles in viral infection. Both proteomic and other studies highlight the importance of the cytoskeleton during viral infection, particularly for movement and formation of replication sites; yet, even in model systems there is still some debate about the precise role of each cytoskeletal component. Undoubtedly this is an area where significant advances will be made in the coming years. It is also likely that, as proteomics technologies continue to improve, further light will be shed on the effects of viral infection on proteins that are low in abundance or difficult to extract, which tend to be identified less frequently in current proteome approaches that rely on a relatively high threshold of abundance in protein extractions for detection.

The use of mass spectrometry for protein identification requires a well-

annotated database for the host species of interest, which is not available for many plant species. In most cases this issue is solved by the use of a database from one or more related species; however, a database which more nearly approximates the actual possible proteins present in a sample will certainly improve the number and accuracy of protein identifications. One possible solution is to bypass genome sequencing and instead perform RNA-seq under the conditions of interest, as proteomic studies do not require any information about untranscribed regions of the genome. Recent work has shown that protein identification can be achieved using a transcriptome for searching, which is much faster and easier to obtain than a fully annotated genome (Lopez-Casado et al., 2012). An additional issue is the lack of annotation or known function for a not-insignificant proportion of proteins in any database, as "hypothetical proteins" and proteins with "unknown function" were identified as differentially regulated in a number of proteomic experiments reviewed here. A yeast two-hybrid study using the CaMV movement protein as bait (not included in this review) could not find significant structural homology for any of the three protein interaction partners discovered (Huang et al., 2001). Structural information, including post-translational modifications, composition of oligomers, enzymatic active sites, and the three-dimensional structure of proteins, is also important to understand the proteome.

Another consideration for proteomics studies is choice of tissue. Although plant roots and fruit can be a major site of viral damage and/or replication, only three reviewed papers included one of these tissues (Casado-Vela et al., 2006; Giribaldi et al., 2011; Larson et al., 2008). Most experiments in this field have focused on leaf tissue, which, while informative, may be biased toward photosynthetic and related proteins due to their abundance relative to other proteins. In some cases, however, performing proteomics on other tissues may present unique challenges: some tissues are difficult to harvest in sufficient quantity, difficult to clean (e.g., of soil) or to grind,

or are enriched in proteins or other compounds that complicate extraction or downstream sample preparation (protein digestion, sample clean-up, etc). These challenges are surmountable with careful planning and alteration of protocols (Isaacson et al., 2006; Mehta et al., 2008). As the field of plant virology advances, it will become increasingly important to move beyond the use of model systems and easy tissues to assess what occurs in the hosts and tissues that are most important for each pathosystem.

The overwhelming majority of publications in plant-virus proteomics use 2-dimensional electrophoresis or 2-dimensional fluorescence difference gel electrophoresis (2D DIGE) or, more rarely, mass spectrometry and spectral counting for protein quantification. Both of these approaches search for differences in the quantity of particular proteins or protein isoforms between treatments (i.e., infected vs. healthy). While these studies can be very informative, they do not necessarily account for proteins for which viral infection changes their subcellular localization, structure, post-translational modifications, or simply co-opts them for their own purposes. For example, viral remodeling of the host cytoskeleton likely plays an important role in intra- and intercellular trafficking of many viruses, but may be accomplished without altering levels of actin or tubulin. At the same time, these types of quantification-based analyses may be enriched for proteins far downstream in signaling pathways that are manipulated or perturbed by viruses. This may be part of the reason that some proteins, like beta-1,3-glucanases, are found to be upregulated in nearly all proteomic studies dealing with both viral and non-viral pathogens. To compliment these types of experiments, it will be imperative to elucidate which proteins interact with the viral proteins of interest, either directly or as part of a protein complex, and furthermore, to define the protein complexes that form with each viral protein so that the functions during infection can be elucidated in combination with traditional plant virology

studies (for example: see Ref. (DeBlasio et al., 2015b)). This can be done by co-immunoprecipitation of tagged or antibody-reactive viral components (DeBlasio et al., 2015a), far Western analysis (Bencharki et al., 2010), or using mass spectrometry-based technologies (Chavez et al., 2012; Cilia et al., 2012). In the field of human and animal virus-host interactions, significant progress has been made through proteomic studies utilizing co-immunoprecipitation coupled to mass spectrometry, demonstrating the value of these approaches for studying these unique and highly recalcitrant systems (Cristea et al., 2006; Moorman et al., 2010; Rowles et al., 2013; Rowles et al., 2015).

Analysis of large data sets, like those often generated in proteomic experiments, remains a challenge in the "-omic" era. Some tools, such as gene ontology (GO) and STRING (http://string-db.org) analysis, are available to help identify the primary pathways, networks, or functions represented in a data set (for examples: see Refs. (DeBlasio et al., 2015a; Lin et al., 2015; Rodrigo et al., 2011; Wu et al., 2013a)), but teasing out candidate genes for validation and downstream analysis is a significant hurdle. Some groups, primarily in vertebrate biology, seek to solve this issue using systems biology: a computational modeling approach that aims to simulate the complex interconnected network of genes and proteins in a cell. Systems biology models can be used to predict effects of perturbing a particular gene/protein, predict disease outcomes for a given dataset (Das et al., 2015), or identify novel or key genes in disease. Despite the potential applications, however, systems biology has not been appreciably applied to crop disease, likely due primarily to the difficulty in setting up these models, which require carefully curated databases containing multiple "-omics" data sets, as well as a significant knowledge of programming and mathematics. Systems biology in plant pathology, further application of proteomics to non-model hosts and tissues, and integrating information about the plant host, pathogen, and in

some cases the vector, will open new avenues for crop disease management.

11. Viruses in the Luteoviridae

Plant pathogenic viruses influence and interact with their hosts in complex and diverse ways. Although it is possible to identify commonly affected pathways, it is often difficult to make broad statements about plant-virus interactions across species, as noted in many of the sections above. To conclude this review, we spotlight host-virus and vector-virus interactions for viruses in the family *Luteoviridae*.

The family *Luteoviridae* contains diverse species of plant-pathogenic viruses, which are characterized as having a positive sense, monopartite, single-stranded RNA genome (Mayo et al., 1982). Luteovirids (members of the *Luteoviridae*) have non-enveloped, T=3 icosehedral capsids . Most known luteovirid species are classified in either the *Polerovirus* or *Luteovirus* genera, which contain species that are transmitted exclusively by aphids in a circulative, non-propagative manner (Day, 1955). Poleroviruses and luteoviruses are found only in phloem tissues in natural infections – a phenomenon believed to be an adaptation facilitating acquisition by sap-feeding aphids – and are distinguished primarily by their genome organization. The third genus in the *Luteoviridae*, *Enamovirus*, contains relatively few known species. Unlike other luteovirids, enamoviruses require co-infection with an umbravirus for replication and systemic movement in plants, can be found in non-phloem tissues, and are often mechanically transmissible.

11.1 The luteovirid proteome

Polerovirus, the largest genus in the *Luteoviridae,* is comprised of species with nine known open reading frames (ORFs). ORF0 encodes P0, a silencing suppressor

protein which promotes degradation of select host Argonaute (AGO) proteins (Baumberger et al., 2007; Bortolamiol et al., 2007). ORFs 1 and 2 encode P1, a polyprotein containing a protease domain and the putative VPg, as well as a P1-P2 fusion protein, which is homologous to RNA-dependent RNA polymerases (RdRPs) . P3a and P4 (also known as P17) are encoded by ORFs 3a and 4, respectively, and have functions in systemic movement (Miller et al., 2011; Smirnova et al., 2015; Tacke et al., 1993). The protein products of ORFs 6 and 7 are largely uncharacterized (Ashoub et al., 1998). ORF3 produces the viral coat protein (CP), which makes up the majority of the icosahedral capsid. Sporadic readthrough of an amber stop codon produces a C-terminal extension from ORF5, known as the readthrough domain (RTD) (Bahner et al., 1990; Dinesh-Kumar et al., 1992; Reutenauer et al., 1993; Veidt et al., 1988). The full-length readthrough protein (RTP) is incorporated into the capsid at a low but unknown frequency via the CP domain.

Luteoviruses have a similar genome structure to poleroviruses, differing only in the absence of P0 and P7. In contrast, enamoviruses do encode P0, but lack P3a, P4, P6, and P7. Additionally, ORF5 is truncated in enamoviruses, resulting in an RTP lacking the C-terminal half of the RTD. Unlike other luteovirids, enamoviruses require co-infection with an umbravirus, which compensates for missing functions in exchange for enamoviral capsid proteins.

11.2 Structural biology of luteovirids

Although no crystal structure has been published for any luteovirid virion or structural protein, luteovirids are known to have non-enveloped, icosahedral capsids with T=3 symmetry, comprised primarily of CP with a minor RTP component (Kojima et al., 1968, 1969; Shikata et al., 1966). The CP can be divided into two

regions: the R-domain, which is arginine-rich and lines the interior of the capsid, and the S-domain, which forms the capsid surface (Chavez et al., 2012). The S-domain is believed to adopt a jellyroll conformation, similar to many other viral coat proteins, based on homology modeling (Alexander et al., 2017; Chavez et al., 2012; DeBlasio et al., 2016a; Terradot et al., 2001).

The RTD can also be divided into two domains of roughly equal size. The N-RTD, or N-terminal half, is highly conserved, and is present in all three genera of luteovirids. The C-RTD, or C-terminal half, is poorly conserved, is predicted to be highly disordered (Gray et al., 2014), and is present only in the *Luteovirus* and *Polerovirus* genera. Importantly, luteovirids are believed to move systemically in both plant hosts and aphid vectors as assembled virions. Accordingly, mutational studies have identified regions in the CP and RTD which are critical for aphid transmission, systemic movement, phloem tropism, and virion assembly (Brault et al., 2003; Kaplan et al., 2007; Lee et al., 2005; Peter et al., 2009; Peter et al., 2008). These studies and the structural biology of luteovirids are discussed in greater detail in Chapter 2.

Although no crystal structure for the luteovirid capsid is available, several groups have utilized computational modeling and cross-linking data to make predictions about capsid structure (Brault et al., 2003; Chavez et al., 2012; DeBlasio et al., 2016a; Terradot et al., 2001). In Chapter 2, we extend these techniques to *Turnip yellows virus* (TuYV; *Luteoviridae*: *Polerovirus*).

In addition to its incorporated form, the RTP is also found in a free, soluble configuration, which is independently important for systemic movement and phloem restriction (Boissinot et al., 2014; Peter et al., 2009). Interestingly, virions tend to be enriched for a C-terminally truncated form of the RTP, whereas the full-length RTP seems to exist primarily in the soluble form (Boissinot et al., 2014)(Chapter 2).

11.3 Vector biology of luteovirids

Luteovirids are transmitted exclusively by aphids in a circulative, non-propagative manner in nature, and are one of only three genera of plant viruses transmitted in this mode (Gray et al., 2014). As with luteovirid behavior in plants, much of what we know about luteovirid transmission comes from early TEM studies (for review: (Brault et al., 2007)). The process begins when a compatible vector feeds on the phloem sap of an infected plant, taking up virions while feeding. Through interactions with unidentified receptors, the virions are taken up by epithelial cells in either the midgut or hindgut (depending on virus species) and transported in vesicles to the basal plasmalemma, where they are released into the hemocoel (Gildow et al., 2000). Virions in the hemocoel circulate through the aphid body until they reach the salivary glands, where they are taken up into accessory salivary glands by a second receptor-mediated endocytosis event (Gray and Gildow, 2003). Virions are then redeposited with saliva during subsequent feeding events. The two receptor-mediated endocytosis events critical for luteovirid transmission are often referred to as the gut and salivary barriers to transmission (Gray et al., 2014; Gray and Gildow, 2003), and are important factors in vector specificity. Although luteovirids are not believed to replicate in their insect vectors (Eskandari et al., 1979), viruliferous aphids retain the ability to transmit luteovirids for the remainder of their lives (for review: (Gray et al., 2014)).

Successful acquisition of luteovirids by aphids can induce changes in vector health and behavior to promote pathogen spread to additional plants. Aphids carrying luteovirids often produce more offspring, mature more quickly, and are more likely produce winged morphs (Castle and Berger, 1993; Castle et al., 1998; Jimenez-

Martinez et al., 2004b; Srinivasan et al., 2008).

As luteovirids are not believed to uncoat in aphids, viral structural proteins are likely solely responsible for interactions permitting acquisition and transmission. Mutational analyses have identified the N-RTD as being particularly important for aphid transmission, particularly at the salivary gland barrier (Chay et al., 1996; Gildow et al., 2000; Reinbold et al., 2003). However, very little is known about the aphid proteins involved, in part due to the intractability of the system. The first putative receptors, aminopeptidase N (APN) and ephrin, were only recently identified (Figure 1.2) (Linz et al., 2015; Mulot et al., 2018). Two other proteins, SaM35 and SaM50, found binding *Barley yellow dwarf-MAV* (BYDV-MAV; *Luteoviridae*: *Luteovirus*) virions in a far western assay may also be salivary receptors; however more evidence is needed (Li et al., 2001). Far western analysis has also identified actin, RACK-1, and GAPDH as potential luteovirid interaction partners of unknown function (Seddas et al., 2004).

Other approaches taken to probe luteovirid-vector interactions include microarrays, transcriptomics, 2D-DIGE and earlier versions of this method, and co-immunoprecipitation. In particular, the use of 2D-DIGE or related techniques for comparison of the proteomes of naturally occurring vector and non-vector aphid isolates has been shown to be particularly powerful in identifying aphid proteins, such as cyclophilin, which are important for transmission (Cilia et al., 2011; Papura et al., 2002; Tamborindeguy et al., 2013; Yang et al., 2008).

11.4 Luteovirid-host interactions: Systemic movement

Until recently, relatively little was known about the specific ways in which luteovirids interact with their host plants. Early TEM studies identified luteovirid

virions in the cytoplasm, nucleus, and plasmodesmata of phloem cells of infected plants, and were sometimes seen associated with the endoplasmic reticulum (ER) or small vesicles (Esau and Hoefert, 1972a, b; Gill and Chong, 1975; Shikata and Maramorosch, 1966). These studies also showed an association between luteovirids and microtubules (Esau and Hoefert, 1972b). Based on the observation of virions in plasmodesmata, luteovirids are believed to move from cell to cell as virions, rather than as unencapsidated ribonucleoprotein complexes (RNPs).

The mechanism by which the luteovirid movement protein, P17, functions remains incompletely characterized. Like many other viral movement proteins, P17 localizes to and has been shown to increase the size exclusion limit of plasmodesmata (Hofius et al., 2001; Schmitz et al., 1997). P17 contains a nucleic-acid binding motif, similar to movement proteins from other plant viruses, and has been shown to dimerize *in planta* via an amphipathic helix in the N-terminal half of the protein (DeBlasio et al., 2018b; Tacke et al., 1991; Tacke et al., 1993). Although P17 is translated from the same subgenomic RNA as the CP, P17 has been shown to be translated at a seven-fold higher efficiency in plants (Tacke et al., 1990). Expression of GFP-tagged P17 from PLRV in tobacco found that P17 localized to plasmodesmata of both vascular and non-vascular cells in source leaves, although visible changes in plasmodesmata structure were only visible in phloem cells (Herbers et al., 1997). In sink leaves, GFP-tagged P17 was only visible in the plasmodesmata of trichomes, indicating that P17 may only target plasmodesmata of immature leaves. Expression of PLRV P17 in *Arabidopsis* showed similar trends: GFP-tagged P17 was visible in plasmodesmata of most cells in source leaves, but only in trichomes of sink leaves (Kronberg et al., 2007).

P17 is not required for systemic movement in all plant hosts (Lee et al., 2002),

indicating that it is not the only factor mediating movement in plants. Indeed, mutational analyses have identified regions in the PLRV CP and RTD which are required for systemic movement, as discussed in Section 11.2 above and in Chapter 2. The recent discovery of P3a has further complicated the picture of luteovirid movement. Since its identification in 2015, this small protein has been shown to be important for systemic movement of two different polerovirus species: TuYV and *Brassica yellows virus* (BrYV) (Smirnova et al., 2015; Zhang et al., 2018). A 2018 study in PLRV showed that P3a interacts with itself, P17, and with structural proteins, and that the P3a - structural protein interaction is partially dependent on P17. Based on localization patterns, authors proposed a model for intracellular movement involving translocation through multiple organelles (DeBlasio et al., 2018b).

11.5 Luteovirid-host interactions: Carbon metabolism and transport

Luteovirids also commonly affect carbon metabolism and sugar transport, a phenomenon which has been particularly well-explored for *Sugarcane yellow leaf virus* (SCYLV; *Luteoviridae: Polerovirus*) (ElSayed et al., 2010; ElSayed et al., 2013; Gonçalves et al., 2005; Lehrer et al., 2007; Viswanathan et al., 2014; Wu et al., 2013a; Wu et al., 2013b; Yan et al., 2008).

Functional studies indicate that these effects are likely at least partly mediated by P17. Transgenic tobacco plants expressing P17 were found to accumulate sugars and starch in source leaves in a manner directly proportional to P17 expression levels (Hofius et al., 2001). However, increased plasmodesmata size exclusion limits were found even when P17 was expressed at low levels (Hofius et al., 2001). High levels of P17 expression were also found to cause severe stunting, decreased photosynthetic capacity, chlorosis, and occasional necrosis (Herbers et al., 1997; Hofius et al., 2001).

In a similar study using transgenic *Arabidopsis*, low levels of P17 expression caused minor increases in carbohydrate accumulation in source leaves and increased vegetative growth, but did not impact seed production (Kronberg et al., 2007). In contrast, high levels of P17 expression caused more marked carbohydrate accumulation and negatively affected vegetative growth, but significantly increased seed yield. Although it has been suggested that P17's effects on carbohydrate transport are a direct consequence of its effect on plasmodesmal size exclusion limits, P17 was found to increase size exclusion limits even when expressed at levels too low to affect carbohydrate accumulation (Hofius et al., 2001).

Finally, multiple carbohydrate metabolic proteins have been found in complex or directly interacting with PLRV structural proteins (DeBlasio et al., 2016a; DeBlasio et al., 2015a). Although it is unknown at this time how these associations impact host carbohydrate metabolism or luteovirid replication, if at all, the finding of multiple proteins from this category directly or indirectly interacting with structural proteins is striking.

Although it is unknown at this time whether effects on carbohydrate metabolism and transport are a direct or indirect result of interaction with viral proteins, or how they may be important in the viral life cycle, it has been suggested that manipulation of carbohydrate content may be a form of host manipulation designed to benefit or attract potential vectors (Eigenbrode et al., 2002).

11.6 Luteovirid-host interactions: Chloroplasts and photosynthesis

Multiple co-immunoprecipitation studies have identified chloroplastic proteins in complex with luteovirids (DeBlasio et al., 2015a; DeBlasio et al., 2015b; DeBlasio et al., 2016b). This finding is perhaps unsurprising, given that luteovirid infection is

frequently associated with interveinal chlorosis and altered photosynthesis (examples: (Delfosse et al., 2013; Duffus, 1960; Gonçalves et al., 2005; Herbers et al., 1997; Kamran et al., 2018; Kyselakova et al., 2011; Lehrer and Komor, 2008; Stevens et al., 2005; Yan et al., 2008)). Whether these effects are directly beneficial for virus infection, a side effect of virus infection, or offer vector-related benefits is unknown; however, disruption of chloroplast function using virus-induced gene silencing was recently shown to dramatically increase PLRV titer (DeBlasio et al., 2018a). Similarly, silencing of PsbQ, which also directly interacts with PLRV structural proteins, was found to promote an increase in PLRV titer in local infections (DeBlasio et al., 2016a). These data suggest that inhibiting photosynthesis may be beneficial for replication.

11.7 Luteovirid-host interactions: Host manipulation

Luteovirid infection is also known to alter host plants to promote acquisition and dispersal by insect vectors (for review: (Bosque-Perez and Eigenbrode, 2011)). Luteovirid-infected plants tend to be more effective at attracting aphid vectors and promoting prolonged feeding for acquisition than uninfected plants. These effects appear to be largely due to changes in volatile emissions produced by host plants (Eigenbrode et al., 2002; Jimenez-Martinez et al., 2004a; Medina-Ortega et al., 2009; Ngumbi et al., 2007; Rajabaskar et al., 2014; Srinivasan et al., 2006; Werner et al., 2009), but tissue chlorosis and nutritional content of phloem may also be involved (Ajayi, 1986; Ajayi and Dewar, 1983; Blua et al., 1994; Eckel and Lampert, 1996; Fereres et al., 1990; Jensen, 1972; Macias and Mink, 1969; Markkula and Laurema, 1964). Viruliferous aphids are less responsive to these cues than non-viruliferous aphids, and the strength of these cues seems to intensify as infection progresses

(Medina-Ortega et al., 2009; Werner et al., 2009). Co-immunoprecipitation and cross-linking studies have identified proteins involved in volatile compound synthesis and amino acid metabolism in complex or interacting with PLRV (DeBlasio et al., 2015a) (Figure 1.2).

11.8 Viruses in the Luteoviridae: Conclusion

In this dissertation, we apply cross-linking proteomics and computational modeling, in tandem with plant molecular biology, to examine the structural biology of luteovirids, and to probe direct host-virus interactions. In addition to insights in luteovirid biology, we detail technical advances, and show how cutting-edge proteomics can be linked to more traditional techniques, with powerful results.

REFERENCES

Aarabe, A., Chebli, B., Afechtal, M., 2018. First report of *Cucurbit aphid-borne yellows virus* from Morocco. Australasian Plant Disease Notes 13.

Afroz, A., Zahur, M., Zeeshan, N., Komatsu, S., 2013. Plant-bacterium interactions analyzed by proteomics. Frontiers in Plant Science 4, 21.

Agranovsky, A.A., Boyko, V.P., Karasev, A.V., Koonin, E.V., Dolja, V.V., 1991. Putative 65 kDa protein of *Beet yellows closterovirus* is a homologue of HSP70 heat shock proteins. J Mol Bio 217, 603-6010.

Ahmad, A., Ashfaq, M., Riaz, T., Ahsan, M., Hyder, S., Manglli, A., Tomassoli, L., 2018. First Report of *Pepper vein yellows virus* infecting hot pepper in Pakistan. Plant Disease 102, 258-258.

Ajayi, O., 1986. The effect of *Barley yellow dwarf virus* on the amino acid composition of spring wheat. Annals of Applied Biology 108, 145-149.

Ajayi, O., Dewar, A.M., 1983. The Effect of *Barley yellow dwarf virus* on field populations of the cereal aphids, Sitobion-Avenae and Metopolophium-Dirhodum. Annals of Applied Biology 103, 1-11.

Alexander, M.M., Mohr, J.P., DeBlasio, S.L., Chavez, J.D., Ziegler-Graff, V., Brault, V., Bruce, J.E., Heck, M.C., 2017. Insights in luteovirid structural biology guided by chemical cross-linking and high resolution mass spectrometry. Virus Res 241, 42-52.

Alzhanova, D.V., Prokhnevsky, A.I., Peremyslov, V.V., Dolja, V.V., 2007. Virion tails of *Beet yellows virus*: Coordinated assembly by three structural proteins. Virology 359, 220-226.

Amari, K., Lerich, A., Schmitt-Keichinger, C., Dolja, V.V., Ritzenthaler, C., 2011. Tubule-guided cell-to-cell movement of a plant virus requires class XI myosin motors. PLoS Pathog 7, e1002327.

Arias, M.C., Lenardon, S., Taleisnik, E., 2003. Carbon metabolism alterations in sunflower plants infected with the *Sunflower chlorotic mottle virus*. Journal of Phytopathology 151, 267-273.

Asada, K., 2006. Production and scavenging of reactive oxygen species in chloroplasts and their functions. Plant Physiol 141, 391-396.

Ashoub, A., Rohde, W., Prüfer, D., 1998. *In planta* transcription of a second subgenomic RNA increases the complexity of the subgroup 2 luteovirus genome. Nucleic Acids Research 26, 420-426.

Ashraf, M., Zafar, Z.U., 2000. Patterns of free carbohydrates and starch accumulation in the leaves of cotton (*Gossypium hirsutum* L.) cultivars differing in resistance to *Cotton leaf curl virus*. Archives of Agronomy and Soil Science 45, 1-9.

Ashraf, M., Zafar, Z.U., McNeilly, T., Veltkamp, C.J., 1999. Some morpho-anatomical characteristics of cotton (*Gossypium hirsutum* L.) in relation to reistance to *Cotton leaf curl virus* (CLCuV). Journal of Applied Botany 73, 76-82.

Avisar, D., Prokhnevsky, A.I., Dolja, V.V., 2008. Class VIII myosins are required for plasmodesmatal localization of a closterovirus Hsp70 homolog. J Virol 82, 2836-2843.

Bahner, I., Lamb, J., Mayo, M.A., Hay, R.T., 1990. Expression of the genome of *Potato leafroll virus*: Readthrough of the coat protein termination codon in vivo. Journal of General Virology 71 (Pt 10), 2251-2256.

Balachandran, S., Hull, R.J., Vaadia, Y., Wolf, S., Lucas, W.J., 1995. Alteration in carbon partitioning induced by the movement protein of *Tobacco mosaic virus* originates in the mesophyll and is independent of change in the plasmodesmal size exclusion limit. Plant, Cell & Environment 18, 1301-1310.

Bauer, M.R., 2000. Role of reactive oxygen species and antioxidant enzymes in systemic virus infections of plants. Journal of Phytopathology 148, 297-302.

Baumberger, N., Tsai, C.H., Lie, M., Havecker, E., Baulcombe, D.C., 2007. The polerovirus silencing suppressor P0 targets ARGONAUTE proteins for degradation. Curr Biol 17, 1609-1614.

Bekele, B., Kumari, S., Ahmed, S., Fininsa, C., Yusuf, A., Abraham, A., 2018. Non-cultivated grass hosts of yellow dwarf viruses in Ethiopia and their epidemiological consequences on cultivated cereals. Journal of Phytopathology 166, 103-115.

Bencharki, B., Boissinot, S., Revollon, S., Ziegler-Graff, V., Erdinger, M., Wiss, L., Dinant, S., Renard, D., Beuve, M., Lemaitre-Guillier, C., Brault, V., 2010. Phloem protein partners of *Cucurbit aphid borne yellows virus*: possible involvement of phloem proteins in virus transmission by aphids. Mol Plant Microbe Interact 23, 799-810.

Blanc, S., Schmidt, I., Vantard, M., Scholthof, H.B., Kuhl, G., Esperandieu, P., Cerutti, M., Louis, C., 1996. The aphid transmission factor of *Cauliflower mosaic virus* forms a stable complex with microtubules in both insect and plant cells. Proceedings of the National Academy of Sciences of the United States of America 93, 15158-15163.

Blua, M.J., Perring, T.M., Madore, M.A., 1994. Plant virus-induced changes in aphid population development and temporal fluctuations in plant nutrients. J Chem Ecol 20, 691-707.

Boissinot, S., Erdinger, M., Monsion, B., Ziegler-Graff, V., Brault, V., 2014. Both structural and non-structural forms of the readthrough protein of *Cucurbit aphid-borne yellows virus* are essential for efficient systemic infection of plants. PLoS One 9, e93448.

Bortolamiol, D., Pazhouhandeh, M., Marrocco, K., Genschik, P., Ziegler-Graff, V., 2007. The polerovirus F box protein P0 targets ARGONAUTE1 to suppress RNA silencing. Curr Biol 17, 1615-1621.

Bosque-Perez, N.A., Eigenbrode, S.D., 2011. The influence of virus-induced changes in plants on aphid vectors: Insights from luteovirus pathosystems. Virus Res 159, 201-205.

Boyko, V., Ferralli, J., Ashby, J., Schellenbaum, P., Heinlein, M., 2000. Function of microtubules in intercellular transport of plant virus RNA. Nature Cell Biology 2, 826-832.

Boyko, V., Hu, Q., Seemanpillai, M., Ashby, J., Heinlein, M., 2007. Validation of microtubule-associated *Tobacco mosaic virus* RNA movement and involvement of microtubule-aligned particle trafficking. Plant J 51, 589-603.

Braam, J., Campbell, P., 1999. Xyloglucan endotransglycosylases: Diversity of genes, enzymes and potential wall-modifying functions. Trends in Plant Science 4, 361-366.

Brault, V., Bergdoll, M., Mutterer, J., Prasad, V., Pfeffer, S., Erdinger, M., Richards, K.E., Ziegler-Graff, V., 2003. Effects of point mutations in the major capsid protein of *Beet western yellows virus* on capsid formation, virus accumulation, and aphid transmission. Journal of Virology 77, 3247-3256.

Brault, V., Herrbach, E., Reinbold, C., 2007. Electron microscopy studies on luteovirid transmission by aphids. Micron 38, 302-312.

Brizard, J.P., Carapito, C., Delalande, F., Van Dorsselaer, A., Brugidou, C., 2006. Proteome analysis of plant-virus interactome: Comprehensive data for virus multiplication inside their hosts. Mol Cell Proteomics 5, 2279-2297.

Buzkan, N., Arpaci, B.B., Yarali, F., Koç, M., 2018. Occurence of *Beet western yellows virus* on squash and broad bean in Turkey. Journal of Plant Pathology 100, 305-307.

Cantú, M.D., Mariano, a.G., Palma, M.S., Carrilho, E., Wulff, N.a., 2008. Proteomic analysis reveals suppression of bark chitinases and proteinase inhibitors in citrus plants affected by the citrus sudden death disease. Phytopathology 98, 1084-1092.

Carmo, L.S., Resende, R.O., Silva, L.P., Ribeiro, S.G., Mehta, A., 2013. Identification of host proteins modulated by the virulence factor AC2 of *Tomato chlorotic mottle virus* in *Nicotiana benthamiana*. Proteomics 13, 1947-1960.

Carvajal-Yepes, M., Olaya, C., Lozano, I., Cuervo, M., Castano, M., Cuellar, W.J., 2014. Unraveling complex viral infections in cassava (*Manihot esculenta* Crantz) from Colombia. Virus Res 186, 76-86.

Casado-Vela, J., Selles, S., Martinez, R.B., 2006. Proteomic analysis of *Tobacco mosaic virus*-infected tomato (*Lycopersicon esculentum* M.) fruits and detection of viral coat protein. Proteomics 6 Suppl 1, S196-206.

Castle, S.J., Berger, P.H., 1993. Rates of growth and increase of *Myzus persicae* on virus-infected potatoes according to type of virus-vector relationship. Entomologia Experimentalis et Applicata 69, 51-60.

Castle, S.J., Mowry, T.M., Berger, P.H., 1998. Differential settling by *Myzus persicae* (Homoptera : Aphididae) on various virus infected host plants. Annals of the Entomological Society of America 91, 661-667.

Chavez, J.D., Cilia, M., Weisbrod, C.R., Ju, H.J., Eng, J.K., Gray, S.M., Bruce, J.E., 2012. Cross-linking measurements of the *Potato leafroll virus* reveal protein interaction topologies required for virion stability, aphid transmission, and virus-plant interactions. J Proteome Res 11, 2968-2981.

Chay, C.A., Gunasinge, U.B., Dinesh-Kumar, S.P., Miller, W.A., Gray, S.M., 1996. Aphid transmission and systemic plant infection determinants of *Barley yellow dwarf luteovirus*-PAV are contained in the coat protein readthrough domain and 17-kDa protein, respectively. Virology 219, 57-65.

Chen, L., Shimamoto, K., 2010. Emerging roles of molecular chaperones in plant innate immunity. Journal of General Plant Pathology 77, 1-9.

Chen, M.H., Sheng, J., Hind, G., Handa, a.K., Citovsky, V., 2000. Interaction between the *Tobacco mosaic virus* movement protein and host cell pectin methylesterases is required for viral cell-to-cell movement. The EMBO Journal 19, 913-920.

Cho, S.Y., Cho, W.K., Kim, K.H., 2012. Identification of tobacco proteins associated with the stem-loop 1 RNAs of *Potato virus X*. Mol Cells 33, 379-384.

Cilia, M., Peter, K.A., Bereman, M.S., Howe, K., Fish, T., Smith, D., Gildow, F., MacCoss, M.J., Thannhauser, T.W., Gray, S.M., 2012. Discovery and targeted LC-MS/MS of purified polerovirus reveals differences in the virus-host interactome associated with altered aphid transmission. PLoS One 7, e48177.

Cilia, M., Tamborindeguy, C., Fish, T., Howe, K., Thannhauser, T.W., Gray, S., 2011. Genetics coupled to quantitative intact proteomics links heritable aphid and endosymbiont protein expression to circulative polerovirus transmission. J Virol 85, 2148-2166.

Cotton, S., Grangeon, R., Thivierge, K., Mathieu, I., Ide, C., Wei, T., Wang, A., Laliberte, J.F., 2009. *Turnip mosaic virus* RNA replication complex vesicles are mobile, align with microfilaments, and are each derived from a single viral genome. J Virol 83, 10460-10471.

Cristea, I.M., Carroll, J.W., Rout, M.P., Rice, C.M., Chait, B.T., MacDonald, M.R., 2006. Tracking and elucidating alphavirus-host protein interactions. The Journal of Biological Chemistry 281, 30269-30278.

Csorba, T., Kontra, L., Burgyan, J., 2015. Viral silencing suppressors: Tools forged to fine-tune host-pathogen coexistence. Virology 479-480, 85-103.

Csorba, T., Lozsa, R., Hutvagner, G., Burgyan, J., 2010. Polerovirus protein P0 prevents the assembly of small RNA-containing RISC complexes and leads to degradation of ARGONAUTE1. Plant J 62, 463-472.

Dangl, J.L., Dietrich, R.A., Richberg, M.H., 1996. Death don't have no mercy: Cell death programs in plant-microbe interactions. The Plant Cell 8, 1793-1807.

Das, J., Gayvert, K.M., Bunea, F., Wegkamp, M.H., Yu, H., 2015. ENCAPP: elastic-net-based prognosis prediction and biomarker discovery for human cancers. BMC Genomics 16, 263.

Day, M.F., 1955. The mechanism of the transmission of *Potato leaf roll virus* by aphids. Australian Journal of Biological Sciences 8, 498 - 513

DeBlasio, S.L., Chavez, J.D., Alexander, M.M., Ramsey, J., Eng, J.K., Mahoney, J., Gray, S.M., Bruce, J.E., Cilia, M., 2016a. Visualization of host-polerovirus interaction topologies using Protein Interaction Reporter technology. J Virol 90, 1973-1987.

DeBlasio, S.L., Johnson, R., Mahoney, J., Karasev, A., Gray, S.M., MacCoss, M.J., Cilia, M., 2015a. Insights into the polerovirus-plant interactome revealed by co-immunoprecipitation and mass spectrometry. Mol Plant Microbe Interact 28, 467-481.

DeBlasio, S.L., Johnson, R., Sweeney, M.M., Karasev, A., Gray, S.M., MacCoss, M.J., Cilia, M., 2015b. *Potato leafroll virus* structural proteins manipulate overlapping, yet distinct protein interaction networks during infection. Proteomics 15, 2098-2112.

DeBlasio, S.L., Johnson, R.S., MacCoss, M.J., Gray, S.M., Cilia, M., 2016b. Model system-guided protein interaction mapping for virus isolated from phloem tissue. J Proteome Res 15, 4601-4611.

DeBlasio, S.L., Rebelo, A.R., Parks, K., Gray, S.M., Heck, M.C., 2018a. Disruption of chloroplast function through downregulation of phytoene desaturase enhances the systemic accumulation of an aphid-borne, phloem-restricted virus. Mol Plant Microbe Interact 31, 1095-1110.

DeBlasio, S.L., Xu, Y., Johnson, R.S., Rebelo, A.R., MacCoss, M.J., Gray, S.M., Heck, M., 2018b. The interaction dynamics of two *Potato leafroll virus* movement proteins affects their localization to the outer membranes of mitochondria and plastids. Viruses 10.

Delfosse, V.C., Casse, M.F., Agrofoglio, Y.C., Kresic, I.B., Hopp, H.E., Ziegler-Graff, V., Distefano, A.J., 2013. Agroinoculation of a full-length cDNA clone of *Cotton leafroll dwarf virus* (CLRDV) results in systemic infection in cotton and the model plant *Nicotiana benthamiana*. Virus Res 175, 64-70.

Demler, S.A., De Zoeten, G.A., Adam, G., Harris, K.F., 1996. Pea enation mosaic enamovirus: Properties and aphid transmission, in: Harrison, B.D. (Ed.), The Plant Viruses. Springer, pp. 303-344.

Denison, F.C., Paul, A.L., Zupanska, A.K., Ferl, R.J., 2011. 14-3-3 proteins in plant physiology. Semin Cell Dev Biol 22, 720-727.

Derrien, B., Clavel, M., Baumberger, N., Iki, T., Sarazin, A., Hacquard, T., Ponce, M.R., Ziegler-Graff, V., Vaucheret, H., Micol, J.L., Voinnet, O., Genschik, P., 2018. A suppressor screen for AGO1 degradation by the viral F-Box P0 protein uncovers a role for AGO DUF1785 in sRNA duplex unwinding. Plant Cell 30, 1353-1374.

Di Carli, M., Benvenuto, E., Donini, M., 2012. Recent insights into plant-virus interactions through proteomic analysis. J Proteome Res 11, 4765-4780.

Di Carli, M., Villani, M.E., Bianco, L., Lombardi, R., Perrotta, G., Benvenuto, E., Donini, M., 2010. Proteomic analysis of the plant-virus interaction in *Cucumber mosaic virus* (CMV) resistant transgenic tomato. J Proteome Res 9, 5684-5697.

Diaz-Vivancos, P., Rubio, M., Mesonero, V., Periago, P.M., Barcelo, A.R., Martinez-Gomez, P., Hernandez, J.A., 2006. The apoplastic antioxidant system in *Prunus*: response to long-term plum pox virus infection. J Exp Bot 57, 3813-3824.

Dinesh-Kumar, S.P., Brault, V., Miller, W.A., 1992. Precise mapping and *in vitro* translation of a trifunctional subgenomic RNA of *Barley yellow dwarf virus*. Virology 187, 711-722.

Duffus, J.E., 1960. Radish yellows, a disease of radish, sugar beet, and other crops. Phytopathology 50.

Dunwell, J.M., Gibbings, J.G., Mahmood, T., Saqlan Naqvi, S.M., 2008. Germin and germin-like proteins: Evolution, structure, and function. Critical Reviews in Plant Sciences 27, 342-375.

Eckel, R.V.W., Lampert, E.P., 1996. Relative attractiveness of *Tobacco etch virus*-infected and healthy flue-cured tobacco plants to aphids (Homoptera: Aphididae). Journal of Economic Entomology 89, 1017-1027.

Edreva, A., 2005. Pathogenesis-related proteins: Research progress in the last 15 years. General Applied Plant Physiology 31, 105-124.

Eicholtz, M., Grinstead, S., Wu, L.P., Kinard, G., Li, R., 2018. First report of *Beet western yellows virus* infecting *Epiphyllum* spp. Plant Disease 102, 464-464.

Eigenbrode, S.D., Ding, H., Shiel, P., Berger, P.H., 2002. Volatiles from potato plants infected with *Potato leafroll virus* attract and arrest the virus vector, *Myzus persicae* (Homoptera: Aphididae). Proc Biol Sci 269, 455-460.

ElSayed, A.I., Ramadan, M.F., Komor, E., 2010. Expression of sucrose transporter (ShSUT1) in a Hawaiian sugarcane cultivar infected with *Sugarcane yellow leaf virus* (SCYLV). Physiological and Molecular Plant Pathology 75, 56-63.

ElSayed, A.I., Weig, A.R., Sariyeva, G., Hummel, E., Yan, S.-L., Bertolini, A., Komor, E., 2013. Assimilate export inhibition in *Sugarcane yellow leaf virus*-infected sugarcane is not due to less transcripts for sucrose transporters and sucrose-phosphate synthase or to callose deposition in sieve plates. Physiological and Molecular Plant Pathology 81, 64-73.

Elvira, M.I., Galdeano, M.M., Gilardi, P., Garcia-Luque, I., Serra, M.T., 2008. Proteomic analysis of pathogenesis-related proteins (PRs) induced by compatible and incompatible interactions of *Pepper mild mottle virus* (PMMoV) in *Capsicum chinense* L3 plants. J Exp Bot 59, 1253-1265.

Ephraim, N., Yona, B., Evans, A., Sharon, A., Titus, A., 2015. Effect of cassava brown streak disease (CBSD) on cassava (*Manihot esculenta* Crantz) root storage components , starch quantities and starch quality properties. International Journal of Plant Physiology and Biochemistry 7, 12-22.

Esau, K., Hoefert, L.L., 1972a. Development of infection with *Beet western yellows virus* in the sugarbeet. Virology 48, 724-738.

Esau, K., Hoefert, L.L., 1972b. Ultrastructure of sugarbeet leaves infected with *Beet western yellows virus*. Journal of ultrastructure research 40, 556-571.

Eskandari, F., Sylvester, E.S., Richardson, J., 1979. Evidence for lack of propagation of *Potato leaf roll virus* in its aphid vector, *Myzus persicae*. Phytopathology 69, 45-47.

Fereres, A., Araya, J.E., Housley, T.L., Foster, J.E., 1990. Carbohydrate-composition of wheat infected with *Barley yellow dwarf virus*. Z Pflanzenk Pflanzen 97, 600-608.

Fernandez-Calvino, L., Osorio, S., Hernandez, M.L., Hamada, I.B., del Toro, F.J., Donaire, L., Yu, A., Bustos, R., Fernie, A.R., Martinez-Rivas, J.M., Llave, C., 2014. Virus-induced alterations in primary metabolism modulate susceptibility to *Tobacco rattle virus* in *Arabidopsis*. Plant Physiol 166, 1821-1838.

Fox, A., Fowkes, A.R., Skelton, A., Harju, V., Buxton-Kirk, A., Kelly, M., Forde, S.M.D., Pufal, H., Conyers, C., Ward, R., Weekes, R., Boonham, N., Adams, I.P., 2018. Using high-throughput sequencing in support of a plant health outbreak reveals novel viruses in *Ullucus tuberosus* (Basellaceae). Plant Pathology.

Gampala, S.S., Kim, T.W., He, J.X., Tang, W., Deng, Z., Bai, M.Y., Guan, S., Lalonde, S., Sun, Y., Gendron, J.M., Chen, H., Shibagaki, N., Ferl, R.J., Ehrhardt, D., Chong, K., Burlingame, A.L., Wang, Z.Y., 2007. An essential role for 14-3-3 proteins in brassinosteroid signal transduction in *Arabidopsis*. Dev Cell 13, 177-189.

Gao, J.-G., Nassuth, A., 1993. Alteration of major cellular organelles in wheat leaf tissue infected with *Wheat streak mosaic rymovirus* (*Potyviridae*). Phytopathology 83, 206-213.

Garcia-Ruiz, H., Carbonell, A., Hoyer, J.S., Fahlgren, N., Gilbert, K.B., Takeda, A., Giampetruzzi, A., Garcia Ruiz, M.T., McGinn, M.G., Lowery, N., Martinez Baladejo, M.T., Carrington, J.C., 2015. Roles and programming of *Arabidopsis* ARGONAUTE proteins during *Turnip mosaic virus infection*. PLoS Pathog 11, e1004755.

Gibson, K.E., Landis, B.J., Klostermeyer, E.C., 1951. Effect of aphid control on the spread of leafroll in potatoes. American Potato Journal 28, 658-666.

Gildow, F.E., 1982. Coated-vesicle transport of luteoviruses through salivary-glands of *Myzus-persicae*. Phytopathology 72, 1289-1296.

Gildow, F.E., Reavy, B., Mayo, M.A., Duncan, G.H., Woodford, J.A., Lamb, J.W., Hay, R.T., 2000. Aphid acquisition and cellular transport of *Potato leafroll virus*-like particles lacking P5 readthrough protein. Phytopathology 90, 1153-1161.

Gill, C.C., Chong, J., 1975. Development of the infection in oat leaves inoculated with *Barley yellow dwarf virus*. Virology 66, 440-453.

Gill, S.S., Tuteja, N., 2010. Reactive oxygen species and antioxidant machinery in abiotic stress tolerance in crop plants. Plant Physiol Biochem 48, 909-930.

Gillespie, T., 2002. Functional analysis of a DNA-shuffled movement protein reveals that microtubules are dispensable for the cell-to-cell movement of *Tobacco mosaic virus*. The Plant Cell Online 14, 1207-1222.

Giribaldi, M., Purrotti, M., Pacifico, D., Santini, D., Mannini, F., Caciagli, P., Rolle, L., Cavallarin, L., Giuffrida, M.G., Marzachi, C., 2011. A multidisciplinary study on the effects of phloem-limited viruses on the agronomical performance and berry quality of *Vitis vinifera* cv. Nebbiolo. J Proteomics 75, 306-315.

Glenney, J.R., Kaulfus, P., Matsudaira, P., Weber, K., 1981. F-actin binding and bundling properties of fimbrin, a major cytoskeletal protein of microvillus core filaments. Journal of Biological Chemistry 256, 9283-9288.

Golinowski, W., Tomenius, K., Oxelfelt, P., 1987. Ultrastructural studies on potato phloem cells infected with *Potato leaf roll virus*—comparison of two potato varieties. Acta Agriculturae Scandinavica 37, 3-19.

Gonçalves, M.C., Vega, J., Oliveira, J.G., Gomes, M.M.a., 2005. *Sugarcane yellow leaf virus* infection leads to alterations in photosynthetic efficiency and carbohydrate accumulation in sugarcane leaves. Fitopatologia Brasileira 30, 10-16.

Grangeon, R., Jiang, J., Laliberte, J.F., 2012. Host endomembrane recruitment for plant RNA virus replication. Curr Opin Virol 2, 683-690.

Gray, S., Cilia, M., Ghanim, M., 2014. Circulative, "nonpropagative" virus transmission: An orchestra of virus-, insect-, and plant-derived instruments. Adv Virus Res 89, 141-199.

Gray, S., Gildow, F.E., 2003. Luteovirus-aphid interactions. Annu Rev Phytopathol 41, 539-566.

Greber, U.F., Way, M., 2006. A superhighway to virus infection. Cell 124, 741-754.

Greenberg, J.T., Yao, N., 2004. The role and regulation of programmed cell death in plant-pathogen interactions. Cellular Microbiology 6, 201-211.

Guadie, D., Abraham, A., Tesfaye, K., Winter, S., Menzel, W., Knierim, D., 2018. First report of *Maize yellow mosaic virus* infecting maize (*Zea mays*) in Ethiopia. Plant Disease 102, 1044-1044.

Harries, P.a., Park, J.-W., Sasaki, N., Ballard, K.D., Maule, A.J., Nelson, R.S., 2009. Differing requirements for actin and myosin by plant viruses for sustained intercellular movement. Proceedings of the National Academy of Sciences of the United States of America 106, 17594-17599.

Haupt, S., Cowan, G.H., Ziegler, A., Roberts, A.G., Oparka, K.J., Torrance, L., 2005. Two plant-viral movement proteins traffic in the endocytic recycling pathway. Plant Cell 17, 164-181.

Heinlein, M., 2015. Plant virus replication and movement. Virology 479-480, 657-671.

Heinlein, M., Epel, B.L., Padgett, H.S., Beachy, R.N., 1995. Interaction of tobamovirus movement proteins with the plant cytoskeleton. Science 270, 1983-1985.

Heinlein, M., Padgett, H.S., Gens, J.S., Pickard, B.G., Casper, S.J., Epel, B.L., Beachy, R.N., 1998. Changing patterns of localization of the *Tobacco mosaic virus* movement protein and replicase to the endoplasmic reticulum and microtubules during infection. Plant Cell 10, 1107-1120.

Herbers, K., Tacke, E., Hazirezaei, M., Krause, K.P., Melzer, M., Rohde, W., Sonnewald, U., 1997. Expression of a luteoviral movement protein in transgenic plants leads to carbohydrate accumulation and reduced photosynthetic capacity in source leaves. Plant J 12, 1045-1056.

Hofius, D., Herbers, K., Melzer, M., 2001. Expression level-dependent modulation of carbohydrate status and viral resistance by the *Potato leafroll virus* movement protein in transgenic tobacco plants. The Plant Journal 28, 529-543.

Holmes, J.C., Bethel, W.M., 1972. Modification of intermediate host behaviour by parasites, in: Canning, E.U., Wright, C.A. (Eds.), Behavioural aspects of parasite transmission. Academic Press, London, pp. 123-149.

Huang, Z., Andrianov, V.M., Han, Y., Howell, S.H., 2001. Identification of *Arabidopsis* proteins that interact with the *Cauliflower mosaic virus* (CaMV) movement protein. Plant Molecular Biology 47, 663-675.

Huber, S.C., MacKintosh, C., Kaiser, W.M., 2002. Metabolic enzymes as targets for 14-3-3 proteins. Plant Molecular Biology 50, 1053-1063.

Ilbagi, H., Citir, A., Kara, A., Uysal, M., 2018. Poaceae weed hosts of *Yellow dwarf viruses* (YDVs) in the Trakya region of Turkey. Ekin J. 4, 8-19.

Ingwell, L.L., Eigenbrode, S.D., Bosque-Pérez, N.A., 2012. Plant viruses alter insect behavior to enhance their spread. Scientific Reports 2.

Isaacson, T., Damasceno, C.M., Saravanan, R.S., He, Y., Catala, C., Saladie, M., Rose, J.K., 2006. Sample extraction techniques for enhanced proteomic analysis of plant tissues. Nature Protocols 1, 769-774.

Jensen, S.G., 1972. Metabolism and carbohydrate composition in *Barley yellow dwarf virus*-infected wheat. Phytopathology 62, 587-&.

Jimenez-Martinez, E.S., Bosque-Perez, N.A., Berger, P.H., Zemetra, R., Ding, H.J., Eigenbrode, S.D., 2004a. Volatile cues influence the response of *Rhopalosiphum padi* (Homoptera : Aphididae) to *Barley yellow dwarf virus*-infected transgenic and untransformed wheat. Environmental Entomology 33, 1207-1216.

Jimenez-Martinez, E.S., Bosque-Perez, N.A., Berger, P.H., Zemetra, R.S., 2004b. Life history of the bird cherry-oat aphid, *Rhopalosiphum padi* (Homoptera: Aphididae), on transgenic and untransformed wheat challenged with *Barley yellow dwarf virus*. J Econ Entomol 97, 203-212.

Ju, H.J., Samuels, T.D., Wang, Y.S., Blancaflor, E., Payton, M., Mitra, R., Krishnamurthy, K., Nelson, R.S., Verchot-Lubicz, J., 2005. The *Potato virus X* TGBp2 movement protein associates with endoplasmic reticulum-derived vesicles during virus infection. Plant Physiol 138, 1877-1895.

Kamran, A., Lotos, L., Amer, M.A., Al-Saleh, M.A., Alshahwan, I.M., Shakeel, M.T., Ahmad, M.H., Umar, M., Katis, N.I., 2018. Characterization of *Pepper leafroll chlorosis virus*, a new polerovirus causing yellowing disease of bell pepper in Saudi Arabia. Plant Dis 102, 318-326.

Kaplan, I.B., Lee, L., Ripoll, D.R., Palukaitis, P., Gildow, F., Gray, S.M., 2007. Point mutations in the *Potato leafroll virus* major capsid protein alter virion stability and aphid transmission. J Gen Virol 88, 1821-1830.

Karasev, A.V., Kashina, A.S., Gelfand, V.I., Dolja, V.V., 1992. HSP70-related 65 kDa protein of *Beet yellows closterovirus* is a microtubule-binding protein. Federation of European Biochemical Societies 304, 12-14.

Kawakami, S., Watanabe, Y., Beachy, R.N., 2004. *Tobacco mosaic virus* infection spreads cell to cell as intact replication complexes. Proceedings of the National Academy of Sciences of the United States of America 101, 6291-6296.

Kenesi, E., Carbonell, A., Lozsa, R., Vertessy, B., Lakatos, L., 2017. A viral suppressor of RNA silencing inhibits ARGONAUTE 1 function by precluding target RNA binding to pre-assembled RISC. Nucleic Acids Res 45, 7736-7750.

Kojima, M., Shikata, E., Sugawara, M., Murayama, D., 1968. Isolation and electron microscopy of *Potato leafroll virus* from plants. Virology 35, 612-615.

Kojima, M., Shikata, E., Sugawara, M., Murayama, D., 1969. Purification and electron microscopy of *Potato leafroll virus*. Virology 39, 162-173.

Kronberg, K., Vogel, F., Rutten, T., Hajirezaei, M.R., Sonnewald, U., Hofius, D., 2007. The silver lining of a viral agent: increasing seed yield and harvest index in *Arabidopsis* by ectopic expression of the *Potato leaf roll virus* movement protein. Plant Physiol 145, 905-918.

Kumar, L.M., Foster, J.A., McFarland, C., Malapi-Wight, M., 2018. First report of *Barley virus* G in switchgrass (*Panicum virgatum*). Plant Disease 102, 466-466.

Kundu, S., Chakraborty, D., Kundu, A., Pal, A., 2013. Proteomics approach combined with biochemical attributes to elucidate compatible and incompatible plant-virus interactions between *Vigna mungo* and *Mungbean yellow mosaic India virus*. Proteome Science 11.

Kundu, S., Chakraborty, D., Pal, A., 2011. Proteomic analysis of salicylic acid induced resistance to *Mungbean yellow mosaic India virus* in *Vigna mungo*. J Proteomics 74, 337-349.

Kyselakova, H., Prokopova, J., Naus, J., Novak, O., Navratil, M., Safarova, D., Spundova, M., Ilik, P., 2011. Photosynthetic alterations of pea leaves infected systemically by *Pea enation mosaic virus*: A coordinated decrease in efficiencies of CO_2 assimilation and photosystem II photochemistry. Plant Physiol Biochem 49, 1279-1289.

Lai, T., Deng, Y., Zhang, P., Chen, Z., Hu, F., Zhang, Q., Hu, Y., Shi, N., 2013. Proteomics-based analysis of *Phalaenopsis amabilis* in response toward *Cymbidium mosaic virus* and/or *Odontoglossum ringspot virus* infection. American Journal of Plant Sciences 04, 1853-1862.

Lam, E., Kato, N., Lawton, M., 2001. Programmed cell death, mitochondria and the plant hypersensitive response. Nature 411, 848-853.

Laporte, C., 2003. Involvement of the secretory pathway and the cytoskeleton in intracellular targeting and tubule assembly of *Grapevine fanleaf virus* movement protein in tobacco BY-2 cells. The Plant Cell Online 15, 2058-2075.

Larson, R.L., Wintermantel, W.M., Hill, A., Fortis, L., Nunez, A., 2008. Proteome changes in sugar beet in response to *Beet necrotic yellow vein virus*. Physiological and Molecular Plant Pathology 72, 62-72.

Lee, B.J., Kwon, S.J., Kim, S.K., Kim, K.J., Park, C.J., Kim, Y.J., Park, O.K., Paek, K.H., 2006. Functional study of hot pepper 26S proteasome subunit RPN7 induced by *Tobacco mosaic virus* from nuclear proteome analysis. Biochem Biophys Res Commun 351, 405-411.

Lee, L., Kaplan, I.B., Ripoll, D.R., Liang, D., Palukaitis, P., Gray, S.M., 2005. A surface loop of the *Potato leafroll virus* coat protein is involved in virion assembly, systemic movement, and aphid transmission. J Virol 79, 1207-1214.

Lee, L., Palukaitis, P., Gray, S.M., 2002. Host-dependent requirement for the *Potato leafroll virus* 17-kDa protein in virus movement. MOL PLANT MICROBE INTERACT 15, 1086-1094.

Lee, S.J., Saravanan, R.S., Damasceno, C.M., Yamane, H., Kim, B.D., Rose, J.K., 2004. Digging deeper into the plant cell wall proteome. Plant Physiology and Biochemistry 42, 979-988.

Lehrer, A.T., Komor, E., 2008. Carbon dioxide assimilation by virus-free sugarcane plants and by plants which were infected by *Sugarcane yellow leaf virus*. Physiological and Molecular Plant Pathology 73, 147-153.

Lehrer, A.T., Moore, P.H., Komor, E., 2007. Impact of *Sugarcane yellow leaf virus* (ScYLV) on the carbohydrate status of sugarcane: Comparison of virus-free plants with symptomatic and asymptomatic virus-infected plants. Physiological and Molecular Plant Pathology 70, 180-188.

Lenz, O., Sarkisova, T., Koloniuk, I., Franova, J., Pribylova, J., Spak, J., 2018. *Red clover-associated luteovirus* - a newly classifiable member of the genus *Luteovirus* with an enamo-like P5 protein. Arch Virol 163, 3439-3442.

Levy, A., Erlanger, M., Rosenthal, M., Epel, B.L., 2007a. A plasmodesmata-associated β-1,3-glucanase in *Arabidopsis*. The Plant Journal 49, 669-682.

Levy, A., Guenoune-Gelbart, D., Epel, B.L., 2007b. Beta-1,3-glucanases: plasmodesmal gate keepers for intercellular communication. Plant Signaling & Behavior 2, 404-407.

Levy, A., Zheng, J.Y., Lazarowitz, S.G., 2015. Synaptotagmin SYTA forms ER-plasma membrane junctions that are recruited to plasmodesmata for plant virus movement. Curr Biol 25, 2018-2025.

Lewis, J.D., Lazarowitz, S.G., 2010. *Arabidopsis* synaptotagmin SYTA regulates endocytosis and virus movement protein cell-to-cell transport. Proc Natl Acad Sci U S A 107, 2491-2496.

Li, C., Cox-Foster, D., Gray, S.M., Gildow, F., 2001. Vector specificity of *Barley yellow dwarf virus* (BYDV) transmission: Identification of potential cellular receptors binding BYDV-MAV in the aphid, Sitobion avenae. Virology 286, 125-133.

Li, K., Xu, C., Zhang, J., 2011. Proteome profile of maize (*Zea mays* L.) leaf tissue at the flowering stage after long-term adjustment to *Rice black-streaked dwarf virus* infection. Gene 485, 106-113.

Li, Y., Sun, Q., Zhao, T., Xiang, H., Zhang, X., Wu, Z., Zhou, C., Zhang, X., Wang, Y., Zhang, Y., Wang, X., Li, D., Yu, J., Dinesh-Kumar, S.P., Han, C., 2019. Interaction between *Brassica yellows virus* silencing suppressor P0 and plant SKP1 facilitates stability of P0 *in vivo* against degradation by proteasome and autophagy pathways. New Phytol.

Lim, S., Yoon, Y., Jang, Y.W., Bae, D.H., Kim, B.S., Maharjan, R., Yi, H., Bae, S., Lee, Y.H., Lee, B.C., Park, C.Y., Lee, S.H., Moon, J.S., 2018a. First report of *Maize yellow mosaic virus* infecting *Panicum miliaceum* and *Sorghum bicolor* in South Korea. Plant Disease 102, 689-689.

Lim, S., Yoon, Y., Jang, Y.W., Bae, S., Lee, Y.H., Lee, B.C., 2018b. First report of *Maize yellow mosaic virus* on *Zea mays* in South Korea. Plant Dis 102, 1864.

Lin, P.C., Hu, W.C., Lee, S.C., Chen, Y.L., Lee, C.Y., Chen, Y.R., Liu, L.Y., Chen, P.Y., Lin, S.S., Chang, Y.C., 2015. Application of an integrated omics approach for identifying host proteins that interact with *Odontoglossum ringspot virus* capsid protein. Mol Plant Microbe Interact 28, 711-726.

Linz, L.B., Liu, S., Chougule, N.P., Bonning, B.C., 2015. *In vitro* evidence supports membrane alanyl aminopeptidase N as a receptor for a plant virus in the pea aphid vector. J Virol 89, 11203-11212.

Liu, C., Nelson, R.S., 2013. The cell biology of *Tobacco mosaic virus* replication and movement. Frontiers in Plant Science 4, 12.

Liu, H., Wu, L., Nikolaeva, E., Peter, K., Liu, Z., Mollov, D., Cao, M., Li, R., 2018. Characterization of a new apple luteovirus identified by high-throughput sequencing. Virol J 15, 85.

Liu, J.Z., Blancaflor, E.B., Nelson, R.S., 2005. The *Tobacco mosaic virus* 126-kilodalton protein, a constituent of the virus replication complex, alone or within the complex aligns with and traffics along microfilaments. Plant Physiol 138, 1853-1865.

Lopez-Casado, G., Covey, P.A., Bedinger, P.A., Mueller, L.A., Thannhauser, T.W., Zhang, S., Fei, Z., Giovannoni, J.J., Rose, J.K., 2012. Enabling proteomic studies with RNA-Seq: The proteome of tomato pollen as a test case. Proteomics 12, 761-774.

Lozano-Duran, R., Robatzek, S., 2015. 14-3-3 proteins in plant-pathogen interactions. Mol Plant Microbe Interact 28, 511-518.

Lucas, W.J., Olesinski, A., Hull, R.J., Haudenshield, J.S., Deom, C.M., Beachy, R.N., Wolf, S., 1993. Influence of the *Tobacco mosaic virus* 30-kDa movement protein on carbon metabolism and photosynthate partitioning in transgenic tobacco plants. Planta 190, 88-96.

Ma, Y., Tan, S.T., Liu, Q.L., Li, Y.Y., Chen, X.J., Chen, H.R., Li, F., 2018. First report of *Tobacco vein distorting virus* infecting *Eupatorium adenophorum* in China. Plant Dis, PDIS12172021PDN.

Ma, Y., Zhou, T., Hong, Y., Fan, Z., Li, H., 2008. Decreased level of ferredoxin I in *Tobacco mosaic virus*-infected tobacco is associated with development of the mosaic symptom. Physiological and Molecular Plant Pathology 72, 39-45.

Macias, W., Mink, G.I., 1969. Preference of green peach aphids for virus-infected sugarbeet leaves. Journal of Economic Entomology 62, 28-29.

Magyarosy, A.C., Buchanan, B.B., Schürmann, P., 1973. Effect of a systemic virus infection on chloroplast function and structure. Virology 55, 426-438.

Malter, D., Wolf, S., 2011. Melon phloem-sap proteome: developmental control and response to viral infection. Protoplasma 248, 217-224.

Markkula, M., Laurema, S., 1964. Changes in concentration of free amino acids in plants induced by virus diseases and the reproduction of aphids. Ann. Ag. Fenn. 3, 265–271.

Martinez, F., Rodrigo, G., Aragones, V., Ruiz, M., Lodewijk, I., Fernandez, U., Elena, S.F., Daros, J.A., 2016. Interaction network of *Tobacco etch potyvirus* NIa protein with the host proteome during infection. BMC Genomics 17, 87.

Martinière, A., Gargani, D., Uzest, M., Lautredou, N., Blanc, S., Drucker, M., 2009. A role for plant microtubules in the formation of transmission-specific inclusion bodies of *Cauliflower mosaic virus*. The Plant Journal 58, 135-146.

Más, P., Beachy, R.N., 1999. Replication of *Tobacco mosaic virus* on endoplasmic reticulum and role of the cytoskeleton and virus movement protein in intracellular distribution of viral RNA. Journal of Cell Biology 147, 945-958.

Massawe, D.P., Stewart, L.R., Kamatenesi, J., Asiimwe, T., Redinbaugh, M.G., 2018. Complete sequence and diversity of a maize-associated polerovirus in East Africa. Virus Genes 54, 432-437.

Mayo, M.A., Barker, H., Robinson, D.J., Tamada, T., Harrison, B.D., 1982. Evidence that *Potato leafroll virus* RNA is positive-stranded, is linked to a small protein and does not contain polyadenylate. Journal of General Virology 59, 163-167.

McLean, B.G., Zupan, J., Zambryski, P.C., 1995. *Tobacco mosaic virus* movement protein associates with the cytoskeleton in tobacco cells. The Plant Cell 7, 2101-2114.

Medina-Ortega, K.J., Bosque-Perez, N.A., Ngumbi, E., Jimenez-Martinez, E.S., Eigenbrode, S.D., 2009. *Rhopalosiphum padi* (Hemiptera: Aphididae) responses to volatile cues from *Barley yellow dwarf virus*-infected wheat. Environ Entomol 38, 836-845.

Mehta, A., Magalhães, B.S., Souza, D.S.L., Vasconcelos, E.a.R., Silva, L.P., Grossi-de-Sa, M.F., Franco, O.L., da Costa, P.H.a., Rocha, T.L., 2008. Rooteomics: the challenge of discovering plant defense-related proteins in roots. Current Protein & Peptide Science 9, 108-116.

Miller, W.A., Dinesh-Kumar, S.P., Paul, C.P., 2011. Luteovirus Gene Expression. Critical Reviews in Plant Sciences 14, 179-211.

Mochizuki, T., Ohki, S.T., 2011. Single amino acid substitutions at residue 129 in the coat protein of *Cucumber mosaic virus* affect symptom expression and thylakoid structure. Arch Virol 156, 881-886.

Mohnen, D., 2008. Pectin structure and biosynthesis. Curr Opin Plant Biol 11, 266-277.

Moorman, N.J., Sharon-Friling, R., Shenk, T., Cristea, I.M., 2010. A targeted spatial-temporal proteomics approach implicates multiple cellular trafficking pathways in human cytomegalovirus virion maturation. Molecular and Cellular Proteomics 9, 851-860.

Mooseker, M.S., 1983. Actin binding proteins of the brush border. Cell 35, 11-13.

Mulot, M., Monsion, B., Boissinot, S., Rastegar, M., Meyer, S., Bochet, N., Brault, V., 2018. Transmission of *Turnip yellows virus* by *Myzus persicae* is reduced by feeding aphids on double-stranded RNA targeting the ephrin receptor protein. Front Microbiol 9, 457.

Napuli, A.J., Falk, B.W., Dolja, V.V., 2000. Interaction between HSP70 homolog and filamentous virions of the *Beet yellows virus*. Virology 274, 232-239.

Ngumbi, E., Eigenbrode, S.D., Bosque-Perez, N.A., Ding, H., Rodriguez, A., 2007. *Myzus persicae* is arrested more by blends than by individual compounds elevated in headspace of PLRV-Infected potato. Journal of Chemical Ecology 33, 1733-1747.

Novakova, S., Flores-Ramirez, G., Glasa, M., Danchenko, M., Fiala, R., Skultety, L., 2015. Partially resistant *Cucurbita pepo* showed late onset of the *Zucchini yellow mosaic virus* infection due to rapid activation of defense mechanisms as compared to susceptible cultivar. Front Plant Sci 6, 263.

O'Brien, J.A., Daudi, A., Butt, V.S., Bolwell, G.P., 2012. Reactive oxygen species and their role in plant defence and cell wall metabolism. Planta 236, 765-779.

Obrepalska-Steplowska, A., Wieczorek, P., Budziszewska, M., Jeszke, A., Renaut, J., 2013. How can plant virus satellite RNAs alter the effects of plant virus infection? A study of the changes in the *Nicotiana benthamiana* proteome after infection by *Peanut stunt virus* in the presence or absence of its satellite RNA. Proteomics 13, 2162-2175.

Oh, M.H., Wang, X., Clouse, S., Huber, S., 2009. 14-3-3 proteins bind to the brassinosteroid receptor kinase, BRI1 and are positive regulators of brassinosteroid signaling, American Society of Plant Biologists Annual Meeting.

Olesinski, A.a., Lucas, W.J., Galun, E., Wolp, S., 1995. Pleiotropic effects of *Tobacco-mosaic-virus* movement protein on carbon metabolism in transgenic tobacco plants. Planta, 118-126.

Osborn, H., 1935. Incubation period of pea mosaic in the aphid, *Macrosiphum pisi*. Phytopathology 25, 160-177.

Oswald, J.W., Houston, B.R., 1951. A new virus disease of cereals, transmissible by aphids. Plant Disease Reporter 11, 471-475.

Padgett, H.S., Epel, B.L., Kahn, T.W., Heinlein, M., Watanabe, Y., Beachy, R.N., 1996. Distribution of tobamovirus movement protein in infected cells and implications for cell-to-cell spread of infection. The Plant Journal 10, 1079-1088.

Papura, D., Jacquot, E., Dedryver, C.A., Luche, S., Riault, G., Bossis, M., Rabilloud, T., 2002. Two-dimensional electrophoresis of proteins discriminates aphid clones of *Sitobion avenae* differing in BYDV-PAV transmission. Arch Virol 147, 1881-1898.

Patarroyo, C., Laliberte, J.F., Zheng, H., 2012. Hijack it, change it: how do plant viruses utilize the host secretory pathway for efficient viral replication and spread? Front Plant Sci 3, 308.

Pavan Kumar, B.K., Kanakala, S., Malathi, V.G., Gopal, P., Usha, R., 2016. Transcriptomic and proteomic analysis of yellow mosaic diseased soybean. Journal of Plant Biochemistry and Biotechnology 26, 224-234.

Pazhouhandeh, M., Dieterle, M., Marrocco, K., Lechner, E., Berry, B., Brault, V., Hemmer, O., Kretsch, T., Richards, K.E., Genschik, P., Ziegler-Graff, V., 2006. F-box-like domain in the polerovirus protein P0 is required for silencing suppressor function. Proc Natl Acad Sci U S A 103, 1994-1999.

Pennell, R.I., Lamb, C., 1997. Programmed cell death in plants. The Plant Cell 9, 1157-1168.

Perez-Bueno, M.L., Rahoutei, J., Sajnani, C., Garcia-Luque, I., Baron, M., 2004. Proteomic analysis of the oxygen-evolving complex of photosystem II under biotic stress: Studies on *Nicotiana benthamiana* infected with tobamoviruses. Proteomics 4, 418-425.

Peter, K.A., Gildow, F., Palukaitis, P., Gray, S.M., 2009. The C terminus of the polerovirus P5 readthrough domain limits virus infection to the phloem. J Virol 83, 5419-5429.

Peter, K.A., Liang, D., Palukaitis, P., Gray, S.M., 2008. Small deletions in the *Potato leafroll virus* readthrough protein affect particle morphology, aphid transmission, virus movement and accumulation. J Gen Virol 89, 2037-2045.

Pineda, M., Sajnani, C., Baron, M., 2010. Changes induced by the *Pepper mild mottle tobamovirus* on the chloroplast proteome of *Nicotiana benthamiana*. Photosynth Res 103, 31-45.

Postnikova, O.A., Nemchinov, L.G., 2012. Comparative analysis of microarray data in *Arabidopsis* transcriptome during compatible interactions with plant viruses. Virol J 9, 101.

Printz, B., Dos Santos Morais, R., Wienkoop, S., Sergeant, K., Lutts, S., Hausman, J.F., Renaut, J., 2015. An improved protocol to study the plant cell wall proteome. Frontiers in Plant Science 6, 237.

Prokhnevsky, A.I., Peremyslov, V.V., Dolja, V.V., 2005. Actin cytoskeleton is involved in targeting of a viral Hsp70 homolog to the cell periphery. J Virol 79, 14421-14428.

Prokhnevsky, A.I., Peremyslov, V.V., Napuli, A.J., Dolja, V.V., 2002. Interaction between long-distance transport factor and Hsp70-related movement protein of *Beet yellows virus*. Journal of Virology 76, 11003-11011.

Quanjer, H.M., Van der Lek, H.A.A., Botjes, O., 1916. Aard, verspreiding en bestrijding van Phloeemnecroses en hare beteekenis voor de aardappelcultuur. Mededeelingen van de Landbouwhoogeschool 17, 1-74.

Rahoutei, J., García-Luque, I., Barón, M., 2000. Inhibition of photosynthesis by viral infection: Effect on PSII structure and function. Physiologia Plantarum 110, 286-292.

Rajabaskar, D., Bosque-Perez, N.A., Eigenbrode, S.D., 2014. Preference by a virus vector for infected plants is reversed after virus acquisition. Virus Res 186, 32-37.

Reichel, C., Beachy, R.N., 1998. *Tobacco mosaic virus* infection induces severe morphological changes of the endoplasmic reticulum. Proceedings of the National Academy of Sciences of the United States of America 95, 11169-11174.

Reinbold, C., Herrbach, E., Brault, V., 2003. Posterior midgut and hindgut are both sites of acquisition of Cucurbit aphid-borne yellows virus in *Myzus persicae* and Aphis gossypii. J Gen Virol 84, 3473-3484.

Reutenauer, A., Ziegler-Graff, V., Lot, H., Scheidecker, D., Guilley, H., Richards, K., Jonard, G., 1993. Identification of *Beet western yellows luteovirus* genes implicated in viral replication and particle morphogenesis. Virology 195, 692-699.

Rodrigo, G., Carrera, J., Ruiz-Ferrer, V., del Toro, F.J., Llave, C., Voinnet, O., Elena, S.F., 2011. Characterization of the *Arabidopsis thaliana* interactome targeted by viruses. Santa Fe Institute Working Paper.

Rodrigues, S.P., Da Cunha, M., Ventura, J.A., Fernandes, P.M.B., 2009. Effects of the *Papaya meleira virus* on papaya latex structure and composition. Plant Cell Reports 28, 861-871.

Rodrigues, S.P., Ventura, J.A., Aguilar, C., Nakayasu, E.S., Almeida, I.C., Fernandes, P.M., Zingali, R.B., 2011. Proteomic analysis of papaya (*Carica papaya* L.) displaying typical sticky disease symptoms. Proteomics 11, 2592-2602.

Rodrigues, S.P., Ventura, J.A., Aguilar, C., Nakayasu, E.S., Choi, H., Sobreira, T.J., Nohara, L.L., Wermelinger, L.S., Almeida, I.C., Zingali, R.B., Fernandes, P.M., 2012. Label-free quantitative proteomics reveals differentially regulated proteins in the latex of sticky diseased *Carica papaya* L. plants. J Proteomics 75, 3191-3198.

Rodriguez, M., Taleisnik, E., Lenardon, S., Lascano, R., 2010. Are *Sunflower chlorotic mottle virus* infection symptoms modulated by early increases in leaf sugar concentration? Journal of Plant Physiology 167, 1137-1144.

Rowles, D.L., Terhune, S.S., Cristea, I.M., 2013. Discovery of host-viral protein complexes during infection. Methods in Molecular Biology 1064, 43-70.

Rowles, D.L., Tsai, Y.C., Greco, T.M., Lin, A.E., Li, M., Yeh, J., Cristea, I.M., 2015. DNA methyltransferase DNMT3A associates with viral proteins and impacts HSV-1 infection. Proteomics 15, 1968-1982.

Ruiz-May, E., Rose, J.K., 2013. Progress toward the tomato fruit cell wall proteome. Frontiers in Plant Science 4, 159.

Sampol, B., Bota, J., Riera, D., Medrano, H., Flexas, J., 2003. Analysis of the virus-induced inhibition of photosynthesis in malmsey grapevines. New Phytologist 160, 403-412.

Sanfaçon, H., 2005. Replication of positive-strand RNA viruses in plants: contact points between plant and virus components. Canadian Journal of Botany 83, 1529-1549.

Sappl, P.G., Carroll, A.J., Clifton, R., Lister, R., Whelan, J., Harvey Millar, A., Singh, K.B., 2009. The *Arabidopsis* glutathione transferase gene family displays complex stress regulation and co-silencing multiple genes results in altered metabolic sensitivity to oxidative stress. Plant J 58, 53-68.

Schmitz, J., Stussi-Garaud, C., Tacke, E., Prüfer, D., Rohde, W., Rohfritsch, O., 1997. In situ localization of the putative movement protein (pr17) from *Potato leafroll luteovirus* (PLRV) in infected and transgenic potato plants. Virology 235, 311-322.

Schrotenboer, A.C., Allen, M.S., Malmstrom, C.M., 2011. Modification of native grasses for biofuel production may increase virus susceptibility. GCB Bioenergy 3, 360-374.

Seddas, P., Boissinot, S., Strub, J.M., Van Dorsselaer, A., Van Regenmortel, M.H., Pattus, F., 2004. Rack-1, GAPDH3, and actin: proteins of *Myzus persicae* potentially involved in the transcytosis of *Beet western yellows virus* particles in the aphid. Virology 325, 399-412.

Serra-Soriano, M., Navarro, J.A., Genoves, A., Pallas, V., 2015. Comparative proteomic analysis of melon phloem exudates in response to viral infection. J Proteomics 124, 11-24.

Shalitin, D., Wolf, S., 2000. *Cucumber mosaic virus* infection affects sugar transport in melon plants. Plant Physiology 123, 597-604.

Shen, P., Tian, X., Zhang, S., Ren, F., Li, P., Yu, Y.Q., Li, R., Zhou, C., Cao, M., 2018. Molecular characterization of a novel luteovirus infecting apple by next-generation sequencing. Arch Virol 163, 761-765.

Shepardson, S., Esau, K., McCrum, R., 1980. Ultrastructure of potato leaf phloem infected with *Potato leafroll virus*. Virology 105, 379-392.

Shikata, E., Maramorosch, K., 1966. Electron microscopy of *Pea enation mosaic virus* in plant cell nuclei. Virology 30, 439-454.

Shikata, E., Maramorosch, K., Granados, R.R., 1966. Electron microscopy of *Pea enation mosaic virus* in plants and aphid vectors. Virology 29, 426-436.

Shirasu, K., 2009. The HSP90-SGT1 chaperone complex for NLR immune sensors. Annu Rev Plant Biol 60, 139-164.

Skelton, A., Uzayisenga, B., Fowkes, A.R., Adams, I.P., Buxton-Kirk, A., Harju, V., Forde, S.M.D., Ward, R., Ritchie, B., Rutherford, M., Offord, L., Umulisa, C., Waweru, B., Kagiraneza, B., Karangwa, P., Fox, A., 2018. First report of *Pepper veinal mottle virus*, *Pepper yellows virus* and a novel enamovirus in chili pepper (*Capsicum* sp.) in Rwanda. New Disease Reports 37, 5.

Smirnova, E., Firth, A.E., Miller, W.A., Scheidecker, D., Brault, V., Reinbold, C., Rakotondrafara, A.M., Chung, B.Y., Ziegler-Graff, V., 2015. Discovery of a small non-AUG-initiated ORF in poleroviruses and luteoviruses that is required for long-distance movement. PLoS Pathog 11, e1004868.

Srinivasan, R., Alvarez, J.M., Bosque-Perez, N.A., Eigenbrode, S.D., Novy, R.G., 2008. Effect of an alternate weed host, hairy nightshade, *Solanum sarrachoides*, on the biology of the two most important *Potato leafroll virus* (*Luteoviridae*: *Polerovirus*) vectors, *Myzus persicae* and *Macrosiphum euphorbiae* (Aphididae: Homoptera). Environ Entomol 37, 592-600.

Srinivasan, R., Alvarez, J.M., Eigenbrode, S.D., Bosque-pérez, N.A., 2006. Influence of hairy nightshade *Solanum sarrachoides* (Sendtner) and *Potato leafroll virus* (*Luteoviridae*:*Polerovirus*) on the Host Preference of *Myzus persica e*(Sulzer) (Homoptera: Aphididae). Environmental Entomology 35, 546-553.

Stare, T., Ramsak, Z., Blejec, A., Stare, K., Turnsek, N., Weckwerth, W., Wienkoop, S., Vodnik, D., Gruden, K., 2015. Bimodal dynamics of primary metabolism-related responses in tolerant potato-*Potato virus Y* interaction. BMC Genomics 16, 716.

Stevens, M., Freeman, B., Liu, H.Y., Herrbach, E., Lemaire, O., 2005. Beet poleroviruses: close friends or distant relatives? Mol Plant Pathol 6, 1-9.

Su, S., Liu, Z., Chen, C., Zhang, Y., Wang, X., Zhu, L., Miao, L., Wang, X.C., Yuan, M., 2010. *Cucumber mosaic virus* movement protein severs actin filaments to increase the plasmodesmal size exclusion limit in tobacco. Plant Cell 22, 1373-1387.

Tacke, E., Prufer, D., Salamini, F., Rohde, W., 1990. Characterization of a *Potato leafroll luteovirus* subgenomic RNA: differential expression by internal translation initiation and UAG suppression. J Gen Virol 71 (Pt 10), 2265-2272.

Tacke, E., Prüfer, D., Schmitz, J., Rohde, W., 1991. The *Potato leafroll luteovirus* 17K protein is a single-stranded nucleic acid-binding protein. Journal of General Virology 72, 2035-2038.

Tacke, E., Schmitz, J., Prüfer, D., Rohde, W., 1993. Mutational analysis of the nucleic acid-binding 17 kDa phosphoprotein of *Potato leafroll luteovirus* identifies an amphipathic alpha-helix as the domain for protein/protein interactions. Virology 197, 274-282.

Tamborindeguy, C., Bereman, M.S., DeBlasio, S., Igwe, D., Smith, D.M., White, F., MacCoss, M.J., Gray, S.M., Cilia, M., 2013. Genomic and proteomic analysis of *Schizaphis graminum* reveals cyclophilin proteins are involved in the transmission of *Cereal yellow dwarf virus*. PLoS One 8, e71620.

Técsi, L., Maule, A., Smith, A., Leegood, R., 1994. Complex, localized changes in CO_2 assimilation and starch content associated with the susceptible interaction between *Cucumber mosaic virus* and a cucurbit host. The Plant Journal 5, 837-847.

Tecsi, L.I., Maule, a.J., Smith, a.M., Leegood, R.C., 1994. Metabolic alteration in cotyledons of *Cucurbita pepo* infected by *Cucumber mosaic virus*. Journal of Experimental Botany 45, 1541-1551.

Tecsi, L.I., Smith, A.M., Maule, A.J., Leegood, R.C., 1996. A spatial analysis of physiological changes associated with infection of cotyledons of marrow plants with *Cucumber mosaic virus*. Plant Physiology 111, 975-985.

Terradot, L., Souchet, M., Tran, V., Giblot Ducray-Bourdin, D., 2001. Analysis of a three-dimensional structure of *Potato leafroll virus* coat protein obtained by homology modeling. Virology 286, 72-82.

Tilsner, J., Linnik, O., Louveaux, M., Roberts, I.M., Chapman, S.N., Oparka, K.J., 2013. Replication and trafficking of a plant virus are coupled at the entrances of plasmodesmata. J Cell Biol 201, 981-995.

van Loon, L.C., Rep, M., Pieterse, C.M., 2006. Significance of inducible defense-related proteins in infected plants. Annu Rev Phytopathol 44, 135-162.

Vanholme, R., Demedts, B., Morreel, K., Ralph, J., Boerjan, W., 2010. Lignin biosynthesis and structure. Plant Physiol 153, 895-905.

Veidt, I., Lot, H., Leiser, M., Scheidecker, D., Guilley, H., Richards, K., Jonard, G., 1988. Nucleotide sequence of *Beet western yellows virus* RNA. Nucleic Acids Research 16, 9917-9932.

Ventelon-Debout, M., Delalande, F., Brizard, J.P., Diemer, H., Van Dorsselaer, A., Brugidou, C., 2004. Proteome analysis of cultivar-specific deregulations of *Oryza sativa* indica and *O. sativa* japonica cellular suspensions undergoing *Rice yellow mottle virus* infection. Proteomics 4, 216-225.

Verchot, J., 2012. Cellular chaperones and folding enzymes are vital contributors to membrane bound replication and movement complexes during plant RNA virus infection. Front Plant Sci 3, 275.

Vidal, A.H., Sanches, M.M., Alves-Freitas, D.M.T., Abreu, E.F.M., Lacorte, C., Pinheiro-Lima, B., Rosa, R.C.C., Jesus, O.N., Campos, M.A., Varsani, A., Ribeiro, S.G., 2018. First world report of *Cucurbit aphid-borne yellows virus* infecting passionfruit. Plant Disease 102, 2665-2665.

Vigers, A.J., Wiedemann, S., Roberts, W.K., Legrand, M., Selitrennikoff, C.P., Fritig, B., 1992. Thaumatin-like pathogenesis-related proteins are antifungal. Plant Science 83, 155-161.

Villamor, D.E., Mekuria, T.A., Pillai, S.S., Eastwell, K.C., 2016. High-throughput sequencing identifies novel viruses in nectarine: Insights to the etiology of stem-pitting disease. Phytopathology 106, 519-527.

Viswanathan, R., Chinnaraja, C., Malathi, P., Gomathi, R., Rakkiyappan, P., Neelamathi, D., Ravichandran, V., 2014. Impact of *Sugarcane yellow leaf virus* (ScYLV) infection on physiological efficiency and growth parameters of sugarcane under tropical climatic conditions in India. Acta Physiologiae Plantarum 36, 1805-1822.

Wang, B., Hajano, J.U., Ren, Y., Lu, C., Wang, X., 2015. iTRAQ-based quantitative proteomics analysis of rice leaves infected by *Rice stripe virus* reveals several proteins involved in symptom formation. Virol J 12, 99.

Wang, J., Wang, X.R., Zhou, Q., Yang, J.M., Guo, H.X., Yang, L.J., Liu, W.Q., 2016. iTRAQ protein profile analysis provides integrated insight into mechanisms of tolerance to TMV in tobacco (*Nicotiana tabacum*). J Proteomics 132, 21-30.

Ward, B.M., 2011. The taking of the cytoskeleton one two three: How viruses utilize the cytoskeleton during egress. Virology 411, 244-250.

Werner, B.J., Mowry, T.M., Bosque-Perez, N.A., Ding, H., Eigenbrode, S.D., 2009. Changes in green peach aphid responses to *Potato leafroll virus*-induced volatiles emitted during disease progression. Environ Entomol 38, 1429-1438.

Williams, D.B., 2005. Beyond lectins: The calnexin/calreticulin chaperone system of the endoplasmid reticulum. Journal of Cell Science 119, 615-623.

Wright, K.M., Cowan, G.H., Lukhovitskaya, N.I., Tilsner, J., Roberts, A.G., Savenkov, E.I., Torrance, L., 2010. The N-terminal domain of PMTV TGB1 movement protein is required for nucleolar localization, microtubule association, and long-distance movement. Molecular Plant-Microbe Interactions 23, 1486-1497.

Wu, J.-Q., Bähler, J., Pringle, J.R., 2001. Roles of a fimbrin and an α-actinin-like protein in fission yeast cell polarization and cytokinesis. Molecular Biology of the Cell 12, 1061-1077.

Wu, L., Han, Z., Wang, S., Wang, X., Sun, A., Zu, X., Chen, Y., 2013a. Comparative proteomic analysis of the plant-virus interaction in resistant and susceptible ecotypes of maize infected with *Sugarcane mosaic virus*. J Proteomics 89, 124-140.

Wu, L., Wang, S., Chen, X., Wang, X., Wu, L., Zu, X., Chen, Y., 2013b. Proteomic and phytohormone analysis of the response of maize (*Zea mays* L.) seedlings to *Sugarcane mosaic virus*. PLoS One 8, e70295.

Xu, Q., Ni, H., Chen, Q., Sun, F., Zhou, T., Lan, Y., Zhou, Y., 2013. Comparative proteomic analysis reveals the cross-talk between the responses induced by H_2O_2 and by long-term *Rice black-streaked dwarf virus* infection in rice. PLoS One 8, e81640.

Xu, X.M., Wang, J., Xuan, Z., Goldshmidt, A., Borrill, P.G.M., Hariharan, N., Kim, J.-Y., Jackson, D., 2011. Chaperonins facilitate KNOTTED1 cell-to-cell trafficking and stem cell function. Science 333, 1141-1144.

Yan, S.L., Lehrer, A.T., Hajirezaei, M.R., Springer, A., Komor, E., 2008. Modulation of carbohydrate metabolism and chloroplast structure in sugarcane leaves which were infected by *Sugarcane yellow leaf virus* (SCYLV). Physiological and Molecular Plant Pathology 73, 78-87.

Yang, H., Huang, Y., Zhi, H., Yu, D., 2011. Proteomics-based analysis of novel genes involved in response toward *Soybean mosaic virus* infection. Mol Biol Rep 38, 511-521.

Yang, X., Thannhauser, T.W., Burrows, M., Cox-Foster, D., Gildow, F.E., Gray, S.M., 2008. Coupling genetics and proteomics to identify aphid proteins associated with vector-specific transmission of polerovirus (*Luteoviridae*). J Virol 82, 291-299.

Yoo, R.H., Lee, S.W., Lim, S., Zhao, F., Igori, D., Baek, D., Hong, J.S., Lee, S.H., Moon, J.S., 2017. Complete genome analysis of a novel umbravirus-polerovirus combination isolated from *Ixeridium dentatum*. Arch Virol 162, 3893-3897.

Zarzyńska-Nowak, A., Hasiów-Jaroszewska, B., Budzyńska, D., Borodynko-Filas, N., 2019. First Report of *Cucurbit aphid-borne yellows virus* infecting zucchini plants (*Cucurbita pepo* convar. giromontiina) in Poland. Plant Disease.

Zeier, J., 2013. New insights into the regulation of plant immunity by amino acid metabolic pathways. Plant Cell Environ 36, 2085-2103.

Zhang, X., Yuan, Y.R., Pei, Y., Lin, S.S., Tuschl, T., Patel, D.J., Chua, N.H., 2006. *Cucumber mosaic virus*-encoded 2b suppressor inhibits *Arabidopsis* Argonaute1 cleavage activity to counter plant defense. Genes Dev 20, 3255-3268.

Zhang, X.Y., Zhao, T.Y., Li, Y.Y., Xiang, H.Y., Dong, S.W., Zhang, Z.Y., Wang, Y., Li, D.W., Yu, J.L., Han, C.G., 2018. The conserved proline-18 in the polerovirus P3a is important for *Brassica yellows virus* systemic infection. Front Microbiol 9, 613.

Zheng, H.Y., Wu, X.Y., Han, K.L., Chen, Z.Q., Song, X.J., Peng, J.J., Lu, Y.W., Lin, L., Chen, J.P., Yan, F., Wu, X.Y., Han, K.L., 2018. First report of *Beet western yellows virus* infecting *Crocus sativus* in China. Plant Disease 102, 1471-1471.

CHAPTER 2

INSIGHTS IN LUTEOVIRID STRUCTURAL BIOLOGY GUIDED BY CHEMICAL CROSS-LINKING AND HIGH-RESOLUTION MASS SPECTROMETRY[2]

Abstract

Interactions between plant pathogenic viruses in the family *Luteoviridae* and their plant hosts and insect vectors are governed by the topology of the viral capsid, which is the sole vehicle for long distance movement of the viral genome. Previous application of a mass spectrometry-compatible cross-linker to preparations of the luteovirid *Potato leafroll virus* (PLRV; *Luteoviridae*: *Polerovirus*) revealed a detailed network of interactions between viral structural proteins and enabled generation of the first cross-linking guided coat protein models. In this study, we extended application of chemical cross-linking technology to the related *Turnip yellows virus* (TuYV; *Luteoviridae*: *Polerovirus*). Remarkably, all cross-links found between sites in the viral coat protein found for TuYV were also found in PLRV. Guided by these data, we present two models for the TuYV coat protein trimer, the basic structural unit of luteovirid virions. Additional cross-links found between the TuYV coat protein and a site in the viral protease domain suggest a possible role for the luteovirid protease in regulating the structural biology of these viruses.

[2]This chapter has been published as: Alexander, M.M., Mohr, J.P., DeBlasio, S.L., Chavez, J.D., Ziegler-Graff, V., Brault, V., Bruce, J.E., Heck, M.C., 2017. Insights in luteovirid structural biology guided by chemical cross-linking and high resolution mass spectrometry. Virus Res 241, 42-52.

1. Introduction

Viruses in the family *Luteoviridae*, referred to in this paper as luteovirids, are plant pathogenic, icosahedral viruses with a monopartite, positive-sense, single stranded RNA genome. With the exception of viruses in the genus Enamovirus, luteovirids are transmitted exclusively by aphids in a persistent, circulative manner and are restricted to the plant vascular tissue, or phloem, in a natural infection. Luteovirids as a group have an extensive host and geographical range, with six new species characterized in 2016 alone (Bag et al., 2015; Bejerman et al., 2016; Chen et al., 2016; Ibaba et al., 2017; Lotos et al., 2016; Sharman et al., 2016; Villamor et al., 2016). These viruses are important pathogens of many major crops, including small grains (yellow dwarf viruses; *Luteoviridae*: *Polerovirus* and *Luteovirus*), brassicas (*Turnip yellows virus*, TuYV; *Luteoviridae*: *Polerovirus*), sugarcane (*Sugarcane yellow leaf virus*, SCYLV; *Luteoviridae*: *Polerovirus*), potato (*Potato leafroll virus*; *Luteoviridae*: *Polerovirus*), and soybean (*Soybean dwarf virus*, SbDV; *Luteoviridae*: *Luteovirus*). Management of these pathogens relies on cultural practices and control of the aphid vectors, as no chemicals means are available to target luteovirids directly. However, insecticide resistance and environmental impact are significant and growing concerns.

The luteovirid genome is 5-6kB in length and includes five to nine overlapping open reading frames depending on genera. Luteovirids have a non-enveloped icosahedral capsid with T=3 symmetry, which is comprised primarily of the 20-25kDa coat protein. Sporadic readthrough of an amber stop codon following the coat protein gene leads to translation of a 25-50kDa C-terminal extension known as the readthrough domain (Bahner et al., 1990; Dinesh-Kumar et al., 1992; Reutenauer et al., 1993; Veidt et al., 1988). The resulting readthrough protein is believed to be incorporated in the capsid with a low but undetermined frequency (Brault et al., 1995;

Cheng et al., 1994). Interestingly, the full length readthrough protein can be readily detected by western blot in protein extracts from luteovirid-infected plants; however, the signal for the full-length protein is weak or absent in purified virions (Bahner et al., 1990; Brault et al., 1995; Bruyere et al., 1997; Filichkin et al., 1994; Jolly and Mayo, 1994; Wang et al., 1995). Instead, one or more lower molecular weight bands attributed to C-terminal truncation(s) of the readthrough protein can be detected. Truncated readthrough protein is sporadically detectable in whole protein extracts. Recently, a function in systemic movement was demonstrated for the truncated readthrough protein of *Cucurbit aphid-borne yellows virus* (CABYV; *Luteoviridae*: *Polerovirus*) (Boissinot et al., 2014), indicating that readthrough protein truncation is not simply a byproduct of host defense or virus purification. Although the protein(s) responsible for this cleavage are unknown, it has been suggested that the viral protease, encoded by ORF 1 and referred to as the P1 protease hereafter, may be involved (Boissinot et al., 2014). Currently, the only experimentally verified function of the P1 protease is in processing of the P1 polyprotein (Li et al., 2007; Li et al., 2000).

Early studies in luteovirid structural biology included epitope mapping of the PLRV virion, identifying twelve epitopes within the PLRV coat protein (Torrance, 1992). Several other studies assessed the effect of targeted mutations in the coat protein and readthrough domain on capsid assembly, aphid transmission, viral replication, and systemic movement (Brault et al., 2003; Bruyere et al., 1997; Hipper et al., 2014; Kaplan et al., 2007; Lee et al., 2005; Peter et al., 2009; Peter et al., 2008). These studies enabled the generation of a detailed map of the functional biology of the coat protein; however, the complete lack of available crystal structures for any luteovirid virion or structural protein has been a significant hurdle to link structure to function. The first computational model of a luteovirid coat protein was obtained for

PLRV in 2001, by homology modeling against the crystal structure of other icosahedral plant viruses, despite a less than 30% sequence identity between the coat proteins of PLRV and the nearest relative with an available crystal structure at the time (Terradot et al., 2001). Like the coat proteins of many other icosahedral viruses, the PLRV coat protein can be subdivided into a shell (S-) domain, which forms the capsid surface, and an arginine-rich (R-) domain, which likely interacts with viral nucleic acid inside the capsid. Alternate luteovirid coat protein monomer and trimer models have since been proposed for PLRV and TuYV based on new mutational analyses, cross-linking data, and alternate computational modeling (Brault et al., 2003; Chavez et al., 2012; DeBlasio et al., 2016a). However, without a crystal structure for any luteovirid, full validation of any of these models remains impossible. The recalcitrance of luteovirids to crystallization is likely due in part to the highly disordered readthrough domain projecting outward from the capsid surface, which may not uniformly adopt an ordered conformation (Chavez et al., 2012). Computational modeling of the readthrough domain has also proved difficult, as it does not bear homology to any protein for which a crystal structure is available, and *de novo* modeling is also negatively affected by the high degree of disorder predicted in this domain (Chavez et al., 2012). Luteovirid structural biology studies are further hampered by their phloem limitation, as phloem cells are relatively low in abundance and are difficult to separate from other tissues (DeBlasio et al., 2016b). Further advances in luteovirid structural biology could lead to new strategies for management of these pathogens. In particular, luteovirid-aphid vector interactions are known to be governed by capsid topology (Brault et al., 1995; Bruyere et al., 1997; Chavez et al., 2012; Chay et al., 1996; Gray et al., 2014; Kaplan et al., 2007; Lee et al., 2005; Linz et al., 2015; Peter et al., 2008; Reinbold et al., 2003; Ziegler-Graff et al., 1996).

Protein Interaction Reporter (PIR) technology utilizes mass spectrometry-cleavable cross-linkers to detect direct protein-protein interactions, both *in vivo* and *in vitro* (Chavez et al., 2012; Tang et al., 2005; Weisbrod et al., 2013). The unique composition of the PIR cross-linker permits large-scale identification of cross-linked peptides, including the identity of specific cross-linked residues. Using these cross-linked residues and the known length of the PIR cross-linker, protein-protein interactions can be computationally modeled. The usefulness of PIR technology in probing both the structural biology and virus-host interactions of luteovirids has already been shown with PLRV, generating not only the first large-scale map of direct luteovirid interactions, but also the first predictions of specific PLRV-binding sites on several host proteins (Chavez et al., 2012; DeBlasio et al., 2016a). Although extensive, these data were limited to a single virus species. As PIR had never before been applied to two species within the same genus, it was unknown to what extent cross-links were likely to be conserved. If cross-linking data from one species can reasonably be extended to its relatives, the potential applications of a single PIR experiment would be much greater. To begin to address this question, and to expand on our previous studies, we applied PIR technology to probe the structural biology of TuYV, a related pathogen of plants in the Brassicaceae. Our results enable the generation of new structural protein models that are supported by cross-linking data as well as previous literature, and represent the first comparison of PIR cross-linking data between related viruses.

2. Materials and Methods

2.1 Preparation of plant material

N. benthamiana leaves were inoculated by infiltration with *A. tumefaciens* C58C1 (Holsters et al., 1980) containing a cDNA clone of TuYV (Leiser et al., 1992).

Infiltrated leaves were harvested six to eight days after inoculation and immediately frozen in liquid nitrogen. Leaf tissue was stored frozen until use.

2.2 Virus purification and aphid transmission assays

TuYV was purified from infected *N. benthamiana* leaves by sucrose density centrifugation as previously described (van den Heuvel et al., 1991), and virus was recovered after the 30% sucrose cushion. Aphid transmissibility of virus used for cross-linking was verified by feeding *Myzus persicae* for 24 hours on membranes containing 50ug of purified TuYV in a total volume of 500ul of a nutrient solution, or nutrient solution alone as a negative control (Kim and Jander, 2007). Ten aphids per plant were transferred to five young *A. thaliana* plants per treatment, and allowed to feed for 72 hours before they were removed by fumigation. Infection status of recipient plants was analyzed three weeks after inoculation by double antibody sandwich enzyme-linked immunosorbent assay (DAS-ELISA) using a commercially available anti-TuYV antibody set (Loewe Biochemica GmbH). Young leaf tissue was collected and homogenized in 200µL of phosphate-buffered saline per 12mg of tissue, using a Mixer Mill 400 (Retsch GmbH). Samples with a blank-subtracted Abs405 value greater than 0.5 were considered positive. Samples from a plant previously confirmed to be infected with TuYV were used as a positive control.

2.3 Cross-linking of purified virus

Synthesis of the biotin aspartate proline-PIR (BDP-NHP) cross-linker was carried out as previously described (Weisbrod et al., 2013). A total of 1.3mg of purified TuYV was diluted to a volume of 250µL with 100mM citrate buffer, pH 6.0, containing 0.5% ethanol. A 250mM stock solution of PIR cross-linker in methanol

was added to samples to a final concentration of 1mM, and the sample was incubated at room temperature with vigorous shaking for one hour. Urea was then added to a final concentration of 8M. Reduction and alkylation, protein digestion, and desalting were performed as previously described for PLRV (DeBlasio et al., 2016a).

Peptide samples were fractionated by strong cation exchange (SCX) chromatography using an Agilent 1200 HPLC system equipped with a Phenomenex Luna SCX column. A binary linear gradient consisting of buffer A (5mM KH_2PO_4, pH 2.6, 30% acetonitrile [ACN]) and buffer B (5mM KH_2PO_4, pH 2.6, 30% ACN, 350mM KCl) was applied at a flow rate of 1.5 mL/min for 97.5 min as follows: 0% B at 0 min, 5% B at 7.5 min, 60% B at 47.5 min, 100% B at 67.5 min, 100% B at 77.5 min, 0% B at 77.51 min, 0% B at 97.5 min. Fractions were taken every 5 min starting at 17.5 min, and fractions were pooled (6 total) as follows: 1-5, 6-7, 8, 9, 10, 11-14. Fraction pools were then dried to a final volume of ~2mL in a vacuum centrifuge and adjusted to a pH of 8.0 with 1.5M NaOH. These samples were then enriched by incubation with Ultralink monomeric avidin (ThermoFisher). Briefly, 100µl of avidin resin was added to each fraction and samples were incubated at room-temperature with mixing for 1 hour. Cross-linked peptides were washed on the avidin matrix using 100mM ABC, and subsequently eluted from the avidin resin by the addition of 70% acetonitrile-0.5% formic acid.

2.4 Generation of a stage I database

To maximize our ability to identify cross-links in TuYV, a stage I database enriched for PIR-reactive proteins was generated (DeBlasio et al., 2016a; Navare et al., 2015) for searching of avidin-enriched fractions using 0.5mg of the same purified TuYV used in Section 2.3. The stage I database approach enriches for proteins that

have reacted with the cross-linker by incubating the cross-linked protein sample with monomeric avidin prior to trypsin digestion. Protein samples are then eluted from the avidin resin using a solution containing 8M urea, 2mM biotin in 100mM ABC. Following elution the sample is diluted by a factor of 10 to bring the urea concentration to less than 1M and the reduction, alkylation and digestion are performed as described in Section 2.2.

Peptides resulting from digestion of avidin enriched proteins were analyzed using a Thermo n-LC coupled to a Q Exactive Plus mass spectrometer. Peptides were fractionated over a 60cm x 75µm inner diameter fused silica analytical column packed with ReproSil-Pur C8, 5µm diameter, 120Å pore size particles by applying a linear gradient from 98% solvent A (0.1% formic acid in water), 2% solvent B (0.1% formic acid in acetonitrile) to 70% solvent A, 30% solvent B over either 90 minutes at a flow rate of 300nL/min. Peptides eluting from the column were ionized by ESI by applying a voltage of 2-2.5 kV to the laser pulled fused silica spray tip at the end of the column. The mass spectrometer was operated using a data dependent analysis (DDA) method performing one high resolution (70,000 resolving power (RP) at *m/z* 200) MS1 scan from 400-2000 *m/z* followed by MS2 (17,500 RP) on the 20 most abundant ions detected in the MS1. Settings for MS2 analysis included at automatic gain control target value of 50,000 ions, a maximum ion accumulation time of 50ms, an isolation window of 1.6m/z and a normalized collision energy of 25. Ions selected for MS2 were dynamically excluded from further selection for 30s. A stage I database was generated by searching the resulting spectra with Comet against a concatenated target-decoy database containing proteins from *N. benthamiana* and TuYV. At a 1% FDR, 106 unique *N. benthamiana* proteins had at least 1 peptide-spectrum match. These proteins were merged with all 12 proteins from the TuYV database, yielding the complete stage I database.

2.5 ReACT

Enriched cross-linked peptide samples were resuspended in 0.1% formic acid and analyzed using a Waters nano-Acquity UPLC system coupled to a Velos-FTICR mass spectrometer. Peptides were fractionated using a 60cm x 75µm inner diameter fused silica analytical column packed with ReproSil-Pur C8, 5µm diameter, 120Å pore size particles by applying a linear gradient from 95% solvent A, 5% solvent B to 60% solvent A, 40% solvent B over either 120 or 240 minutes at a flow rate of 300nL/min. The mass spectrometer was operated utilizing a Real-time Analysis for Cross-linked peptide Technology (ReACT) method (Weisbrod et al., 2013), where ions with a charge state of four or greater were selected for high resolution MS2 analysis in the ICR cell where an "on-the-fly" check of the observed fragment ion masses against the PIR mass relationship (Mass Precursor = Mass Reporter Ion + Mass Peptide 1 + Mass Peptide 2) is performed. Masses that satisfied the PIR relationship within a tolerance of 20ppm mass error triggered subsequent low resolution MS3 analyses of the released cross-linked peptide ions.

2.6 Mass spectrometry data analysis

The database for searching the stage I sample consisted of version 0.4.4 of the predicted *N. benthamiana* proteome from the Sol Genomics Network (solgenomics.net), in addition to the proteome of the TuYV infectious clone used in this study, which was manually curated in house (Bombarely et al., 2012).

Data generated from ReACT analyses was searched using Comet version 2016.01 rev. 2 with the stage I database (Eng et al., 2013). Search settings included a precursor mass tolerance of 20.0ppm, standard C13 error, tryptic peptides with up to

two missed cleavages, and a fragment mass tolerance of 1.005Da. The mass modifications included: a variable modification of oxidation on Met (15.9949Da), a variable mod of acetylation on Lys (42.010565Da), and a required modification of the cross-linker stump mass on Lys (197.032422Da). Peptides are sorted by ascending e-value, and the FDR was calculated as the ratio of twice the number of decoy hits divided by the total number of hits at a given e-value. Peptides were filtered to a 1% FDR, yielding 261 unique peptide-spectrum matches.

2.7 Modeling of the coat protein trimer

The structure of the TuYV coat protein monomer was modeled by the I-TASSER server (Yang et al., 2015). The most recent model of the PLRV coat protein (DeBlasio et al., 2016a) was included as a user-supplied input for multi-template threading. The top five I-TASSER models were subjected to analysis with the R-package XLmap (Schweppe et al., 2016) to assess their fit with cross-linking data for TuYV and PLRV, using a maximum distance of 50Å for both contact mapping and contact map score (CMscore) calculation. The top-ranking I-TASSER model had the best CMscore of the five coat protein models, and was therefore used for all subsequent modeling. The root-mean-square deviation (RMSD) of atomic positions in the PLRV and TuYV coat protein S-domains (designated as amino acids 42-208 and 36-202, respectively) was calculated by Molsoft (Molsoft LLC) by weighted iterative superposition. Modeling of the coat protein trimer was performed using SymmDock (Schneidman-Duhovny et al., 2005), with a 3-fold order of symmetry. The unambiguous homodimer cross-link found for the TuYV coat protein, as well as three other homologous homodimer cross-links found for PLRV, were supplied as distance constraints, with a maximum allowable distance of 35Å between cross-linked

residues. Sidechain and flexible backbone refinement of the 77 models produced by SymmDock was performed by SymmRef (Mashiach-Farkash et al., 2011). As SymmDock's distance calculations are strictly Euclidean and may pass through the interior of a protein, XWALK was used to calculate the solvent accessible distance between residues used as distance constraints (Kahraman et al., 2011). Images of the monomer and trimer models were generated in MolSoft (MolSoft LLC), and final figures assembled in Adobe Photoshop (Adobe Systems).

2.8 SDS-PAGE and detection of PLRV readthrough protein isoforms

N. benthamiana leaves were inoculated with an infectious clone of PLRV by agroinfiltration (DeBlasio et al., 2016a). Infiltrated leaves were harvested and frozen three days after inoculation. Frozen tissue was roughly ground with mortar and pestle without being allowed to thaw. PLRV virions were isolated from ground tissue, and their aphid transmissibility verified, as previously described (Chavez et al., 2012).

Five micrograms of purified PLRV were mixed with an equal volume of 2X Laemmli Sample Buffer (Bio-Rad) containing 5% beta-mercaptoethanol, and incubated at 98°C in a thermocycler (Bio-Rad) for five minutes prior to separation on a 10% Mini-Protean TGX SDS-polyacrylamide gel (Bio-Rad) in a Mini-Protean Tetra cell (Bio-Rad). Crude protein extracts from a PLRV agroinfiltrated and a mock infiltrated *N. benthamiana* leaf, also diluted with an equal volume of Laemmli buffer, were included as positive and negative controls, respectively. The Precision Plus Protein Kaleidoscope Ladder (Bio-Rad) was included for estimation of band molecular weights. Western blotting for detection of PLRV coat protein/readthrough protein was performed as previously described (DeBlasio et al., 2015b). The blot was imaged using a document scanner and brightness/contrast adjusted in Adobe

Photoshop (Adobe Systems).

2.9 Analysis of potential P1 cleavage sites in the luteovirid readthrough protein

Luteovirid readthrough protein and P1 polyprotein sequences were downloaded from NCBI on November 22, 2016 and sorted by virus species. A consensus readthrough protein sequence for each species was built using MUSCLE (http://www.ebi.ac.uk/Tools/msa/muscle/), the Los Alamos National Laboratory Consensus Maker tool (https://www.hiv.lanl.gov/content/sequence/CONSENSUS/consensus.html), and manual curation. The sequences for the TuYV infectious clone used in these studies were used as the representative sequences for TuYV, and TuYV was considered as a species distinct from the related *Beet western yellows virus* (BWYV; *Luteoviridae*: *Polerovirus*) as per the most recent International Committee on Taxonomy of Viruses (ICTV) Release (Adams et al., 2016). Multiple sequence alignment of the P1 polyprotein consensus sequences was performed by MUSCLE (Edgar, 2004). A simple script using BioPython (Chapman and Chang, 2000) was used to identify potential P1 cleavage sites in each consensus sequence and calculate the molecular weight of the truncated product. The Gaussian kernel density plot summarizing the cleavage site positions was generated in R using the ggplot2 package, using a smoothing bandwidth equal to one-half of the standard deviation of the smoothing kernel (Wickham, 2009).

3. Results and Discussion

3.1 Purified TuYV virions were transmissible by aphids

TuYV virions were purified by sucrose density purification from *Nicotiana*

benthamiana leaves 6-8 days after infiltration with a wild-type TuYV clone (Veidt et al., 1992). To verify the integrity and infectivity of purified virions, the aphid transmissibility of the purified virus preparation was tested by feeding *M. persicae* on membranes containing purified virus diluted with a nutrient solution. Of the five *A. thaliana* plants colonized with aphids fed on membranes containing purified TuYV, one died prior to sampling, and the remaining four gave clear positive ELISA readings (data not shown). All five plants colonized by aphids fed on virus-free nutrient solution gave negative ELISA readings.

3.2. PIR enabled the identification of TuYV cross-linked peptides

After verifying the integrity and infectivity of purified virions, 1.3mg of the purified sample was subjected to PIR cross-linking and mass spectrometry. Two cross-links between reactive lysines on the TuYV coat protein were observed, between K150 and K179, and an unambiguous homodimer from K179 – K179 (Table 2.1). Strikingly, all coat protein – coat protein cross-links observed in TuYV were also observed in PIR cross-linked PLRV samples, as these lysines are conserved (DeBlasio et al., 2016a). In addition to representing the first cross-linking data for TuYV, these results also show that PIR data are applicable to related species with good conservation of lysine residues.

Table 2.1. Intra-virus cross-links found in purified TuYV

Protein1	Protein2	Peptide 1[a]	Peptide 2[a]	FDR1[b]	FDR2[b]
TuYV CP/RTP	TuYV CP/RTP	TINK.FGITK$_{150}$PGK.RAFT	DQFR.ILYK$_{179}$GNGSSSIAGSFR.IAGS	0.00E+00	0.00E+00
TuYV CP/RTP	TuYV CP/RTP	**DQFR.ILYK$_{179}$GNGSSSIAGSFR.IAGS**	**DQFR.ILYK$_{179}$GNGSSSIAGSFR.IAGS**	0.00E+00	0.00E+00
TuYV CP/RTP	TuYV P1	DQFR.ILYK$_{179}$GNGSSSIAGSFR.IAGS	AEFK.TIAK$_{284}$SDK.GDVT	0.00E+00	0.00E+00
TuYV CP/RTP	TuYV P1	GSFR.ITIK$_{195}$CQFHNPK.VDEE	AEFK.TIAK$_{284}$SDK.GDVT	0.00E+00	0.00E+00

[a]Amino acid sequence of cross-linked peptides deduced from MS3 fragmentation and database searching. The four amino acids before and after each peptide are given as a reference, with peptide boundaries denoted by periods. K residue numbers indicate cross-linked lysines. The bolded peptides were found cross-linked in an unambiguous homodimer.

[b]False discovery rates (FDR) for MS3 identification of the indicated peptides.

Unexpectedly, two additional cross-links were found between the coat protein and a viral non-structural protein. Two additional reactive lysines in the TuYV coat protein (K179 and K195) were found cross-linked to a reactive lysine in TuYV ORF 1. The residue in ORF 1 could not be confidently assigned to a single viral protein, as this residue is present in both the viral P1 polyprotein, and in a fusion protein generated by a frameshift (the P1-P2 fusion protein) which contains the viral RNA-dependent RNA polymerase (RdRP). Although several variants of another peptide in ORF 1 could be detected during creation of the stage I database, these peptides are also shared between P1 and the P1-P2 fusion protein. No peptides unique to either P1 or the P1-P2 fusion protein were detected in the stage I database sample. However, the ORF 1 lysine found cross-linked to the TuYV coat protein is located near the center of the P1 serine protease domain. The P1 protease is responsible for processing of the P1 polyprotein by cleavage at a site N-terminal and a site C-terminal to the protease domain. While it cannot be ruled out that either the immature polyprotein or the P1-P2 fusion protein interact with the TuYV coat protein, the location of the reactive lysine residue as well as the high efficiency of the P1 protease even when expressed separately in insect cells suggests that the coat protein is most likely to interact with the free, mature protease (Li et al., 2000).

3.3 Modeling of the TuYV coat protein monomer

The TuYV coat protein monomer was modeled by multi-template threading with the I-TASSER server, using the PLRV coat protein model as an additional user-supplied template (DeBlasio et al., 2016a; Yang et al., 2015). The PLRV coat protein was the top template for threading, with 100% coverage and over 60% identity, followed by the crystal structures of the *Ryegrass mottle virus* (RGMoV; Unclassified:

Sobemovirus) and *Turnip crinkle virus* (TCV; *Tombusviridae*: *Carmovirus*) coat proteins. The five top I-TASSER models were evaluated using XLmap, an R package, to assess which models best matched the cross-linking data (Figure 2.1) (Schweppe et al., 2016). XLmap constructs a contact map showing the distance between every pair of residues in the protein, then maps the cross-linking data onto the contact map and calculates the CMscore, which measures the goodness of fit between the cross-linking data and the model, where a lower score indicates a better fit (Schweppe et al., 2016). Due to the high degree of homology between the TuYV and PLRV coat proteins (RMSD = 0.82Å for the S-domains), including near-perfect conservation of reactive lysine residues, the TuYV coat protein models were evaluated for goodness of fit both with the only potentially intra-protein cross-link found for TuYV (K150-K179) and with cross-links homologous to eight others previously found for PLRV (Supplementary Table 1). Model rankings relative to one another were the same regardless of which set of cross-links were used for analysis. The top-ranking I-TASSER model also had the lowest CMscore and a contact map most similar to the most recently published PLRV monomer (Figure 2.1) (DeBlasio et al., 2016a), and was therefore used for the remainder of the modeling in this study. In agreement with other icosahedral coat protein structures, the S-domain of the TuYV monomer consists primarily of an eight-stranded beta jelly-roll, as previously postulated for luteovirids (Chavez et al., 2012; DeBlasio et al., 2016a; Qu et al., 2000; Rossmann, 2013; Terradot et al., 2001). The arginine-rich, N-terminal region of the coat protein, hypothesized to interact with the viral genome, lines the underside of the S-domain and is predicted to extend into the capsid interior.

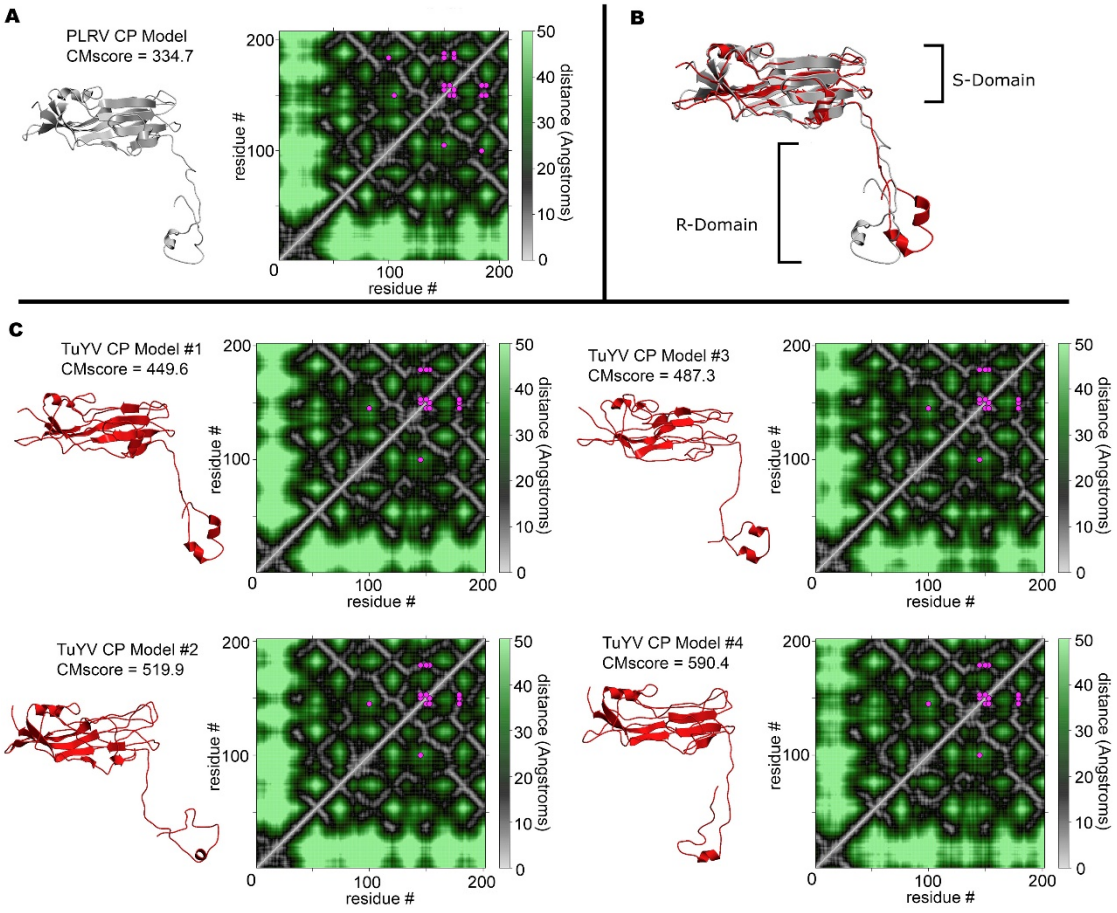

Figure 2.1: Application of XLmap in selecting a TuYV coat protein model. A) Coat protein model for PLRV (DeBlasio et al., 2016a) and the corresponding contact map, showing the distance (angstroms) between all possible residue pairs. Residues which have been found to be cross-linked in previous studies are marked by purple dots (Supplementary Table 2.1). These cross-links are also used to calculate the CMscore, a measure of how well the model is supported by the given cross-linking data, where lower scores denote better support. B) Overlay of the top TuYV coat protein model (red) on the PLRV coat protein model (grey). The shell (S) domain forms the surface of the capsid, while the arginine-rich (R) domain interacts with the viral genome. C) The four top-ranking I-TASSER models for the TuYV coat protein monomer, each with their corresponding contact map and CMscore. Contact maps shown were generated using the K150-K179 cross-link found in this study, as well as the PLRV cross-links from A) mapped onto the TuYV coat protein.

3.4 Cross-linking-assisted modeling of the TuYV coat protein trimer

One TuYV coat protein cross-link, K179-K179, was confidently ascribed to an inter-coat-protein interaction (Table 2.1). This was the only cross-link from these data used for modeling of the TuYV coat protein trimer. Previous cross-linking work with PLRV identified five unambiguous homodimer cross-links between PLRV coat protein monomers (Chavez et al., 2012; DeBlasio et al., 2016a). Of these, one was homologous to the TuYV K179-K179 cross-link, and one did not have a lysine at the homologous position in TuYV (Supplementary Table 1). Lysine residues in the TuYV coat protein homologous to the remaining three PLRV homodimer cross-links were used as additional distance constraints for modeling with SymmDock. Of the resulting 77 models for the TuYV coat protein trimer, two were selected based on their fit with the PLRV and TuYV cross-linking data, taking into account the shortest solvent accessible distance between the lysine pairs and similarity to previous models for luteovirid coat protein trimers (Brault et al., 2003; Chavez et al., 2012; DeBlasio et al., 2016a; Terradot et al., 2001).

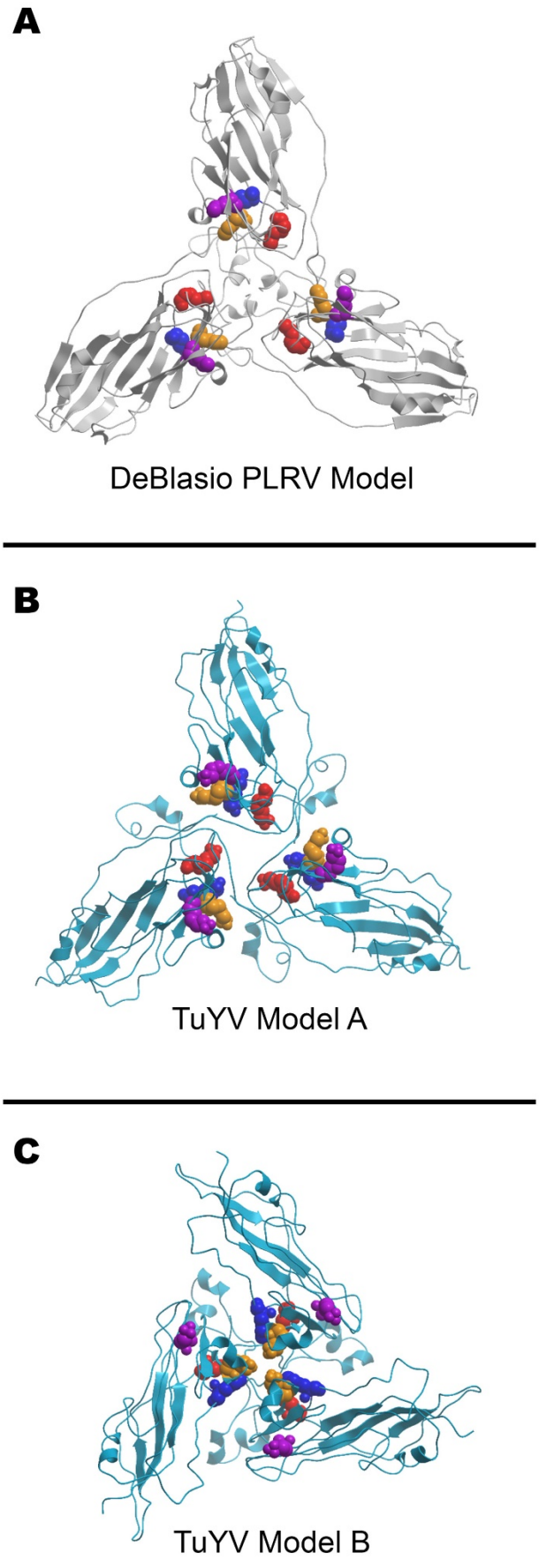

Figure 2.2: Comparison of cross-linking guided luteovirid trimer models. A) The most recent PLRV coat protein trimer model (DeBlasio et al., 2016a). B) TuYV trimer Model A. C) TuYV trimer Model B. All models are shown as viewed from the capsid exterior. Four lysine residues found cross-linked as unambiguous homodimers, used for generation of the models, are space-filled and shown in red, orange, blue, and purple.

Of the four previously proposed luteovirid trimer models, only the DeBlasio and Chavez/Cilia models were PIR-derived (Chavez et al., 2012; DeBlasio et al., 2016a). Of these two, the DeBlasio model was based on a greater number of cross-links, and these cross-links were also used to guide modeling of the TuYV trimer. Therefore, comparisons of the TuYV trimer here and elsewhere in this study were performed against the DeBlasio model, except where otherwise noted. As shown in Figure 2.2, Model A was most similar in shape to the PLRV trimer model. The S-domains project outward radially from the beta-annulus at a ~120° angle. The relative positions of the lysine residues used as distance constraints were also very similar to the PLRV model, indicating that the rotation of the monomers relative to the radial axis was also similar.

In contrast, Model B was the only one of the 77 SymmDock models to satisfy solvent-accessible distance constraints for all four lysine pairs, including the K179-K179 pair found cross-linked in TuYV samples. Model B is similar in shape to the trimeric asymmetric unit of other icosahedral viruses, including RGMoV and *Rice yellow mottle virus* (RYMV; Unclassified: *Sobemovirus*) – the nearest relatives for which crystal structures are available. The monomers in Model B are more tightly packed than in Model A, and are rotated, as shown by the difference in positioning of the reactive lysine residues.

Although Model B was the only model with all four unambiguous homodimers within acceptable solvent accessible distance constraints, it should be noted that a model can be correct without satisfying all distance constraints. A limitation of PIR and other cross-linking technologies is the inability to determine which region of the capsid any given cross-link was found in. While all four cross-links may occur near the trimer center, as presented here, it is also possible that one or more of these cross-

links occurred at the interface between trimer units, at the five-fold axis of symmetry, or even in unincorporated coat protein dimers (DeBlasio et al., 2016a). For this reason it may not be advisable to dismiss or accept a model on the sole basis of the solvent-accessible distance between residues. In this particular case it seems likely that all four cross-links occurred in the same area of the capsid, given their proximity to one another on the monomer model, but this cannot be determined with certainty.

The conformation of R-domain of the TuYV and PLRV coat proteins, which interacts with viral RNA inside the capsid, is markedly different between both the PLRV and TuYV coat protein trimer models. However, it is unlikely that the conformation of the R-domains can be accurately predicted, as modeling software cannot account for their interaction with viral nucleic acid inside the capsid. Protein-RNA interactions, such as in the R-domain, cannot yet be accurately modeled; the generated models instead assume a neutral aqueous environment surrounding the entire protein complex. This is likely a large part of the reason why there is so much variability in models for the R-domain, as evidenced by the top four I-TASSER models for the TuYV coat protein (Figure 2.1).

3.5 Comparison of epitope and critical residue locations between models

The high degree of conservation between the PLRV and TuYV coat protein sequences permits the superimposition of data from both species on the TuYV trimer models. Residues previously identified in mutational studies as important for virion assembly in TuYV (red) and PLRV (yellow) map primarily to the center of the exterior surface of each S-domain in Model A, whereas in Model B these residues map more to the outer edges of the trimer (Figure 2.3A, 2.3B). A 2005 study of PLRV identified residues which, when mutated to alanine residues, completely abolished

virion assembly (Lee et al., 2005). Four such residues, E170, W171, H172, and D177, were located at the predicted center of the capsid asymmetric unit and were hypothesized to stabilize the asymmetric unit via formation of a negatively charged depression. These residues are in a similar position in TuYV Model A, forming a small pit at the center of the asymmetric unit. In Model B, this pit is wider and occurs instead at the five- and three-fold axes of symmetry, and has an outer rim lined with the aforementioned EWH motif alternating with a short alpha helix created at one of the acidic patches – another highly conserved, charged region of the coat protein. As with the EWH motif, mutation of the KAY motif at the end of this helix (positions 100-102 in TuYV, or 105-107 in PLRV) completely blocks virion assembly (Kaplan et al., 2007).

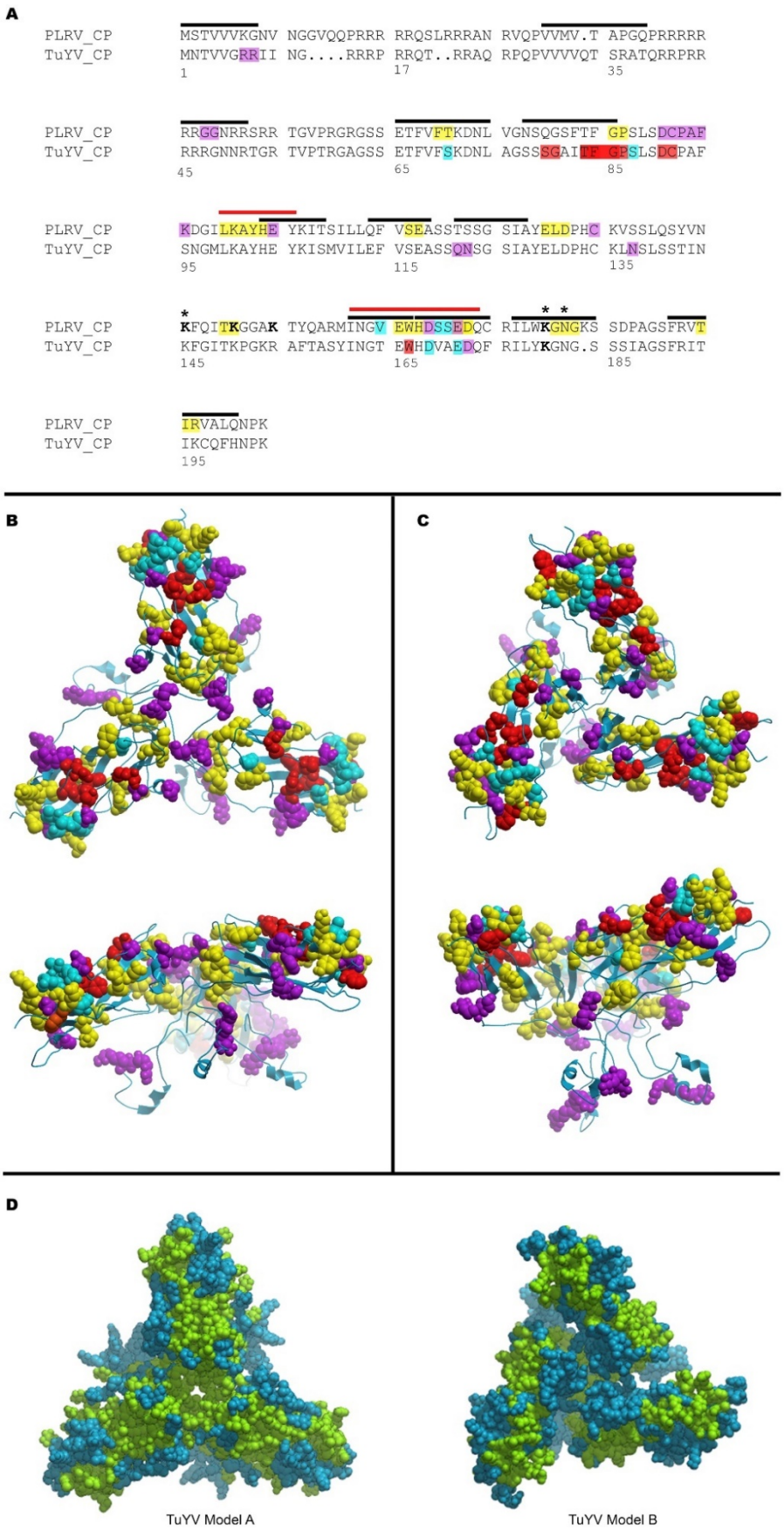
A
PLRV_CP MSTVVVKGNV NGGVQQPRRR RRQSLRRRAN RVQPVVMV.T APGQPRRRRR
TuYV_CP MNTVVGRRII NG....RRRP RRQT..RRAQ RPQPVVVVQT SRATQRRPRR
1 17 35
PLRV_CP RRGGNRRSRR TGVPRGRGSS ETFVFTKDNL VGNSQGSFTF GPSLSDCPAF
TuYV_CP RRRGNNRTGR TVPTRGAGSS ETFVFSKDNL AGSSSGAITF GPSLSDCPAF
45 65 85
PLRV_CP KDGILKAYHE YKITSILLQF VSEASSTSSG SIAYELDPHC KVSSLQSYVN
TuYV_CP SNGMLKAYHE YKISMVILEF VSEASSQNSG SIAYELDPHC KLNSLSSTIN
95 115 135
PLRV_CP KFQITKGGAK TYQARMINGV EWHDSSEDQC RILWKGNGKS SDPAGSFRVT
TuYV_CP KFGITKPGKR AFTASYINGT EWHDVAEDQF RILYKGNG.S SSIAGSFRIT
145 165 185
PLRV_CP IRVALQNPK
TuYV_CP IKCQFHNPK
195
B
C
D
TuYV Model A
TuYV Model B

Figure 2.3: Mapping of functional data onto the TuYV trimer models. A) Alignment of the PLRV and TuYV coat protein sequences. Black bars designate known epitopes (Torrance, 1992), while red bars denote previously described acidic patches (Terradot et al., 2001). Residues highlighted in yellow have been shown to be important for PLRV virion assembly (Kaplan et al., 2007; Lee et al., 2005). Residues highlighted in red have been shown to be important for TuYV virion assembly (Brault et al., 2003; Hipper et al., 2014). Residues highlighted in purple have been shown to be important for systemic movement, aphid transmission, or titer. Mutants in cyan residues have no measurable phenotype. Bolded residues were found cross-linked as unambiguous coat protein homodimers (DeBlasio et al., 2016a). Asterisks mark positions where homologous residues in *Cereal yellow dwarf virus*-RPV (CYDV; *Luteoviridae*: *Polerovirus*) have been shown to have secondary modifications (Cilia et al., 2014). Numbers below alignment designate TuYV coat protein residue number. B) and C): TuYV coat protein trimer Models A and B, respectively, shown from the capsid exterior (above) and from the side (below). Residues of functional importance highlighted in A) are space-filled and colored accordingly. For residues with differing data in PLRV and TuYV, the residues are colored according to the TuYV data. D) Surface maps of TuYV coat protein trimer Model A (left) and B (right) constructed by MolSoft. Green areas are homologous to known epitopes for PLRV (Torrance, 1992).

Mutational studies in TuYV by Brault and colleagues found that a double substitution mutant, Q121E/N122D, conferred no measurable phenotype (Brault et al., 2003). Virions assembled normally and were aphid-transmissible. The authors noted that this was surprising, given that the PLRV trimer model proposed by Terradot and colleagues, referred to as the Terradot model hereafter, predicts these residues to lie at the three- and five-fold axes of symmetry (Terradot et al., 2001). A double mutant within the Terradot structure would have to tolerate the presence of 10-12 negatively charged amino acids in proximity at 32 different places on the capsid. This incongruity also holds true for the DeBlasio PLRV model and TuYV Model A. However, in TuYV Model B these residues fall near the midpoint of the sides of the asymmetrical unit, on the underside of the trimer. In this case, the QN motifs from multiple monomers do not converge at any one point. The additional negative charges are spread out over a larger area, where they are more likely to be tolerated, and also partially face the positively-charged interior of the capsid. TuYV Model B is very similar in both shape and placement of the QN residues to the TuYV trimer model proposed by Brault *et al.* in light of their findings (Brault et al., 2003). Although there are significant differences in other aspects of the trimer structure between the Brault model and TuYV Model B, partially owing to major differences in the predicted structure of the coat protein monomer, the convergence of the two models with regards to the QN motif is nonetheless interesting.

In 1992, twelve regions of the PLRV coat protein were identified as solvent accessible based on epitope mapping (Torrance, 1992). Surprisingly, one such epitope was located at the coat protein N-terminus, a region believed to be on the capsid interior. Another epitope in the R-domain was found for *Barley yellow dwarf virus* (BYDV; *Luteoviridae*: *Luteovirus*) (Rizzo and Gray, 1992). A mechanism for solvent accessibility of these epitopes was first proposed by DeBlasio *et al*. Looser packing in

the DeBlasio PLRV trimer model created an opening in the trimer center, through which the R-domains may be partially solvent exposed (DeBlasio et al., 2016a). The looser packing of monomers in TuYV Model A creates a similar opening, while the tighter packing in Model B does not (Figure 2.3C). Additional support for partial or conditional solvent exposure of the coat protein R-domain comes from PIR-assisted modeling of a direct interaction between the PLRV coat protein and a host luminal binding protein (BiP) (DeBlasio et al., 2016a). A stretch of seven hydrophobic amino acids in the coat protein R-domain, homologous to the known binding site for human BiP-family proteins, was shown to fit in the substrate binding pocket of the *N. benthamiana* BiP. These hydrophobic amino acids, an anomaly in a region otherwise highly charged, are well conserved across luteovirid species (DeBlasio et al., 2016a). In both models A and B, at least one epitope other than the N-terminal epitope is located on the interior side of the trimer. This may be attributed to the interaction of soluble, non-incorporated readthrough protein with virions (Boissinot et al., 2014).

3.6 Comparison of models in the context of the capsid

Although the shape of Model B appears to be more similar to the PLRV trimer model computationally derived by Terradot and colleagues (Terradot et al., 2001), mapping both models to a more three-dimensional projection reveals that the orientation of the monomers in the Terradot PLRV model is actually more similar to TuYV Model A, as well as the DeBlasio PLRV model (DeBlasio et al., 2016a). The visual difference between the models lies primarily in which unit of three monomers is denoted the "trimer": the DeBlasio PLRV model and TuYV Model A place the center of the trimer unit at the three-fold axis of symmetry, such that the monomers in the trimer are each in a different face of the capsid. The three monomers in these models

are all in equivalent contexts, but account for, at most, two-thirds of the monomers in the capsid, assuming that the second trimer unit at the three-fold axis is identical to the first (Figure 2.4A, 2.4B). The remaining third of the monomers are located at the five-fold axes of symmetry, which are not contained within these models, but could be similarly oriented. In contrast, the Terradot PLRV model, TuYV Model B, and the RYMV crystal structure place the center of the trimer at the quasi-three-fold axis of symmetry, such that the trimer is effectively the asymmetric unit of the capsid (Figure 2.4C, 2.4D). These models contain all three quasi-equivalent monomers and therefore all of the monomers in the capsid, but they do not model the relationship between capsid faces at the 3- or 5- fold axes of symmetry. Importantly, the orientation of the monomers relative to the quasi-three-fold axes of symmetry is similar in the Terradot and DeBlasio PLRV models, and in TuYV Model A. This can be visualized more easily by highlighting the position of a tryptophan residue found to be critical for virion assembly in both TuYV and PLRV (W166/W178, respectively, Figure 2.4) (Brault et al., 2003; Lee et al., 2005). The Terradot and DeBlasio PLRV models, and TuYV Model A, have the aforementioned tryptophan residue positioned at the quasi-three-fold axis. However, in TuYV Model B, residue W166 is instead positioned at the three- and five-fold axes of symmetry. Thus, the orientation of the monomers in Model B relative to the quasi-three-fold axis is the inverse of the other models.

As an alternative to choosing either Model A or B for the TuYV coat protein trimer, a hybrid of both could be proposed, with two subunits from Model A and one from Model B. In this case one would also expect to find cross-links between residues at opposite ends of the S-domain. Such cross-links were, in fact, among those found in a previous PIR study with PLRV (e.g. K100-K184) (DeBlasio et al., 2016a), but were not used for trimer modeling because it could not be determined whether they were intra- or inter-protein cross-links.

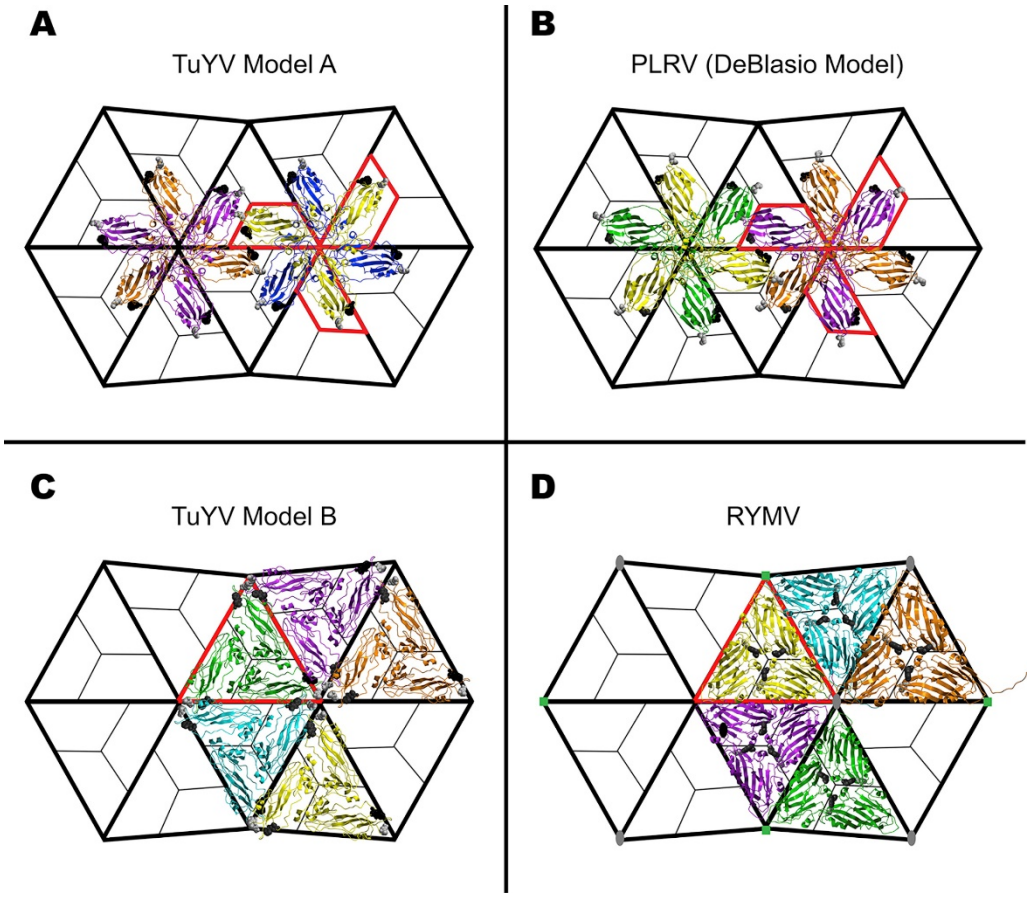

Figure 2.4: Cage diagrams of trimer models in their three-dimensional context. Each trimer is shown in a different color to facilitate visualization, and one trimer is outlined in red. The last amino acid in the coat protein is shown space-filled in white. A tryptophan residue critical for virion assembly is shown space-filled in black in A-C (Brault et al., 2003; Lee et al., 2005). A) Cage diagram of TuYV trimer Model A. B) Cage diagram of the DeBlasio PLRV model (DeBlasio et al., 2016a). C) Cage diagram of TuYV trimer Model B. D) Cage diagram of the crystal structure of the RYMV asymmetric unit, also a trimer. The three- and five-fold axes of symmetry are marked with gray ovals and green squares, respectively.

3.7 Direct interaction of a luteovirid non-structural protein with the coat protein

The cross-linked residue in ORF1 is present in both the P1 polyprotein and the P1-P2 fusion protein, but is located in a serine protease domain present in both proteins. The finding of a direct interaction between the TuYV coat protein and P1 protease domain supports the hypothesis that readthrough protein truncation is performed by the viral protease, as discussed in Section 1. Although no cross-links were detected between P1 and the readthrough domain of the readthrough protein, the proximity between P1 and the capsid surface during cleavage could easily account for the coat protein-P1 interaction. Additionally, the low abundance of the readthrough protein compared to coat protein in purified samples makes it difficult to detect any interactions with the readthrough domain, as evidenced by the low number of cross-links involving the readthrough domain that have been identified for PLRV (DeBlasio et al., 2016a).

To determine the plausibility of P1 truncation of the luteovirid readthrough protein, the distribution of putative cleavage sites in luteovirid readthrough proteins was assessed. Although the only experimentally verified P1 cleavage site for a luteovirid is a glutamate$_{204}$-arginine$_{205}$ (ER) motif in the PLRV polyprotein, a putative second glutamate-serine (ES) site has been identified based on the estimated sizes of the polyprotein cleavage products (Li et al., 2007; Prüfer et al., 1999). This agrees with literature showing that closely related sobemovirus proteases cleave at ES, glutamate-threonine (ET), and glutamate-asparagine (EN) sites in their corresponding polyproteins (Makinen et al., 2000; Nair and Savithri, 2010; Satheshkumar et al., 2004). An ER cleavage site in the related *Sesbania mosaic virus* (SeMV; Unclassified: *Sobemovirus*) has also been proposed, but not yet verified (Nair and Savithri, 2010). Both luteovirid and sobemovirus proteases are believed to cleave between the two amino acids comprising the recognition site. The 3C-like serine proteases from the

more distant genus *Arterivirus* cleave at (E/Q)-(G/S/A/N/K) sites in their respective polyproteins (Snijder and Gorbalenya, 2013). Additionally, it has been noted for PLRV, SeMV, and *Lactate dehydrogenase-elevating virus* (LDV; *Nidovirales*: *Arteriviridae*: *Arterivirus*) that the one or two amino acids immediately following the diresidue cleavage site are often aliphatic (Godeny et al., 1993; Li et al., 2007; Nair and Savithri, 2010). To determine the most likely cleavage sites in other luteovirid species, a multiple sequence alignment of the PLRV P1 polyprotein and the P1 polyproteins of other luteovirids was generated (supplementary materials). Using this alignment and the preferences of the aforementioned proteases, the luteovirid P1 cleavage motif was tentatively hypothesized to be (E)-(R/K/S/T/I)-(X), where X is a small aliphatic or polar amino acid. To assess the distribution of putative cleavage sites in luteovirid readthrough proteins, readthrough protein consensus sequences were generated for thirty luteovirid species and searched for sites satisfying the above criteria (supplementary materials). A probability density plot of putative P1 cleavage sites by the molecular weight of the resulting putative truncated readthrough proteins is shown in Figure 2.5B. Molecular weight, rather than amino acid position, was chosen as a basis for comparison due to the relatively poor conservation of readthrough protein sequence across luteovirid species. Although the criteria used to identify potential P1 cleavage sites in the readthrough protein are only an estimate based on available data, a striking pattern in the distribution of putative cleavage sites in the luteovirid consensus sequences could be seen. Putative sites were found most frequently in the C-terminal ~25kDa of the readthrough protein, generating truncated products between 50-75kDa in size. This corresponds remarkably with the typical size estimates for luteovirid truncated readthrough protein isoforms, between 50-70kDa. In contrast, there are relatively few predicted products in the 0-50kDa range. The dramatic difference in prevalence of putative cleavage sites beginning around 50kDa

suggests that the distribution of these sites is not random, particularly given the relative dearth of putative cleavage sites in the coat protein, which is required for virion assembly and readthrough protein incorporation.

These cleavage site predictions are interesting overall, but it should be noted that they likely represent a simplified view, even if the P1 protease is responsible for truncation. Accessibility of putative cleavage sites may be affected by post-translational modifications or conformation of the readthrough protein. Additionally, P1 protease site preferences may vary by virus species or the presence and conformation of the adjacent VPg, as has been shown for sobemoviruses (Makinen et al., 2000; Nair et al., 2008; Nair and Savithri, 2010; Satheshkumar et al., 2005; Satheshkumar et al., 2004). Of course, readthrough protein truncation by host proteases, at sites either disparate from or similar to the P1 cleavage motifs proposed here, cannot be ruled out. Significant further work is necessary to determine the mechanism behind truncation of the readthrough protein. However, the finding of a direct interaction between the TuYV coat protein and protease domain of the P1 polyprotein, together with the striking similarity in the distribution of putative P1 cleavage sites to the estimated sizes of truncated readthrough protein isoforms, suggest involvement of the viral protease. The P1 polyprotein and the P1-P2 fusion protein were both found to co-immunoprecipitate with PLRV in samples extracted from infected *N. benthamiana* leaves (DeBlasio et al., 2017; DeBlasio et al., 2015a; DeBlasio et al., 2015b). PLRV P1 was also found to co-immunoprecipitate with PLRV in protein extracts from systemically infected potato (*S. tuberosum*), a natural host of PLRV (DeBlasio et al., 2016b).

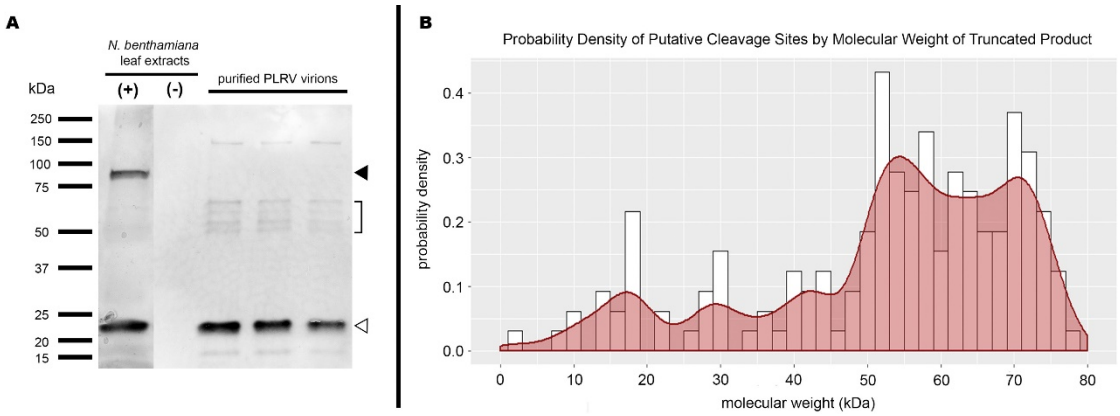

Figure 2.5: Truncation of the luteovirid readthrough protein and putative cleavage sites. A) Western blot showing detected PLRV coat protein/readthrough protein in crude protein extract from infected (+) and uninfected (-) *N. benthamiana*, and in three biological replicates of virions purified from *N. benthamiana*. The band corresponding to the PLRV coat protein (23kDa) is marked by an open triangle. The full-length readthrough protein (80kDa) is marked by a closed triangle. Putative truncated readthrough protein isoforms are bracketed. Image is from a single Western blot, but some redundant lanes have been cropped out. B) Probability density plot of P1 cleavage sites by molecular weight of truncated product (kDa). Shaded area represents the area under the smoothed Gaussian kernel density curve.

4. Conclusion

Application of PIR technology to TuYV provided direct experimental evidence that cross links, and therefore protein topologies, can be highly conserved between species. This finding opens opportunities for broader application of cross-linking data; for example, the PLRV and TuYV coat protein cross-links reported here and previously may also be useful for modeling of other luteovirid coat protein trimers. The similarity in coat protein topology between PLRV and TuYV also implies that the comprehensive mutational and epitope mapping studies which have been performed in the most commonly studied luteovirid species can be extended to the many economically important luteovirids which are poorly understood.

5. Acknowledgements

The authors would like to thank Jason Ingram, Rogerio Santos, August Kronstadt-Brennan, and Brian Bell for excellent aphid and plant care at Cornell University. We also thank Jimmy Eng and the staff at the University of Washington Proteome Resource (UWPR) center.

Funding for this work was provided by the National Science Foundation (NSF grant number 1354309) and the United States Department of Agriculture – National Institute of Food and Agriculture (USDA-NIFA grant number 1008590).

6. Author Contributions

Conceived and designed the analysis: MMA*, SLD, MCH, JDC, JEB, JPM

Collected the data: MMA*, JPM*, JDC

Contributed data or analysis tools: MMA*, JPM, SLD, JDC, VZG, VB, JEB, MCH

Performed the analysis: MMA*, JPM, JDC, MCH, JEB

Wrote the paper: MMA*, MCH

*Primary contributor

7. Supplementary Materials

Supplementary Table 2.1. Sites in TuYV coat protein homologous to cross-links found in purified PLRV

PLRV Peptide1	PLRV Peptide 2	TuYV Peptide 1 Homolog	TuYV Peptide 2 Homolog
PHCK.VSSLQSYVNK$_{150}$FQITK.GGAK	**PHCK.VSSLQSYVNK$_{150}$FQITK.GGAK**	**PHCK.LNSLSSTINK$_{145}$FGITK.PGKR**	**PHCK.LNSLSSTINK$_{145}$FGITK.PGKR**
YVNK.FQITK$_{155}$GGAK.TYQAR	**YVNK.FQITK$_{155}$GGAK.TYQAR**	**TINK.FGITK$_{150}$PGK.RAFT**	**TINK.FGITK$_{150}$PGK.RAFT**
QITK.GGAK$_{159}$TYQAR.MING	**QITK.GGAK$_{159}$TYQAR.MING**	**GITK.PGK$_{153}$R.AFTA**	**GITK.PGK$_{153}$R.AFTA**
DQCR.ILWK$_{184}$GNGK.SSDP	**DQCR.ILWK$_{184}$GNGK.SSDP**	**DQFR.ILYK$_{179}$GNGSSSIAGSFR.IAGS**	**DQFR.ILYK$_{179}$GNGSSSIAGSFR.IAGS**
YVNK.FQITK$_{155}$GGAK.TYQAR	QITK.GGAK$_{159}$TYQAR.MING	TINK.FGITK$_{150}$PGK.RAFT	GITK.PGK$_{153}$R.AFTA
PAFK.DGILK$_{105}$AYHEYK.ITSI	PHCK.VSSLQSYVNK$_{150}$FQITK.GGAK	PHCK.LNSLSST$_{145}$INKFGITK.PGKR	PHCK.LNSLSSTINK$_{145}$FGITK.PGKR
YVNK.FQITK$_{155}$GGAK.TYQAR	PHCK.VSSLQSYVNK$_{150}$FQITK.GGAK	TINK.FGITK$_{150}$PGK.RAFT	PHCK.LNSLSSTINK$_{145}$FGITK.PGKR
QITK.GGAK159TYQAR.MING	PHCK.VSSLQSYVNK$_{150}$FQITK.GGAK	GITK.PGK$_{153}$R.AFTA	PHCK.LNSLSSTINK$_{145}$FGITK.PGKR
DQCR.ILWK184GNGK.SSDP	PHCK.VSSLQSYVNK$_{150}$FQITK.GGAK	DQFR.ILYK$_{179}$GNGSSSIAGSFR.IAGS	PHCK.LNSLSSTINK$_{145}$FGITK.PGKR
ILWK.GNGK$_{188}$SSDPAGSFR.VTIR	PHCK.VSSLQSYVNK$_{150}$FQITK.GGAK	No homologous lysine[b]	PHCK.LNSLSSTINK$_{145}$FGITK.PGKR
PRGR.GSSETFVFTK$_{76}$DNLVGNSQGSFTFGPSLSDcPAFK.DGIL	DQCR.ILWK$_{184}$GNGK.SSDP	VPTR.GAGSSETFVFSK$_{71}$DNLAGSSSGAITFGPSLSDCPAFSNGLK.AYHE	DQFR.ILYK$_{179}$GNGSSSIAGSFR.IAGS
GVPR.GRGSSETFVFTK$_{76}$DNLVGNSQGSFTFGPSLSDcPAFK.DGIL	DQCR.ILWK$_{184}$GNGK.SSDP	VPTR.GAGSSETFVFSK$_{71}$DNLAGSSSGAITFGPSLSDCPAFSNGLK.AYHE	DQFR.ILYK$_{179}$GNGSSSIAGSFR.IAGS
VFTK.DNLVGNSQGSFTFGPSLSDcPAFK$_{100}$DGILK.AYHE	DQCR.ILWK$_{184}$GNGK.SSDP	No homologous lysine[b]	DQFR.ILYK$_{179}$GNGSSSIAGSFR.IAGS
PAFK.DGILK$_{105}$AYHEYK.ITSI	DQCR.ILWK$_{184}$GNGK.SSDP	VFSK.DNLAGSSSGAITFGPSLSDCPAFSNGMLK$_{100}$AYHEYK.ISMV	DQFR.ILYK$_{179}$GNGSSSIAGSFR.IAGS
YVNK.FQITK$_{155}$GGAK.TYQAR	DQCR.ILWK$_{184}$GNGK.SSDP	TINK.FGITK$_{150}$PGK.RAFT	DQFR.ILYK$_{179}$GNGSSSIAGSFR.IAGS
ILWK.GNGK$_{188}$SSDPAGSFR.VTIR	DQCR.ILWK$_{184}$GNGK.SSDP	No homologous lysine[b]	DQFR.ILYK$_{179}$GNGSSSIAGSFR.IAGS

[a]Amino acid sequence of cross-linked PLRV peptides deduced from MS3 fragmentation and database searching (DeBlasio 2015), or TuYV peptides deduced from sequence alignment. The four amino acids before and after each peptide are given as a reference, with peptide boundaries denoted by periods. K residue numbers indicate predicted or actual cross-linked lysines. The bolded peptides represent unambiguous homodimers used for modeling of the coat protein trimer. Blue peptides were found cross-linked in TuYV samples (see Table 2.1).

[b]Residues aligning to lysines at positions 100 and 188 in the PLRV coat protein are a serine and a missing amino acid, respectively, in the TuYV coat protein sequence.

REFERENCES

Adams, M.J., Lefkowitz, E.J., King, A.M., Harrach, B., Harrison, R.L., Knowles, N.J., Kropinski, A.M., Krupovic, M., Kuhn, J.H., Mushegian, A.R., Nibert, M., Sabanadzovic, S., Sanfacon, H., Siddell, S.G., Simmonds, P., Varsani, A., Zerbini, F.M., Gorbalenya, A.E., Davison, A.J., 2016. Ratification vote on taxonomic proposals to the International Committee on Taxonomy of Viruses (2016). Archives of Virology 161, 2921-2949.

Bag, S., Al Rwahnih, M., Li, A., Gonzalez, A., Rowhani, A., Uyemoto, J.K., Sudarshana, M.R., 2015. Detection of a new luteovirus in imported nectarine trees: A case study to propose adoption of metagenomics in post-entry quarantine. Phytopathology 105, 840-846.

Bahner, I., Lamb, J., Mayo, M.A., Hay, R.T., 1990. Expression of the genome of *Potato leafroll virus*: Readthrough of the coat protein termination codon in vivo. Journal of General Virology 71 (Pt 10), 2251-2256.

Bejerman, N., Giolitti, F., Trucco, V., de Breuil, S., Dietzgen, R.G., Lenardon, S., 2016. Complete genome sequence of a new enamovirus from Argentina infecting alfalfa plants showing dwarfism symptoms. Arch Virol 161, 2029-2032.

Boissinot, S., Erdinger, M., Monsion, B., Ziegler-Graff, V., Brault, V., 2014. Both structural and non-structural forms of the readthrough protein of *Cucurbit aphid-borne yellows virus* are essential for efficient systemic infection of plants. PLoS One 9, e93448.

Bombarely, A., Rosli, H.G., Vrebalov, J., Moffett, P., Mueller, L.A., Martin, G.B., 2012. A draft genome sequence of *Nicotiana benthamiana* to enhance molecular plant-microbe biology research. Mol Plant Microbe Interact 25, 1523-1530.

Brault, V., Bergdoll, M., Mutterer, J., Prasad, V., Pfeffer, S., Erdinger, M., Richards, K.E., Ziegler-Graff, V., 2003. Effects of point mutations in the major capsid protein of *Beet western yellows virus* on capsid formation, virus accumulation, and aphid transmission. Journal of Virology 77, 3247-3256.

Brault, V., van den Heuvel, J.F.J.M., Verbeek, M., Ziegler-Graff, V., Reutenauer, a., Herrbach, E., Garaud, J.C., Guilley, H., Richards, K., Jonard, G., 1995. Aphid transmission of *Beet western yellows luteovirus* requires the minor capsid read-through protein P74. The EMBO Journal 14, 650-659.

Bruyere, A., Brault, V., Ziegler-Graff, V., Simonis, M.T., Van den Heuvel, J.F., Richards, K., Guilley, H., Jonard, G., Herrbach, E., 1997. Effects of mutations in the *Beet western yellows virus* readthrough protein on its expression and packaging and on virus accumulation, symptoms, and aphid transmission. Virology 230, 323-334.

Chapman, B.A., Chang, J.T., 2000. Biopython: Python tools for computational biology. ACM SIGBIO Newsletter 20, 15-19.

Chavez, J.D., Cilia, M., Weisbrod, C.R., Ju, H.J., Eng, J.K., Gray, S.M., Bruce, J.E., 2012. Cross-linking measurements of the *Potato leafroll virus* reveal protein interaction topologies required for virion stability, aphid transmission, and virus-plant interactions. J Proteome Res 11, 2968-2981.

Chay, C.A., Gunasinge, U.B., Dinesh-Kumar, S.P., Miller, W.A., Gray, S.M., 1996. Aphid transmission and systemic plant infection determinants of *Barley yellow dwarf luteovirus*-PAV are contained in the coat protein readthrough domain and 17-kDa protein, respectively. Virology 219, 57-65.

Chen, S., Jiang, G., Wu, J., Liu, Y., Qian, Y., Zhou, X., 2016. Characterization of a novel polerovirus infecting maize in China. Viruses 8.

Cheng, S.L., Domier, L.L., D'Arcy, C.J., 1994. Detection of the readthrough protein of *Barley yellow dwarf virus*. Virology 202, 1003-1006.

Cilia, M., Johnson, R., Sweeney, M., DeBlasio, S.L., Bruce, J.E., MacCoss, M.J., Gray, S.M., 2014. Evidence for lysine acetylation in the coat protein of a polerovirus. J Gen Virol 95, 2321-2327.

DeBlasio, S.L., Bereman, M.S., Mahoney, J., Thannhauser, T.W., Gray, S.M., MacCoss, M.J., Cilia Heck, M., 2017. Evaluation of a bead-free co-immunoprecipitation technique for identification of virus-host protein interactions using high-resolution mass spectrometry. J Biomol Tech 28, 111-121.

DeBlasio, S.L., Chavez, J.D., Alexander, M.M., Ramsey, J., Eng, J.K., Mahoney, J., Gray, S.M., Bruce, J.E., Cilia, M., 2016a. Visualization of host-polerovirus interaction topologies using Protein Interaction Reporter technology. J Virol 90, 1973-1987.

DeBlasio, S.L., Johnson, R., Mahoney, J., Karasev, A., Gray, S.M., MacCoss, M.J., Cilia, M., 2015a. Insights into the polerovirus-plant interactome revealed by co-immunoprecipitation and mass spectrometry. Mol Plant Microbe Interact 28, 467-481.

DeBlasio, S.L., Johnson, R., Sweeney, M.M., Karasev, A., Gray, S.M., MacCoss, M.J., Cilia, M., 2015b. *Potato leafroll virus* structural proteins manipulate overlapping, yet distinct protein interaction networks during infection. Proteomics 15, 2098-2112.

DeBlasio, S.L., Johnson, R.S., MacCoss, M.J., Gray, S.M., Cilia, M., 2016b. Model system-guided protein interaction mapping for virus isolated from phloem tissue. J Proteome Res 15, 4601-4611.

Dinesh-Kumar, S.P., Brault, V., Miller, W.A., 1992. Precise mapping and in vitro translation of a trifunctional subgenomic RNA of *Barley yellow dwarf virus*. Virology 187, 711-722.

Edgar, R.C., 2004. MUSCLE: multiple sequence alignment with high accuracy and high throughput. Nucleic Acids Res 32, 1792-1797.

Eng, J.K., Jahan, T.A., Hoopmann, M.R., 2013. Comet: an open-source MS/MS sequence database search tool. Proteomics 13, 22-24.

Filichkin, S.A., Lister, R.M., McGrath, P.F., Young, M.J., 1994. In vivo expression and mutational analysis of the *Barley yellow dwarf virus* readthrough gene. Virology 205, 290-299.

Godeny, E.K., Chen, L., Kumar, S.N., Methven, S.L., Koonin, E.V., Brinton, M.A., 1993. Complete genomic sequence and phylogenetic analysis of the *Lactate dehydrogenase-elevating virus* (LDV). Virology 194, 585-596.

Gray, S., Cilia, M., Ghanim, M., 2014. Circulative, "nonpropagative" virus transmission: An orchestra of virus-, insect-, and plant-derived instruments. Adv Virus Res 89, 141-199.

Hipper, C., Monsion, B., Bortolamiol-Becet, D., Ziegler-Graff, V., Brault, V., 2014. Formation of virions is strictly required for *Turnip yellows virus* long-distance movement in plants. J Gen Virol 95, 496-505.

Holsters, M., Silva, B., Van Vliet, F., Genetello, C., De Block, M., Dhaese, P., Depicker, A., Inzé, D., Engler, G., Villarroel, R., 1980. The functional organization of the nopaline *A. tumefaciens* plasmid pTiC58. Plasmid 3, 212-230.

Ibaba, J.D., Laing, M.D., Gubba, A., 2017. *Pepo aphid-borne yellows virus*: a new species in the genus Polerovirus. Virus Genes 53, 134-136.

Jolly, C.A., Mayo, M.A., 1994. Changes in the amino acid sequence of the coat protein readthrough domain of *Potato leafroll luteovirus* affect the formation of an epitope and aphid transmission. Virology 201, 182-185.

Kahraman, A., Malmstrom, L., Aebersold, R., 2011. Xwalk: Computing and visualizing distances in cross-linking experiments. Bioinformatics 27, 2163-2164.

Kaplan, I.B., Lee, L., Ripoll, D.R., Palukaitis, P., Gildow, F., Gray, S.M., 2007. Point mutations in the *Potato leafroll virus* major capsid protein alter virion stability and aphid transmission. J Gen Virol 88, 1821-1830.

Kim, J.H., Jander, G., 2007. *Myzus persicae* (green peach aphid) feeding on *Arabidopsis* induces the formation of a deterrent indole glucosinolate. Plant J 49, 1008-1019.

Lee, L., Kaplan, I.B., Ripoll, D.R., Liang, D., Palukaitis, P., Gray, S.M., 2005. A surface loop of the *Potato leafroll virus* coat protein is involved in virion assembly, systemic movement, and aphid transmission. J Virol 79, 1207-1214.

Leiser, R.M., Ziegler-Graff, V., Reutenauer, A., Herrbach, E., Lemaire, O., Guilley, H., Richards, K., Jonard, G., 1992. Agroinfection as an alternative to insects for infecting plants with *Beet western yellows virus*. Proceedings of the National Academy of Sciences 89, 9136-9140.

Li, X., Halpin, C., Ryan, M.D., 2007. A novel cleavage site within the *Potato leafroll virus* P1 polyprotein. J Gen Virol 88, 1620-1623.

Li, X., Ryan, M.D., Lamb, J.W., 2000. *Potato leafroll virus* protein P1 contains a serine proteinase domain. Journal of General Virology 81, 1857-1864.

Linz, L.B., Liu, S., Chougule, N.P., Bonning, B.C., 2015. *In vitro* evidence supports membrane alanyl aminopeptidase N as a receptor for a plant virus in the pea aphid vector. J Virol 89, 11203-11212.

Lotos, L., Maliogka, V.I., Katis, N.I., 2016. New poleroviruses associated with yellowing symptoms in different vegetable crops in Greece. Arch Virol 161, 431-436.

Makinen, K., Makelainen, K., Arshava, N., Tamm, T., Merits, A., Truve, E., Zavriev, S., Saarma, M., 2000. Characterization of VPg and the polyprotein processing of *Cocksfoot mottle virus* (genus *Sobemovirus*). Journal of General Virology 81, 2783-2789.

Mashiach-Farkash, E., Nussinov, R., Wolfson, H.J., 2011. SymmRef: a flexible refinement method for symmetric multimers. Proteins 79, 2607-2623.

Nair, S., Gayathri, P., Murthy, M.R., Savithri, H.S., 2008. Stacking interactions of W271 and H275 of SeMV serine protease with W43 of natively unfolded VPg confer catalytic activity to protease. Virology 382, 83-90.

Nair, S., Savithri, H.S., 2010. Processing of SeMV polyproteins revisited. Virology 396, 106-117.

Navare, A.T., Chavez, J.D., Zheng, C., Weisbrod, C.R., Eng, J.K., Siehnel, R., Singh, P.K., Manoil, C., Bruce, J.E., 2015. Probing the protein interaction network of *Pseudomonas aeruginosa* cells by chemical cross-linking mass spectrometry. Structure 23, 762-773.

Peter, K.A., Gildow, F., Palukaitis, P., Gray, S.M., 2009. The C terminus of the polerovirus P5 readthrough domain limits virus infection to the phloem. J Virol 83, 5419-5429.

Peter, K.A., Liang, D., Palukaitis, P., Gray, S.M., 2008. Small deletions in the *Potato leafroll virus* readthrough protein affect particle morphology, aphid transmission, virus movement and accumulation. J Gen Virol 89, 2037-2045.

Prüfer, D., Kawchuk, L., Monecke, M., Nowok, S., Fischer, R., Rohde, W., 1999. Immunological analysis of *Potato leafroll luteovirus* (PLRV) P1 expression identifies a 25 kDa RNA-binding protein derived via P1 processing. Nucleic Acids Research 27, 421-425.

Qu, C., Liljas, L., Opalka, N., Brugidou, C., Yeager, M., Beachy, R.N., Fauquet, C.M., Johnson, J.E., Lin, T., 2000. 3D domain swapping modulates the stability of members of an icosahedral virus group. Structure 8, 1095-1103.

Reinbold, C., Herrbach, E., Brault, V., 2003. Posterior midgut and hindgut are both sites of acquisition of Cucurbit aphid-borne yellows virus in *Myzus persicae* and *Aphis gossypii*. J Gen Virol 84, 3473-3484.

Reutenauer, A., Ziegler-Graff, V., Lot, H., Scheidecker, D., Guilley, H., Richards, K., Jonard, G., 1993. Identification of *Beet western yellows luteovirus* genes implicated in viral replication and particle morphogenesis. Virology 195, 692-699.

Rizzo, T.M., Gray, S.M., 1992. Localization of a surface domain of the capsid protein of *Barley yellow dwarf virus*. Virology 186, 300-302.

Rossmann, M.G., 2013. Structure of viruses: A short history. Quarterly Reviews of Biophysics 46, 133-180.

Satheshkumar, P.S., Lokesh, G.L., Murthy, M.R., Savithri, H.S., 2005. The role of arginine-rich motif and beta-annulus in the assembly and stability of *Sesbania mosaic virus* capsids. J Mol Biol 353, 447-458.

Satheshkumar, P.S., Lokesh, G.L., Savithri, H.S., 2004. Polyprotein processing: *cis* and *trans* proteolytic activities of *Sesbania mosaic virus* serine protease. Virology 318, 429-438.

Schneidman-Duhovny, D., Inbar, Y., Nussinov, R., Wolfson, H.J., 2005. PatchDock and SymmDock: Servers for rigid and symmetric docking. Nucleic Acids Res 33, W363-367.

Schweppe, D.K., Chavez, J.D., Bruce, J.E., 2016. XLmap: an R package to visualize and score protein structure models based on sites of protein cross-linking. Bioinformatics 32, 306-308.

Sharman, M., Kehoe, M., Coutts, B., van Leur, J., Filardo, F., Thomas, J., 2016. Two complete genome sequences of *Phasey bean mild yellows virus*, a novel member of the *Luteoviridae* from Australia. Genome Announc 4.

Snijder, E.J., Gorbalenya, A.E., 2013. Arterivirus Serine Endopeptidase, in: Rawlings, N.D., Salvesen, G. (Eds.), Handbook of Proteolytic Enzymes, 3 ed. Academic Press, San Diego, CA, pp. 3137-3141.

Tang, X., Munske, G.R., Siems, W.F., Bruce, J.E., 2005. Mass spectrometry identifiable cross-linking strategy for studying protein-protein interactions. Analytical Chemistry 77, 311-318.

Terradot, L., Souchet, M., Tran, V., Giblot Ducray-Bourdin, D., 2001. Analysis of a three-dimensional structure of *Potato leafroll virus* coat protein obtained by homology modeling. Virology 286, 72-82.

Torrance, L., 1992. Analysis of epitopes on *Potato leafroll virus* capsid protein. Virology 191, 485-489.

van den Heuvel, J.F.J.M., Boerma, T.M., Peters, D., 1991. Transmission of *Potato leafroll virus* from plants and artificial diets by *Myzus persicae*. Phytopathology 81, 150-154.

Veidt, I., Bouzoubaa, S.E., Leiser, R.M., Ziegler-Graff, V., Guilley, H., Richards, K., Jonard, G., 1992. Synthesis of full-length transcripts of *Beet western yellows virus* RNA: Messenger properties and biological activity in protoplasts. Virology 186, 192-200.

Veidt, I., Lot, H., Leiser, M., Scheidecker, D., Guilley, H., Richards, K., Jonard, G., 1988. Nucleotide sequence of *Beet western yellows virus* RNA. Nucleic Acids Research 16, 9917-9932.

Villamor, D.E., Mekuria, T.A., Pillai, S.S., Eastwell, K.C., 2016. High-throughput sequencing identifies novel viruses in nectarine: Insights to the etiology of stem-pitting disease. Phytopathology 106, 519-527.

Wang, J.Y., Chay, C., Gildow, F.E., Gray, S.M., 1995. Readthrough protein associated with virions of *Barley yellow dwarf luteovirus* and its potential role in regulating the efficiency of aphid transmission. Virology 206, 954-962.

Weisbrod, C.R., Chavez, J.D., Eng, J.K., Yang, L., Zheng, C., Bruce, J.E., 2013. *In vivo* protein interaction network identified with a novel real-time cross-linked peptide identification strategy. J Proteome Res 12, 1569-1579.

Wickham, H., 2009. ggplot2: Elegant graphics for data analysis. Springer-Verlag New York.

Yang, J., Yan, R., Roy, A., Xu, D., Poisson, J., Zhang, Y., 2015. The I-TASSER Suite: protein structure and function prediction. Nature Methods 12, 7-8.

Ziegler-Graff, V., Brault, V., Mutterer, J.D., Simonis, M.-T., Herrbach, E., Guilley,

H., Richards, K.E., Jonard, G., 1996. The coat protein of Beet western yellows luteovirus is essential for systemic infection but the viral gene products P29 and P19 are disposable for systemic infection and aphid transmission. Mol Plant Microbe Interact 9, 501-510.

CHAPTER 3

A DELICATE BALANCE: NEW FACETS OF THE COMPLEX RELATIONSHIP BETWEEN POLEROVIRUSES AND ARGONAUTE1

Abstract

Potato leafroll virus (PLRV) is a model plant pathogenic virus in the genus *Polerovirus*. Despite the ubiquity and economic importance of poleroviruses, technical challenges have limited our ability to understand their direct molecular interactions with host plants. Expanding on a previous study, we discovered several new interactions between PLRV and host proteins, including a putative interaction between PLRV coat protein and plant Argonaute1 (AGO1). Using *Tobacco rattle virus* (TRV) -based virus-induced gene silencing, we probed the role of AGO1 in systemic PLRV infection, finding that knocking down AGO1 expression increases both PLRV and TRV titer, as well as variability in PLRV titer only. Combined infection of plants with PLRV and TRV silencing AGO1 was found to be uniquely lethal. In a GFP-based silencing suppressor assay, co-expression of PLRV CP with P0, the PLRV silencing suppressor, was found to enhance silencing suppression relative to co-expression of P0 with a control protein. However, PLRV CP co-expression did not enhance silencing suppression by P19, the silencing suppressor from tombusviruses. Based on these data, we propose that the relationship between poleroviruses and AGO1 is more complex than previously thought, and suggest some potential functions for the putative CP-AGO1 interaction.

1. Introduction

The genus *Polerovirus* (family: *Luteoviridae*) contains numerous plant pathogens of current and historic importance, including the type species *Potato leafroll virus* (PLRV). Poleroviruses are unusual among plant-pathogenic viruses in that they are restricted to phloem tissue in natural infections, and are transmitted exclusively by aphids in a circulative, non-propagative manner (Gray et al., 2014). Poleroviruses are believed to move from cell-to-cell in both plants and aphids as icosahedral virions, which are comprised primarily of coat protein (CP; encoded by ORF3) with a minor component of readthrough protein (RTP; encoded by readthrough of an amber stop codon separating ORFs 3 and 5) (Bahner et al., 1990). Luteovirids are believed to move systemically in both plant hosts and aphid vectors as virions, meaning that interactions important for cell-cell movement are likely to be mediated by structural proteins (Esau and Hoefert, 1972a, b; Gildow, 1982; Shepardson et al., 1980). This hypothesis is supported by several seminal studies identifying residues in the luteovirid CP and RTP which are critical for aphid transmission, systemic movement in plants, and phloem restriction (Brault et al., 2000; Kaplan et al., 2007; Lee et al., 2005; Peter et al., 2009; Peter et al., 2008).

In 2016, the first application of cross-linking proteomics for host-virus interaction discovery in poleroviruses was published (DeBlasio et al., 2016a). This work in the PLRV pathosystem utilized Protein Interaction Reporter (PIR) technology - a mass spectrometry-compatible cross-linker which can be used to detect direct protein-protein interactions occurring in a complex mixture (Hoopmann et al., 2010; Tang and Bruce, 2010; Weisbrod et al., 2013). Functional validation using virus-induced gene silencing (VIGS) to knock down expression of host interaction partners definitively showed that this method successfully identifies biologically relevant host-virus interactions (DeBlasio et al., 2016a). Here, we perform additional studies with

the PIR cross-linker on partially purified PLRV virions, and find evidence suggesting a novel direct interaction between PLRV CP/RTP and AGO1, a plant Argonaute-family protein involved in RNA silencing.

RNA silencing is plants' primary defense against plant viral infection. To combat silencing by the plant immune system, most plant viruses encode one or more silencing suppressor proteins. These proteins have highly diverse modes of action, including direct protection of dsRNA, sequestration of siRNAs, and inhibition or degradation of RNA silencing pathway proteins (Csorba et al., 2015). The silencing suppressor protein for PLRV and other poleroviruses is P0, which binds to and promotes the degradation of unloaded plant AGO1 (Baumberger et al., 2007; Bortolamiol et al., 2007; Csorba et al., 2010; Derrien et al., 2012). P0 contains a F-BOX domain which is required for its silencing suppressor activity (Baumberger et al., 2007; Pazhouhandeh et al., 2006). F-BOX proteins typically act as a component of the SKP/CULLIN/FBOX complex (SCF complex), which targets a protein substrate for ubiquitination and subsequent degradation by the proteasome (for review: (Correa et al., 2013)). P0 has been found to interact directly with SKP1 or the SCF complex in multiple systems (Derrien et al., 2018; Li et al., 2019; Pazhouhandeh et al., 2006; Pfeffer et al., 2002), and abolishing a short amino acid sequence in AGO1 required for interaction with SCF also confers insensitivity to P0 (Derrien et al., 2018). However, at least one PLRV isolate has been found to encode a P0 that does not interact with SCF (Zhuo et al., 2014). Furthermore, P0-mediated degradation of AGO1 is insensitive to proteasome inhibitors, indicating that P0-mediated degradation is not proteasome-dependent (Baumberger et al., 2007; Derrien et al., 2012). Instead, AGO1 degradation appears to proceed through the autophagy pathway (Derrien et al., 2012).

In this study, we use VIGS to compare and contrast the function of AGO1 in

systemic infection with PLRV and *Tobacco rattle virus* (TRV; *Virgaviridae*: *Tobravirus*), which has markedly different biological properties. Based on our observations, we propose possible functions for the putative CP-AGO1 interaction, and discuss the implications of these hypotheses.

2. Materials and Methods

2.1 Virion Purification

Infected *Nicotiana benthamiana* tissue inoculated with an infectious clone of PLRV by *Agrobacterium tumefaciens* infiltration (agroinfiltration) was prepared as previously described (DeBlasio et al., 2016a) to generate purified virus preparations for PIR analysis. Frozen tissue was used for partial virion purification, stopping after the sucrose cushion step to preserve host-virus protein-protein interactions, as in similar previous experiments (DeBlasio et al., 2016a). Quantification of PLRV in the resulting preparations was performed using a Nanovue (GE), and the presence of intact virions was confirmed by enzyme-linked immunosorbent assay (ELISA) and verification of aphid transmissibility (see below).

2.2 Aphid Transmission Assays

Aphid transmissibility of partially purified virions was performed as previously described (Alexander et al., 2017; DeBlasio et al., 2016a) to verify purified virions were infectious. Infection status of recipient plants and virion presence in purified virion samples was assessed by double antibody sandwich enzyme-linked immunosorbent assay (DAS-ELISA) using an Agdia PLRV DAS-ELISA antibody set as previously described (DeBlasio et al., 2016a), except that 2% nonfat dry milk in phosphate buffered saline + 0.05% Tween-20 was used for the wash steps between

coating and sample incubation.

2.3 Cross-Linking and Sample Preparation

To obtain three biological replicates with at least 500ng of virion each, the products of multiple purifications were combined after testing the aphid transmissibility of each. Synthesis of the PIR cross-linker was performed as previously described (Tang and Bruce, 2010). PIR cross-linker was added to partially purified samples to a final concentration of 1mM. Samples were incubated with vigorous shaking at room temperature for one hour. Urea was added to cross-linked samples to a final concentration of 8M. Tris(2-carboxyethyl)phosphine (TCEP) was added to a final concentration of 5mM, and samples were incubated for 45 minutes at room temperature with shaking. Iodoacetamide (IAA) in 100mM ammonium bicarbonate (ABC) was added to a final IAA concentration of 10mM, and samples were incubated for 45 minutes in the dark at room temperature, with shaking. Samples were then diluted in 100mM ABC to reduce the urea concentration below 1M. Trypsin digestion was performed overnight at 37°C with 1µg of trypsin per 100µg of purified virus. Undiluted formic acid was added to samples until they reached a pH ≤3. Samples were then desalted using Sep Pak C_{18} columns as previously described (DeBlasio et al., 2016a) and dried down in a vacuum centrifuge.

2.4 Stage I database sample generation

To perform the bioinformatics analysis of the PIR data, we used a stage I database search strategy (Anderson et al., 2007), which we have previously shown to improve the statistical analysis of cross-linked peptides using mass spectrometry (Weisbrod et al., 2013). A 500µg sample pooled from all three biological replicates

was cross-linked as above, stopping immediately prior to trypsin digestion. The undigested protein was enriched through biotin capture to generate a reduced database by identifying a set of proteins modified by the cross-linker. The samples were incubated for one hour with mixing with 100µL of UltraLink monomeric avidin (Thermofisher). The resin was washed 10 times with 3mL aliquots of 100mM ABC. Cross-linked proteins were eluted from the beads by two additions of 250µL of 2mM d-biotin in a buffer containing 8M urea and 100mM ABC. The captured proteins were digested overnight with trypsin, and the resulting peptides were desalted using Sep Pak C_{18} columns. The desalted peptides were resuspended at approximately 1µg/µl in 0.1% formic acid.

2.5 Data dependent acquisition for stage I sample

Stage I samples were analyzed by mass spectrometry. The reconstituted peptides were analyzed on a Q-Exactive Plus (Thermo Scientific) mass spectrometer coupled to an EASY-nLC (Thermo Scientific). Peptides were fractionated over a 60cm by 75µm inner diameter fused silica analytical column packed with Reprosil-Pur C8 (5µM diameter, 120 Å pore size particles) by applying a linear gradient from 90% solvent A (0.1% formic acid in water), 10% solvent B (0.1% formic acid in acetonitrile) to 70% solvent A, 30% solvent B over 90 minutes at a flow rate of 300nL/min. The mass spectrometer was operated in data dependent analysis (DDA) mode, where a higher resolution (70,000 resolving power) MS1 scan was taken, followed by up to 20 MS2 scans (17,500 resolving power) on the most abundant ions from MS1. Parameters for the MS2 scan include an AGC of 50,000, a maximum ion time of 50ms, an isolation window of 1.6 Da, and a normalized collision energy of 25. The resulting data were searched using comet 2018.01 rev. 3 against a concatenated database of *N. benthamiana* and PLRV using comet's concatenated decoy search

(Bombarely et al., 2012; Eng et al., 2013). The search output was analyzed using ProteinProphet (Nesvizhskii et al., 2003), and all proteins of probability 0.95 or greater were added to the stage I database. Stage I samples from a previous PLRV study (DeBlasio et al., 2016a) were re-processed with the same informatics pipeline, and their proteins were also added to the stage I database to generate the final database used for cross-linking searches.

2.6 Preparation of cross-linked peptides

The desalted cross-linked peptides were fractionated by strong cation exchange (SCX) chromatography using an Agilent 1200 HPLC system equipped with a Phenomenex Luna SCX column. A binary linear gradient consisting of buffer A (5mM KH_2PO_4, pH 2.6, 30% acetonitrile (ACN)) and buffer B (5mM KH_2PO_4, pH 2.6, 30% ACN, 350mM KCl) was applied at a flow rate of 1.5mL/min for 97.5 min as follows: 0% B at 0 min, 5% B at 7.5 min, 60% B at 47.5 min, 100% B at 67.5 min, 100% B at 77.5 min, 0% B at 77.51 min to completion. Fractions were taken every 5 min starting at 17.5 min, and fractions were pooled as follows: 1-5, 6-7, 8, 9, 10, 11-14. Fractions 1-5 were not processed any further. The remaining fractions were then reduced to a final volume of 1-2 mL by vacuum centrifugation and adjusted to pH 8.0 with 1.5M NaOH. Following pH adjustment, each sample was incubated with 100µL of UltraLink monomeric avidin (Thermofisher) for 1 hour with gentle mixing. The avidin matrix was then washed 5 times with 3mL aliquots of 100mM ABC. Cross-linked peptides were eluted from the avidin matrix by two serial additions of 500µL of 70% acetonitrile-0.5% formic acid. The final eluent was dried to completion via vacuum centrifugation and resuspended in 30µL of 0.1% formic acid.

2.7 MS1 quantification of AGO1 peptides in wild-type and mutant PLRV co-IPs

Sample preparation, analysis, and MS1 quantification were performed as described in a previous publication from the same co-immunoprecipitation dataset (DeBlasio et al., 2018b). Ten peptides were used for MS1 quantification of PLRV CP as previously described (DeBlasio et al., 2018b). The following peptides were used for quantification of AGO1: SLYTAGPLPFVQK, QADAPQEALQVLDIVLR, RQPLGEGLESWR, DILQTVHHNAYADDPYAK, DILETVHHNAYANDPYAK, QELIQDLYTTR. Statistical analysis was performed on six replicates per treatment (two technical replicates for each of three biological replicates) using Microsoft Excel and R Studio. Graphs were generated using the ggplot2 R package (Wickham, 2009).

2.8 ReACT analysis of cross-linked peptides

A method to analyze cross-linked peptides in real time called, Real-time Analysis of Cross-linked peptides Technology (ReACT) was used to identify host-virus protein interactions (Weisbrod et al., 2013). Enriched cross-linked peptides were analyzed using a Waters NanoAcquity UPLC coupled to a Thermo Velos Fourier transform ion cyclotron resonance mass spectrometer (Velos-FT). Peptides were fractionated over a 60cm by 75µm inner diameter fused silica analytical column packed with Reprosil-Pur C8 (5µM diameter, 120Å pore size particles) by applying a linear gradient from 90% solvent A (0.1% formic acid in water), 10% solvent B (0.1% formic acid in acetonitrile) to 70% solvent A, 40% solvent B over 120 minutes at a flow rate of 300nL/min. The mass spectrometer was operated with the ReACT method (Weisbrod et al., 2013), in which a high resolution MS1 scan (50,000 resolving power at *m/z* 400) is taken and followed by a high resolution MS2 scan (50,000 resolving power at *m/z* 400) on the most abundant ion of charge state four or greater at a

normalized collision energy of 25. This MS2 scan is processed in real time to identify if the resulting fragments fulfill a mass relationship (precursor mass = reporter ion mass + peak 1 mass + peak 2 mass) within 20ppm, and if a pair is found then each peak is targeted for two MS3 scans in the ion trap. The MS3 spectra were searched using comet 2018.01 rev. 3 against the stage I database with a required modification of +197.032422 at an internal lysine (cross-linker stump), and a variable modification of +42.010565 (acetylation) at lysine (Eng et al., 2013). Cross-linking search results from comet were analyzed using XlinkProphet (Keller et al., 2019) and filtered to a minimum composite probability of 0.99.

2.9 AGO1 Silencing During PLRV Infection

Virus-induced gene silencing (VIGS) was used for functional analysis of the AGO1-CP interaction. The bipartite *Tobacco rattle virus* (TRV) system for VIGS in *N. benthamiana* was used essentially as previously described (DeBlasio et al., 2018a). The silencing construct for AGO1 was designed using the Sol Genomics VIGS tool to identify a region unique to the four AGO1 paralogs in *N. benthamiana* (Fernandez-Pozo et al., 2015). A TRV VIGS construct targeting GFP was used as a negative control for AGO1 silencing. *A. tumefaciens* strain LB4404 harboring an infectious clone of PLRV was used for agroinoculation of PLRV, as previously described (DeBlasio et al., 2016a). Mock inoculations were performed with the *A. tumefaciens* strain GV2260. All *A. tumefaciens* used for TRV and PLRV agroinoculation were diluted to an OD_{600} of 0.3 with fresh infiltration buffer before infiltration. TRV1 and TRV2-AGO1/GFP were mixed at a 1:1 ratio shortly before infiltration.

2.10 Optimization of Experimental Design for AGO1 VIGS

To determine the best sampling strategy for assessment of the effect of AGO1 VIGS on PLRV infection, plants were inoculated with PLRV and TRV at 3-4 weeks old by agroinfiltration of the third and fourth true leaves, respectively. Six plants each were inoculated with PLRV + TRV-AGO1 and PLRV + TRV-GFP. An uninoculated plant was used as a negative control for titer analysis.

Tissue samples for analysis of PLRV, TRV, and AGO1 expression were taken from the eighth true leaf at 14 days post infiltration and frozen in liquid nitrogen. One half of the leaf, excluding the midrib, was excised and frozen directly ('half leaf' samples). For leaf halves too large to fit in a 2mL tube, the ~2cm of leaf tissue nearest the midrib were taken instead. Leaf disc samples were taken from the other half of the leaf using a #3 cork borer. Petiole and midrib samples consisted of the entire petiole or midrib of the leaf, respectively, cut into several pieces when required to fit in a 2mL centrifuge tube. All samples were cryoground for 3 cycles of 3 minutes each at 25Hz in 2mL centrifuge tubes using a Mixer Mill 400 (Retsch). Sample tubes and Mixer Mill cassettes were cooled in liquid nitrogen for at least 3 minutes between cycles. Cryoground samples were stored at –80°C until use.

Tissue lysis was performed as follows: Powdered leaf discs were thawed on ice with 200µL of PBS per disc. Cryoground petiole and midrib samples were thawed on ice with 200µL of PBS per 12mg of tissue. For samples larger than 150mg, $1/10^{th}$ of the final volume of PBS was added directly to the samples, and a 100µL aliquot was diluted 10-fold in PBS after thawing. Due to the large volume of tissue in the half-leaf samples, an aliquot of tissue powder was transferred to a clean tube pre-chilled in liquid nitrogen and weighed, before thawing on ice with 200µL of PBS per 12mg of powdered tissue. 100µL of each sample was added to each well for ELISA analysis.

Sufficiently large samples were run in technical duplicate or triplicate and averaged after analysis; all others were run in singlet.

2.13 Assessment of AGO1 VIGS Effects on PLRV

Identical to the above with the following exceptions: Thirty plants each were inoculated with PLRV + TRV-AGO1 and PLRV + TRV+GFP. Ten plants each were inoculated with TRV-AGO1 + mock (*A. tumefaciens* strain GV2260) and TRV-GFP + mock. Five plants were inoculated with PLRV + mock. All plants were sampled at 12dpi, and petiole samples were cut up longitudinally to improve cryolysis. PLRV titer, TRV titer, and AGO1 expression were quantified by RT-qPCR as described below.

Photos were taken using a Canon Eos Rebel T6 or a Samsung Galaxy S6. Cropping, rotation, and minor adjustments to brightness/contrast were performed in Adobe Photoshop.

2.11 RNA Extraction and qRT-PCR

To validate AGO1 silencing and quantify virus titer, qRT-PCR was performed. RNA was extracted from cyroground samples using a Qiagen Plant RNeasy mini kit (Qiagen) following manufacturer's instructions, with the following changes: Tissue samples were incubated on ice with 10µL of lysis buffer per 1mg tissue with occasional vortexing until samples had thawed. RNA yields were quantified using a Nanovue (GE Healthcare Life Sciences), and 700µg of RNA for each sample was treated with TURBO DNase (Thermo Fisher) prior to cDNA synthesis with SuperScript III Reverse Transcriptase (Thermo Fisher), both following manufacturers' instructions.

Quantitative real-time PCR was performed on a QuantStudio 6K Flex qPCR Instrument using Fast SYBR Green Master Mix (Thermo), with the manufacturer-recommended thermocycling conditions. Two microliters of 10-fold diluted cDNA were used for each 10µL reaction, and all reactions were performed in technical triplicate. Two reference genes (clathrin and AP2) were used for normalization. Primer sequences can be found in Supplementary Table 3.1. A standard curve for each primer set was generated on a ten-fold dilution series of a mixture of all cDNA samples to calculate reaction efficiencies. Following the run, amplification and melt curves were manually inspected, and clear outliers or samples with erroneous melt curves were discarded. The remaining technical replicates were averaged to generate the mean Ct for each sample-primer combination. Samples for which less than two technical replicates remained were re-run. The relative abundance of PLRV, TRV, and AGO1 mRNA was calculated using the Pfaffl method, averaged across the two reference genes .

RNA extraction and cDNA synthesis were performed in randomized batches, and the plate layout for qPCR was randomized.

2.12 Silencing suppressor assay

Silencing suppressor assays were performed as previously described (Baumberger et al., 2007). Briefly, leaves were inoculated by agroinfiltration with a 1:1:1:1 mixture of *A. tumefaciens* containing expression constructs for GFP, a double-stranded GFP silencing construct (dsGFP), a silencing suppressor (P0 alone, P19 alone, or a cDNA infectious clone of PLRV), and either the PLRV CP or a negative control protein (FLAG-tagged GUS). The first three constructs were diluted to an OD_{600} of 0.3 prior to mixing and infiltration; PLRV CP and FLAG-GUS were diluted

to an OD_{600} of 0.6 prior to mixing and infiltration, due to low expression of the PLRV CP construct. Two leaves per plant on six plants were inoculated with GFP + dsGFP + P0 + CP/FLAG-GUS. Of these plants, half were inoculated on the same leaves with GFP + dsGFP + P19 + CP/FLAG-GUS, and half were inoculated with GFP + dsGFP + WT PLRV + CP/FLAG-GUS. The infiltrated area was marked with a black permanent marker on the upper side of leaves. GFP fluorescence in infiltrated areas was visualized under blacklight at 2 and 3 days post infiltration (data not shown) to confirm silencing suppression. GFP fluorescence was measured at 3 days post infiltration in leaf discs using a Biotek Synergy 2 microplate reader, as previously described (Pasin et al., 2014). The following parameters were used: excitation: 485/20 filter; emission: 528/20 filter; sensitivity = 70; endpoint mode; 510nm dichroic mirror. Relative fluorescence units were calculated by the Gen5 software. The average normalized fluorescence from two leaf discs per infiltrated spot was considered to be one biological replicate.

2.13 Data Analysis and Statistics

All data analysis was performed using Microsoft Excel and R Studio (Team, 2015; Team, 2013). Titer data were transformed by natural logarithm to improve normality. The following R packages were used during data analysis: readr, plyr, car, FSA, reshape (Ogle et al., 2019). The ggplot2, ggcorrplot, and RColorBrewer packages for R was used for graphical analysis of data (Wickham, 2009). Specific information on individual statistical tests can be found accompanying results.

3. Results

3.1 Partially Purified PLRV is Aphid-Transmissible

To obtain preparations of PLRV virions, protein was extracted from *N. benthamiana* leaves inoculated with an infectious clone of PLRV by agroinfiltration. As in other similar experiments, a PLRV virion purification protocol was used, stopping before sucrose gradient centrifugation, to enrich samples for virions without completely removing plant proteins (Alexander et al., 2017; DeBlasio et al., 2016a). To test that the resulting preparations contained intact virions, the aphid vector *Myzus persicae* was fed on artificial diet containing 50ng of partially purified PLRV, then transferred to uninfected recipient plants (Kim and Jander, 2007). Infection status of recipients was assessed by ELISA 3-4 weeks after aphid inoculation. All PLRV preparations used in this study were found to be aphid-transmissible, confirming the presence of intact, infectious virions.

3.2 PIR-based identification of host-virus interactions

Protein Interaction Reporter (PIR) technology uses a mass spectrometry-compatible protein-protein cross-linker to explore direct protein-protein interactions in a complex mixture (DeBlasio et al., 2016a; Tang and Bruce, 2010; Weisbrod et al., 2013). PIR has been successfully applied to partially purified preparations of PLRV virions, as well as the related *Turnip yellows virus* (TuYV; *Luteoviridae*: *Polerovirus*), in previous studies (Alexander et al., 2017; Chavez et al., 2012; DeBlasio et al., 2016a). To search for additional host-virus cross-links, we applied PIR to larger quantities of purified virions and included some optimizations in sample preparation and data analysis, as outlined above. Using the new protocol, a total of four host-virus cross-links were found (Table 3.1). Of these, two cross-links were confidently identified as between peptides in PLRV CP/RTP and the large chain of RuBisCO, and

a 60S ribosomal subunit. The remaining two cross-links also involved peptides in the CP region of the PLRV CP/RTP; however, the host peptide could not be confidently assigned to a single *N. benthamiana* protein.

Table 3.1: Host-virus cross-links in partially purified PLRV samples

Protein1 Name	Peptide 1[a]	Protein2 Name	Protein2 Gene ID[b]	Peptide 2[a]
PLRV CP/RTP	PHCK.VSSLQSYVNK$_{150}$FQITK.GGAK	Nb AGO1/10	Niben101Scf08137g02022.1*, Niben101Scf00887g01007.1, Niben101Scf01571g04001.1, Niben101Scf05146g06007.1 Niben101Scf11262g01008.1, Niben101Scf10638g02001.1	DRVK.I<u>K</u>K$_{179}$ALR.GVKV
		Nb RuBisCO large subunit	Niben101Scf11178g01008.1*, Niben101Scf05750g00009.1, Niben101Scf00173g09004.1	IHFR.VLAK$_{201}$ALR.MSGG
PLRV CP/RTP	QITK.GGAK$_{159}$TYQAR.MING	Nb AGO1/10	Niben101Scf08137g02022.1*, Niben101Scf00887g01007.1, Niben101Scf01571g04001.1, Niben101Scf05146g06007.1 Niben101Scf11262g01008.1, Niben101Scf10638g02001.1	DRVK.I<u>K</u>K$_{179}$ALR.GVKV
		Nb RuBisCO large subunit	Niben101Scf11178g01008.1*, Niben101Scf05750g00009.1, Niben101Scf00173g09004.1	IHFR.VLAK$_{201}$ALR.MSGG
PLRV CP/RTP	QITK.GGAK$_{159}$TYQAR.MING	Nb RuBisCO large subunit	Niben101Scf01734g01047.1 ,Niben101Scf11178g01008.1*, Niben101Scf00173g09004.1, Niben101Scf00568g04029.1	IKPK.LGLSAK$_{68}$NYGR.AVYE
PLRV CP/RTP	QITK.GGAK$_{159}$TYQAR.MING	Nb 60S ribosomal subunit	Niben101Scf02182g18008.1*, Niben101Scf02182g18003.1, Niben101Scf02073g04012.1 ,Niben101Scf02459g09004.1, Niben101Scf21171g00004.1	LGYK. AK$_{56}$QGYVVYR.VRVK

[a]Amino acid sequence of cross-linked peptides deduced from MS3 fragmentation and database searching. The four amino acids before and after each peptide are given as a reference, with peptide boundaries denoted by periods. Numbered lysines indicate cross-linking sites, where the number indicates amino acid position. Underlining indicates sidechain acetylation. Split rows for first two cross-links indicate ambiguous assignment for Peptide 2 (see Figure 3.1).

[b]Gene ID from *N. benthamiana* genome v1.0.1 (solgenomics.net). Asterisk denotes gene sequence from which flanking sequences and residue numbers for Peptide 2 are based.

The top hit was a peptide with the sequence VLAKALR, from homologs of the RuBisCO large chain, for which peaks corresponding to 11 of 12 b/y ions could be identified in one or more cross-linked spectra (Figure 3.1). The next best hit was a peptide with the sequence IKKALR, from homologs of AGOs 1 and 10, for which peaks corresponding to 9 of 10 b/y-ions could be identified in at least one cross-linked spectra. Of the 11 and 9 b/y-ions identified from RuBisCO or AGO1/10, respectively, 8 are common to both peptides, due to the shared KALR motif and the fact that the monoisotopic mass of VLA and IK(Ac), where K(Ac) is an acetylated lysine, are exactly equal. Three of the four remaining b- or y-ions unique to VLAKALR were found in at least one cross-linked spectrum, whereas one of two ions unique to IKKALR were identified.

As unique ions from both peptides were identified in at least one cross-linked spectrum, it is not possible to determine whether the CP/RTP was cross-linked to Rubisco, AGO1/10, or all three, without additional information.

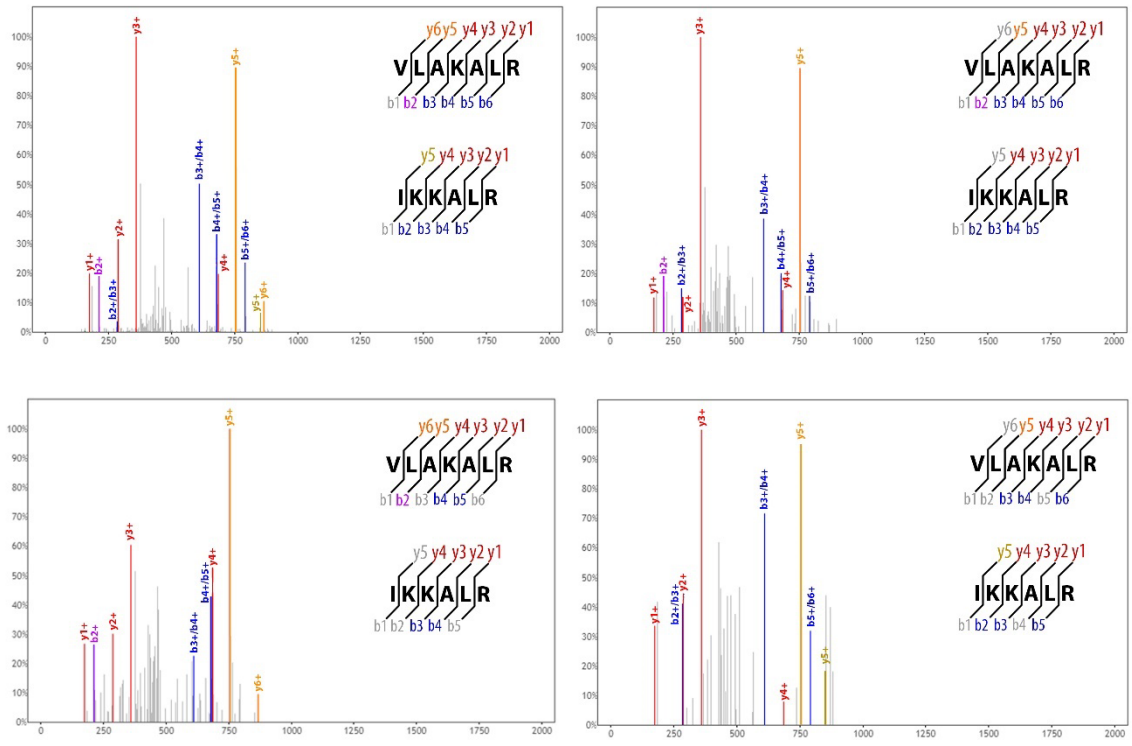

Figure 3.1: MS3 fragmentation pattern of one or more peptides found cross-linked to PLRV CP/RTP, with m/z (mass-to-charge ratio) on the x-axis and relative intensity on the y-axis. The sequence of the two top peptide hits for the spectra with their corresponding b- and y-ions are given on the right hand side. Gray represents ions that were not identified in the given spectrum. Blue and red represent b- and y-ions, respectively, which are shared between both peptides and were identified in the given spectrum. Magenta represents an ion unique to the VLAKALR peptide found in the given spectrum; gold denotes the same for the IKKALR peptide.

3.3 AGO1 co-immunoprecipitates with PLRV

To determine the most likely identity of the *N. benthamiana* peptide cross-linked to CP/RTP, we investigated whether the RuBisCO large chain homologs and/or the AGO1/10 homologs were found in complex with PLRV by co-immunoprecipitation. Previous data from our group has shown that *N. benthamiana* AGO1 homologs co-immunoprecipitate with PLRV CP in both locally infected *N. benthamiana* and systemically infected potato (DeBlasio et al., 2015b; DeBlasio et al., 2016b). In addition to wild-type (WT) PLRV, AGO1 was found to co-immunoprecipitate with a PLRV mutant lacking the RTD (ΔRTD PLRV), a mutant lacking the C-terminal half of the RTD (ΔRTC PLRV), and an amber stop codon mutant which produces RTP but not free CP (ΔCP PLRV), indicating that neither the RTD nor virions are required for interaction (DeBlasio et al., 2015a; DeBlasio et al., 2015b). No peptides from the RuBisCO large chain were found to be significantly enriched in any of the PLRV co-immunoprecipitations.

Although these studies clearly established that AGO1 is found in complex with WT PLRV, ΔRTD PLRV, ΔRTC PLRV, and ΔCP PLRV, we were interested in quantifying more accurately whether AGO1 is differentially abundant in the mutant PLRV co-IPs. To do so, we quantified the MS1 peak areas for AGO1 and CP peptides in a previously published co-immunoprecipitation dataset (DeBlasio et al., 2018b).

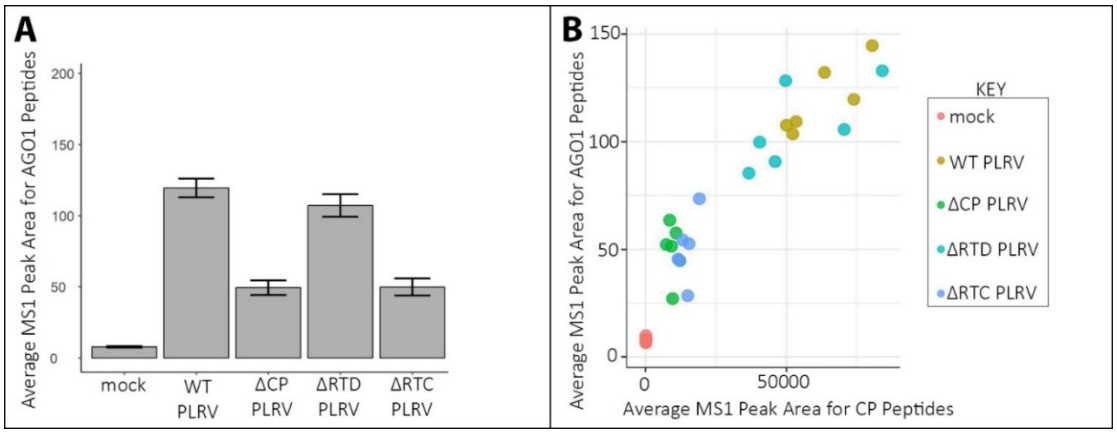

Figure 3.2: AGO1 is found in complex with PLRV CP. A): Average MS1 peak area for peptides from AGO1 found co-immunoprecipitating with PLRV CP/RTP. B) Average MS1 peak area for AGO1 peptides versus average MS1 peak area for CP peptides. Each point represents one biological replicate averaged over two technical replicates.

MS1 peak quantification clearly verified that AGO1 is enriched in all PLRV co-IPs, compared to mock-inoculated controls (Figure 3.2A). While it appeared from the raw data that AGO1 was less enriched in the ΔRTC and ΔCP mutants, plotting the average MS1 peak area for AGO1 peptides versus the average MS1 peak area for CP peptides revealed that this difference is likely due to the reduced levels of CP (bait) in these samples (Figure 3.2B).

Overall these data support an association between PLRV CP and AGO1, although we cannot determine whether it is direct or indirect from the co-immunoprecipitation data. Notably, none of the RuBisCO large chain or AGO10 homologs in *N. benthamiana* were found to be significantly enriched in PLRV vs control co-immunoprecipitations. Therefore, we have evidence independent of the cross-linking data for a CP-AGO1 association, but not for a CP-Rubisco or CP-AGO10 association. Furthermore, because RuBisCO is a key photosynthetic enzyme in plants, it cannot be knocked out *in vitro*, which greatly limits our ability to study its function in viral infection. For these reasons, we chose to perform further functional experiments only on AGO1.

3.4 Optimization of a PLRV/TRV Co-Infection Protocol for VIGS

The use of *Tobacco rattle virus* (TRV; *Virgaviridae*: *Tobravirus*) for targeted virus-induced gene silencing (VIGS) in *N. benthamiana* is well established for functional characterization of plant proteins, both in healthy plants and in the context of infection with other pathogens (DeBlasio et al., 2015a; DeBlasio et al., 2018a; Odokonyero et al., 2017; Senthil-Kumar and Mysore, 2014; Velasquez et al., 2009). To explore the role of AGO1 during PLRV infection, a TRV VIGS construct was developed which contained a small fragment of the AGO1 gene (TRV-AGO1). As TRV infection causes mild symptoms in *N. benthamiana* even when no plant genes

are targeted for silencing, a TRV construct targeting GFP (TRV-GFP) was used as a negative control.

Assessment of PLRV titer in *N. benthamiana* is typically performed on leaf discs, to ensure sample size consistency and facilitate tissue lysis. However, we have observed that PLRV titer is relatively variable in leaf discs taken from systemically infected plants, even within a single leaf. Initial experiments showed that the variability in PLRV titer was further exaggerated in plants co-infected with TRV-AGO1, hampering statistical analysis. Because PLRV is phloem-limited, and does not move uniformly throughout a leaf (Esau and Hoefert, 1972b), we hypothesized that the variability in titer between leaf discs may be attributed to a combination of spatial variation within a leaf and varying quantities of phloem tissue in different disc samples.

To test whether modifying sampling method would reduce variability, the eighth true leaf of plants systemically infected with PLRV and recombinant TRV for VIGS of AGO1 (TRV-AGO1) or a TRV control targeting GFP (TRV-GFP) was split into six sample types at 12 days post inoculation (dpi) (Figure 3.3). The left half of the leaf was sampled as in previous studies, taking one disc each from the proximal, center, and distal portion of the leaf. The midrib and petiole of the leaf were then taken as separate samples. Finally, the remaining half of the leaf was taken in its entirety. Analysis of PLRV titer in these samples revealed that titer was more variable in leaf discs taken from the distal portion of the leaf than the proximal (Figure 3.3). Titer in both the midrib and half-leaf samples was highly variable, particularly in plants co-infected with TRV-AGO1. In contrast, variability in PLRV titer was noticeably reduced in petiole samples, as compared to all other sample types. Therefore, a petiole sampling strategy was used for all subsequent experiments.

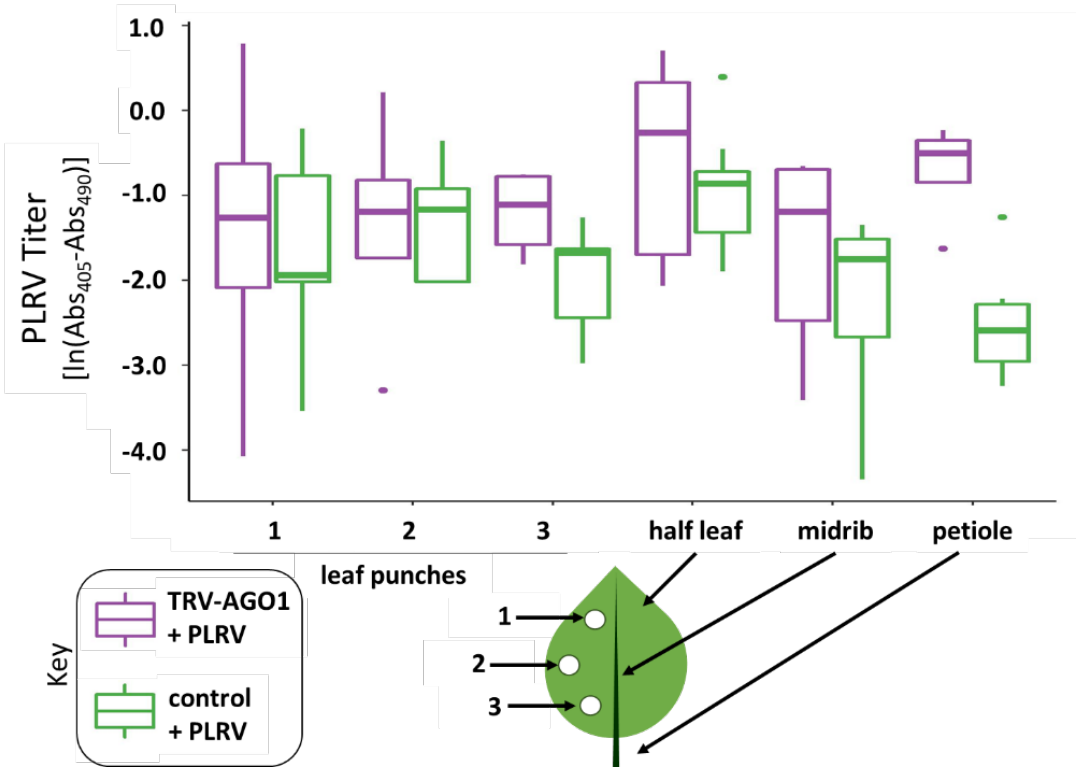

Figure 3.3: Optimization of sampling strategy for VIGS in PLRV-infected *N. benthamiana*. Top: Box-and-whisker plot of PLRV titer in plants co-infected with TRV targeting AGO1 (purple) or TRV targeting GFP (green; negative control), as measured by DAS-ELISA. PLRV titer is given as the natural log of the blank-subtracted difference in absorbance from 405 to 490nm. A diagram below shows the different tissues sampled.

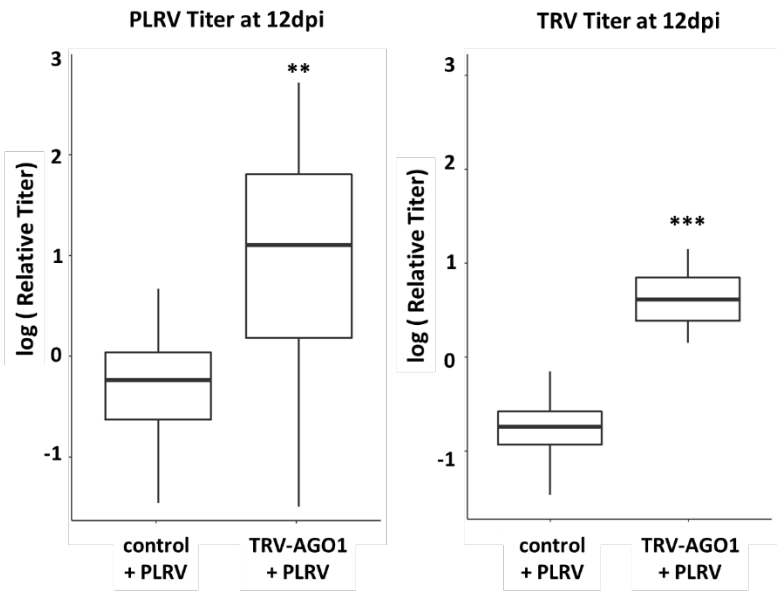

Figure 3.4: Effects of VIGS of AGO1 on PLRV and TRV titer. Box-and-whisker plots of PLRV (left) and TRV (right) titer in plants co-infected with TRV targeting AGO1 or GFP (control), as measured by RT-qPCR. Titer is given as the natural log of the blank-subtracted expression relative to a sample containing equal quantities of cDNA from all samples, normalized to two reference genes. **$p \leq 0.01$, ***$p \leq 0.001$ by Welch's two-tailed t-test.

3.5 Knocking down AGO1 affects PLRV and TRV titer

To probe the role of AGO1 in PLRV infection, plants were co-inoculated by agroinfiltration with PLRV and either TRV-AGO1 or TRV-GFP (negative control). At 15dpi, the petiole of the eighth true leaf of each plant was weighed and frozen for RNA extraction, cDNA synthesis, and qPCR. Although analysis of PLRV titer by ELISA has the advantage of measuring the presence of virions, rather than viral RNA, titer analysis was performed by qPCR to facilitate concurrent assessment of TRV titer and AGO1 expression.

Plants co-infected with TRV-AGO1 and PLRV were found to support significantly higher PLRV titer than plants infected with the TRV-GFP control and PLRV ($t(20) = 3.7$, $p= 0.0013$ by Welch's t-test; Figure 3.4A). Additionally, PLRV titer was about 4.9 times more variable in TRV-AGO1 plants than in the controls ($F = 4.9$, $p = 0.0013$ by two-tailed F-test). Silencing AGO1 by VIGS also significantly increased TRV titer ($t(33) = 13$, $p = 1.3E-14$ by Welch's t-test; Figure 3.4B), but did not impact variability ($F = 0.93$, $p = 0.90$ by two-tailed F-test).

Unlike leaf discs, petiole samples are somewhat recalcitrant to disruption by cryogrinding, even after multiple cycles. This is particularly noticeable for large petioles. To determine whether petiole size affected efficiency of PLRV extraction, a correlation analysis was performed. No significant correlation was found between sample weight and PLRV titer in petiole samples ($p= 0.611$, $tau = -0.0857$ by Kendall's rank correlation tau), indicating that PLRV was extracted with equal efficiency from small and large petioles (Supplementary Figure 3.1).

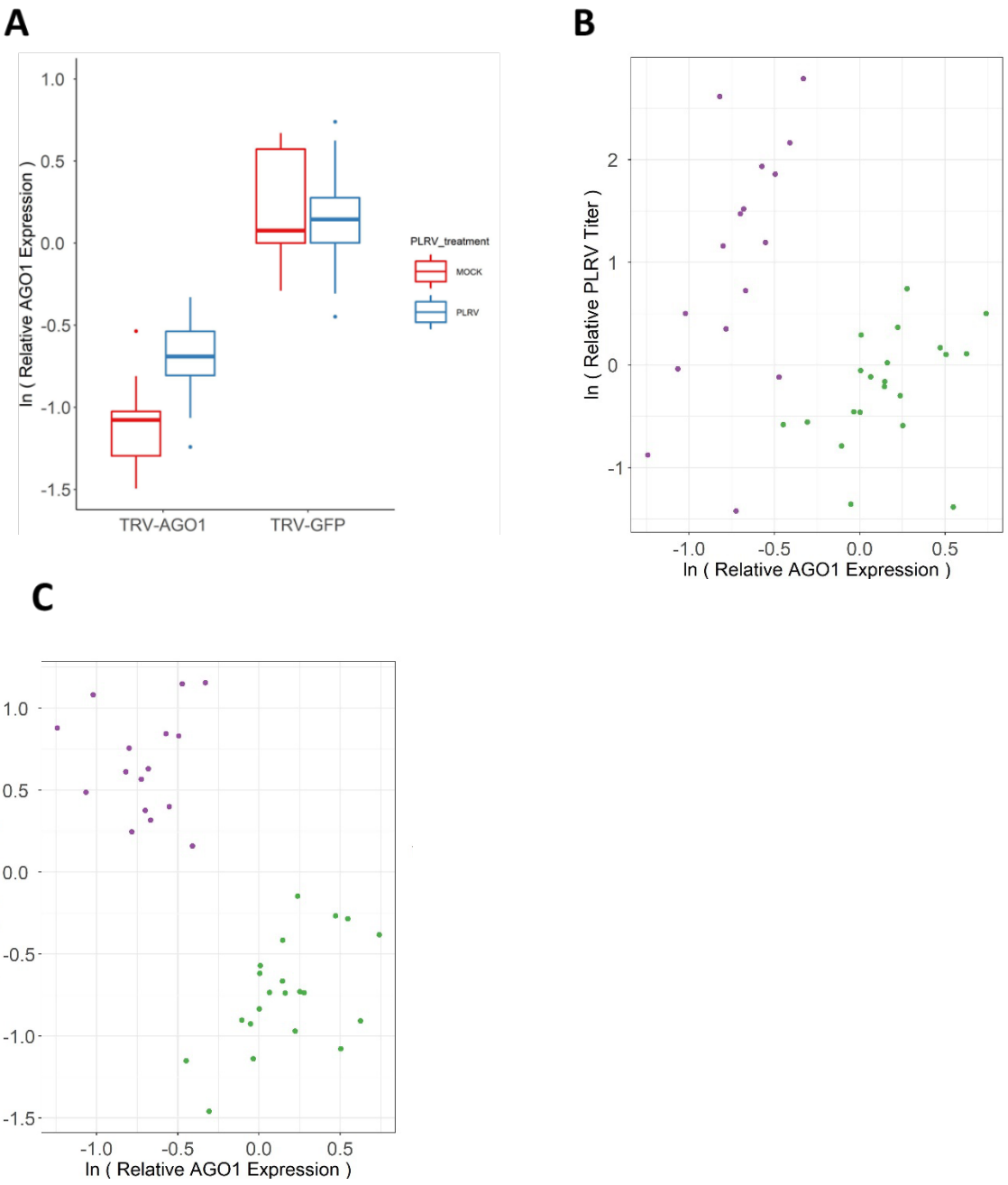
A
1.0
0.5
0.0
-0.5
-1.0
-1.5
ln (Relative AGO1 Expression)
TRV-AGO1
TRV-GFP
PLRV_treatment
MOCK
PLRV
B
2
1
0
-1
ln (Relative PLRV Titer)
-1.0
-0.5
0.0
0.5
ln (Relative AGO1 Expression)
C
1.0
0.5
0.0
-0.5
-1.0
-1.5
ln (Relative TRV Titer)
-1.0
-0.5
0.0
0.5
ln (Relative AGO1 Expression)

Figure 3.5: Interrelationships between PLRV titer, TRV titer, and AGO1 expression.

A: Box-and-whisker plots of relative AGO1 expression in PLRV-infected (red) or mock-inoculated (blue) plants co-infected with TRV targeting AGO1 or GFP (control), as measured by RT-qPCR. AGO1 expression is given as the natural log of the blank-subtracted expression relative to a sample containing equal quantities of cDNA from all samples, normalized to two reference genes. **$p \leq 0.01$ by Welch's two-tailed t-test.

B: Scatterplot of PLRV titer (y-axis) versus AGO1 expression (x-axis) in plants co-infected with PLRV and TRV-GFP (green) or PLRV and TRV-AGO1 (purple). Titer and expression were measured by RT-qPCR and are given as the natural log of the blank-subtracted expression relative to a sample containing equal quantities of cDNA from all samples, normalized to two reference genes. Each data point represents one sample averaged over technical replicates.

C: Scatterplot of TRV titer (y-axis) versus AGO1 expression (x-axis) in plants co-infected with PLRV and TRV-GFP (green) or PLRV and TRV-AGO1 (purple). Titer and expression were measured by RT-qPCR and given as the natural log of the blank-subtracted expression relative to a sample containing equal quantities of cDNA from all samples, normalized to two reference genes. Each data point represents one sample averaged over technical replicates.

3.6 PLRV infection only affects AGO1 homeostasis when AGO1 is also knocked down by VIGS

In addition to PLRV and TRV titer, AGO1 expression was assessed by qPCR. TRV-mediated silencing of AGO1 was clearly evident in TRV-AGO1-infected plants, which had markedly reduced AGO1 expression compared to TRV-GFP-infected plants, regardless of PLRV infection status ($t(52) = -12.1$, $p = 8.8e-17$ by Welch's t-test).

Because AGO1 expression in plants is auto-regulated by a feedback loop, we expected that P0-mediated degradation of AGO1 protein may result in a compensatory rise in AGO1 expression. However, PLRV infection was found to significantly increase AGO expression only in plants co-infected with TRV-AGO1, where AGO1 homeostasis was already disrupted by VIGS ($t(17) = -3.61$, $p = 0.0021$ by Welch's t-test; Figure 3.5A). AGO1 expression was unaffected by PLRV expression in plants co-infected with TRV-GFP.

3.7 Correlations between AGO1 expression and virus titer

Finally, we investigated whether changes in AGO1 expression were correlated with changes in PLRV titer, TRV titer, or both, in individual samples. There was a significant positive correlation between PLRV titer and AGO1 expression among plants co-infected with PLRV and TRV-AGO1 ($r = 0.57$, $n = 14$, $p = 0.022$ by Pearson's product-moment correlation), although variation in AGO1 expression accounted for only ~32% of the variation in PLRV titer (Figure 3.5B). There was a weaker positive correlation, which was not statistically significant, between PLRV titer and AGO1 expression in control plants co-infected with PLRV and TRV-GFP ($r = 0.37$, $n = 19$, $p = 0.099$). However, plants infected with TRV-AGO1 on average had higher PLRV titer and lower AGO1 expression than plants infected with TRV-GFP.

In contrast, there was a significant positive correlation between TRV titer and AGO1 expression in plants co-infected with PLRV and TRV-GFP ($r = 0.55$, $n = 19$, $p = 0.0098$), but not in plants infected with PLRV and TRV-AGO1 ($r = -0.0012$, $n = 14$, $p = 0.9964$) (Figure 3.5C). Variation in AGO1 expression accounted for about 30% of the variation in PLRV titer in plants co-infected with PLRV and TRV-GFP. As with PLRV titer, however, TRV titer was, on average, higher, and AGO1 expression lower in plants infected with PLRV and TRV-AGO1 than in plants infected with PLRV and TRV-GFP.

Importantly, qPCR measures only AGO1 expression, which does not necessarily correlate with AGO1 protein levels. While AGO1 expression and virus titer were weakly correlated, at best, the relationships may be quite different with respect to AGO1 protein, particularly as P0 is known to promote AGO1 degradation at the protein level (Baumberger et al., 2007; Bortolamiol et al., 2007).

No significant correlation was found between TRV titer and PLRV titer, either in plants infected with PLRV and TRV-GFP ($r = 0.14$, $n = 19$, $p = 0.54$) or those infected with PLRV and TRV-AGO1 ($r = -0.0075$, $n = 14$, $p = 0.98$).

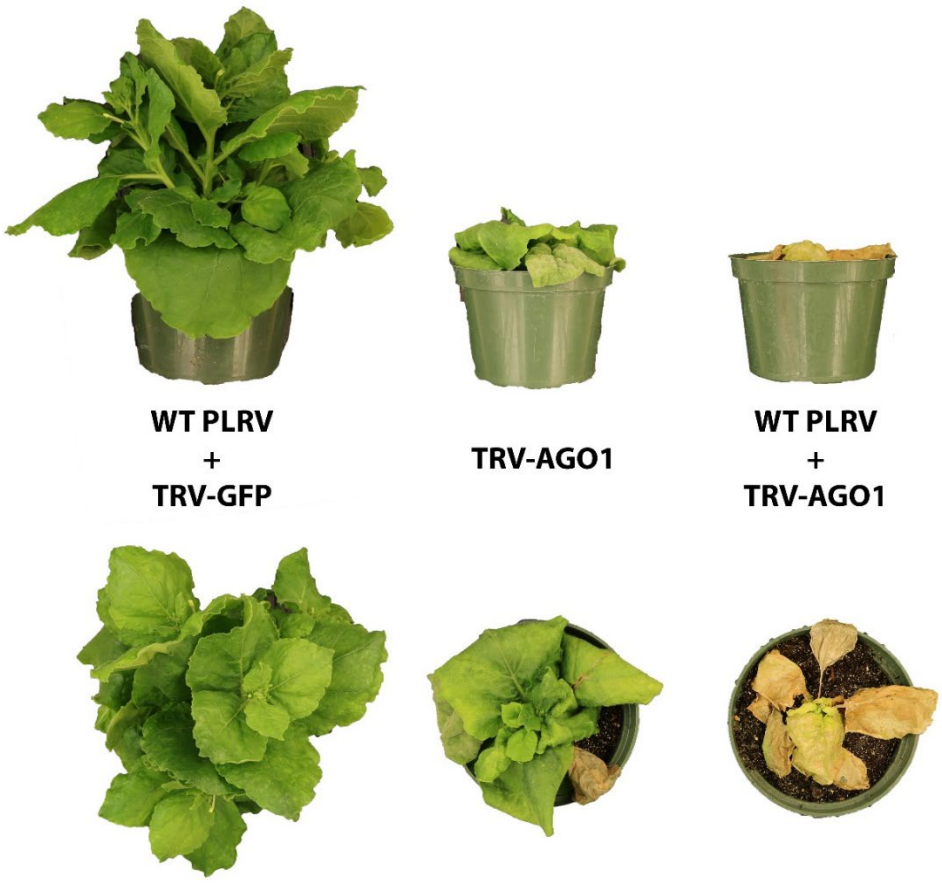

Figure 3.6: Combined effects of VIGS targeting AGO1 and PLRV infection are lethal. Representative photos of *N. benthamiana* plants at 24dpi infected with (left to right): WT PLRV and TRV-GFP; TRV-AGO1 alone; WT PLRV and TRV-AGO1.

3.8 Combined effects of TRV-AGO1 and PLRV

Knocking down AGO1 expression by infection with TRV-AGO1 caused moderate developmental defects in *N. benthamiana*, including stunting and leaf deformities (Figure 3.6), similar to the phenotype of published AGO1 mutants (Morel et al., 2002). Nonetheless, plants infected with TRV-AGO1 alone exhibited continual growth and would often flower if left long enough.

In contrast, plants co-infected with PLRV and TRV-AGO1 entered a rapid decline 2-4 weeks after inoculation (Figure 3.6). Necrosis and collapse, beginning with the oldest leaves, typically gave way to complete or near-complete defoliation, and often death, of the plant within 3-6 weeks, depending on the age of the plants at the time of inoculation. This effect cannot be attributed to PLRV infection alone, which causes only mild stunting and chlorosis in *N. benthamiana.* Co-infection with PLRV and TRV-GFP is also non-lethal, causing mild stunting and mottled chlorosis. The rapid decline only of plants co-infected with TRV-AGO1 and PLRV was reproducible over more than three iterations of this experiment.

3.9 Silencing suppression by P0 is enhanced by co-expression of PLRV CP

Finally, we tested whether PLRV CP has a positive or negative effect on silencing suppression by P0. To do so, we used a classic silencing suppressor assay, in which *N. benthamiana* leaves are co-agroinfiltrated with constructs for both expression and silencing of GFP (GFP and dsGFP, respectively), as well as the silencing suppressor protein(s) of interest. Without a silencing suppressor present, the GFP-silencing construct effectively prevents GFP expression. However, co-infiltration with a silencing suppressor restores GFP expression and fluorescence.

To test the effect of PLRV CP on silencing suppression, we co-infiltrated

leaves with GFP + dsGFP and either PLRV CP or a control protein (FLAG-tagged GUS), and a variety of silencing suppressors. Three days after infiltration, 5mm leaf discs were taken from the infiltrated area, and GFP fluorescence was measured using a 96-well plate reader. We found that GFP fluorescence was significantly brighter, indicating stronger silencing suppression, when P0 was co-expressed with PLRV CP than when P0 was co-expressed with the FLAG-GUS control on the same leaf (Figure 3.7; $p = 0.009$ by paired Wilcoxan signed rank test). This finding suggests that the PLRV CP may also have silencing suppressor activity, or that the CP assists P0 in promoting AGO1 degradation.

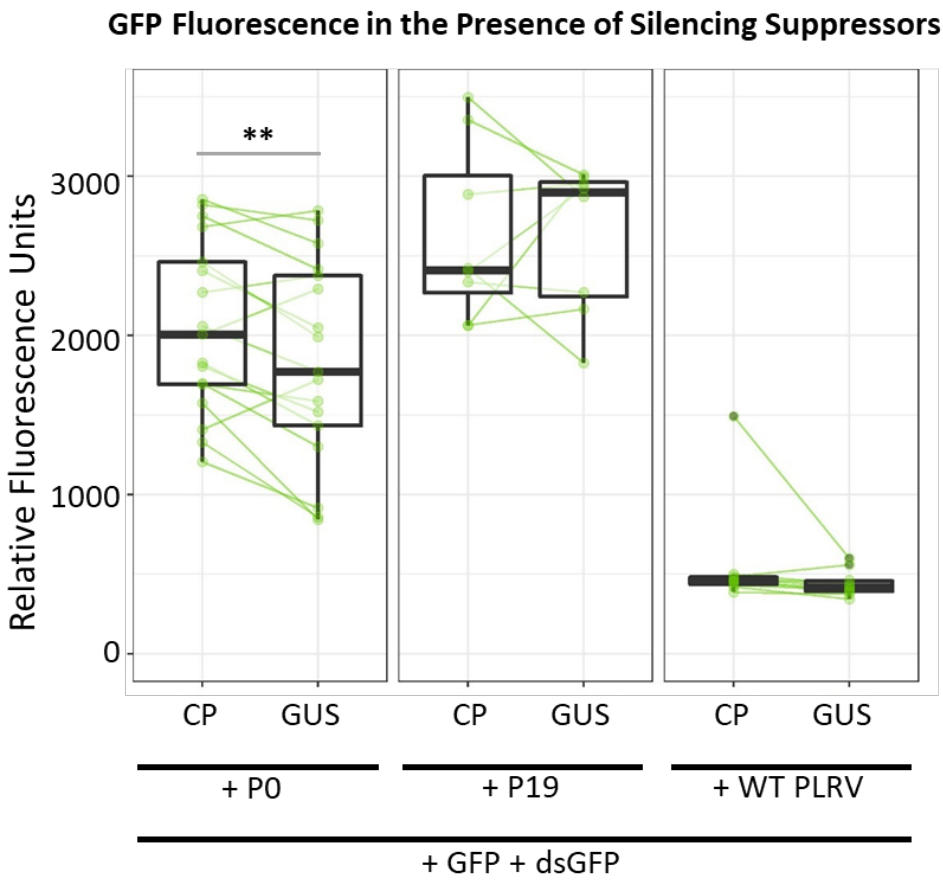

Figure 3.7: PLRV CP enhances silencing suppression by P0. Box-and-whisker plot of average relative fluorescence units (RFU) in leaf discs co-infiltrated with the designated constructs at 5dpi, overlaid with RFU values from individual leaf discs (green dots). Green lines connect leaf discs taken from the same leaf. **$p \leq 0.01$ by paired Wilcoxan signed rank test.

Substitution of a full-length cDNA clone of PLRV for P0 in silencing suppression assays markedly decreased silencing suppression, likely due to reduced expression of P0. No significant difference in GFP fluorescence was found between areas co-infiltrated with PLRV and CP versus PLRV and FLAG-GUS ($p=0.06$ by paired Wilcoxan signed rank test). While this may indicate that virions or other viral proteins interfere with CP's effect on silencing suppression, it may also be that the baseline level of silencing suppression in these treatments was too weak to detect differences.

We also tested whether CP expression affected the silencing suppressor activity of the protein P19: a silencing suppressor from tombusviruses, which is believed to function by sequestering siRNAs. GFP fluorescence was found to be similar in plants co-expressing P19 and PLRV CP as in controls co-expressing P19 and FLAG-GUS ($p=0.84$ by paired Wilcoxan signed rank test), suggesting that PLRV does not have silencing suppressor activity independent of P0, and that PLRV CP does not affect P19 activity.

4. Discussion

4.1 Evidence for an association between PLRV CP/RTP and plant AGO1

While peptide identification by mass spectrometry is often presented as a straightforward process, several situations can complicate peptide-spectral matching. In our data set, we found a peptide cross-linked to PLRV CP which we were unable to confidently assign to a single *N. benthamiana* protein due to the highly similar sequence of a peptide from the RuBisCO large chain to an unrelated peptide found in four homologs of AGO1 and two homologs of AGO10. In addition to eight b- and y-ions common to both peptides, at least one transition unique to each peptide was

present in one or more analyzed spectra. Notably, one of the most intense peaks in all four spectra was assigned to the unique y5 ion of the RuBisCO peptide. We were unable to assign a single peptide identity to these spectra; however, the presence of unique ions from both peptides suggests that these spectra may, in fact, be chimeric, containing both peptides.

Argonaute proteins are a highly conserved family of proteins present in both eukaryotes and prokaryotes. In eukaryotes, AGO proteins have been studied primarily for their role in generation and function of small interfering RNAs (siRNAs), which silence genes at the transcriptional and post-transcriptional levels. RNA silencing is important for regulation of many endogenous genes, but is also believed to be plants' primary defense against viruses. Triggered by the presence of double-stranded RNA (dsRNA), which may be produced during replication or as secondary structure in the viral genome, RNA silencing begins with cleavage of dsRNAs by DICER-like (DCL) proteins, producing primary small interfering RNAs (siRNAs): short, single-stranded fragments 21-24 nucleotides (nt) in length. Primary siRNAs may be amplified by RNA-dependent RNA polymerases, producing secondary siRNAs, or loaded into proteins in the Argonaute family, forming the RNA-induced silencing complex (RISC). The RISC targets ssRNA molecules with homology to its loaded siRNA for silencing via translation inhibition or cleavage, often through endogenous slicer activity of AGO proteins. siRNAs are mobile over short and long distances, and can trigger systemic silencing of homologous transcripts.

An association between poleroviruses and AGO1 has been known since 2007, when the ability of P0 to promote AGO1 degradation was discovered (Baumberger et al., 2007; Bortolamiol et al., 2007). Although a direct interaction between P0 and virions or any other polerovirus proteins has not been demonstrated previously, AGO1

has been shown to co-immunoprecipitate with wild-type PLRV in multiple hosts, as well as with mutants which do not produce the RTD, RTC, or free CP and virions (DeBlasio et al., 2015a; DeBlasio et al., 2015b; DeBlasio et al., 2016b). These data indicate that virions are not required for the AGO1-CP association, nor is any part of the RTD. Across all samples, there was an approximately linear relationship between the average MS1 peak area for CP peptides and the average MS1 peak area for AGO1 peptides, suggesting that the CP-AGO1 association is mediated by the CP domain, as is also suggested by the PIR data.

The AGO1 peptide putatively cross-linked to a CP/RTP peptide was found to be acetylated at the lysine immediately prior to the cross-linked residue. The single report of lysine acetylation in AGO1 in the current literature is in human AGO1 (Zhao et al., 2010), at a site about 200 amino acids downstream of the *N. benthamiana* acetylation site in our dataset. Both sites are located within the MID domain, which is involved in recognition of the 5' end of the guide sRNA. The functional and structural importance of lysine acetylation in AGO1 is currently unknown.

Although we do not have co-immunoprecipitation data to support an association between CP and AGO10 or RuBisCO, we cannot rule out that either one occurs but was not captured in these data sets. Many other chloroplastic proteins have been found to co-immunoprecipitate with PLRV, and silencing of phytoene desaturase, a chloroplastic enzyme, has been shown to increase PLRV titer (DeBlasio et al., 2015a; DeBlasio et al., 2015b; DeBlasio et al., 2016b; DeBlasio et al., 2018a). However, it is also possible that the putative CP-RuBisCO interaction found here was the result of non-specific binding, particularly as RuBisCO is the most abundant enzyme in plants.

4.2 PLRV titer is less variable in petiole samples

To explore the function of the CP/RTP-AGO1 association, we used a TRV-based VIGS approach. However, optimization of sampling strategy was necessary to maximize statistical power, as PLRV titer was found to be especially variable in leaf discs from plants co-infected with PLRV and TRV-AGO1. This observation is not unique to our system, as the distribution of luteovirid virions in infected plants has been observed to be non-uniform, with some heavily infected cells neighboring cells that do not appear infected at all (Esau and Hoefert, 1972b). Six different sample types (three leaf discs, midrib, petiole, and half of the leaf) were assessed for variability in PLRV titer.

Mean titer was found to similar in all leaf disc samples in a treatment, regardless of where on the leaf the sample was taken from. However, variability in PLRV titer was noticeably greater in samples from the distal portion of the leaf than the proximal. Although PLRV infection begins from the proximal portion of the leaf and moves distally, the similar mean titer across leaf samples suggests that variability is not due to incomplete infection of the distal portion of the leaf at the time of sampling. However, it is possible that tissue in the proximal part of the leaf has had more time for virus replication and host defenses to reach an equilibrium, decreasing variability in titer, whereas random variation is a more dominant factor in the distal part of the leaf.

We predicted that sampling one entire half of each leaf might reduce variability, as each sample would represent the average titer across the full length of the leaf. However, half-leaf samples were found to be just as variable as leaf punches, indicating that plant-to-plant variability was as important as, or more important than, spatial variation within a leaf.

We also hypothesized that variability in leaf disc samples may be due in part to the phloem-limited nature of PLRV. Perhaps some leaf discs had more phloem tissue in them than others, which, compounded with the random nature of PLRV movement from cell-to-cell on a small scale, would account for the large variability seen in leaf disc samples. Therefore, we predicted that sampling midribs or petioles, which should contain a more consistent number of phloem cells, might reduce variability in observed PLRV titer. Interestingly, we found that PLRV titer was just as variable in midrib samples as in leaf discs; however, PLRV titer was markedly more consistent in petiole samples. Perhaps this is due to small amounts of residual leaf tissue attached to midrib samples, or to the putatively stronger influence of random variability in the distal portion of the leaf. Based on the leaf disc samples, PLRV titer may be less variable in the proximal part of the leaf in general; therefore the sampling strategy likely to be least variable would be one that sampled the proximal part of the leaf in a way that captured a consistent number of phloem cells each time. This would explain why petioles, which are the most proximal of all samples tested, were found to have less variable PLRV titer.

To show that the difference in mean PLRV titer between TRV-GFP- and TRV-AGO1-infected plants was not due simply to the smaller size, and therefore easier lysis, of the TRV-AGO1 petioles, we looked for a correlation between sample size and PLRV titer. As no correlation could be found, we concluded that sample size did not have an inherent effect on PLRV titer. This may be because the contents of the phloem and xylem in petioles diffuse out into the lysis buffer from the cut ends, as in sap collection protocols using cut-end exudates, passive diffusion into buffer, or centrifugation (Hijaz and Killiny, 2014; Tetyuk et al., 2013). Although not explored here, it would be interesting to see if titer variability in different sample types varies similarly for TRV or another virus that is not phloem-limited.

4.3 PLRV titer, TRV titer, and AGO1 expression are interconnected

Argonaute-family proteins, including AGO1, are major components of the RNA silencing pathway, which is the primary plant defense against RNA viruses, and AGO1 mutants have been shown to be hypersensitive to virus infection (Morel et al., 2002). Additionally, P0, which functions by promoting AGO1 degradation, is generally required for systemic movement of poleroviruses (Rashid et al., 2019; Zhuo et al., 2014) and also affects accumulation of virions in local infections (Zhuo et al., 2014; Ziegler-Graff et al., 1996). It is unsurprising, therefore, that knocking down AGO1 expression by VIGS was found to significantly increase both PLRV and TRV titer. That said, PLRV's response to AGO1 silencing was markedly different than TRV's with respect to titer variability: only PLRV titer was significantly more variable in plants co-infected with TRV-AGO1 plants than in the TRV-GFP controls. This may be attributed to the complex relationship between poleroviruses and AGO1, which both influence one another; however, it is not known at this time whether TRV and AGO1 are similarly intertwined. It has been shown that 16K, the tobravirus silencing suppressor protein, inhibits the formation of RISCs, but it is unknown to what extent this impacts AGO1 in particular (Fernandez-Calvino et al., 2016). Unfortunately, previous studies on virus infection in AGO1 knockdown or hypomorphic plants utilized northern blotting to assess virus titer; therefore, no estimate of variability was performed (Dzianott et al., 2012; Garcia-Ruiz et al., 2015; Morel et al., 2002; Qu et al., 2008).

Although both PLRV and TRV titer were both clearly higher in TRV-AGO1-infected plants, which had lower AGO1 expression, there was, at best, a weak positive correlation between virus titer and AGO1 expression (accounting for, at most, ~32%

of the variability in titer). However, it should be noted that AGO1 expression may not result in (or from) changes in AGO1 protein levels, particularly in a system like this where outside manipulation of both AGO1 expression (by VIGS) and AGO1 protein levels (by P0) are occurring simultaneously.

Interestingly, PLRV infection was not found to significantly affect AGO1 expression in TRV-GFP control plants. This agrees with a recent report that levels of FLAG-tagged AGO1 appeared similar in plants infected with TuYV as in uninfected plants (Bortolamiol-Becet et al., 2018). Both our results and the TuYV study appear to disagree with previous literature showing that P0 promotes degradation of AGO1; however, the latter studies utilized transient expression of P0 alone, rather than systemic infection with the entire virus. It's likely that smaller effects on AGO1 during systemic infection are masked by our inability to effectively separate phloem tissue from other tissues. Additionally, our data from the silencing suppressor assay shows that silencing suppression even in infiltrated tissue is much stronger when P0 is expressed alone than as part of an infectious clone. It may be that silencing suppression in systemically infected tissue is not strong enough to affect AGO1 homeostasis, either because P0 is expressed to lower levels, or because other viral proteins modulate P0 activity, as posited below.

However, PLRV infection was found to significantly increase AGO1 expression in plants co-infected with TRV-AGO1. This increased expression may be an attempt by the plant to compensate for low AGO1 activity in plants with high levels of P0. Alternatively, or additionally, silencing AGO1 at the transcript level by VIGS may render the plant more sensitive to P0 activity.

4.4 Phenotypic effects of infection with TRV-AGO1 and PLRV

In addition to its role in antiviral defense, AGO1 is also critical for growth and development in plants. AGO1 null mutants in *Arabidopsis* exhibit severe developmental and morphological defects and are infertile (Arribas-Hernandez et al., 2016; Bohmert et al., 1998; Carbonell et al., 2012; Vaucheret et al., 2004). The stunting and morphological defects present in TRV-AGO1-infected plants in this study are similar to previously published phenotypes of plants with hypomorphic AGO1 alleles (Fagard et al., 2000; Jones et al., 2006; Morel et al., 2002) and a previous study also using TRV for VIGS of AGO1 (Odokonyero et al., 2017). Despite the relatively severe stunting, *N. benthamiana* plants infected with TRV-AGO1 alone remained green and growing throughout the experiment, even several months after inoculation.

In contrast, plants co-infected with PLRV and TRV-AGO1 were consistently observed to experience severe necrosis and leaf drop beginning around 2-4 weeks post inoculation, which often resulted in complete defoliation and plant death. These effects could be related to the abnormally high PLRV and TRV titer in these plants. However, a recent study showing that VIGS of phytoene desaturase dramatically increases PLRV titer without significant additive phenotypic effects suggests that high titer alone may not be sufficient to cause plant death (DeBlasio et al., 2018a).

Alternatively, we hypothesize that the lethal effects of co-infection with PLRV and TRV-AGO1 are the result of extremely low levels of AGO1. While TRV-AGO1 and PLRV P0 individually knock down AGO1 at the transcript and protein levels, respectively, the combination of both may effectively silence AGO1 entirely, resulting in death in plants already compromised by virus infection. Similarly, a previous study showed that infection of *Arabidopsis* with *Cucumber mosaic virus* (CMV;

Bromoviridae: *Cucumovirus*) was lethal only in plants with hypomorphic AGO1 alleles (Morel et al., 2002). At the time, the authors proposed that lethality was due to the high CMV titer in AGO1-deficient plants. However, the CMV silencing suppressor protein (2b) inhibits AGO1 activity (Zhang et al., 2006); therefore, low AGO1 levels/activity could also have been a factor in the death of these plants.

The possibility that P0 could promote degradation of AGO1 to an extent that causes adverse effects is not far-fetched. Previous experiments illuminating P0's mode of action have shown that transient overexpression of P0 alone in plant tissue causes a dramatic reduction in AGO1 levels, even when AGO1 is also overexpressed (Bortolamiol et al., 2007; Cascardo et al., 2015; Fusaro et al., 2012; Hendelman et al., 2013). Additionally, stable expression of P0 from various polerovirus species in plants has been shown to induce dwarfing and morphological defects (Bortolamiol et al., 2007; Fusaro et al., 2012; Hendelman et al., 2013; Prufer et al., 2006; Wang et al., 2018), and can be seedling lethal if not controlled by an inducible promoter (Bortolamiol et al., 2007; Hendelman et al., 2013). These effects are often remarkably similar to the phenotype of AGO1 mutants. Furthermore, a common and particularly damaging symptom of PLRV infection of potato is necrosis of stem or tuber phloem (Douglas and Pavek, 1972; Marsh et al., 2000; Quanjer et al., 1916).

Overall, these data suggest that the polerovirus silencing suppressor may be a double-edged sword: knocking down AGO1 impairs host defense, enabling greater virus replication, but may have severe and even lethal consequences for the host plant. To some extent this balancing act likely exists for many viral proteins that disrupt endogenous pathways, but is particularly important for viruses that are circulatively transmitted by insects, like poleroviruses. Circulative transmission requires long periods of sustained insect feeding, both to acquire the virus and to transmit it to a new

host. In this case, it is likely more important for the virus to maintain a long-lived host that is attractive to insects than to produce as many infectious particles as possible. The concept that the activity of P0 must be tightly controlled for optimal virus infection has been proposed previously (Csorba et al., 2010).

4.5 Possible functions of the CP/RTP-AGO1 interaction

These data, combined with the possibility of a direct interaction found between the PLRV CP/RTP and AGO1, led us to hypothesize that the CP/RTP may bind to AGO1 to protect it from P0, indirectly modulating P0's activity. This is an attractive possibility for several reasons. P0 is encoded by the first known ORF in the polerovirus genome, and is therefore likely to be one of the first proteins produced in a newly infected cell (Klein et al., 2014). In contrast, the CP/RTP is produced from a subgenomic RNA, which suggests that it may be produced later in infection. P0 activity is likely to be most important during early stages of infection, when the replicating viral genome is vulnerable to RNA silencing. Protection of AGO1 by CP/RTP would dampen P0 activity during later stages of replication, when its activity may no longer be necessary, or when P0 accumulates to higher-than-optimal levels. Additionally, although the stoichiometry of polerovirus protein production is largely unexplored, it is reasonable to suppose that CP/RTP levels correlate with P0 levels, such that cells with a very high virus titer would also have high levels of P0. Protection of AGO1 by the CP/RTP would provide a scaling safety net against overabundant P0 when titer is high.

Furthermore, the fact that VIGS works in PLRV-infected plants strongly suggests the presence of a mechanism to regulate P0 activity, as AGO1 degradation would be expected to diminish or abolish VIGS. In experiments like this one, where the VIGS vector is not phloem-restricted, it could be argued that the number of P0-

expressing phloem cells is small enough that it doesn't affect the measurable efficacy of VIGS on a macroscopic scale, even if VIGS is not functional in polerovirus-infected cells at all. However, the recent development of a TuYV-based VIGS system provides clear evidence to the contrary (Bortolamiol-Becet et al., 2018). Additionally, TRV-based VIGS of a reporter gene, such as phytoene desaturase, does not appear to be diminished near veins of PLRV-infected plants, despite elevated PLRV titer (DeBlasio et al., 2018a).

Despite these argments, we were unable to find evidence for our CP protection hypothesis in a silencing suppressor assay. In fact, co-infiltration of P0 with PLRV CP strengthened silencing suppression relative to areas co-infiltrated with P0 and a control protein (FLAG-GUS). This result suggests that PLRV CP either has its own silencing suppressor activity, or that it enhances P0 activity, for example by stabilizing the P0-AGO1 interaction. This is an interesting alternative hypothesis for the function of the putative CP-AGO1 interaction. The CP and RTP are already known to be multifunctional, with regions of specific importance for systemic movement, capsid assembly, aphid transmission, and phloem restriction, and functional redundancy is common in viruses. Additionally, silencing suppressor activity has been shown for at least one other plant virus structural protein (Iki et al., 2017). However, if the PLRV CP had inherent silencing suppressor activity, we would also expect that its expression would strengthen silencing suppression of silencing suppressors from other virus species. As GFP fluorescence was similarly strong in samples co-expressing P19 (the potyvirus silencing suppressor) and CP as in samples co-expressing P19 and FLAG-GUS, it is likely that the CP does not have silencing suppressor activity independent of P0.

We cannot conclusively say that the CP enhances silencing suppression,

though, as the ORF for the polerovirus movement protein, P17, is contained entirely within the ORF for the CP, in a different frame, and is believed to be expressed by leaky scanning. As our CP expression construct also contains the P17 ORF, we cannot rule out that P17 was also expressed. Although silencing suppressor activity in the polerovirus movement protein has not been identified, the luteovirus P17 has been shown to act as a silencing suppressor in at least one species (Fusaro et al., 2017). Given the close evolutionary relationship between poleroviruses and luteoviruses, as well as the sequence homology and synteny of their movement proteins, it is certainly possible that the polerovirus P17 has some silencing suppressor activity. To more rigorously test this hypothesis, a construct for expression of PLRV CP containing a silent mutation abolishing the P17 start codon would need to be generated.

5. Conclusion

Although our cross-linking evidence for an AGO1-CP/RTP interaction is uncertain, the functional work in this study clearly delineates the importance of AGO1 in viral infection, and suggests that the relationship between poleroviruses and AGO1 may be more complex than previously thought. This is also the first direct evidence showing that AGO1 expression affects polerovirus titer in systemic infections, which was previously assumed based on other plant viruses and the P0 mechanism of action; the first study of AGO1 expression during systemic polerovirus infection; and the first report of a potential role for the polerovirus CP in silencing suppression. This research provides a foundation for future work in polerovirus silencing suppression.

6. Acknowledgements

This work was funded by USDA-NIFA grants # 2016-67011-24683 and #1907-22000-021-20.

PIR data collection and analysis were performed by Jared P. Mohr, Juan D. Chavez, and James E. Bruce. Co-immunoprecipitation data was provided by Stacy L. DeBlasio and Michelle C. Heck. Stacy L. DeBlasio, Michelle C. Heck, and Ana Rita Rebelo assisted with experimental design and data collection. Mariko M. Alexander was the primary or sole contributor to experimental design, *in planta* data collection, data analysis, figure generation, and manuscript authorship.

6. Supplementary Materials

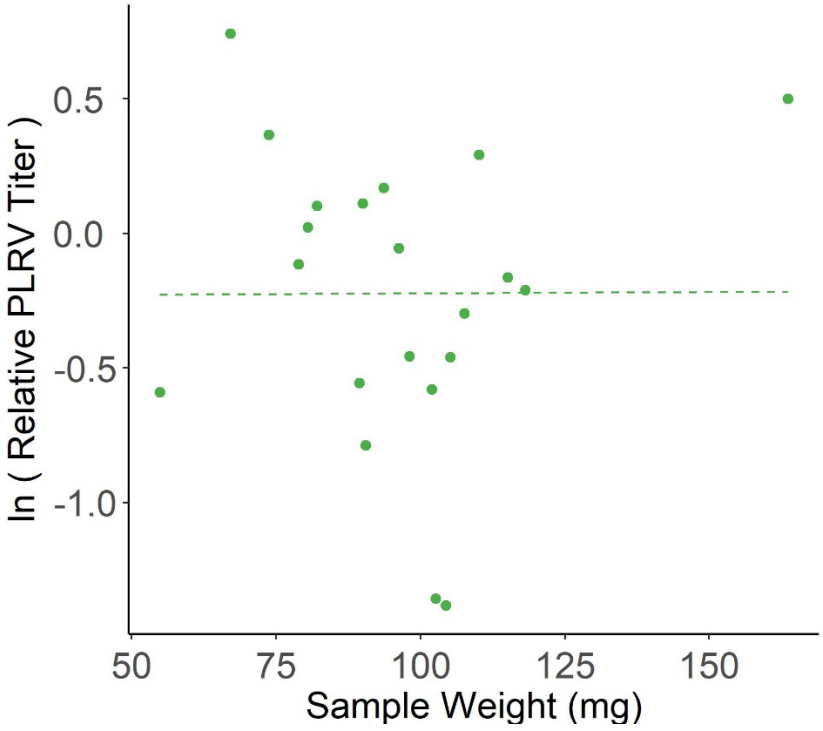

Supplementary Figure 3.1: PLRV titer is not correlated with petiole weight. Plot of relative PLRV titer (y-axis) versus weight of petiole samples in mg (x-axis) from plants co-infected with PLRV and TRV-GFP (control). Titer is given as the natural log of the blank-subtracted expression relative to a sample containing equal quantities of cDNA from all samples, normalized to two reference genes. Each data point represents one sample averaged over technical replicates. Dashed line is the linear best fit line (p= 0.611, tau = - 0.0857 by Kendall's rank correlation tau).

Supplementary Table 3.1: Primers used for qPCR analysis

Target Transcript	Forward Primer (5' - 3')	Reverse Primer (5' - 3')	Final Primer Concentration for qPCR (nM)	Amplicon Size (bp)
PLRV	CTAACAGAGTTCAG CCAGTGG	TGTCCTTTGTAAAC ACGAATGTC	300	147
TRV	ACTCACGGGCTAAC AGTGCT	TCGTAACCGTTGTG TTTGGA	600	126
AGO1	TCAGGATCTGTACA CGACTAGG	GCTCTTCGGAAGGA TATAAGTAAGT	600	98
AP-2	CGTACACGAATGGA AGTGAA	GTCAATGGATGGAT TGTACTTTG	600	156
Clathrin	TATTCCAGAGTTCA TTGAGGGT	ATACTTCATCGGCG AGCT	300	164

REFERENCES

Alexander, M.M., Mohr, J.P., DeBlasio, S.L., Chavez, J.D., Ziegler-Graff, V., Brault, V., Bruce, J.E., Heck, M.C., 2017. Insights in luteovirid structural biology guided by chemical cross-linking and high resolution mass spectrometry. Virus Res 241, 42-52.

Anderson, G.A., Tolic, N., Tang, X., Zheng, C., Bruce, J.E., 2007. Informatics strategies for large-scale novel cross-linking analysis. J Proteome Res 6, 3412-3421.

Arribas-Hernandez, L., Kielpinski, L.J., Brodersen, P., 2016. mRNA decay of most *Arabidopsis* miRNA targets requires slicer activity of AGO1. Plant Physiol 171, 2620-2632.

Bahner, I., Lamb, J., Mayo, M.A., Hay, R.T., 1990. Expression of the genome of *Potato leafroll virus*: Readthrough of the coat protein termination codon in vivo. Journal of General Virology 71 (Pt 10), 2251-2256.

Baumberger, N., Tsai, C.H., Lie, M., Havecker, E., Baulcombe, D.C., 2007. The polerovirus silencing suppressor P0 targets ARGONAUTE proteins for degradation. Curr Biol 17, 1609-1614.

Bencharki, B., Boissinot, S., Revollon, S., Ziegler-Graff, V., Erdinger, M., Wiss, L., Dinant, S., Renard, D., Beuve, M., Lemaitre-Guillier, C., Brault, V., 2010. Phloem protein partners of *Cucurbit aphid borne yellows virus*: possible involvement of phloem proteins in virus transmission by aphids. Mol Plant Microbe Interact 23, 799-810.

Bohmert, K., Camus, I., Bellini, C., Bouchez, D., Caboche, M., Benning, C., 1998. AGO1 defines a novel locus of *Arabidopsis* controlling leaf development. EMBO J 17, 170-180.

Bombarely, A., Rosli, H.G., Vrebalov, J., Moffett, P., Mueller, L.A., Martin, G.B., 2012. A draft genome sequence of *Nicotiana benthamiana* to enhance molecular plant-microbe biology research. Mol Plant Microbe Interact 25, 1523-1530.

Bortolamiol-Becet, D., Monsion, B., Chapuis, S., Hleibieh, K., Scheidecker, D., Alioua, A., Bogaert, F., Revers, F., Brault, V., Ziegler-Graff, V., 2018. Phloem-triggered virus-induced gene silencing using a recombinant polerovirus. Front Microbiol 9, 2449.

Bortolamiol, D., Pazhouhandeh, M., Marrocco, K., Genschik, P., Ziegler-Graff, V., 2007. The polerovirus F box protein P0 targets ARGONAUTE1 to suppress RNA silencing. Curr Biol 17, 1615-1621.

Brault, V., Mutterer, J., Scheidecker, D., Simonis, M.T., Herrbach, E., Richards, K., Ziegler-Graff, V., 2000. Effects of point mutations in the readthrough domain of the *Beet western yellows virus* minor capsid protein on virus accumulation *in planta* and on transmission by aphids. J Virol 74, 1140-1148.

Carbonell, A., Fahlgren, N., Garcia-Ruiz, H., Gilbert, K.B., Montgomery, T.A., Nguyen, T., Cuperus, J.T., Carrington, J.C., 2012. Functional analysis of three *Arabidopsis* ARGONAUTES using slicer-defective mutants. Plant Cell 24, 3613-3629.

Cascardo, R.S., Arantes, I.L., Silva, T.F., Sachetto-Martins, G., Vaslin, M.F., Correa, R.L., 2015. Function and diversity of P0 proteins among *Cotton leafroll dwarf virus* isolates. Virol J 12, 123.

Chavez, J.D., Cilia, M., Weisbrod, C.R., Ju, H.J., Eng, J.K., Gray, S.M., Bruce, J.E., 2012. Cross-linking measurements of the *Potato leafroll virus* reveal protein interaction topologies required for virion stability, aphid transmission, and virus-plant interactions. J Proteome Res 11, 2968-2981.

Correa, R.L., Bruckner, F.P., de Souza Cascardo, R., Alfenas-Zerbini, P., 2013. The role of F-box proteins during viral infection. Int J Mol Sci 14, 4030-4049.

Csorba, T., Kontra, L., Burgyan, J., 2015. Viral silencing suppressors: Tools forged to fine-tune host-pathogen coexistence. Virology 479-480, 85-103.

Csorba, T., Lozsa, R., Hutvagner, G., Burgyan, J., 2010. Polerovirus protein P0 prevents the assembly of small RNA-containing RISC complexes and leads to degradation of ARGONAUTE1. Plant J 62, 463-472.

DeBlasio, S.L., Chavez, J.D., Alexander, M.M., Ramsey, J., Eng, J.K., Mahoney, J., Gray, S.M., Bruce, J.E., Cilia, M., 2016a. Visualization of host-polerovirus interaction topologies using Protein Interaction Reporter technology. J Virol 90, 1973-1987.

DeBlasio, S.L., Johnson, R., Mahoney, J., Karasev, A., Gray, S.M., MacCoss, M.J., Cilia, M., 2015a. Insights into the polerovirus-plant interactome revealed by co-immunoprecipitation and mass spectrometry. Mol Plant Microbe Interact 28, 467-481.

DeBlasio, S.L., Johnson, R., Sweeney, M.M., Karasev, A., Gray, S.M., MacCoss, M.J., Cilia, M., 2015b. *Potato leafroll virus* structural proteins manipulate overlapping, yet distinct protein interaction networks during infection. Proteomics 15, 2098-2112.

DeBlasio, S.L., Johnson, R.S., MacCoss, M.J., Gray, S.M., Cilia, M., 2016b. Model system-guided protein interaction mapping for virus isolated from phloem tissue. J Proteome Res 15, 4601-4611.

DeBlasio, S.L., Rebelo, A.R., Parks, K., Gray, S.M., Heck, M.C., 2018a. Disruption of chloroplast function through downregulation of phytoene desaturase enhances the systemic accumulation of an aphid-borne, phloem-restricted virus. Mol Plant Microbe Interact 31, 1095-1110.

DeBlasio, S.L., Xu, Y., Johnson, R.S., Rebelo, A.R., MacCoss, M.J., Gray, S.M., Heck, M., 2018b. The interaction dynamics of two *Potato leafroll virus* movement proteins affects their localization to the outer membranes of mitochondria and plastids. Viruses 10.

Derrien, B., Baumberger, N., Schepetilnikov, M., Viotti, C., De Cillia, J., Ziegler-Graff, V., Isono, E., Schumacher, K., Genschik, P., 2012. Degradation of the antiviral component ARGONAUTE1 by the autophagy pathway. Proc Natl Acad Sci U S A 109, 15942-15946.

Derrien, B., Clavel, M., Baumberger, N., Iki, T., Sarazin, A., Hacquard, T., Ponce, M.R., Ziegler-Graff, V., Vaucheret, H., Micol, J.L., Voinnet, O., Genschik, P., 2018. A suppressor screen for AGO1 degradation by the viral F-Box P0 protein uncovers a role for AGO DUF1785 in sRNA duplex unwinding. Plant Cell 30, 1353-1374.

Douglas, D.R., Pavek, J.J., 1972. Net necrosis of potato tubers associated with primary, secondary, and tertiary infection of leafroll. American Potato Journal 49, 330-333.

Dzianott, A., Sztuba-Solinska, J., Bujarski, J.J., 2012. Mutations in the antiviral RNAi defense pathway modify *Brome mosaic virus* RNA recombinant profiles. Mol Plant Microbe Interact 25, 97-106.

Eng, J.K., Jahan, T.A., Hoopmann, M.R., 2013. Comet: An open-source MS/MS sequence database search tool. Proteomics 13, 22-24.

Esau, K., Hoefert, L.L., 1972a. Development of infection with *Beet western yellows virus* in the sugarbeet. Virology 48, 724-738.

Esau, K., Hoefert, L.L., 1972b. Ultrastructure of sugarbeet leaves infected with *Beet western yellows virus*. Journal of Ultrastructure Research 40, 556-571.

Fagard, M., Boutet, S., Morel, J.B., Bellini, C., Vaucheret, H., 2000. AGO1, QDE-2, and RDE-1 are related proteins required for post-transcriptional gene silencing in plants, quelling in fungi, and RNA interference in animals. Proc Natl Acad Sci U S A 97, 11650-11654.

Fernandez-Calvino, L., Martinez-Priego, L., Szabo, E.Z., Guzman-Benito, I., Gonzalez, I., Canto, T., Lakatos, L., Llave, C., 2016. *Tobacco rattle virus* 16K silencing suppressor binds ARGONAUTE 4 and inhibits formation of RNA silencing complexes. J Gen Virol 97, 246-257.

Fernandez-Pozo, N., Rosli, H.G., Martin, G.B., Mueller, L.A., 2015. The SGN VIGS tool: User-friendly software to design virus-induced gene silencing (VIGS) constructs for functional genomics. Mol Plant 8, 486-488.

Fusaro, A.F., Barton, D.A., Nakasugi, K., Jackson, C., Kalischuk, M.L., Kawchuk, L.M., Vaslin, M.F.S., Correa, R.L., Waterhouse, P.M., 2017. The luteovirus P4 movement protein is a suppressor of systemic RNA silencing. Viruses 9.

Fusaro, A.F., Correa, R.L., Nakasugi, K., Jackson, C., Kawchuk, L., Vaslin, M.F., Waterhouse, P.M., 2012. The enamovirus P0 protein is a silencing suppressor which inhibits local and systemic RNA silencing through AGO1 degradation. Virology 426, 178-187.

Garcia-Ruiz, H., Carbonell, A., Hoyer, J.S., Fahlgren, N., Gilbert, K.B., Takeda, A., Giampetruzzi, A., Garcia Ruiz, M.T., McGinn, M.G., Lowery, N., Martinez Baladejo, M.T., Carrington, J.C., 2015. Roles and programming of *Arabidopsis* ARGONAUTE proteins during *Turnip mosaic virus* infection. PLoS Pathog 11, e1004755.

Gildow, F.E., 1982. Coated-vesicle transport of luteoviruses through salivary-glands of *Myzus-persicae*. Phytopathology 72, 1289-1296.

Gray, S., Cilia, M., Ghanim, M., 2014. Circulative, "nonpropagative" virus transmission: An orchestra of virus-, insect-, and plant-derived instruments. Adv Virus Res 89, 141-199.

Hendelman, A., Kravchik, M., Stav, R., Zik, M., Lugassi, N., Arazi, T., 2013. The developmental outcomes of P0-mediated ARGONAUTE destabilization in tomato. Planta 237, 363-377.

Hijaz, F., Killiny, N., 2014. Collection and chemical composition of phloem sap from *Citrus sinensis* L. Osbeck (sweet orange). PLoS One 9, e101830.

Hoopmann, M.R., Weisbrod, C.R., Bruce, J.E., 2010. Improved strategies for rapid identification of chemically cross-linked peptides using Protein Interaction Reporter technology. Journal of proteome research 9, 6323-6333.

Iki, T., Tschopp, M.A., Voinnet, O., 2017. Biochemical and genetic functional dissection of the P38 viral suppressor of RNA silencing. RNA 23, 639-654.

Jones, L., Keining, T., Eamens, A., Vaistij, F.E., 2006. Virus-induced gene silencing of Argonaute genes in *Nicotiana benthamiana* demonstrates that extensive systemic silencing requires Argonaute1-like and Argonaute4-like genes. Plant Physiol 141, 598-606.

Kaplan, I.B., Lee, L., Ripoll, D.R., Palukaitis, P., Gildow, F., Gray, S.M., 2007. Point mutations in the *Potato leafroll virus* major capsid protein alter virion stability and aphid transmission. J Gen Virol 88, 1821-1830.

Keller, A., Chavez, J.D., Bruce, J.E., 2019. Increased sensitivity with automated validation of XL-MS cleavable peptide crosslinks. Bioinformatics 35, 895-897.

Kim, J.H., Jander, G., 2007. *Myzus persicae* (green peach aphid) feeding on *Arabidopsis* induces the formation of a deterrent indole glucosinolate. Plant J 49, 1008-1019.

Klein, E., Brault, V., Klein, D., Weyens, G., Lefebvre, M., Ziegler-Graff, V., Gilmer, D., 2014. Divergence of host range and biological properties between natural isolate and full-length infectious cDNA clone of the *Beet mild yellowing virus* 2ITB. Mol Plant Pathol 15, 22-30.

Lee, L., Kaplan, I.B., Ripoll, D.R., Liang, D., Palukaitis, P., Gray, S.M., 2005. A surface loop of the *Potato leafroll virus* coat protein is involved in virion assembly, systemic movement, and aphid transmission. J Virol 79, 1207-1214.

Li, Y., Sun, Q., Zhao, T., Xiang, H., Zhang, X., Wu, Z., Zhou, C., Zhang, X., Wang, Y., Zhang, Y., Wang, X., Li, D., Yu, J., Dinesh-Kumar, S.P., Han, C., 2019. Interaction between *Brassica yellows virus* silencing suppressor P0 and plant SKP1 facilitates stability of P0 *in vivo* against degradation by proteasome and autophagy pathways. New Phytol.

Marsh, T.L., Huffaker, R.G., Long, G.E., 2000. Optimal control of vector-virus-plant interactions: The case of *Potato leafroll virus* net necrosis. American Journal of Agricultural Economics 82, 556-569.

Morel, J.-B., Godon, C., Mourrain, P., Béclin, C., Boutet, S., Feuerbach, F., Proux, F., Vaucheret, H., 2002. Fertile hypomorphic ARGONAUTE (ago1) mutants impaired in post-transcriptional gene silencing and virus resistance. The Plant Cell 14, 629-639.

Natti, J.J., Ross, A.F., 1953. Branch-trace necrosis, a symptom of *Potato leafroll virus* infection American Potato Journal 31, 12-19.

Nesvizhskii, A.I., Keller, A., Kolker, E., Aebersold, R., 2003. A statistical model for identifying proteins by tandem mass spectrometry. Anal Chem 75, 4646-4658.

Odokonyero, D., Mendoza, M.R., Moffett, P., Scholthof, H.B., 2017. *Tobacco rattle virus* (TRV)-mediated silencing of *Nicotiana benthamiana* ARGONAUTES (NbAGOs) reveals new antiviral candidates and dominant effects of TRV-NbAGO1. Phytopathology 107, 977-987.

Ogle, D.H., Wheeler, P., Dinno, A., 2019. FSA: Fisheries Stock Analysis.

Pasin, F., Kulasekaran, S., Natale, P., Simon-Mateo, C., Garcia, J.A., 2014. Rapid fluorescent reporter quantification by leaf disc analysis and its application in plant-virus studies. Plant Methods 10, 22.

Pazhouhandeh, M., Dieterle, M., Marrocco, K., Lechner, E., Berry, B., Brault, V., Hemmer, O., Kretsch, T., Richards, K.E., Genschik, P., Ziegler-Graff, V., 2006. F-box-like domain in the polerovirus protein P0 is required for silencing suppressor function. Proc Natl Acad Sci U S A 103, 1994-1999.

Peter, K.A., Gildow, F., Palukaitis, P., Gray, S.M., 2009. The C terminus of the polerovirus P5 readthrough domain limits virus infection to the phloem. J Virol 83, 5419-5429.

Peter, K.A., Liang, D., Palukaitis, P., Gray, S.M., 2008. Small deletions in the *Potato leafroll virus* readthrough protein affect particle morphology, aphid transmission, virus movement and accumulation. J Gen Virol 89, 2037-2045.

Pfaffl, M.W., 2001. A new mathematical model for relative quantification in real-time RT-PCR. Nucleic Acids Res 29, e45.

Pfeffer, S., Dunoyer, P., Heim, F., Richards, K.E., Jonard, G., Ziegler-Graff, V., 2002. P0 of *Beet western yellows virus* is a suppressor of posttranscriptional gene silencing. Journal of virology 76, 6815-6824.

Prufer, D., Kawchuk, L., Rohde, W., 2006. Polerovirus ORF0 genes induce a host-specific response resembling viral infection. Can. J. Plant Pathol. 28, 302-309.

Qu, F., Ye, X., Morris, T.J., 2008. *Arabidopsis* DRB4, AGO1, AGO7, and RDR6 participate in a DCL4-initiated antiviral RNA silencing pathway negatively regulated by DCL1. Proc Natl Acad Sci U S A 105, 14732-14737.

Quanjer, H.M., Van der Lek, H.A.A., Botjes, O., 1916. Aard, verspreiding en bestrijding van Phloeemnecroses en hare beteekenis voor de aardappelcultuur. Mededeelingen van de Landbouwhoogeschool 17, 1-74.

Rashid, M.O., Zhang, X.Y., Wang, Y., Li, D.W., Yu, J.L., Han, C.G., 2019. The three essential motifs in P0 for suppression of RNA silencing activity of *Potato leafroll virus* are required for virus systemic infection. Viruses 11.

Sadowy, E., Maasen, A., Juszczuk, M., David, C., Zagorski-Ostoja, W., Gronenborn, B., Hulanicka, M.D., 2001. The ORF0 product of *Potato leafroll virus* is indispensable for virus accumulation. J Gen Virol 82, 1529-1532.

Senthil-Kumar, M., Mysore, K.S., 2014. *Tobacco rattle virus*-based virus-induced gene silencing in *Nicotiana benthamiana*. Nat Protoc 9, 1549-1562.

Shepardson, S., Esau, K., McCrum, R., 1980. Ultrastructure of potato leaf phloem infected with *Potato leafroll virus*. Virology 105, 379-392.

Tang, X., Bruce, J.E., 2010. A new cross-linking strategy: Protein Interaction Reporter (PIR) technology for protein-protein interaction studies. Mol Biosyst 6, 939-947.

Team, R., 2015. RStudio: Integrated Development Environment for R. RStudio, Inc.

Team, R.C., 2013. R: A language and environment for statistical computing. R Foundation for Statistical Computing.

Tetyuk, O., Benning, U.F., Hoffmann-Benning, S., 2013. Collection and analysis of *Arabidopsis* phloem exudates using the EDTA-facilitated method. J Vis Exp, e51111.

van der Wilk, F., Houterman, P., Molthoff, J., Hans, F., Dekker, B., van den Heuvel, J., Huttinga, H., Goldbach, R., 1997. Expression of the *Potato leafroll virus* ORF0 induces viral-disease-like symptoms in transgenic potato plants. Mol Plant Microbe Interact 10, 153-159.

Vaucheret, H., Vazquez, F., Crete, P., Bartel, D.P., 2004. The action of ARGONAUTE1 in the miRNA pathway and its regulation by the miRNA pathway are crucial for plant development. Genes Dev 18, 1187-1197.

Velasquez, A.C., Chakravarthy, S., Martin, G.B., 2009. Virus-induced gene silencing (VIGS) in *Nicotiana benthamiana* and tomato. J Vis Exp.

Wang, F., Zhao, X., Dong, Q., Zhou, B., Gao, Z., 2018. Characterization of an RNA silencing suppressor encoded by *Maize yellow dwarf virus*-RMV2. Virus Genes 54, 570-577.

Weisbrod, C.R., Chavez, J.D., Eng, J.K., Yang, L., Zheng, C., Bruce, J.E., 2013. *In vivo* protein interaction network identified with a novel real-time cross-linked peptide identification strategy. J Proteome Res 12, 1569-1579.

Wickham, H., 2009. ggplot2: Elegant graphics for data analysis. Springer-Verlag New York.

Zhang, X., Yuan, Y.R., Pei, Y., Lin, S.S., Tuschl, T., Patel, D.J., Chua, N.H., 2006. *Cucumber mosaic virus*-encoded 2b suppressor inhibits *Arabidopsis* Argonaute1 cleavage activity to counter plant defense. Genes Dev 20, 3255-3268.

Zhao, S., Xu, W., Jiang, W., Yu, W., Lin, Y., Zhang, T., Yao, J., Zhou, L., Zeng, Y., Li, H., Li, Y., Shi, J., An, W., Hancock, S.M., He, F., Qin, L., Chin, J., Yang, P., Chen, X., Lei, Q., Xiong, Y., Guan, K.L., 2010. Regulation of cellular metabolism by protein lysine acetylation. Science 327, 1000-1004.

Zhuo, T., Li, Y.Y., Xiang, H.Y., Wu, Z.Y., Wang, X.B., Wang, Y., Zhang, Y.L., Li, D.W., Yu, J.L., Han, C.G., 2014. Amino acid sequence motifs essential for P0-mediated suppression of RNA silencing in an isolate of *Potato leafroll virus* from Inner Mongolia. Mol Plant Microbe Interact 27, 515-527.

Ziegler-Graff, V., Brault, V., Mutterer, J.D., Simonis, M.-T., Herrbach, E., Guilley, H., Richards, K.E., Jonard, G., 1996. The coat protein of Beet western yellows luteovirus is essential for systemic infection but the viral gene products P29 and P19 are disposable for systemic infection and aphid transmission. Mol Plant Microbe Interact 9, 501-510.

CHAPTER 4

ELUCIDATION OF HOST-VIRUS INTERACTIONS IN *TURNIP YELLOWS VIRUS* USING CROSS-LINKING PROTEOMICS

1. Introduction

Viruses in the genus *Polerovirus* are plant pathogens of diverse crops worldwide. Although the type species, *Potato leafroll virus* (PLRV; *Luteoviridae: Polerovirus*), was first identified in 1916, and poleroviruses have been the subject of active research for decades since, relatively little is known about the specific ways in which poleroviruses interact with host plants. This is due, in part, to technical challenges posed by polerovirus biology, including phloem restriction, low titer, and restrictions on genome size imposed by the capsid (Nurkiyanova et al., 2000).

The single-stranded, positive-sense RNA genome of PLRV and other poleroviruses encodes only nine known proteins. As poleroviruses move systemically in both plants hosts and aphid vectors as virions, the virus capsid is likely to mediate many of the protein-protein interactions important for successful infection. Although the precise structure of the icosahedral capsid is unknown, it is known to be comprised primarily of coat protein (CP). Sporadic readthrough of an amber stop codon terminating the CP gene produces read-through protein (RTP), which consists of CP plus a C-terminal extension known as the read-through domain (RTD). The RTP is believed to exist in both virion-incorporated and unincorporated forms, both of which are required for efficient systemic movement in plants (Boissinot et al., 2014). The importance of polerovirus structural proteins is further underscored by the many sites in the CP and RTD identified by mutational analyses as critical for proper virion assembly, phloem restriction, movement in plants, and circulative transmission by aphids, which is the sole means of polerovirus transmission in nature (Bruyere et al.,

1997; Jolly and Mayo, 1994; Kaplan et al., 2007; Lee et al., 2005; Peter et al., 2009; Peter et al., 2008; Reutenauer et al., 1993; Ziegler-Graff et al., 1996).

To assess direct interactions between polerovirus CP/RTP and host proteins, we have previously utilized Protein Interaction Reporter (PIR) Technology, which utilizes a mass spectrometry-compatible cross-linker for identification of protein-protein interactions in a complex mixture (DeBlasio et al., 2016; Tang et al., 2005). In this study, we expand on this work by applying PIR technology to the related *Turnip yellows virus* (TuYV; *Luteoviridae*: *Polerovirus*).

2. Materials and Methods

2.1 TuYV Purification, Cross-Linking, and Mass Spectrometry

TuYV virions were purified as previously described (Alexander et al., 2017) from frozen *N. benthamiana leaves* harvested 6-8 days after infiltration with *Agrobacterium tumefaciens* C58C1 containing a cDNA clone of TuYV. Aphid transmissibility of virions harvested following the 30% sucrose cushion was verified as previously described (Alexander et al., 2017).

Cross-linking of virion preparations, sample preparation, cross-linking, mass spectrometry, and database searching was performed as previously described (Alexander et al., 2017). A total of 1.3mg of partially purified TuYV was used for cross-linking.

2.2 Arabidopsis Plant Growth

Arabidopsis thaliana seeds were stratified by incubation in deionized water at 4°C for at least seven days prior to planting in 3x6-well flats filled with moist

Osmocote-supplemented soil. All subsequent plant growth was carried out in a growth chamber set to 24°C and ambient humidity, with either 12-hour (for seed production or transformation) or 8-hour (for vegetative growth and TuYV infection assays) light cycles. Seeds were germinated under a dome for 3-5 days before thinning to 1-2 seedlings per cell. Plants grown for seed production were contained in floral bouquet wraps after onset of flowering to support bolts and prevent cross-pollination.

Ecotype identity of Col-0 WT plants was verified using previously published markers. Confirmation of the t-DNA insertion in AtPLL25 mutants was performed using primers recommended by the SALK T-DNA Primer Design Tool (http://signal.salk.edu/tdnaprimers.2.html).

2.3 Arabidopsis thaliana t-DNA mutant lines

t-DNA mutant lines were obtained from the *Arabidopsis* Biological Resource center (ABRC; https://www.*Arabidopsis*.org/abrc/). The AtPLL25 mutant line originated from the verified homozygous ABRC stock SALK_031335C (Alonso et al., 2003). For comparison of rosette diameter between AtPLL25 mutants and wild-type Col-0, two flats of each genotype were grown in short-day conditions. Rosette diameter was measured with a ruler approximately two months after planting.

The PGDH mutant line originated from ABRC stock CS379467 (Rosso et al., 2003). Seed increases were performed by sterilizing and sowing seeds on MS agar as described below containing sulfadiazine for selection of the transgene. Surviving seedlings were transplanted to soil and allowed to grow to maturity. The progeny of one of the survivors was tested for zygosity and lethality by plating on selective media, as previously, and survivors were transferred to soil. Crude DNA extractions from leaf tissue were performed as previously described for PCR testing of zygosity

(Chabi Sika et al., 2015). Primer sequences for testing were obtained from the GABI-Kat primer tool (https://www.gabi-kat.de/db/primerdesign.php) (Huep et al., 2014).

2.4 TuYV-SUL infection timecourse

Wild-type Col-0 and AtPLL25 mutant plants were grown without selection as described above in short-day conditions. Approximately three weeks after sowing, seedlings were inoculated with TuYV-SUL or infiltration buffer alone (negative control) by agroinfiltration as previously described (Bortolamiol-Becet et al., 2018; Veidt et al., 1988). Plants were monitored daily for the appearance of chlorotic leaves indicating the presence of TuYV-SUL. The 15th and 20th true leaves of plants were harvested at either 12 or 16 days post infiltration (dpi) and snap frozen in liquid nitrogen. Leaf samples were cryolysed with a Mixer Mill (Retsch) before adding 10µL PBS per mg of tissue. The resulting lysate was used immediately to quantify TuYV titer by double antibody sandwich enzyme-linked immunosorbent assay (DAS-ELISA) using a commercially available TuYV antibody set (Loewe Biochemica, Germany). Samples were measured in technical triplicate or duplicate for larger leaves, and singlet for smaller leaves. Absorbance values were normalized between plates using a dilution series of partially purified TuYV for generation of a standard curve.

2.5 Statistical analysis

Statistical analyses were performed and graphs generated using Microsoft Excel and R Studio, including the following R packages: ggplot2, readr, plyr, and scales (Team, 2015; Team, 2013; Wickham, 2009).

2.6 Promoter::GUS assays for AtPLL25

The AtPLL25 promoter was cloned, Gateway sites added, and fused to a GUS expression ORF using fusion PCR. The resulting PCR product was gel-purified and recombined into a Gateway donor plasmid using BP Clonase II (Thermo) following manufacturer's instructions. Recombinant plasmids were transformed into Mach1 *E. coli* (Thermo) following manufacturer's instructions and plated on selective media. Plasmid was extracted from positive clones, and the correctness of the sequence confirmed by Sanger sequencing. This procedure was then repeated using LR Clonase II (Thermo) to move the AtPLL25 promoter into the binary expression vector pEarley100 (Earley et al., 2006). Sequence-verified plasmid was transformed into *Agrobacterium tumefaciens* for plant transformation.

Arabidopsis seeds were stratified and planted as described above. Plants were transformed by the floral dip method as previously published, using *A. tumefaciens* strain GV3101 + pMP90 (Clough and Bent, 1998). T0 seed was sterilized as recommended by the *Arabidopsis* Biological Resource Center (https://abrc.osu.edu/seed-handling) and plated on Murashige-Skoog agar with 1% sucrose, 20µg/mL glufosinate ammonium, and Murashige and Skoog vitamin solution (Sigma) at a final concentration of 1X. Surviving T1 plants were transplanted to individual pots when large enough.

Single leaves and flower clusters from mature T1 plants for GUS staining were harvested and incubated on ice in 90% acetone. Samples were fixed in FAA buffer (50% ethanol, 10% glacial acetic acid, 5% formaldehyde) under vacuum. Staining was performed as previously described (Li, 2011). Staining was photographed with an Olympus SZX12 stereo microscope with a ProgRes C14 attachment .

2.7 Photography and figure generation

Macroscopic photos were taken using a Samsung Galaxy S5 or a Canon Eos Rebel T6. Minor adjustment of brightness, contrast, and color balance were performed using Adobe Photoshop. TuYV-SUL infected leaves were scanned using an Epson office scanner.

3. Results and Discussion

3.1 Purified TuYV virions are aphid-transmissible

TuYV virions were partially purified from infected *N. benthamiana* using a sucrose density centrifugation protocol, stopping after the sucrose cushion to retain host-virus interactions, as in previous work with PLRV (DeBlasio et al., 2016). The integrity of purified virions was verified by testing aphid transmissibility. All virion preparations used in this study were verified to be aphid-transmissible, as determined by DAS-ELISA of recipient plants. Of the five plants colonized with *Myzus persicae* fed on purified virions, one died and four were ELISA positive for TuYV three weeks after inoculation. None of the five plants colonized with *M. persicae* fed on artificial diet alone were found to be TuYV-infected. Therefore, the partially purified preparations of TuYV used for cross-linking were intact and biologically active.

3.2 N. benthamiana host proteins interact with TuYV coat protein

Protein Interaction Reporter (PIR) technology utilizes a mass spectrometry-compatible cross-linker to detect direct protein-protein interactions in samples. Previous applications of PIR technology to luteovirids have enabled modeling of PLRV and TuYV coat protein trimers, the fundamental unit of the capsid (Alexander et al., 2017; Chavez et al., 2012; DeBlasio et al., 2016), and generated new insight into

host-virus interactions in PLRV (DeBlasio et al., 2016). In this study, host-virus interactions in TuYV were measured by PIR for the first time.

Application of the PIR cross-linker to partially purified TuYV found cross-links between a site in the TuYV CP/RTP and three host proteins, annotated as a pectate lyase-like protein (PLL), a 3-phosphoglycerate dehydrogenase (PGDH), and a peptide-N4-(N-acetyl-beta-glucosaminyl)asparagine amidase A (PNGase A) (Table 4.1). The CP/RTP lysines found cross-linked to these proteins were also identified as cross-linked to other TuYV proteins and are believed to be surface-exposed (Alexander et al., 2017).

Table 4.1: TuYV-Host Cross-Links

Protein1 Name	**Protein2 ID**	**Protein2 Description**	**Protein2 Name**	**Peptide 1[a]**	**Peptide 2[a]**
TuYV CP/RTP	Niben101Scf03412g05009.1	peptide-N4-(N-acetyl-beta-glucosaminyl) asparagine amidase A	PNGase A	DQRF.ILYK$_{179}$GNGSSSIAGSFR.ITIK	LHLR.ELKFK$_{426}$N<u>K</u>.KINF
TuYV CP/RTP	Niben101Scf01350g03009.1	3-phospho-glycerate dehydrogenase, chloroplastic	PGDH	DQRF.ILYK$_{179}$GNGSSSIAGSFR.ITIK	ATKK.ILNDETFAK$_{257}$<u>M</u>K.KGVR
TuYV CP/RTP	Niben101Scf00171g00014	pectin lyase-like protein	PLL	GDFR.ITIK$_{195}$CQFHNPK.VDEE	MA<u>M</u>GSLISKK$_{10}$K.GVRI

[a]Amino acid sequence of cross-linked peptides deduced from MS3 fragmentation and database searching. The four amino acids before and after each peptide are given as a reference, with peptide boundaries denoted by periods. K residue numbers indicate cross-linked lysines. Sidechains of underlined residues were modified by either acetylation (lysine) or oxidation (methionine).

3.3 Pectate lyase single-gene knockout plants are largely indistinguishable from wild-type plants during TuYV infection

Pectate lyases in plants were first discovered in pollen, where they tend to be highly expressed and are major allergenic proteins in some plant species. Pectate lyase expression has also been observed in ripening fruit, floral tissues, and actively growing cells, where they are believed to be involved in cell wall loosening to facilitate expansion (Palusa et al., 2007). Although originally believed to have fewer than 30 pectin lyase genes, the most recent bioinformatic analysis found a total of 67 putative pectin lyase genes in *Arabidopsis thaliana* (Cao, 2012).

The nearest *A. thaliana* homolog of the *N. benthamiana* pectin lyase found cross-linked to TuYV is a protein designated "pectin lyase-like superfamily protein" (locus ID: At4g13710), which is the reciprocal best hit by BLAST and has 80% identity to the *N. benthamiana* homolog at the protein level. The *A. thaliana* and *N. benthamiana* homologs of this pectin lyase will be referred to hereafter as AtPLL25 and NbPLL25, respectively, according to the designations given by Palusa and colleagues (Palusa et al., 2007).

To further explore the function of PLL25 during TuYV infection, we obtained an *Arabidopsis* mutant homozygous for a t-DNA insertion in the exon of one of two splice variants for AtPLL25 (TAIR stock ID: SALK_031335C) (Alonso et al., 2003). The AtPLL25 mutant (referred to hereafter as ΔAtPLL25) was fertile and appeared phenotypically similar to Col-0 wild-type plants, although mutants were observed to have noticeably larger rosettes than wild-type plants when grown in short-day conditions for long periods (>2 months) ($p = 3.9e\text{-}19$ at 36 days post-planting by Welch's Two Sample T-Test; Figure 4.1).

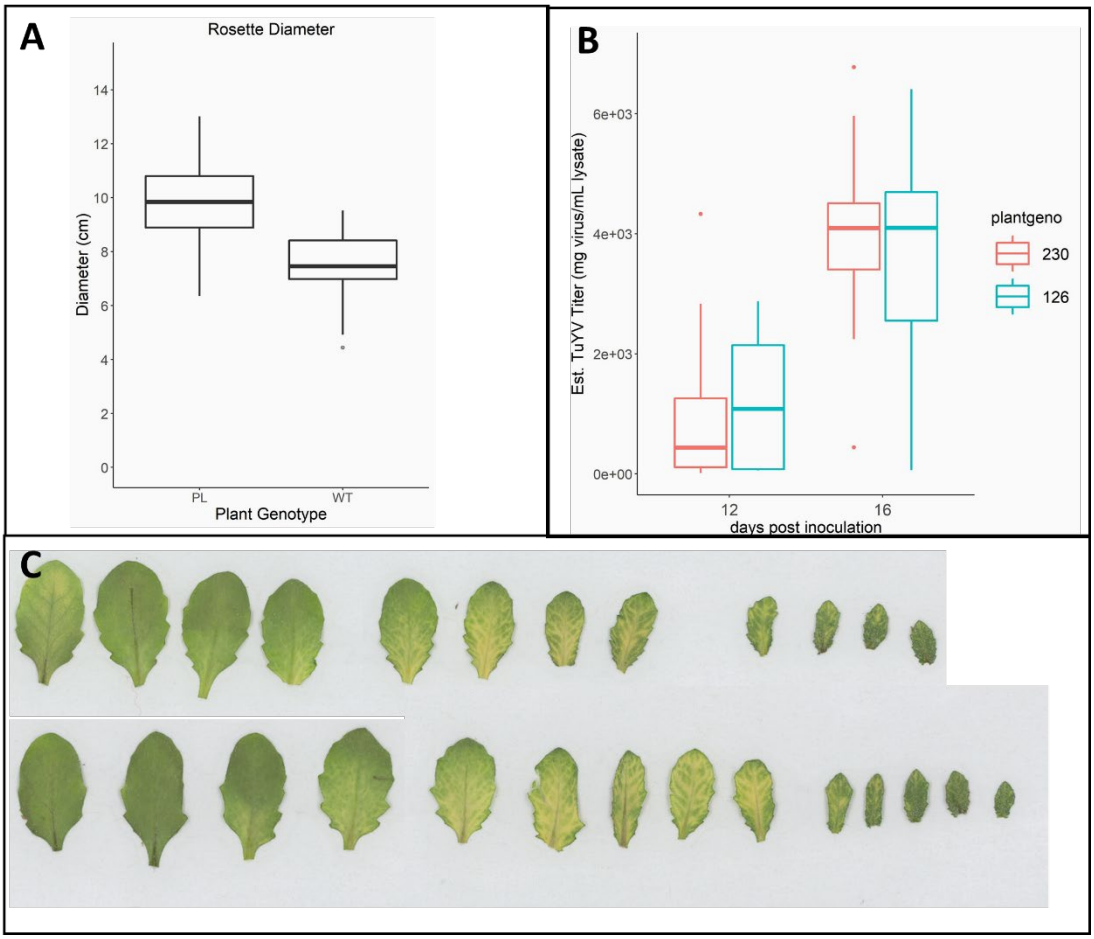

Figure 4.1: Comparison of ΔAtPLL25 and wild-type plants' response to TuYV-SUL infection. A) Uninfected ΔAtPLL25 have significantly larger rosettes at 36 days post planting than uninfected wild-type plants (p= 3.9e-19 at 36 days post-planting by Welch's Two Sample T-Test). B) ΔAtPLL25 support similar TuYV titer as wild-type plants at both 12 and 16 dpi. C) Representative example of chlorosis pattern in wild-type (top) and ΔAtPLL25 (bottom) leaves infected with TuYV-SUL at 13dpi. Each row contains leaves from a single plant, with older leaves on the left and younger on the right.

Using TuYV-SUL, a recently published TuYV recombinant containing a short insert which causes chlorosis in infected cells by virus-induced gene silencing (VIGS) (Bortolamiol-Becet et al., 2018), we assessed TuYV movement, phloem restriction, and titer in ΔAtPLL25 plants (Figure 4.1). We found no statistically significant difference in TuYV titer in ΔAtPLL25 mutants as compared to wild-type plants at either of the time points assessed (12 and 16 dpi). TuYV-SUL also appeared to move systemically at a similar rate in wild-type and ΔAtPLL25 plants. Wild-type plants initially seemed to be infected at a lower frequency than ΔAtPLL25 plants; however, the difference was not statistically significant ($p= 0.2492$ and 0.3472 at 12 and 16 dpi, respectively, by Kruskal-Wallace rank sum test).

The pattern and degree of chlorosis, which indirectly indicate TuYV presence and titer, appeared similar in ΔAtPLL25 and wild-type plants (Figure 4.1). Both groups of plants exhibited chlorosis, usually as small speckles, first in young leaves. The pattern of chlorosis transitioned to the expected pattern, following the vasculature, over the next several days, during which time chlorosis also began to appear in older leaves. Over time, chlorotic areas broadened and became more intense, often nearly overtaking leaves at later stages of infection. The oldest leaves, including those inoculated by agroinfiltration, did not become chlorotic by 30 days post inoculation.

Overall, all aspects of infection assessed, including virus titer, rate of systemic movement, infection frequency, and chlorosis pattern, were similar between wild-type and ΔAtPLL25 plants. It should be noted, though, that the absence of a measurable effect on TuYV-SUL infection in ΔAtPLL25 plants does not necessarily indicate that AtPLL25 is not important in TuYV infection. It is possible that the function of the TuYV- ΔAtPLL25 interaction affects an aspect of the viral life cycle not assessed

here, such as aphid feeding, host specificity, or attractiveness to vectors. As *Arabidopsis* has an estimated 67 pectin lyase genes, it is also very possible that TuYV is able to interact with more than one homolog, and that multiple homologs would need to be knocked out to see an effect. Finally, although AtPLL25 was the reciprocal best hit for NbPLL25 in the *Arabidopsis* genome, we cannot be certain that these two genes are homologous in terms of their function in TuYV infection.

3.4 An Arabidopsis pectate lyase promoter is active in phloem tissue

Next, we explored the expression of AtPLL25 by generating transgenic plants which expressed a GUS reporter under the control of the AtPLL25 promoter in the ΔAtPLL25 background. Whole leaves and flowers from mature transgenic plants were cleared and stained for GUS activity, which is reported as a blue color. Of twelve first generation transgenic plants tested, ten had no discernable staining. The remaining two showed mild to moderate staining at the base of flowers, in anthers, and in vascular elements of leaves and shoots (Figure 4.1). No staining was visualized in any of the untransformed ΔAtPLL25 control plants.

These findings are partially aligned with previous work, also using a GUS reporter system, which found that the AtPLL25 promoter was active in seedling root tips, leaf stipules, styles, filament-anther junctions, the abscission zones of flowers and recently-abscised seeds, and the dehiscion zone of mature siliques (Sun and van Nocker, 2010). AtPLL25 has also shown to be generally expressed in flowers, roots, stems, and leaves (in order from highest to lowest expression) (Palusa et al., 2007).

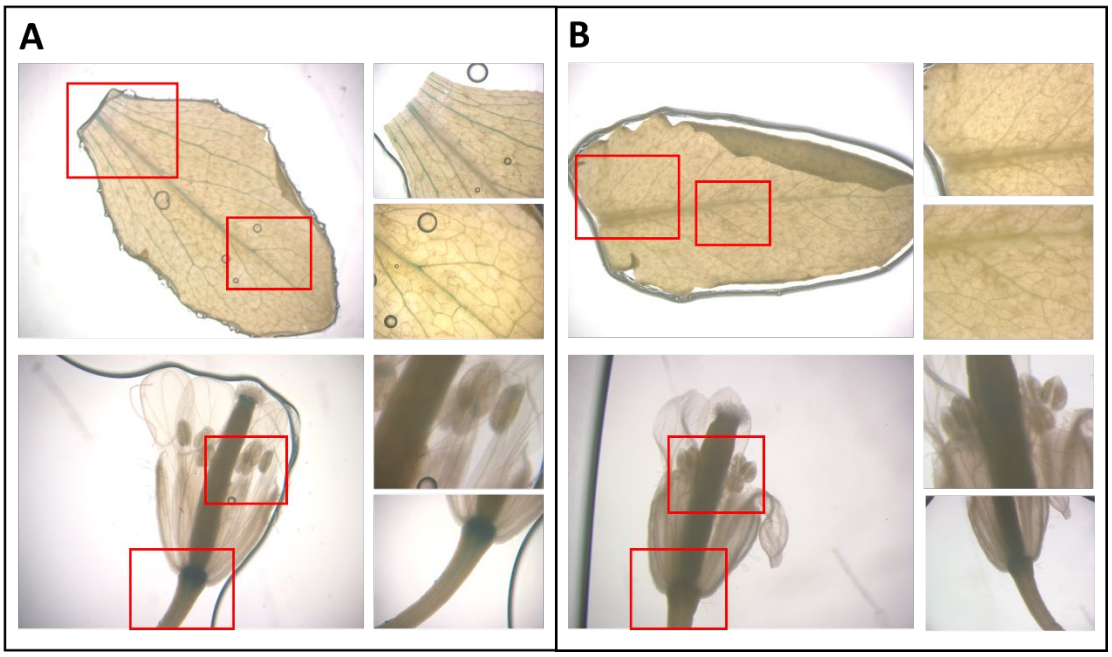

Figure 4.2: AtPLL25 promoter is active in vascular tissues. GUS staining of AtPLL25 promoter activity in uninfected transgenic (left) and untransformed ΔAtPLL25 control (right) plants. Red boxes indicate areas magnified in smaller images on right.

We were surprised to find that the AtPLL25 promoter was particularly active in the vasculature of leaves and shoots, as this localization had not been previously reported. This finding is particularly interesting considering the phloem restriction of poleroviruses, including TuYV. Although locally infiltrated tissue, which is made primarily of mesophyll and other non-phloem cells, was used for cross-linking in this study, this finding suggests that some polerovirus-host interactions are tissue specific, and that those interactions can be identified by this technique. However, it should be noted that AtPLL25 and NbPLL25 may not have the same expression pattern.

3.5 A PGDH knockout line is homozygous seedling lethal

To explore the function of the interaction between TuYV CP/RTP and host PGDH, we obtained a t-DNA knockout line for the nearest *A. thaliana* homolog (locus ID: AT4G34200.1; TAIR stock # CS379467) (Rosso et al., 2003). As the seed from this line is distributed as a segregating population, we sought first to obtain progeny homozygous for the insertion. When grown on selective media, approximately one half of the progeny from a PCR-verified homozygous parent died in the seedling stage, indicating that seedlings homozygous for the tDNA insertion were non-viable. Additionally, random PCR testing of 20 surviving seedlings of varying sizes found only heterozygotes. As PGDH is a critical enzyme for amino acid biosynthesis, it is unsurprising that complete loss of function is lethal.

Plants heterozygous for the PGDH insertion were fertile and indistinguishable in appearance from wild-type plants; therefore, we assumed that the wild-type PGDH allele was dominant, and that heterozygotes would be unlikely to behave differently than wild-type plants during TuYV infection. Accordingly, no further testing was performed.

3.6 TuYV titer is likely similar in wild-type plants and PNGase mutants

Finally, we obtained a confirmed homozygous t-DNA knockout line for the nearest *A. thaliana* homolog of the PNGase found cross-linked to TuYV (locus ID: AT5G05480.1; TAIR stock # SALK_138400C) (Alonso et al., 2003). Uninfected PNGase mutant plants appeared similar to wild-type plants, with no obvious stunting or deformities. Due to technical issues, no wild-type plants inoculated alongside PNGase mutants became infected with TuYV-SUL. However, comparisons could be made to ΔAtPLL25 plants within the same experiment. PNGase mutants were found to support similar levels of TuYV as ΔAtPLL25 plants and had similar patterns of chlorosis (data not shown). As the ΔAtPLL25 plants had already been found to behave similarly to wild-type plants during TuYV-SUL infection, we concluded that the same was likely to be true for the PNGase mutants, and no further testing was performed.

4. Conclusions

Using PIR technology, we identified direct interactions between the TuYV CP/RTP and three *N. benthamiana* proteins: a PNGase A, a pectin lyase, and a PGDH. These interactions were found in infected plant protein extracts enriched for virions, which were confirmed to be aphid-transmissible. This method has been successfully employed in the past for the identification of biologically relevant interactions between PLRV and host plant proteins (DeBlasio et al., 2016).

Although we were unable to ascribe a function to the interaction with pectin lyase, several interesting observations were made. The AtPLL25 promoter was found to be active specifically in vascular tissue of vegetative structures. This activity has not been identified previously for any *Arabidopsis* pectin lyase; however, a recent

study identified a pectin lyase in poplar trees (*Populus trichocarpa*) expressed in and important for development of xylem and phloem (Bai et al., 2017). In the same study, transgenic trees overexpressing this pectin lyase were found to be stunted compared to wild-type controls. Notably, this is the inverse phenotype of that seen in AtPLL25 knockout plants in this study, which grew larger than wild-type plants when kept in short-day conditions for long periods. Although AtPLL25 is not the closest *Arabidopsis* homolog to the poplar pectin lyase, it is in the top five hits and is 78.3% identical at the gene level. This suggests that AtPLL25 may be part of a family of pectin lyases important for vascular development and growth.

AtPLL25 and NbPLL25, like other plant pectate lyases, are predicted to localize to the apoplast, whereas TuYV is believed to be strictly symplastic. Although this seems to indicate that the interaction with PLL25 is unlikely to occur *in vivo*, we can pose several possible explanations. The TuYV-PLL25 interaction may occur prior to export of PLL25 to the apoplast, under conditions that alter the localization of PLL25, or with a form of PLL25 that is not exported. Recent work characterizing extracellular vesicles in plants also provides a potential avenue for export of TuYV virions or structural proteins into the apoplastic space (Baldrich et al., 2019; Rutter and Innes, 2017, 2018). These extracellular vesicles are believed to be associated with defense responses, as they are found in greater frequency in plants infected with *Pseudomonas syringae*, a bacterial pathogen, and have been found to contain stress-responsive proteins and diverse small RNAs (Baldrich et al., 2019; Rutter and Innes, 2017, 2018). Despite these possibilities, however, we cannot rule out that the AtPLL25 interaction with TuYV is not functionally relevant or does not occur *in vivo*.

Although purified virion preparations were obtained from agroinfiltrated tissue, rather strictly from the phloem cells where TuYV is naturally found, we believe

there is substantial evidence for the validity of this approach. A similar workflow was applied previously to PLRV, and successfully identified several host-virus interactions clearly of functional importance (DeBlasio et al., 2016). Although *N. benthamiana* is not a natural host of TuYV, unlike PLRV, a large portion of the current body of work on TuYV biology has utilized *N. benthamiana* as an experimental host, often in conjunction with local, rather than systemic, infection, so it is neither unreasonable nor unprecedented to assume that this system can yield biologically relevant insight (Brault et al., 2002; Pfeffer et al., 2002; Rodriguez-Medina et al., 2015).

The absence of a detectable effect on TuYV-SUL infection found in the AtPLL25 and PNGase mutants does not necessarily indicate that these interactions are not real or biologically relevant. Both proteins have multiple homologs in *Arabidopsis*, which may have redundant functions during infection. Alternatively, these interactions may be important for a part of the virus life cycle not assayed here, such as aphid transmission.

This work highlights some of the challenges in functionally characterizing the role of individual plant proteins in virus infection. Many host interaction partners perform critical functions and cannot be knocked out without severe, or even lethal, consequences (as was the case for PGDH). In cases where the protein of interest can be safely knocked out, perturbations in the viral life cycle may be masked by redundancy with other homologs or even other host proteins entirely. Furthermore, detecting the effect of these knockouts on the viral life cycle, other than by analysis of titer, is not simple. Until recently, it was not possible to easily assess polerovirus localization in systemically infected, live plants. Assessing tissue localization and the rate of systemic movement of TuYV in this study would have been difficult or impossible without the use of the -SUL recombinant, which opens new doors for

future work on polerovirus movement (Bortolamiol-Becet et al., 2018).

5. Acknowledgements

We would like to thank Veronique Brault and Veronique Ziegler-Graff for the use of their TuYV and TuYV-SUL infectious clones, reagents, assistance with virion purification, and other contributions; James Bruce, Juan D. Chavez, and Jared Mohr for cross-linking mass spectrometry and data analysis; Stacy L. DeBlasio for experimental design support; and Ana Rita Rebelo for technical assistance. Microscopy support was provided by Mamta Srivastava and the Boyce Thompson Institute Plant Cell Imaging Center. Funding for this project was provided by USDA-NIFA grant #2016-67011-24683.

PIR data collection and analysis were performed by Jared P. Mohr, Juan D. Chavez, and James E. Bruce. Infectious clones of TuYV, technical assistance, and purified virions were provided by Veronique Ziegler-Graff and Veronique Brault, with assistance from Mariko M. Alexander. Stacy L. DeBlasio, Michelle C. Heck, and Ana Rita Rebelo assisted with experimental design and data collection. Mariko M. Alexander was the primary or sole contributor to experimental design, *in planta* data collection, data analysis, figure generation, and drafting of the manuscript.

REFERENCES

Alexander, M.M., Mohr, J.P., DeBlasio, S.L., Chavez, J.D., Ziegler-Graff, V., Brault, V., Bruce, J.E., Heck, M.C., 2017. Insights in luteovirid structural biology guided by chemical cross-linking and high resolution mass spectrometry. Virus Res 241, 42-52.

Alonso, J.M., Stepanova, A.N., Leisse, T.J., Kim, C.J., Chen, H., Shinn, P., Stevenson, D.K., Zimmerman, J., Barajas, P., Cheuk, R., Gadrinab, C., Heller, C., Jeske, A., Koesema, E., Meyers, C.C., Parker, H., Prednis, L., Ansari, Y., Choy, N., Deen, H., Geralt, M., Hazari, N., Hom, E., Karnes, M., Mulholland, C., Ndubaku, R., Schmidt, I., Guzman, P., Aguilar-Henonin, L., Schmid, M., Weigel, D., Carter, D.E., Marchand, T., Risseeuw, E., Brogden, D., Zeko, A., Crosby, W.L., Berry, C.C., Ecker, J.R., 2003. Genome-wide insertional mutagenesis of *Arabidopsis thaliana*. Science 301, 653-657.

Bai, Y., Wu, D., Liu, F., Li, Y., Chen, P., Lu, M., Zheng, B., 2017. Characterization and functional analysis of the poplar pectate lyase-like gene PtPL1-18 reveal its role in the development of vascular tissues. Front Plant Sci 8, 1123.

Baldrich, P., Rutter, B.D., Karimi, H.Z., Podicheti, R., Meyers, B.C., Innes, R.W., 2019. Plant extracellular vesicles contain diverse small RNA Species and are enriched in 10- to 17-nucleotide "tiny" RNAs. Plant Cell 31, 315-324.

Boissinot, S., Erdinger, M., Monsion, B., Ziegler-Graff, V., Brault, V., 2014. Both structural and non-structural forms of the readthrough protein of *Cucurbit aphid-borne yellows virus* are essential for efficient systemic infection of plants. PLoS One 9, e93448.

Bortolamiol-Becet, D., Monsion, B., Chapuis, S., Hleibieh, K., Scheidecker, D., Alioua, A., Bogaert, F., Revers, F., Brault, V., Ziegler-Graff, V., 2018. Phloem-triggered virus-induced gene silencing using a recombinant polerovirus. Front Microbiol 9, 2449.

Brault, V., Pfeffer, S., Erdinger, M., Mutterer, J.D., Ziegler-Graff, V., 2002. Virus-induced gene silencing in transgenic plants expressing the minor capsid protein of *Beet western yellows virus*. Mol Plant Microbe Interact 15, 799-807.

Bruyere, A., Brault, V., Ziegler-Graff, V., Simonis, M.T., Van den Heuvel, J.F., Richards, K., Guilley, H., Jonard, G., Herrbach, E., 1997. Effects of mutations in the *Beet western yellows virus* readthrough protein on its expression and packaging and on virus accumulation, symptoms, and aphid transmission. Virology 230, 323-334.

Cao, J., 2012. The pectin lyases in *Arabidopsis thaliana*: Evolution, selection and expression profiles. PLoS One 7, e46944.

Chabi Sika, K., Kefela, T., Adoukonou-Sagbadja, H., Ahoton, L., Saidou, A., Baba-Moussa, L., Jno Baptiste, L., Kotconi, S.O., Gachomo, E.W., 2015. A simple and efficient genomic DNA extraction protocol for large scale genetic analyses of plant biological systems. Plant Gene 1, 43-45.

Chavez, J.D., Cilia, M., Weisbrod, C.R., Ju, H.J., Eng, J.K., Gray, S.M., Bruce, J.E., 2012. Cross-linking measurements of the *Potato leafroll virus* reveal protein interaction topologies required for virion stability, aphid transmission, and virus-plant interactions. J Proteome Res 11, 2968-2981.

Clough, S.J., Bent, A.F., 1998. Floral dip: A simplified method for *Agrobacterium*-mediated transformation of *Arabidopsis thaliana*. Plant J 16, 735-743.

DeBlasio, S.L., Chavez, J.D., Alexander, M.M., Ramsey, J., Eng, J.K., Mahoney, J., Gray, S.M., Bruce, J.E., Cilia, M., 2016. Visualization of host-polerovirus interaction topologies using Protein Interaction Reporter technology. J Virol 90, 1973-1987.

Earley, K.W., Haag, J.R., Pontes, O., Opper, K., Juehne, T., Song, K., Pikaard, C.S., 2006. Gateway-compatible vectors for plant functional genomics and proteomics. Plant J 45, 616-629.

Huep, G., Kleinboelting, N., Weisshaar, B., 2014. An easy-to-use primer design tool to address paralogous loci and T-DNA insertion sites in the genome of *Arabidopsis thaliana*. Plant Methods 10, 28.

Jolly, C.A., Mayo, M.A., 1994. Changes in the amino acid sequence of the coat protein readthrough domain of *Potato leafroll luteovirus* affect the formation of an epitope and aphid transmission. Virology 201, 182-185.

Kaplan, I.B., Lee, L., Ripoll, D.R., Palukaitis, P., Gildow, F., Gray, S.M., 2007. Point mutations in the *Potato leafroll virus* major capsid protein alter virion stability and aphid transmission. J Gen Virol 88, 1821-1830.

Lee, L., Kaplan, I.B., Ripoll, D.R., Liang, D., Palukaitis, P., Gray, S.M., 2005. A surface loop of the *Potato leafroll virus* coat protein is involved in virion assembly, systemic movement, and aphid transmission. J Virol 79, 1207-1214.

Li, X., 2011. Histostaining for tissue expression pattern of promoter-driven GUS activity in *Arabidopsis*. Bio-Protocol 1.

Nurkiyanova, K.M., Ryabov, E.V., Commandeur, U., Duncan, G.H., Canto, T., Gray, S.M., Mayo, M.A., Taliansky, M.E., 2000. Tagging *Potato leafroll virus* with the jellyfish green fluorescent protein gene. Journal of General Virology 81, 617-626.

Palusa, S.G., Golovkin, M., Shin, S.B., Richardson, D.N., Reddy, A.S., 2007. Organ-specific, developmental, hormonal and stress regulation of expression of putative pectate lyase genes in *Arabidopsis*. New Phytol 174, 537-550.

Peter, K.A., Gildow, F., Palukaitis, P., Gray, S.M., 2009. The C terminus of the polerovirus P5 readthrough domain limits virus infection to the phloem. J Virol 83, 5419-5429.

Peter, K.A., Liang, D., Palukaitis, P., Gray, S.M., 2008. Small deletions in the *Potato leafroll virus* readthrough protein affect particle morphology, aphid transmission, virus movement and accumulation. J Gen Virol 89, 2037-2045.

Pfeffer, S., Dunoyer, P., Heim, F., Richards, K.E., Jonard, G., Ziegler-Graff, V., 2002. P0 of *Beet western yellows virus* is a suppressor of posttranscriptional gene silencing. Journal of virology 76, 6815-6824.

Reutenauer, A., Ziegler-Graff, V., Lot, H., Scheidecker, D., Guilley, H., Richards, K., Jonard, G., 1993. Identification of *Beet western yellows luteovirus* genes implicated in viral replication and particle morphogenesis. Virology 195, 692-699.

Rodriguez-Medina, C., Boissinot, S., Chapuis, S., Gereige, D., Rastegar, M., Erdinger, M., Revers, F., Ziegler-Graff, V., Brault, V., 2015. A protein kinase binds the C-terminal domain of the readthrough protein of *Turnip yellows virus* and regulates virus accumulation. Virology 486, 44-53.

Rosso, M.G., Li, Y., Strizhov, N., Reiss, B., Dekker, K., Weisshaar, B., 2003. An *Arabidopsis thaliana* T-DNA mutagenized population (GABI-Kat) for flanking sequence tag-based reverse genetics. Plant Mol Biol 53, 247-259.

Rutter, B.D., Innes, R.W., 2017. Extracellular vesicles isolated from the leaf apoplast carry stress-response proteins. Plant Physiol 173, 728-741.

Rutter, B.D., Innes, R.W., 2018. Extracellular vesicles as key mediators of plant-microbe interactions. Curr Opin Plant Biol 44, 16-22.

Sun, L., van Nocker, S., 2010. Analysis of promoter activity of members of the PECTATE LYASE-LIKE (PLL) gene family in cell separation in *Arabidopsis*. BMC Plant Biol 10, 152.

Tang, X., Munske, G.R., Siems, W.F., Bruce, J.E., 2005. Mass spectrometry identifiable cross-linking strategy for studying protein-protein interactions. Analytical Chemistry 77, 311-318.

Team, R., 2015. RStudio: Integrated Development Environment for R. RStudio, Inc.

Team, R.C., 2013. R: A language and environment for statistical computing. R Foundation for Statistical Computing.

Veidt, I., Lot, H., Leiser, M., Scheidecker, D., Guilley, H., Richards, K., Jonard, G., 1988. Nucleotide sequence of *Beet western yellows virus* RNA. Nucleic Acids Research 16, 9917-9932.

Wickham, H., 2009. ggplot2: Elegant graphics for data analysis. Springer-Verlag New York.

Ziegler-Graff, V., Brault, V., Mutterer, J.D., Simonis, M.-T., Herrbach, E., Guilley, H., Richards, K.E., Jonard, G., 1996. The coat protein of Beet western yellows luteovirus is essential for systemic infection but the viral gene products P29 and P19 are disposable for systemic infection and aphid transmission. Mol Plant Microbe Interact 9, 501-510.

CHAPTER 5

CONCLUSIONS, LESSONS LEARNED, AND FUTURE DIRECTIONS

5.1 Trends in intravirus interactions

Of the two CP/RTP - CP/RTP interactions presented in Chapter 2, both had homologous cross-links of each were found in the previously published PLRV dataset (DeBlasio et al., 2016a), as well as in the cross-linked sample used in Chapter 3 (data not shown). Surprisingly, we identified many fewer CP/RTP - CP/RTP cross-links in the TuYV dataset than in the DeBlasio et al. PLRV data set (DeBlasio et al., 2016a), even though a larger quantity of purified virions was used for cross-linking. The TuYV CP sequence does have fewer lysines in tryptic peptides suitable for mass spectrometry than PLRV; however, the number of intra-virus cross-links is still lower even if cross-linked lysines in PLRV missing or in poor peptides in TuYV are discarded. The intra-virus cross-linking data for TuYV was more similar to the first publication of PIR application to PLRV, which identified four intra-virus cross-links from a 1mg sample of partially purified PLRV (Chavez et al., 2012).

Methodologically, the only commonality we could identify between the three datasets identifying few cross-links (Ch. 2 TuYV, Ch. 3 PLRV, Chavez/Cilia PLRV) which was not present in the DeBlasio PLRV dataset was the use of strong cation exchange fractionation (SCX) in sample preparation of the former (Alexander et al., 2017; Chavez et al., 2012; DeBlasio et al., 2016a). SCX is applied to enrich samples for cross-linked peptides, which have a 4+ positive charge, and supplements avidin enrichment (which was also performed for all four datasets) by depleting the sample of unreacted cross-linker and ‘dead end’ cross-links (Merkley et al., 2013). SCX is a well-established method which has been successfully applied as part of the PIR

workflow for other organisms (Chavez et al., 2018; Schweppe et al., 2017; Zhong et al., 2017); however, the partially purified polerovirus samples used for cross-linking are unique in that the quantity is small (1.5mg or less) and the sample is complex. Therefore, peptide losses or sample fractionation may have a larger impact on these samples than on larger or simpler samples. Alternatively, it is possible that factors other than SCX fractionation contributed to the low number of cross-links identified in most polerovirus samples.

In addition to intra-virus interactions between structural proteins, we also identified an interaction between TuYV CP/RTP and a residue in the protease domain of P1 (Chapter 2, (Alexander et al., 2017)). P1 was also identified as directly interacting with the large subunit of RuBisCO in a previous PLRV study (DeBlasio et al., 2016a). P1 is the only polerovirus non-structural protein that has been identified in PIR cross-linked samples.

5.2 Trends in host-virus interactions

In this work, we identified interactions between PLRV or TuYV structural proteins and at least five proteins from *N. benthamiana* (Chapters 3-4). The five host interactors are distinct from any proteins identified as directly interacting with PLRV structural proteins previously, and have diverse native functions, including cell wall modification, protein modification, amino acid biosynthesis, photorespiration, translation, and RNA silencing. Host interaction partners identified in previous work are similarly diverse (DeBlasio et al., 2016a).

Functional validation of these interactions has proved challenging for reasons outlined below. An effect on PLRV or TuYV titer at one or more time points during local or systemic infection has been shown in null mutants or silenced plants for

eleven of these interaction partners (Chapters 3-4, Appendix 1-2, and unpublished data) (DeBlasio et al., 2016a). Of these, we have identified proteins that increase titer, decrease titer, and have different effects at different time points, when knocked down or out. This suggests that the effects on titer observed are not solely due to general stress caused by the silencing/knock-out.

Knocking out/down some interactors, including the PLL from Chapter 4, did not impact titer at the timepoint(s) tested (Chapter 4 and Appendix 1-2). However, as noted in Chapter 4, this does not mean that these interactions are not real or functional, as the testing we have done does not cover all aspects of the viral life cycle.

As noted in this work and the previous PLRV study, host plants silenced for our interaction partners were frequently chlorotic, stunted, had developmental or morphological abnormalities, or perished prematurely (Chapter 3, Chapter 4, Appendix 1-2). The PLL knockouts represent the only case among the interactors we tested where the knockout appears more robust than the wild-type when PLRV is not present (Chapter 4), and this effect was only noticeable after long periods in short-day conditions, which promote vegetative growth. We cannot rule out that the pleiotropic effects of silencing or knockout out our genes of interest may have had indirect effects on polerovirus replication or movement.

5.3 Limitations of our interaction discovery methods

Mass spectrometry-based proteomics are inherently dependent on the quality of the available protein databases used for searching. This is generally a non-issue when working with model organisms, such as *Arabidopsis*, *E. coli*, or human cell lines; however, the genomes for other species often contain errors due to misassembly, incorrect gene models, and missed annotation of genes. These errors may result in the

complete absence, truncation, or incorrect sequence of some proteins in the proteome database. The inherent bias of such databases can become a significant issue when searching mass spectrometry data, as spectra may be incorrectly assigned or not assigned at all. This error may not be noticed at all unless spectra are checked manually. These issues are further magnified in samples, like the cross-linked virion samples in this work, with few identifiable peptides, where presence of a protein may be reported based on a single mass spectrum.

One example of the way database quality can impact peptide-spectrum matching can be found in Chapter 4. The mass spectra for the host peptide(s) in Figure 4.1 are matched solely to AGO1/10 if searched against v0.4.4 of the *N. benthamiana* proteome, as all four of the relevant RuBisCO large chain homologs are truncated in this version. RuBisCO is the most abundant protein in plants and may be the most abundant protein on Earth, so we, and likely other users, would not have expected it to be misannotated. However, searching the data against v1.0.1 of the proteome, which has greatly improved annotations and gene models, matches the spectra to both RuBisCO large chain and AGO1/10. This also underscores the importance of manually checking peptide-spectrum matches, as we would have missed the putative AGO1/10 peptide if we had simply accepted the top hit for each spectrum. As the quality of the *N. benthamiana* proteome is quite good relative to that of many other plants, insects, and plant pathogens, this potential source of error is extremely important to keep in mind for future studies in organisms with newly sequenced or complex genomes.

The need for database reduction in cross-linking studies by creation of a stage I database introduces another source of error. False or missed identifications in the stage I sample are propagated to the resulting database, creating a flawed search space and

increasing the false discovery rate.

PIR also faces the same inherent biases that all mass spectrometry-based proteomics are subject to. Protein identification relies on the presence of tryptic peptides of a certain size that fragment well and have properties that facilitate their detection by mass spectrometry. For PIR, the requirements are even more stringent - the peptide must contain a solvent-exposed lysine within a given distance of another solvent-exposed lysine, which must also be in a suitable peptide. Fortunately, the PLRV CP contains at least eight such peptides; however the same may not be true for other viral proteins. For example, the P0 protein from our PLRV clone contains a total of six lysines, of which only two are in tryptic peptides of a suitable length.

Additionally, mass spectrometry is inherently biased toward the identification of the most abundant peptides in a mixture, which may not be the most important or most interesting. This is especially true for leaf samples, as RuBisCO is by far the most abundant protein in photosynthetic plant tissue. Furthermore, there is a soft limit on the number of variable post-translational modifications which can be reasonably included in a single database search, as each additional variable modification exponentially increases the search space. Consequently, peptides with rare or complex peptide modifications are likely to be missed unless the user is specifically looking for them.

Mapping of cross-linked peptides to proteins/protein complexes is unusually complex for organisms like poleroviruses, which may have multiple proteins with shared peptides (e.g. CP and RTP), proteins that may exist in monomeric and various multimeric forms, and the potential for both intra- and intermolecular cross-links. These issues are highlighted in Chapter 2, where we used only unambiguous homodimers for modeling, and obtained two different CP trimer models depending on

where in the capsid we assume the measured interactions have occurred.

Finally, it is important to acknowledge the inherent biases in our purified virion samples. These samples represent a snapshot of the protein-protein interactions occurring in a specific organ under the given environmental conditions. For our PIR experiments, we utilized leaf tissue that was agroinfiltrated, which causes some mechanical damage and introduces bacteria into leaves. However, poleroviruses are transmitted exclusively by aphids in nature, and are found only in phloem tissue. The complement and concentration of proteins in phloem cells is likely to differ from mesophyll and epidermal cells, which may result in the loss of some biologically important interactions in our samples. Additionally, cells transformed by agroinfiltration were expressing the PLRV genome under the control of the 35S promoter, which likely does not mimic the dynamics of genome and protein production in naturally infected cells. Despite these differences, 80% of host proteins found co-immunoprecipitating with PLRV from agroinfiltrated *N. benthamiana* were also found co-immunoprecipitating with PLRV from systemically infected potato, strongly suggesting that the agroinfiltration system can still provide useful insight (DeBlasio et al., 2016b).

One of the biggest technical challenges in applying PIR to purified polerovirus virions is that large quantities of virions (at least 0.3mg) are required. While it is relatively easy to obtain milligram quantities of many other plant viruses, poleroviruses replicate to low titer, even under the 35S promoter, and a substantial quantity of virions are lost during purification. Consequently, it is necessary to use large quantities of locally infected (agroinfiltrated) tissue. In our hands, at least 200 grams of tissue are needed for one biological replicate, which is not insignificant even for *N. benthamiana*, which is relatively easy to infiltrate. Fortunately, *N. benthamiana*

is also unusually susceptible to many viruses, including those which normally do not infect solanaceous plants (such as TuYV). This is believed to be due to a naturally present mutation in an RNA-dependent RNA polymerase important for defense against viruses (Yang et al., 2004). While this trait was a key factor in our ability to obtain sufficient tissue for TuYV cross-linking, we must also note that *N. benthamiana* is not a natural host for TuYV (and many other viruses), and is unlikely to perfectly imitate natural hosts in terms of host-virus interactions, especially as a key defense pathway is compromised in *N. benthamiana*. We cannot rule out that this was a factor in our inability to use *A. thaliana* (a natural host) to functionally validate *N. benthamiana* - TuYV interactions found by PIR.

Finally, the virion purification protocol itself introduces some biases. As the procedure is designed to enrich for virions, interactions involving other viral proteins that are not tightly associated with virions are lost. Due to the length of the partial virion purification protocol, any protein interactions that are not stable in purification buffer at 4°C for at least ~60 hours will also be lost. It is likely that there are some weak or transient, but important, interactions which cannot be identified by this method. Additionally, cell lysis in the early steps of the purification causes mixing of cellular compartments, which may introduce interactions that are not present in intact cells. While the PIR cross-linker could theoretically be applied earlier in the purification protocol, it is unlikely to efficiently penetrate cell walls, and the low concentration of virions in samples that have not been enriched by purification means that virus-host and virus-virus interactions are unlikely to be abundant enough to detect. Others in our group have experimented with coupling PIR to co-immunoprecipitation of virions; however, the large quantity of antibody in these samples may have been a significant issue (S.L. DeBlasio, *personal communication*).

Despite these limitations, this work and previous studies have clearly shown that PIR is an excellent tool which identifies functionally relevant, direct host-virus and virus-virus interactions - a feat which had never before been accomplished in a high-throughput way for poleroviruses. The importance of these advances is difficult to understate; however, we also wish to clearly acknowledge the inherent biases and blind spots of our methods.

5.4 Structural modeling

One of the primary advantages of PIR technology is that we can use the cross-linked sites with a distance constraint derived from the length of the cross-linker to structurally model protein-protein interactions. This approach was shown to be powerful in Chapter 2, and in previous work from our group, for making predictions about virion structure (Chavez et al., 2012; DeBlasio et al., 2016a). Cross-linking data can also be useful for validating and generating testable hypotheses about interactions. For example, previous work by DeBlasio and colleagues found that a short stretch of residues in the R-domain was predicted to bind to the substrate binding pocket of a host luminal binding protein (BIP, also discussed briefly in Chapter 1) (DeBlasio et al., 2016a). These residues were a highly conserved stretch of hydrophobic amino acids in the otherwise charged R-domain, which correspond with the known substrate binding motif for BIP.

Although informative, interaction modeling does have several limitations. First, it is dependent on the availability of crystal or cryoEM structures of related proteins for homology modeling of each interacting protein. Although some algorithms for *de novo* protein structure modeling are available, they are notoriously unreliable. Even when suitable related structures are available, homology modeling

and interaction modeling have inherent biases: Both assume a standard, uniform environment, without additional proteins, membranes, or nucleic acids present. While often a reasonable assumption, this can be a serious limitation when modeling polerovirus capsid proteins, which contain a highly charged R-domain that is believed to interact with viral RNA. This impacts modeling of the coat protein itself, but may have greater implications for modeling of protein-protein interactions. CP models from Chapter 2 and previous publications have the R-domain as a long 'tail' extending outward from the S-domain. We cannot be certain what the exact orientation of this tail is, and the assumed orientation affects the possible ways the CP can interact with other proteins (including other CP monomers). Furthermore, without an RNA binding partner, interaction modeling software may attempt to pair this charged tail with negatively charged regions on the partner protein(s). We cannot definitively solve this problem by truncating the R-domain *in silico*, as we cannot determine from PIR data alone whether protein-protein interactions occur with free CP/RTP (where the R-domain is solvent-exposed) or with CP/RTP multimers or virions. This limitation does not mean that modeling should not be attempted, but may help to explain why it is difficult to obtain one clear model for some interactions (e.g., the CP-AGO1 interaction from Chapter 3).

5.5 Functional validation challenges

This study, particularly Chapters 3 and 4, clearly demonstrate the challenges of functional validation of host-virus interactions. Many host proteins found interacting with PLRV or TuYV, here or in previous work, have critical functions in metabolism, photosynthesis, development, or other core processes. Silencing or knocking out these proteins typically causes severe defects in plants, which may indirectly influence

polerovirus infection, and are sometimes lethal. Partial knockdowns or hypomorphic mutants may be useful to help skirt this issue, or, in some cases, overexpression of the gene of interest during infection may yield useful insight. The effect of gene silencing on virus infection may also vary depending on environmental conditions, stress, plant age at inoculation, or other outside factors. One can imagine that the importance of some host-virus interactions may only become clear under certain conditions, for example when other pathways with redundant functions are compromised. As always, greenhouse or growth chamber studies may not perfectly mimic actual effects under field conditions, which is important when considering the application of information from functional studies to plant breeding, biotechnology, and management.

The TRV-based VIGS system in *N. benthamiana* is a useful tool for functional validation, as seen in Chapter 3 and Appendix 1-2. However, the introduction of a second, unrelated virus to the system also introduces another potentially confounding variable. As seen in Chapter 3, VIGS of AGO1 results in an increase in both PLRV and TRV titer. In this scenario, we cannot separate the effects of silencing AGO1 on PLRV from effects of high TRV titer on PLRV, although we know from previous work that a high PLRV titer does not always mean that TRV titer will be elevated (DeBlasio et al., 2018a). Analysis of VIGS data from Chapter 3 is further complicated by the presence of silencing suppressor proteins with different mechanisms of action from PLRV and TRV, which may affect not only titer of both viruses but also expression and activity of AGO1. In the future, we believe it would be preferable to use the polerovirus of interest itself as the VIGS vector, as was recently published for TuYV (Bortolamiol-Becet et al., 2018). This approach has the additional advantage of limiting silencing to phloem and nearby tissues, which may reduce pleiotropic effects of silencing, possibly permitting the targeting of proteins that would not be testable by TRV-based VIGS or genetic knockouts.

Another potential issue in functional testing of host-virus interactions is redundancy. Plants typically have several (and sometimes many) homologs of a single protein - for example, *A. thaliana* has over 60 PLL genes. Although our PIR data sets found only one family member for each host interactor cross-linked to PLRV/TuYV, we cannot rule out that the interaction occurs with other family members, as shown in co-immunoprecipitation experiments with PLRV (DeBlasio et al., 2015). In Chapter 4, we were unable to find any effect on the systemic accumulation of TuYV in PLL25-null mutants. However, this may have been because other PLL proteins were able to fill the role of the missing PLL25, particularly as multiple pectate lyases have been found to co-immunoprecipitate with PLRV (DeBlasio et al., 2015). Host-virus interactions may also be redundant outside of a single protein family. For example, poleroviruses likely interact with many different plant proteins to suppress host defense. Knocking out one of these avenues may not always have a significant effect. This issue is also a challenge for scientists studying the biology of other plant pathogens, including non-viral pathogens. In the molecular arms race between plants and pathogens, it is likely advantageous for both parties to build in multiple fail-safes, so that single mutations are not sufficient to confer resistance/susceptibility.

Redundancy is not the only potential explanation for an apparent lack of phenotype when host interaction partners are silenced. The viral life cycle is complex, and not all aspects of it are easy to assess. While most of our functional studies have focused in alterations in virus titer in locally or systemically infected tissue, these measurements may not pick up on changes in tissue localization, short-distance movement, or stoichiometry of viral protein production. Furthermore, we have not explored any aspects of aphid transmission. Poleroviruses, like many other plant viruses, are known to cause changes in host plants to attract or repel aphid vectors, promote long periods of aphid feeding, alter aphid health, and otherwise manipulate

vectors (for review: (Gray et al., 2014; Ingwell et al., 2012)). These functions are extremely important aspects of the viral life cycle which remain unexplored in the studies presented here.

Although gene silencing/knockout is the most common method used to validate host-pathogen interactions, other options can also provide insight. For example, in Chapter 4 we utilized promoter-GUS fusions to assess expression patterns of PLL25. While this method alone does not provide confirmation, or a mechanism of action in polerovirus infection, it can be useful to show that the gene of interest is expressed in tissues of interest under given conditions and may be useful for generating other testable hypotheses. It may also be useful to fluorescently tag the protein of interest, and/or to verify direct interaction using split-YFP. However, live-cell imaging of phloem is challenging, so transient expression in epidermal cells by agroinfiltration may be required, as was presented with PLRV P17 and P3a in a recent publication (DeBlasio et al., 2018b).

Finally, we found functional validation of host-TuYV interactions to be particularly challenging because we were unable to reliably infect plants with TuYV by agroinfiltration. Despite using the same protocol and infectious clones developed by our collaborators, Veronique Brault and Veronique Ziegler-Graff, who reportedly have a near perfect success rate (personal communication), we typically achieved systemic infection in 0-20% of infiltrated plants. We can only assume that our differing results are due either to slight changes in environmental or soil conditions, or to small nuances in technique. Further optimization of this system on our end, or the use of aphid inoculation, will likely be needed if this protocol is to be used in the future. When we were able to obtain infected plants, we found the recombinant TuYV-SUL clone, which contains a small insert that causes photobleaching in infected and

neighboring cells by VIGS (Bortolamiol-Becet et al., 2018), to be a very useful tool, particularly as TuYV does not cause obvious symptoms in *A. thaliana*. Not only did the use of TuYV-SUL allow us to easily distinguish infected from uninfected plants, but it also enabled us to track how quickly the virus moved systemically and which tissues were infected. The latter properties are especially useful for poleroviruses, which are phloem restricted and do not have available protocols for localization using fluorescent *in situ* hybridization. Without the -SUL recombinant, we would be limited to tissue printing or electron microscopy to assess phloem restriction.

5.6 Practical applications and significance

Our initial goal for this project was to identify host-virus interactions important for polerovirus replication or movement, for which the binding interface on the host protein could be edited based on PIR-guided modeling without affecting the protein's native function. We hypothesized that we would be able to use gene editing in such a case to alter the host protein in a way that hindered the host-virus interaction without pleiotropic effects, to improve plant resistance to poleroviruses. However, a suitable target for these purposes would need to fit very specific requirements: the host-virus interaction must be beneficial for the virus; we must be able to confidently model the host-virus interaction; the interaction site must be distinct from the host protein's active site, as well as any other sites important for regulation or activity of the protein; and the interaction must not be functionally redundant. Due to the stringency of these requirements, combined with technical issues outlined above, we were unable to identify a suitable target for gene editing. However, we believe this strategy still offers substantial promise and is worth pursuing in the future. Additionally, this strategy could be used for functional characterization of particularly interesting targets that

cannot be knocked out or overexpressed without substantial deleterious side effects.

Although we were unable to find a suitable target for gene editing to improve resistance, our results have important implications for polerovirus and general plant virus biology, as well as for similar future studies. In Chapter 1, we applied PIR technology to the study of a second polerovirus species, TuYV, for the first time, and found that cross-links between structural proteins were highly conserved. This allowed us to generate models for the TuYV CP trimer. Notably, one of the two proposed models is the first PIR-guided trimer model with its center at the true three-fold axis of symmetry. Both previous models were centered at six-fold axes, as discussed in Chapter 2. On a broader scale, these results indicate that the structural biology of poleroviruses is likely to be well-conserved across species. This allows us to apply what we have already learned to polerovirus species for which a good toolkit is not yet available, saving time and resources. Furthermore, this finding indicates that host specificity of poleroviruses is unlikely to be determined by the structure of the CP, as PLRV and TuYV have quite different host ranges (Solanaceae and Brassicaceae, respectively). Host specificity in poleroviruses is poorly understood, and is both an important factor for management and an attractive target for engineered resistance.

In Chapter 3, we returned to PLRV, finding evidence that may indicate a direct interaction between PLRV CP/RTP and host AGO1. AGO1 is already known to interact with P0; the possibility that the CP also interacts with AGO1 suggests that the relationship between AGO1 and poleroviruses may be more complex than we thought. Our preliminary data indicates that the CP-AGO1 interaction strengthens silencing suppression by P0, either by inherent silencing suppressor function encoded in P0 or by facilitating P0's activity. As P0 has been previously studied largely outside of the context of the rest of the viral genome, this information is important for future work in

this area. We also found evidence that the silencing suppressor activity of poleroviruses (and likely other viruses, particularly those circulatively transmitted) must be delicately balanced to avoid negatively affecting the host plant. Finally, we showed that PLRV titer is more variable in leaf discs, which are commonly sampled in similar studies, than in petioles. Other polerovirus researchers may wish to consider this in planning their own experiments, as high variability can mask subtle effects on titer. It is unknown at this time to what extent this trend in variability in different sample types applies to other hosts or other plant pathogenic viruses; however, these data certainly have implications for future polerovirus studies, particularly for detecting subtle effects on titer.

Finally, in Chapter 4, we used PIR to uncover direct interactions between TuYV CP/RTP and three host proteins. Although we were not able to ascribe a function to these interactions for reasons discussed above, we found that the promotor of the *A. thaliana* homolog of the PLL found interacting with TuYV is active in vascular tissue. Future studies are necessary to further probe the function of these proteins in polerovirus infection.

5.7 Future directions

Overall, this work raises many more questions and presents several avenues for further research.

Scientists have been studying polerovirus structural biology for decades, using epitope mapping, targeted mutagenesis, computational modeling, and, here, cross-linking proteomics. Though these studies have yielded many important insights, we lack a published crystal or cryoEM structure for any polerovirus virion, structural protein, or structural protein domain, which limits our ability to make additional

progress in this field. From our own work and personal communication with other scientists, we can affirm that poleroviruses are challenging subjects for cryoEM and x-ray crystallography; however, we believe that some solutions are on the horizon. Furthermore, we hope that the cross-linking data from this and previous work will be helpful in solving structures, as has been the case in other systems (Greber et al., 2014).

Open questions also remain from our work on AGO1 in Chapter 3. Given the ambiguities of the peptide ID from our cross-linking data, additional evidence (likely using yeast-2-hybrid or split YFP) is needed to determine whether AGO1 directly interacts with CP. Further experiments are also necessary to untangle the relationship between the CP, AGO1, and P0. Our initial hypothesis that the CP-AGO1 interaction protects AGO1 from P0 was supported by co-immunoprecipitation data, showing that P0 is not detected *in complex* with CP and AGO1 by mass spectrometry, as well as qPCR data showing that PLRV infection does not disrupt AGO1 homeostasis under normal conditions. However, the results of our silencing suppressor screen suggested the opposite: that the CP facilitates the P0-AGO1 interaction or has silencing suppressor activity of its own. One possible explanation is that the enhanced silencing suppression seen in the presence of CP is due to leaky expression of P17, which is contained within the CP ORF. Although not demonstrated for poleroviruses, the P17 of the closely related luteoviruses has been shown to have silencing suppressor activity. This hypothesis could be assessed on a surface level by western blot using a P17 antibody; but, a more definitive test would be to repeat the silencing suppressor assays with a CP construct containing a silent mutation to abolish the P17 start codon. If leaky P17 expression is not responsible for the enhanced silencing, it would also be interesting to test whether some of the PLRV CP mutants that have been functionally characterized do not confer improved silencing suppression. In addition to furthering

our understanding of these mutants, these data could also assist with structural modeling of the CP-AGO1 interaction.

In Chapter 3 we also assessed variability of PLRV titer in different tissue types. It would be informative to extend this analysis to other poleroviruses, phloem-restricted viruses, and mechanically transmissible viruses. This relatively simple experiment would help us understand what the source of this variability is, and could have significant implications for future work in plant virology.

Additional experiments are needed to understand the functional importance of the host-TuYV interactions detailed in Chapter 4. For PLL and PNGase, we would suggest testing the effects of knocking out multiple PLL and PNGase homologs, either by broadly-targeted VIGS in *N. benthamiana* or by crossing existing *A. thaliana* knockouts, as redundancy seems a likely explanation for the absence of an effect in the single-gene knockouts. We would also suggest extending functional experiments to encompass potential effects on aphid feeding or transmission, particularly for PLL, which is involved in cell wall modification.

Finally, we must note that the cross-linking data in Chapter 4 was searched using an older version of the *N. benthamiana* proteome. As discussed previously, whether the newer or older version of the *N. benthamiana* proteome was used had an impact on the proteins identified as interacting with PLRV in Chapter 3; therefore, we believe that re-searching our TuYV cross-linking data with this newer database is absolutely critical to ensure accuracy. Furthermore, the spectra for peptides of interest should be manually inspected.

In more general terms, the functional validation work in Chapters 3-4 and Appendix 1-2 demonstrates the value of titer measurements in surveying the viral life cycle. Historically, most studies of luteovirid biology have assessed systemic

movement, virion assembly, and aphid transmission strictly in terms of presence/absence. These studies are responsible for much of what we know about luteovirid structural biology; however, greater resolution can be achieved by quantitatively measuring titer, either by ELISA or RT-qPCR. For example, had we measured systemic movement of PLRV in Chapter 3 in terms of simple presence/absence, we would not have identified any effect of silencing AGO1. Quantifying titer by RT-qPCR allowed us to identify not only an increase in both PLRV and TRV titer, but also highlighted the increased variability in PLRV titer in AGO1-silenced plants, and permitted us to analyze the relationship between AGO1 expression and virus titer in individual plants. This type of quantitative data also enables statistical analysis within an experiment, improving rigor.

5.8 Closing remarks

This work represents the first application of cross-linking proteomics to TuYV, the third to plant virology, and is among the first five applications to plant pathology in general (Chavez et al., 2012; DeBlasio et al., 2016a; Ramsey et al., 2017). Using this technology, we have demonstrated that interactions between CP domains are conserved across poleroviruses, discovered new direct host-virus interactions, shown that PIR can identify biologically important host-virus interactions, and added a new facet to the complex relationship between poleroviruses and AGO1. We hope that these data will encourage other plant virologists to develop new collaborations to incorporate the latest technologies from animal cell biology and biomedical research in their programs, and that this dissertation will provide a solid foundation for further research in polerovirus biology.

REFERENCES

Alexander, M.M., Mohr, J.P., DeBlasio, S.L., Chavez, J.D., Ziegler-Graff, V., Brault, V., Bruce, J.E., Heck, M.C., 2017. Insights in luteovirid structural biology guided by chemical cross-linking and high resolution mass spectrometry. Virus Res 241, 42-52.

Bortolamiol-Becet, D., Monsion, B., Chapuis, S., Hleibieh, K., Scheidecker, D., Alioua, A., Bogaert, F., Revers, F., Brault, V., Ziegler-Graff, V., 2018. Phloem-triggered virus-induced gene silencing using a recombinant polerovirus. Front Microbiol 9, 2449.

Chavez, J.D., Cilia, M., Weisbrod, C.R., Ju, H.J., Eng, J.K., Gray, S.M., Bruce, J.E., 2012. Cross-linking measurements of the *Potato leafroll virus* reveal protein interaction topologies required for virion stability, aphid transmission, and virus-plant interactions. J Proteome Res 11, 2968-2981.

Chavez, J.D., Lee, C.F., Caudal, A., Keller, A., Tian, R., Bruce, J.E., 2018. Chemical crosslinking mass spectrometry analysis of protein conformations and supercomplexes in heart tissue. Cell Syst 6, 136-141 e135.

DeBlasio, S.L., Chavez, J.D., Alexander, M.M., Ramsey, J., Eng, J.K., Mahoney, J., Gray, S.M., Bruce, J.E., Cilia, M., 2016a. Visualization of host-polerovirus interaction topologies using Protein Interaction Reporter technology. J Virol 90, 1973-1987.

DeBlasio, S.L., Johnson, R., Mahoney, J., Karasev, A., Gray, S.M., MacCoss, M.J., Cilia, M., 2015. Insights into the polerovirus-plant interactome revealed by co-immunoprecipitation and mass spectrometry. Mol Plant Microbe Interact 28, 467-481.

DeBlasio, S.L., Johnson, R.S., MacCoss, M.J., Gray, S.M., Cilia, M., 2016b. Model system-guided protein interaction mapping for virus isolated from phloem tissue. J Proteome Res 15, 4601-4611.

DeBlasio, S.L., Rebelo, A.R., Parks, K., Gray, S.M., Heck, M.C., 2018a. Disruption of chloroplast function through downregulation of phytoene desaturase enhances the systemic accumulation of an aphid-borne, phloem-restricted virus. Mol Plant Microbe Interact 31, 1095-1110.

DeBlasio, S.L., Xu, Y., Johnson, R.S., Rebelo, A.R., MacCoss, M.J., Gray, S.M., Heck, M., 2018b. The interaction dynamics of Two *Potato leafroll virus* movement proteins affects their localization to the outer membranes of mitochondria and plastids. Viruses 10.

Gray, S., Cilia, M., Ghanim, M., 2014. Circulative, "nonpropagative" virus transmission: An orchestra of virus-, insect-, and plant-derived instruments. Adv Virus Res 89, 141-199.

Greber, B.J., Boehringer, D., Leitner, A., Bieri, P., Voigts-Hoffmann, F., Erzberger, J.P., Leibundgut, M., Aebersold, R., Ban, N., 2014. Architecture of the large subunit of the mammalian mitochondrial ribosome. Nature 505, 515-519.

Ingwell, L.L., Eigenbrode, S.D., Bosque-Pérez, N.A., 2012. Plant viruses alter insect behavior to enhance their spread. Scientific Reports 2.

Merkley, E.D., Cort, J.R., Adkins, J.N., 2013. Cross-linking and mass spectrometry methodologies to facilitate structural biology: finding a path through the maze. J Struct Funct Genomics 14, 77-90.

Ramsey, J.S., Chavez, J.D., Johnson, R., Hosseinzadeh, S., Mahoney, J.E., Mohr, J.P., Robison, F., Zhong, X., Hall, D.G., MacCoss, M., Bruce, J., Cilia, M., 2017. Protein interaction networks at the host-microbe interface in Diaphorina citri, the insect vector of the citrus greening pathogen. R Soc Open Sci 4, 160545.

Schweppe, D.K., Chavez, J.D., Lee, C.F., Caudal, A., Kruse, S.E., Stuppard, R., Marcinek, D.J., Shadel, G.S., Tian, R., Bruce, J.E., 2017. Mitochondrial protein interactome elucidated by chemical cross-linking mass spectrometry. Proc Natl Acad Sci U S A 114, 1732-1737.

Yang, S.J., Carter, S.A., Cole, A.B., Cheng, N.H., Nelson, R.S., 2004. A natural variant of a host RNA-dependent RNA polymerase is associated with increased susceptibility to viruses by *Nicotiana benthamiana*. Proc Natl Acad Sci U S A 101, 6297-6302.

Zhong, X., Navare, A.T., Chavez, J.D., Eng, J.K., Schweppe, D.K., Bruce, J.E., 2017. Large-scale and targeted quantitative cross-linking MS using isotope-labeled Protein Interaction Reporter (PIR) cross-linkers. J Proteome Res 16, 720-727.

APPENDIX

APPENDIX 1

ADDENDUM TO:

"VISUALIZATION OF HOST-POLEROVIRUS INTERACTION TOPOLOGIES USING PROTEIN INTERACTION REPORTER TECHNOLOGY"

Introduction

In 2014, the first direct host-virus interactions for *Potato leafroll virus* (PLRV) had been observed using Protein Interaction Reporter (PIR) technology; however, a system for testing the function of these interactions had not yet been developed. Using virus-induced gene silencing (VIGS), the role of eleven candidate host interactors in local PLRV infection was tested, and a method for future work developed. Ultimately, these initial data were not included in the final published manuscript; however, we present them here in abbreviated form as a contribution to the discussion of host-polerovirus interactions.

Materials and Methods

All procedures were identical to those described in the published manuscript (DeBlasio et al., 2016), with the following exceptions: *N. benthamiana* was grown and maintained in a growth chamber, rather than a greenhouse; ELISA readout values were normalized to the average value for the control plants on each plant to facilitate comparison across plates, and then were log-transformed to improve normality; graphs were produced in R Studio using the ggplot2 package (Wickham, 2009). Target proteins and corresponding sequences used for VIGS can be found in Table A1.1.

Construct Name	Target Gene	GeneID	VIGS Construct Sequence
BIPn	luminal binding protein	NbS00039676g0017	TTTTTTTAGGTTTGAGGACAAGGAAGTTCAGAGGGATATGAAGCTTGTCCCATACAA GATCGTGAACAAGGATGGGAAGCCTTACATTCAAGTCAAAATCAAGGACGGAGAA GTTAAGGTATTTAGTCCTGAGGAAATCAGTGCGATGATTCTGATAAAGATGAAGGA GACAGCTGAAGCTTTCCTTGGAAAGAAAATTAAGGATGCTGTAGTAACTGTTCCTGC TTATTTCAATGACGCGCAAAGGCAGGCTACTAAGGATGCAGGTGTTATTGCTGGCTT AAATGTTGCAAGAATTAT
BIPb	luminal binding protein	NbS00039676g0017	GCCCAGAGGCAGGCCACTAAGGATGCAGGTGTTATTGCTGGTTTGAACGTGGCAAG AATCATTAACGAGCCAACTGCAGCTGCCATTGCCTATGGATTAGATAAGAAAGGTG GTGAAAAGAACATCCTGGTCTTTGACCTTGGTGGTGGTACATTTGATGTTAGTATCC TCACTATTGACAACGGTGTTTTTGAGGTTCTTGCCACAAATGGAGACACTCATCTTG GAGGAGAGGATTTTGACCAGAGGATTATGGAGTACTTC ATTAAATTGATAAAGAAGAAGCATGGAAAGGACATCAGCAAGGATAACAGGGCTTT GGGAAAGCTCAGGAGAGAAGCTGAGCGTGCCAAGCGAGCA
GLU	beta-glucanase	NbS00006351g0005	TGCTTTAATAGAACAGATTTTTCGTCCGGATTTGACTATATCCGCTTTCAAGAATCCT AATCCAACGCAGCACCACATAATCTCATCATATAGTGATCTTAGTGTTACTTTAGACT TACCATCAAGTAACCTTAGATTCTTTCTGGTTAGAGGTAGTCCTTATTTGACCTTTGC CGTTAGTGGAAACACTTCCATTTCAATCTCAACCGTCGATCCCATACGCAAACTCTCT TGTGATAGTTCTTTCACTAAGTACACAATTAG ACTCCGTAATCGTCAAACATGGATCCTATATGCATCTTCTCCTATACA
GOGC	golgin	NbS00041061g0004	GAAATGGCGTGGTTTAGCGGGAAACTTGATTTGGGGAACTTGGATCTTGCCGGTGC CGTCAATAAGCTCAGTGAGAGTGTCAAAAATATTGAAAAGAATTTCGACACCGCACT TGGCCTCGAGGAGAAATCTGATGAATCTACTAGCACCGAAGCTTCAGGATTATGGC CTTCCAGTACGGATAGGAAGGCCTTGTTTGATCCTGTCATGGCTTTTATGGGACAAA AAGGTGGGGAGACTACTGTAGAATCTATAGAGAAGGCT GAGTCATCAAAGCCTA
MYO	myosin	NbS00058832g0007	ATTAGAACTGTAAGTTATGTCTTCTGTGATTGTGACAACTTATCAGAATATGGGAAG TCTTAGTACACTAGAGCTTATGCTTGAGGAACTTCAACAAGTAGAGGAAAATACAAA TGATTTGCCACCACCTTTGCCTGTTAGGCCAATTACAAAGGCTAGGTTGCCTAAGGG AAAAAGGAAATTGCCAGAGTTTGGTAAAGAAAAGAATAGAGATGAAGAAGATGGA TATTCACAGGTTAGATGT
PRK	phospho-ribulokinase	NbS00031448g0006	ATCTACTTGGATATCAGCAATGAGGTTAAGTTTGCTTGGAAGATTCAGAGGGATAT GGCTGAGAGAGGGCACAGCCTTGAGAGCATTAAGGCCAGTATTGAAGCCAGGAAG CCAGATTTTGATGCTTACATTGGTGCACTACACCCACAAAAGCAATATGCAGATGCA GTAATTGAAGTGCTACCAACTCAGCTGATCCCAGATGACAATGAAGGCAAAGTTTTG AGAGTGAGATTGATAATGAAGGAAGGAGTGAAGAACTTC AACCCGGTTTACCTGTTTGATGAAGGCTCCACCATC
FBP	fructose 1,6-bisphosphatase	NbS00030497g0015	TATTTCAAGTATTTCTTTGGCTTGTAAGCAGATTGCTTCTCTGGTTCAGAGAGCTGGC ATTTCAAAACTTGCTGAGGTCAAGGTGCTGTTAATGTTCGAGGAGAGGACCAAAAG AAGCTTGATGTTGTTTCTAACGAGTGGACGGATAGGGATTATAGCATCAGAGGAAG AAGATGTACCAGTGGCAGTAGAGGAGAGTTATTATGGAAACTACATTGTCGTGTTT GATCCTCTTGACGGATCATCAAATATTGATGCTGCTTT ATCTTCTGGCGCTATCTTTGGAATATACAGCCCAAATGATGATTGCCTCGTCGATC
PSBQ	photosystem II subunit	NbS00010498g0007	TCAGCCCGTTTGAGCACTGTTAGCACCAGCAGAATTGCCTTGGCTAGACCAGGACTC AGCATTAGAGCCCAACAGGGGTCTGCTGACACTGAAACTAGCCGTAGAGCCGTCAT CGGTCTTGTTGCTGCTGGCCTTGCTGGTTCCTTTGCTCAAGCAGCCTTTGCTGCAGCT AAATCAATCAAGATTGGGGGCGCTCCTCCTCCCTCCGGTGGATTACCTGGAACTTTG AACTCGGATGAGGCAAGGGACTTTGGTCTACCATTG AAGAAGAGGTTT
UbL	ubiquitin ligase	NbS00035343g0006	AGATATCAAAGTATCTCCTTTGGCAACCTCTTTCGACTATGAGCTTTATGACGGCGAT CCTGATCATCTTAGAACTGTTGTTGCTGCACCTACCCTACCTGGTCCTTACATTGATG CTGCGTCAATCAAACTTAGACACAGGATTGGTCGTGGATACTTCGGTGATGTTTGGT CAGCCACACATCATCAGTCAGCTACTGATTACGATGAGAA
HIS	histone	NbS00006630g0001	AAAAGGCAGAGAAAGCCCCAGCAGAGAAGAAGGCCAAAGCCGGGAAGAAGCTCC CAAAGGAAGGCGGAGCAGCAGGAGCTGACAAGAAGAAAAAGAGGGGAAAGAAG AGCGTTGAAACCTACAAGATTTACATCTTCAAAGTGCTGAAGCAAGTGCACCCTGAT ATTGGTATTTCTAGTAAGGCAATGGGGATAATGAACAGTTTCATTAACGATATTTTT GAAAAGCTTGCTCAAGAATCTTCTAGATTGGCTAGGTATAATA AGAAGCCTACTATTACT

Table A1.1: VIGS Targeting Constructs. Gene ID numbers are from version 0.4.4 of the *N. benthamiana* genome (solgenomics.net).

Results and Discussion

The use of the bipartite *Tobacco rattle virus* (TRV) for VIGS in *N. benthamiana* has been well-described for use in general gene characterization and functional evaluation during biotic and abiotic stress. Here, we adapted existing protocols to permit fast screening of VIGS constructs during local PLRV infection. For this procedure, plants are inoculated with the VIGS constructs at ~3 weeks old. About two weeks later, when TRV has moved systemically, silencing the gene(s) of interest in emerging leaves, two young, fully expanded leaves are inoculated with PLRV by agroinfiltration. Leaf disc samples are taken from the infiltrated area at 3 and 5 days post infiltration (dpi), and PLRV titer assessed by enzyme-linked immunosorbent assay (ELISA).

Most VIGS constructs caused only mild phenotypes in TRV-infected plants, such as chlorosis (PSBQ, PRK, FBP, UbL) or mild stunting (AGO1, BIP, PRK, FBP). One construct, targeting histone, caused plant death prior to PLRV inoculation. We generated two constructs targeting a luminal binding protein (BIP) due to the large number of homologs in the *N. benthamiana* genome: a narrow construct we named BIPn targeted only a few homologs, while a broader construct we named BIPb targeted many. Both BIP constructs caused morphological and developmental abnormalities, most markedly leaf rolling and distortion; however, the phenotype caused by the BIPn construct was markedly milder than BIPb. As a negative control, we used a TRV construct targeting an *E. coli* gene, EC1, which is not present in *A. tumefaciens* or *N. benthamiana*.

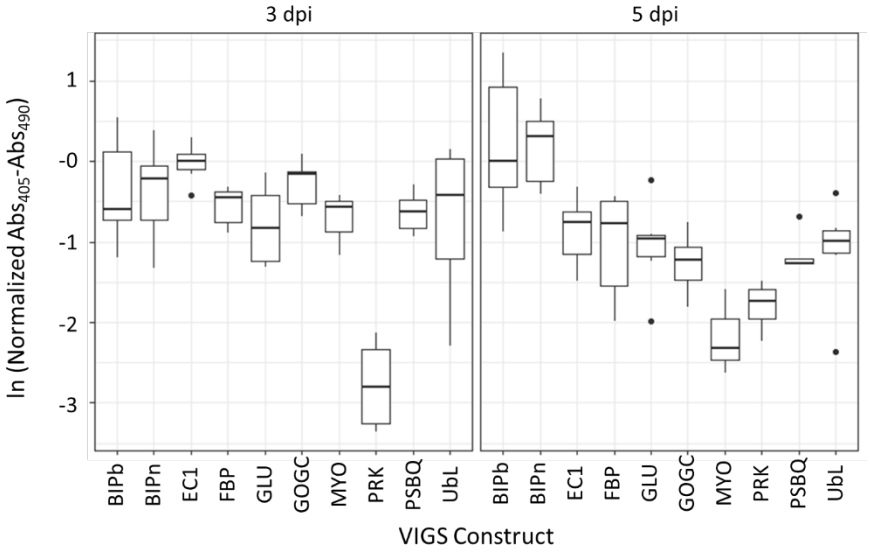

Figure A1.1: Effects of VIGS of host interactors on PLRV titer. PLRV titer in locally infected tissue silenced by systemic infection with different VIGS constructs at 3 and 5 days post infiltration (dpi) with PLRV.

An effect on PLRV titer of silencing the target gene could only be seen at 3dpi for one tested construct, targeting PRK, which had markedly decreased PLRV titer compared to EC1 controls. At 5dpi, effects were more pronounced: plants infected with either of the two BIP constructs exhibited increased PLRV titer, and plants infected with VIGS targeting MYO and PRK had decreased titer, relative to EC1 controls. These effects at 3dpi differed from those included in the published dataset (Appendix 2, and (DeBlasio et al., 2016)), which found significant decreases in PLRV titer in plants infected with TRV targeting PSBQ and BIPn. However, both datasets found that PLRV titer was higher in plants infected with TRV-BIPn at 5dpi.

The disagreements between this dataset and that in Appendix 2 are likely due to differing environmental conditions during the experiment. Here, plants were kept in a growth chamber under high light conditions, whereas below, plants were kept in a greenhouse. Although the greenhouse was climate-controlled and had supplementary lights for cloudy days, the environmental conditions were still much more variable, and we have observed differences even in healthy plants between these two growth conditions.

Additionally, as noted previously in this dissertation, the absence of an effect on PLRV titer in these assays does not indicate the absence of a function. This protocol tests a relatively narrow portion of the virus life cycle, as cells are inoculated by agroinfiltration, and the viral genome is being expressed from the 35S promoter. While some effects on replication may be captured, it is difficult to say for certain how much the constitutive expression of the genome affects titer in these cells. Furthermore, mechanical damage during inoculation and the presence of *Agrobacterium* may induce stress/defense responses that influence PLRV replication. However, as evidenced here and below, this method is useful for quickly screening

candidate host protein interactors. The final publication from DeBlasio et al., follows in Appendix 2.

REFERENCES

DeBlasio, S.L., Chavez, J.D., Alexander, M.M., Ramsey, J., Eng, J.K., Mahoney, J., Gray, S.M., Bruce, J.E., Cilia, M., 2016. Visualization of host-polerovirus interaction topologies using Protein Interaction Reporter technology. J Virol 90, 1973-1987.

Wickham, H., 2009. ggplot2: Elegant graphics for data analysis. Springer-Verlag New York.

APPENDIX 2

VISUALIZATION OF HOST-POLEROVIRUS INTERACTION TOPOLOGIES USING PROTEIN INTERACTION REPORTER TECHNOLOGY[3]

Abstract

Demonstrating direct interactions between host and virus proteins during infection is a major goal and challenge for the field of virology. Most protein interactions are not binary or easily amenable to structural determination. Using infectious preparations of a polerovirus (*Potato leafroll virus* [PLRV]) and protein interaction reporter (PIR), a revolutionary technology that couples a mass spectrometric-cleavable chemical cross-linker with high-resolution mass spectrometry, we provide the first report of a host-pathogen protein interaction network that includes data-derived, topological features for every cross-linked site that was identified. We show that PLRV virions have hot spots of protein interaction and multifunctional surface topologies, revealing how these plant viruses maximize their use of binding interfaces. Modeling data, guided by cross-linking constraints, suggest asymmetric packing of the major capsid protein in the virion, which supports previous epitope mapping studies. Protein interaction topologies are conserved with other species in the *Luteoviridae* and with unrelated viruses in the *Herpesviridae* and *Adenoviridae*. Functional analysis of three PLRV-interacting host proteins *in planta* using a reverse-genetics approach revealed a complex, molecular tug-of-war between host and virus. Structural mimicry and diversifying selection—hallmarks of host-pathogen interactions—were identified within host and viral binding interfaces predicted by our models. These results illuminate the functional diversity of the PLRV-host protein interaction network and demonstrate the usefulness of PIR technology for precision mapping of functional host-pathogen protein interaction topologies.

[3]Originally published as: DeBlasio, S.L., Chavez, J.D., Alexander, M.M., Ramsey, J., Eng, J.K., Mahoney, J., Gray, S.M., Bruce, J.E., Cilia, M., 2016. Visualization of host-polerovirus interaction topologies using Protein Interaction Reporter technology. J Virol 90, 1973-1987.

Introduction

Phloem-limited viruses, such as poleroviruses, are among the most devastating, but least understood pathogens infecting plants due to the technical challenges encountered when studying pathogens that naturally replicate and move within intractable cell types (Stewart et al., 2012). Mutagenesis studies performed with infectious clones have greatly enhanced our understanding of the domains within viral proteins that are responsible for regulating different aspects of the polerovirus life cycle, including virus assembly, systemic movement, phloem retention, and vector transmission (Boissinot et al., 2014; Brault et al., 2003; Brault et al., 2000; Brault et al., 2005; Brault et al., 1995; Kaplan et al., 2007; Lee et al., 2005; Peter et al., 2008). However, very few host proteins have been identified as interacting directly with any polerovirus protein (Bortolamiol et al., 2007; Pazhouhandeh et al., 2006; Reinbold et al., 2013). None have been identified as directly interacting with assembled virions.

Potato leafroll virus (PLRV), the type species of the genus *Polerovirus* in the family *Luteoviridae*, is a positive-sense RNA virus that infects solanaceous hosts (Gray et al., 2014). Encoding only eight proteins, PLRV relies on protein-protein interactions to orchestrate insect transmission and ensure its survival in the host. The icosahedral, nonenveloped virion has two structural proteins: the coat protein (CP) and the readthrough protein (RTP; Fig. A2.1A). The RTP is translated via sporadic readthrough of the CP stop codon (Bahner et al., 1990), producing a protein extension called the readthrough domain (RTD) that protrudes from the capsid surface. The virion is comprised of 180 CP/RTP subunits. While CP is the predominant virion protein, a small but unknown number of RTP subunits are also required in each virion (Fig. A2.1A) for insect transmission (Gray et al., 2014). Assembled virions are the only vehicle for genome movement in plants and aphid vectors (Lee et al., 2005)

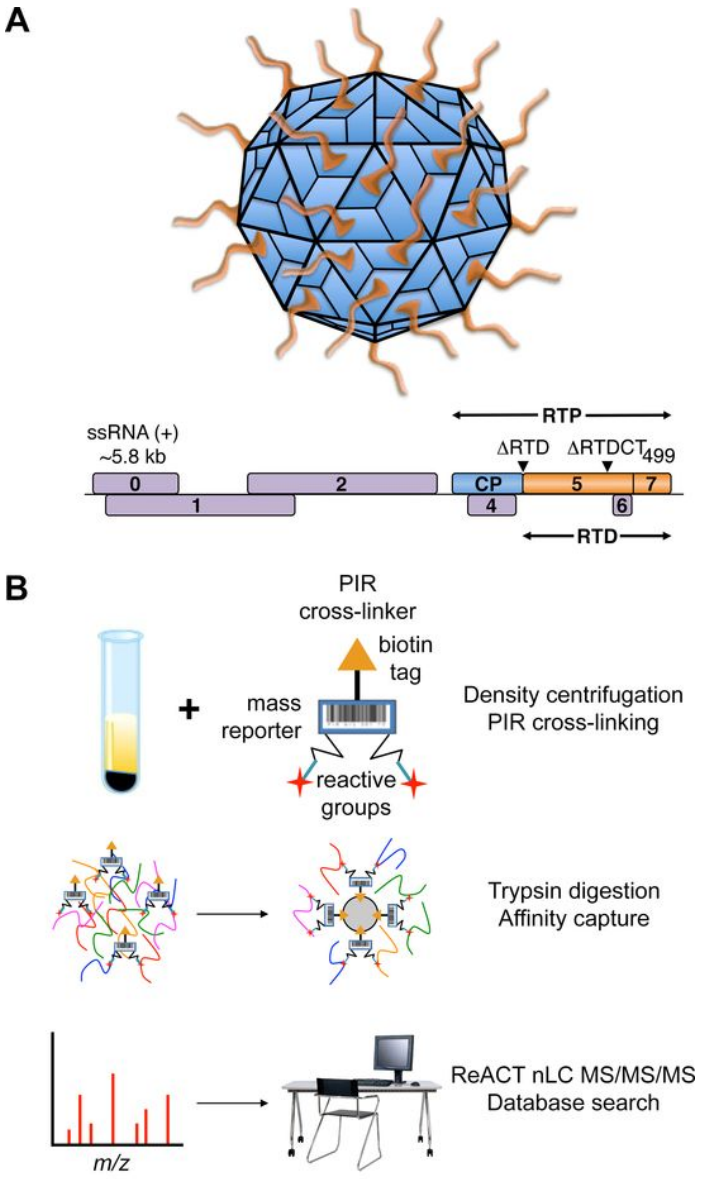
A
RTP
ssRNA (+)
~5.8 kb
ΔRTD
ΔRTDCT499
0
1
2
CP
4
5
6
7
RTD
B
PIR
cross-linker
biotin
tag
mass
reporter
reactive
groups
Density centrifugation
PIR cross-linking
Trypsin digestion
Affinity capture
m/z
ReACT nLC MS/MS/MS
Database search
C
WT
ΔRTDCT499
ΔRTD
PIR
- + - + - +
kDa
150
75
50
37
25
Truncated
RTP
CP dimer
~44 kDa
CP

Figure A2.1: Coupling protein interaction reporter technology and molecular virology to visualize the *Potato leafroll virus*-host interactome. (A) Schematic of a *Potato leafroll virus* (PLRV) virion. The single-stranded, positive-sense RNA [ssRNA(+)] genome of PLRV is shown with positions of the two RTD deletions. (B) PIR workflow used to identify interacting proteins. Virus-host protein complexes were covalently cross-linked using PIR molecules and hydrolyzed into peptides using trypsin, and cross-linked peptide pairs were enriched using avidin-affinity chromatography. A schematic of the PIR molecule with *n*-hydroxyphthalimide (NHP) ester reactive groups, mass spectrometric-labile bonds, mass-encoded reporter, and a biotin affinity tag is shown. (C) Western analysis of viral samples before (−PIR) and after (+PIR) cross-linking with BDP-NHP using a α-PLRV antibody. Monomeric, truncated RTP was detected at ∼58 and 56 kDa in WT and ΔRTDCT$_{499}$, respectively (bracket), while non-cross-linked CP monomer migrates at 23 kDa (black arrow). A protein band migrating at ∼44 kDa in all +PIR samples corresponds to the molecular mass of cross-linked CP homodimer (red arrow).

PLRV is an ideal model virus for protein interaction studies due to its experimental tractability and ability to infect a variety of host plants with genome sequence data available. It is a representative member of a family of economically important plant viruses, and a number of seminal studies using virus mutants have elegantly linked the sequence of the structural proteins to function during plant infection and insect transmission (Kaplan et al., 2007; Lee et al., 2005; Peter et al., 2008). Yet not a single, specific site of protein interaction has been defined between these proteins and host proteins. Such information is necessary for the development of novel virus management tools. However, the disordered nature of the RTP and its confinement to phloem has made protein interaction studies with PLRV and other related viruses challenging (Chavez et al., 2012). In addition, molecular techniques such as yeast-two-hybrid and bimolecular fluorescence, which are traditionally used to probe protein-protein interactions (Nagy, 2008), are not amenable to analyzing interactions that occur between multimeric protein complexes such as assembled virions, nor do they allow for the precise mapping of amino acids involved in the interaction without the generation of additional clones.

Protein interaction reporter (PIR) technology has emerged as a powerful approach to probe *in vivo* and *in vitro* interactions between and within multimeric protein complexes (Chavez et al., 2012; Chavez et al., 2013; Weisbrod et al., 2013). The strategy was developed to identify amino acid residues in interacting proteins that exist close to one another (typically, ≤35Å) by coupling chemical cross-linking with high-resolution mass spectrometry (MS) to derive peptide sequence information. PIR cross-linkers have several features that enable proteome-wide measurements of protein-protein interactions, including *n*-hydroxyphthalimide (NHP) ester reactive groups, MS-labile bonds, an affinity tag, and a mass-encoded reporter ion (Fig. A2.1B). The NHS ester groups enable covalent bond formation with surface exposed

lysine (K) side chains within and between protein molecules to capture interactions, as they exist in cells or solution. The PIR affinity tag enables enrichment of cross-linked products in the sample. This feature is critical for the success of PIR experiments because the majority of proteins are not cross-linked during cross-linker application due to rapid hydrolysis of the cross-linker. Sequence identification of affinity captured cross-linked peptide pairs is achieved using Fourier transform ion cyclotron resonance (FT-ICR) MS coupled with Real-time Analysis Cross-link Technology (ReACT). The MS-labile bonds in PIR molecules allow for the controlled release of the cross-linked peptides within the mass spectrometer so that fragmentation of the peptide backbone can occur on each peptide individually (Chavez et al., 2012; Chavez et al., 2011; Chavez et al., 2013; Weisbrod et al., 2013). The ReACT algorithm allows for the tandem identification of two cross-linked peptides by validating the PIR mass relationship (precursor = mass peptide 1 + mass peptide 2 + mass reporter) of the original cross-linked species in real time. Only peptide ions that are found to satisfy this relationship are selected for peptide fragmentation (Weisbrod et al., 2013). The resulting spectra are mined for protein sequence information using traditional proteomic search engines such as Mascot (Perkins et al., 1999) and SEQUEST (Eng et al., 1994). PIR-derived cross-linked sites identified between or within proteins are then used as distance constraints to develop structural models that enable visualization of proteins and protein complexes, as they exist in cells during cross-linker application (Chavez et al., 2015; Navare et al., 2015; Weisbrod et al., 2013). A recent study using *in vivo* PIR application confirmed OmpA homodimer existence and interfacial regions that were originally identified in bacterial cells by traditional MS methods (Schweppe et al., 2015), demonstrating the ability to derive meaningful structural information from this experimental approach.

In the present study, advances in PIR technology and recent sequencing of

the *Nicotiana benthamiana* genome (Bombarely et al., 2012), a model host plant of PLRV, enabled identification of topological features between host and virus that reveal binding promiscuity, antagonistic coevolution, and structural mimicry, all hallmark features of the coevolutionary race that occurs between viruses and their hosts at the protein level (Daugherty and Malik, 2012; Elde et al., 2009; Franzosa and Xia, 2011). Coupling PIR results to affinity purification and quantitative mass spectrometry, we identified components of the PIR network that are dependent on interactions with the RTD. We used virus-induced gene silencing (Lu, 2003) to probe whether protein interactions identified using PIR are functional and to examine their role during infection.

Materials and Methods

Isolation of virus-host protein complexes

Four- to five-week-old *N. benthamiana* leaves were inoculated with cDNA clones of wild-type (WT) and two PLRV mutants: one that only translates CP and lacks the RTD (ΔRTD) (Peter et al., 2008) and one that translates a truncated RTP lacking the C-terminal 218 amino acids ($\Delta RTDCT_{499}$) (Gray et al., 2014). Plants were infected via *Agrobacterium tumefaciens*-mediated transformation as previously described (DeBlasio et al., 2015a). Infected leaves were harvested 3 days postinfiltration (dpi) and milled into a fine powder under liquid nitrogen using a Mixer mill 400 (Retsch) (DeBlasio et al., 2015a). Virus-host protein complexes were enriched from the cryo-milled tissue using sucrose density centrifugation as described in reference (Chavez et al., 2012). Aphid transmission assays were performed on virus purified from plants infected with wild-type virus to verify that the virus was infectious and transmissible by aphids as described previously (Chavez et al., 2012).

PIR cross-linking of PLRV

PIR chemistry and mass spectrometry were performed on viral host protein complexes purified from plants infected with wild-type (WT) PLRV and the two PLRV RTP mutants in triplicate. Synthesis of the biotin aspartate proline-PIR (BDP-NHP) cross-linker was carried out according to previously described methods (Weisbrod et al., 2013). The BDP cross-linker dissolved in dimethyl sulfoxide was added to 100 to 500 µg of partially purified virus to a final concentration of 1 mM. Concentration of BDP-NHP was selected based on workflows optimized in previous studies (Chavez et al., 2012; Weisbrod et al., 2013). Samples were incubated for 1 h at room temperature with constant mixing. Reacted cross-linker was removed, and cross-linked samples were concentrated to 100 µl using a 30,000-molecular-weight cutoff (MWCO) filter (Millipore, Billerica, MA). Proteins were reduced with 5 mM tris(2-carboxyethyl) phosphine (TCEP) and alkylated with 10 mM iodoacetamide (IAA) in a buffer containing 8 M urea and 100 mM ammonium bicarbonate (ABC). Protein digestion was carried out using a 1:200 (wt/wt) ratio of sequencing-grade, modified trypsin (Promega) to protein in a buffer containing 0.5 M urea and 100 mM ABC. Digests were incubated overnight at 37°C with constant mixing. The samples were desalted using C_{18} Sep-Pak, 3-cm columns (Waters Corporation). Desalted peptide solutions were dried down in a centrifugal concentrator (Genevac) and peptides resuspended in 100 mM ABC. Cross-linked peptides were enriched through biotin affinity using Ultralink monomeric avidin (Pierce). To each sample, 100 µl of avidin resin was added and mixed for 1 h at room temperature. BDP cross-linked peptides were washed and eluted from the avidin resin using 100 mM ABC and 70% acetonitrile–0.5% formic acid, respectively. Enriched peptide samples were dried and stored at −80°C prior to mass spectrometry analysis.

A stage I sample was prepared for the identification of proteins that were

cross-linked using PIR and data-dependent mass spectrometry analysis (see the discussion of mass spectrometry methods below). The stage I sample was necessary for the creation of a stage I database for searching subsequent data sets generated from the avidin-enriched fractions. To generate a stage I protein sample, an aliquot from each virus preparation was combined into one sample (500 μg of total protein) and cross-linked with 1 mM BDP-NHP according to the protocol mentioned above with a few modifications. Reacted cross-linker was removed, proteins were concentrated using the 30,000-MWCO filters (Millipore Co.), and proteins were resuspended in 8 M urea and 100 mM ABC for reduction and alkylation with TCEP and IAA as described above. Urea was removed via buffer exchange using 100 mM ABC. A total of three exchanges were performed, and proteins were concentrated to a volume of 100 μl. An additional 250 μl of 100 mM ABC was added to the sample, and biotin enrichment at the protein level was performed. Avidin-captured cross-linked proteins were washed with 100 mM ABC and eluted in 2 M d-biotin (Pierce) dissolved in a buffer containing 8 M urea and 100 mM ABC. The 2 M d-biotin was removed by buffer exchange in a 30,000-MWCO filter with the urea-ABC buffer. Digestions and C_{18} Sep-Pak solid-phase extraction were performed as described above.

Western blot analysis

To investigate the efficiency of cross-linking reactions, cross-linked and non-cross-linked protein samples (4 to 6 μg) were diluted 1:1 in 2× Laemmli sample buffer (Bio-Rad) and separated on a 8% sodium dodecyl sulfate (SDS)-polyacrylamide resolving gel (Tris/glycine) with a 5% stacking layer (2006). Western blot analysis for PLRV CP/RTP was performed as previously described (2006).

Data-dependent analysis for stage I protein identifications

Tryptic peptides from the stage I sample described above were dissolved at a concentration of 1µM in 0.1% formic acid. One microliter of the stage I peptide sample was injected into the liquid chromatography-mass spectrometry (LC-MS) system consisting of a Waters NanoAcquity LC coupled to a Thermo Velos-FT-ICR mass spectrometer. The sample was loaded onto a 100µm by 3cm trap column packed with Michrom Magic C_{18} 5µm particles with 200Å pores using a flow rate of 2µl/min of 98% solvent A (0.1% formic acid in water) and 2% solvent B (0.1% formic acid in acetonitrile). The sample was washed on the trap column for 10 min before the flow rate was lowered to 300nl/min, and a 120-min linear gradient from 98% solvent A, 2% solvent B to 60% solvent A, and 40% solvent B was used to separate the peptides across a 60cm by 75µm reversed-phase analytical column consisting of fused silica packed with Michrom Magic C_{18} 5µm particles with 100Å pores. Peptides were eluted from the analytical column through a laser pulled tip to which 2kV electrospray voltage was applied. Peptide ions were analyzed by the Velos-FT-ICR mass spectrometer which was operated in a data-dependent manner with a high-resolution MS^1 scan performed in the ICR cell at a resolving power of 50,000 at 400 *m/z*, followed by MS^2scans in the linear ion trap on the 20 most intense ions with charge state greater than 2. Ions selected for MS^2 were dynamically excluded from further MS^2 selection for 45s.

ReACT

Cross-linked peptide samples were analyzed by the LC-MS system described above, which was operated using real-time analysis of cross-linked peptide technology (ReACT) (Weisbrod et al., 2013). Ions detected with a charge state of 4+ or greater were fragmented and analyzed by high-resolution MS^2 where the PIR mass relationship (mass precursor ion = mass peptide 1 + mass peptide 2 + mass reporter)

was queried in real time. If the PIR mass relationship was satisfied within 20ppm or less mass error, then MS^3 scans were performed in the linear ion trap on the two released peptides to obtain peptide fragment ion scans for database searching.

MS data analysis

All databases used for searching were derived from an in-house database created using amino acid sequences corresponding to all coding gene sequences from the released draft sequence of the *N. benthamiana* genome, amino acid sequences from species of *Luteoviridae*, and common animal contaminant protein sequences obtained from the National Center for Biotechnology Information (NCBI). The database is available for download (http://bti.cornell.edu/Nicotiana-benthamiana/). Cross-linking data were searched using an in-house Mascot (Perkins et al., 1999) server v2.3.02 and SEQUEST (Eng et al., 2008) as follows: carbamidomethylation was considered a fixed modification on cysteine residues. The following variable modifications were considered: BDP stump mass (197.032 Da), oxidation of methionine, and deamidation of glutamine and asparagine. Mass measurement accuracy of 30ppm was allowed for precursor ions and 0.8-Da fragment ions. Precursor ion matches were postsearch filtered for a mass measurement accuracy of <10ppm and an expect (E) value of <0.05. Data were searched with SEQUEST against the full database, a stage I database, a reduced internal lysine database, and a reduced plant database of proteins found cross-linked to viral proteins where the observed SEQUEST score for those peptide ions did not fall within the 5% false discovery rate (FDR) cutoff in the previous search strategies but the accurate peptide mass and the largest number of matching fragment ions search yielded the top scoring SEQUEST candidate. All searches were postfiltered for an FDR of 5%. All postfiltered database

matches are available (see Data Set S1 in the supplemental material). For searching the stage I database using Mascot, data were converted into Mascot generic format (mgf) files using tools in Proteowizard (Kessner et al., 2008) and searched using Mascot as described above except the BDP stump mass was used as a fixed modification on lysine residues. The PLRV-plant PIR interaction network was visualized by using Cytoscape (Shannon et al., 2003). The fully labeled Cytoscape network, as well as all raw MS files, is publicly available for download at xlink:DB (http://brucelab.gs.washington.edu/xlinkdb/).

Protein structural modeling

Protein monomer structures were generated by multi-template threading using the Phyre server (Kelley and Sternberg, 2009). The *N. benthamiana* BiP protein model contained 96% of residues modeled at 100% confidence with the top crystal structure of the heat shock protein homolog SSE1 in *Saccharomyces cerevisiae* (PDB c3d2fC). The ACO3 protein model contained 90% of residues modeled at >90% confidence with the top crystal structure (PDB c2b3yB) of human cytosolic aconitase 2 (Dupuy et al., 2006). The PsbQ2 model contained 60% of residues modeled at >90% confidence with the top PDB model, dinzea. All models generated with two or more proteins were made with Patchdock (Schneidman-Duhovny et al., 2005) using the four CP homodimers and cross-linked lysine sites between peptides identified by PIR as distance constraints for the CP trimer, dimer, and plant-virus protein models, respectively. All protein models were labeled and positioned using the Molsoft MolBrowser 3.7-3b (Molsoft L.L.C.). The distance constraints used by Patchdock are linear Euclidean distances between residues, and the possibility exists that the distance penetrates through solvent inaccessible regions of the molecule, occluding cross-link

formation. Therefore, solvent accessible distances (SASD) between cross-linked residues were calculated using XWALK v0.5 (Kahraman et al., 2011) for the top-scoring docked models from Patchdock. Generated models were then filtered according to the criteria of having all cross-linked sites with acceptable SASD values (>49 Å).

Virus-induced gene silencing (VIGS)

DNA sequences (~300-bp fragments) to silence PLRV interacting host proteins were designed using the Sol Genomics VIGS tool with the *N. benthamiana* draft genome as a reference and correspond to the following nucleotide positions in host mRNA sequences: NbS00039676g0017.1 (luminal binding protein, TRV:*BIP*), positions 19 to 311; NbS00028148g0006.1 (aconitase, TRV:*ACO3*), positions 758 to 1039; and NbS00010498g0007.1 (TRV:*PSBQ2*), positions 76 to 351. DNA fragments flanked by *attB*Gateway cloning sequences were synthesized in the pUC57 vector (GenScript) and cloned into the pTRV2 attR2-attR1 binary vector described previously (Liu et al., 2002) using Gateway technology (Life Technologies). VIGS pTRV2 plasmids were transformed into *A. tumefaciens* strain GV22601 and coinfiltrated with pTRV1 into 3-week-old *N. benthamiana* leaves as previously described (Velasquez et al., 2009). A pTRV2 construct targeting *EC-1* (a gene from *Escherichia coli* that is not present in *N. benthamiana* or *A. tumefaciens*) was used as a negative silencing control (Liu et al., 2002; Rosli et al., 2013). Two leaves silenced for target genes were infiltrated with the WT PLRV infectious clone at 3 weeks post-TRV-infiltration. Three, 5mm discs from a single leaf were collected from the PLRV infiltrated area at 3 and 5dpi and stored at −80°C for assessment of virus titer and host gene expression. PLRV titer in infected leaves was measured by double

antibody sandwich enzyme-linked immunosorbent assay (DAS-ELISA) using commercially available α-PLRV antibodies (Agdia) as described earlier (Lee et al., 2005).

Analysis of gene expression

To confirm gene silencing, total RNA was extracted using an RNeasy plant extraction kit (Qiagen) from a pool of three leaf discs per single leaf (n = 8 plants) collected on day zero of infiltration with the PLRV cDNA clone. One microgram was used for oligo(dT) primed cDNA synthesis with a SuperScript III first-strand synthesis kit (Thermo Fisher) according to the manufacturer's instructions. Primers for quantitative PCR (qPCR) were designed to amplify unique regions in target host mRNA sequences described above. The qPCR primers were *BIP*_forward (5′-ATCTGACCGGAATTCCTCCAG-3′) and *BIP*_reverse (5′-TACCAGTGCCCTTATCTTCTGC-3′), *ACO3*_forward (5′-ATCAGCAGCACCGTTCTTTG-3′) and *ACO3*_reverse (5′-TGGCAGTAGTTCTGATCTGAGC-3′), and *PSBQ2*_forward (5′-AACCGTCATCTCTGCTAAGCC-3′) and *PSBQ2*_reverse (5′-GCATAGTACTTCTCTGCTTCAGG-3′). L23 primers were based on reference primer sequences previously published (Liu et al., 2012). Primer annealing temperatures were optimized by RedTaq gradient PCR (Sigma-Aldrich) and determined to be T_a = 60°C for all primers. Real-time qPCR was performed using Fast SYBR green master mix (Life Technologies) and an Applied Biosystems 7900HT (Life Technologies). qPCR was performed on each sample in technical triplicate. A 1:5 and 1:10 dilution series of a 1:1 mix of TRV:*EC1* cDNA samples were used with the target and reference (L23) primers to establish a standard curve and to monitor

reaction efficiency. Reaction products were assessed by melting-curve analysis and gel electrophoresis. Relative quantitation was performed using REST-2009 (http://rest.gene-quantification.info/). Photos of silenced plants were taken with an EOS Rebel T6s (Canon).

PLRV CP sequence alignment

The RTP protein sequences of 19 species of *Luteoviridae* were aligned using the CLUSTALW2 web portal (www.ebi.ac.uk/Tools/msa/clustalw2/). This Clustal alignment was then used to make a graphical consensus sequence with the University of California, Berkeley's Weblogo application (http://weblogo.berkeley.edu/) where the height of the stack indicates the sequence conservation at that position, and the height of the symbols within the stack indicates the relative frequency of each amino acid at that position. Luteoviridae RTP sequences used in the alignment include NP_037637.1(Barley yellow dwarf virus-PAS), NP_054687.1 (Cereal yellow dwarf virus-RPS), NP_563611.1(Bean leafroll virus), NP_620027.1 (Pea enation mosaic virus-1), NP_620066.1(Barley yellow dwarf virus-MAV), NP_620103.1 (Cucurbit aphid-borne yellows virus), NP_620480.1 (Beet mild yellowing virus); NP_050010.2 (Sugarcane yellow leaf virus); NP_620487.1 (Turnip yellow virus); NP_056751.2 (Potato leafroll virus); NP_150434.2(Soybean dwarf virus); NP_813791.1 (Barley yellow dwarf virus-GAV), NP_840017.2(Barley yellow dwarf virus-PAV), NP_840025.2 (Cereal yellow dwarf virus), NP_840098.1(Beet western yellows virus), YP_077188.1 (Carrot red leaf virus), YP_001949872.1(Melon aphid-borne yellows virus), YP_001931932.1 (Tobacco vein distorting virus), and NP_114364.2 (Beet chlorosis virus).

Detection of diversifying selection

The nucleotide sequences corresponding to the coding region of aconitase 3 (*ACO3*) and oxygen-evolving complex protein Q2 (*PSBQ2*) from six and nine species of *Solanaceae*, respectively, were codon aligned using the software program MEGA6 (University Park, PA) and/or the multiple-sequence alignment algorithm MUSCLE, respectively. Residue sites displaying evidence of pervasive diversifying selection with a posterior probability of ≥0.9 were identified using Fast, Unconstrained Bayesian AppRoximation (Murrell et al., 2013) on the DataMonkey web-server (http://www.datamonkey.org). The NCBI accession numbers used for alignments included gi:565370710 (*S. tuberosum*), gi:460395806 (*S. lycopersicum*), gi:11066033 (*N. tabacum*), gi:30407706 (*L. pennellii*), and gi:171854675 (*C. chinense*) for *ACO3* and gi:565400743 (*S. tuberosum*) and gi:350536936 (*S. lycopersicum*) for *PSBQ2*. Sequences obtained from the Sol Genomics Network (http://solgenomics.net/) included NbS00028148g0006.1 (*N. benthamiana*) for ACO3 and NbS00010498g0007.1 (*N. benthamiana*), mRNA_26789_cds (*N. tabacum*), CA02g17690 (*C. chinense*), mRNA_8500_cds (*N. tomentosiformis*), Sme2.5_06605.1_g00005.1 (*S. melongena*), mRNA_32262_cds (*N. sylvestris*), and comp82_c0_seq (*S. dulcamara*) for *PSBQ2*.

Results

PIR measurements of PLRV-host complexes reveal topological features for all cross-linked sites identified by tandem mass spectrometry

Infectious virus-host protein complexes were purified from *N. benthamiana* leaves by sucrose density centrifugation (Cilia et al., 2012) at 3 dpi with wild-type (WT) or mutant PLRV clones containing either of two RTD mutations (ΔRTD, deletion of the entire RTD, and $\Delta RTDCT_{499}$, which lacks the last 218 C-terminal residues, Fig. A2.1A). Mutants were chosen on the bases that both exhibit defects in tissue tropism in plants and aphids compared to the WT (Peter et al., 2009), which could be due to changes in virion structure and/or altered interactions with host proteins. Purified viral samples were reacted with PIR molecules (Fig. A2.1B), and cross-linking was confirmed by Western blot analysis (Fig. A2.1C). Using the PIR ReACT strategy, we identified a total of 375 unique cross-linked peptide pairs from these samples (see Data Set S1 in the supplemental material); 285 were between host proteins, 19 were between or within the two PLRV structural proteins, and 67 were between 33 host and 3 PLRV proteins (Fig. A2.2 and Tables A2.1 and A2.2).

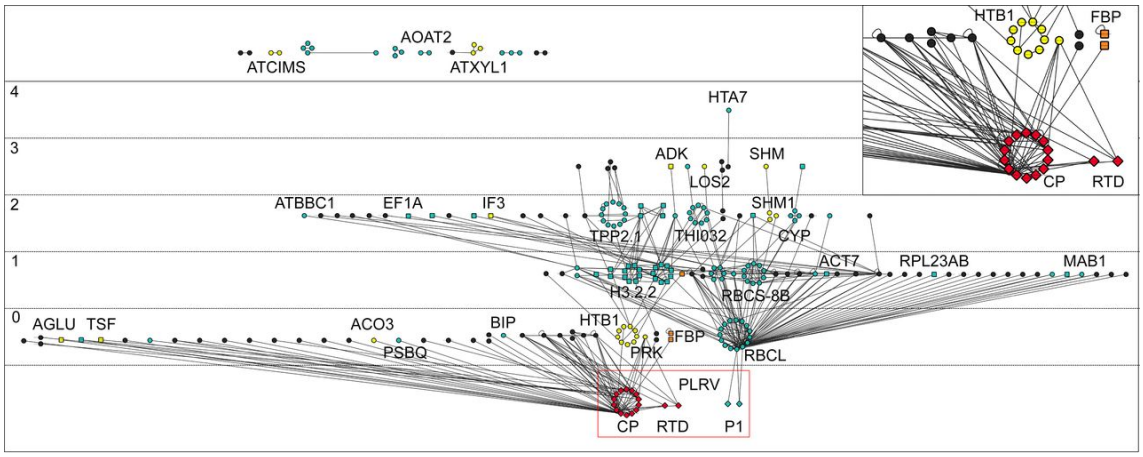

Figure A2.2: PLRV-plant protein interaction network based on PIR and affinity purification-mass spectrometry data (AP-MS). Nodes represent PIR-reactive lysine sites within plant (circles, squares) or viral proteins (diamonds), grouped by protein. Edges connect cross-linked peptides. Nodes are color coded based on their behavior in AP-MS experiments (DeBlasio et al., 2015a; DeBlasio et al., 2015b): aqua, host proteins that affinity purified equally with WT and ΔRTD PLRV; yellow, host proteins enriched in WT compared to ΔRTD; orange, host proteins in which paralogs exhibited different levels in AP-MS experiments; and black, proteins detected in complex with PLRV by PIR but not by AP-MS. Circular nodes represent identical host proteins identified in complex with PLRV by PIR and AP-MS. Squared nodes represent proteins in which functional homologs of PIR plant proteins were detected in AP-MS experiments. Red box highlights PLRV peptides detected. Inset shows zoomed image of the PLRV structural protein cross-links, as well as a subset of virus-host cross-links.

Cross-link[a]	Sequence[b]		FDR[c]	
	Peptide 1	Peptide 2	FDR1	FDR2
CP homodimer	PH**C**K.VSSLQSYVNK$_{150}$FQI**TK**.GGAK	PH**C**K.VSSLQSYVNK$_{150}$FQI**TK**.GGAK	0.00E+00	0.00E+00
	YVNK.FQI**TK**$_{155}$GGAK.TYQAR	YVNK.FQI**TK**$_{155}$GGAK.TYQAR	0.00E+00	3.30E–02
	QI**TK**.GGAK$_{159}$TYQAR.MING	QI**TK**.GGAK$_{159}$TYQAR.MING	0.00E+00	0.00E+00
	DQCR.ILWK$_{184}$**GNG**K.SSDP	DQCR.ILWK$_{184}$**GNG**K.SSDP	0.00E+00	2.79E–02
CP-CP	YVNK.FQI**TK**$_{155}$GGAK.TYQAR	QI**TK**.GGAK$_{159}$TYQAR.MING	0.00E+00	4.88E–02
	PAFK.DGILK$_{105}$AY**HEY**K.ITSI	PH**C**K.VSSLQSYVNK$_{150}$FQI**TK**.GGAK	0.00E+00	0.00E+00
	YVNK.FQI**TK**$_{155}$GGAK.TYQAR	PH**C**K.VSSLQSYVNK$_{150}$FQI**TK**.GGAK	0.00E+00	0.00E+00
	QI**TK**.GGAK$_{159}$TYQAR.MING	PH**C**K.VSSLQSYVNK$_{150}$FQI**TK**.GGAK	0.00E+00	0.00E+00
	DQCR.ILWK$_{184}$**GNG**K.SSDP	PH**C**K.VSSLQSYVNK$_{150}$FQI**TK**.GGAK	2.12E–02	0.00E+00
	ILWK.**GNG**K$_{188}$SSDPAGSFR.VTIR	PH**C**K.VSSLQSYVNK$_{150}$FQI**TK**.GGAK	0.00E+00	0.00E+00
	PRGR.GSSETFV**FT**K$_{76}$DNLVGNSQGSFTF**GP**SLS**DcPAFK**.DGI**L**	DQCR.ILWK$_{184}$**GNG**K.SSDP	0.00E+00	3.95E–02
	GVPR.GRGSSETFV**FT**K$_{76}$DNLVGNSQGSFTF**GP**SLS**DcPAFK**.DGI**L**	DQCR.ILWK$_{184}$**GNG**K.SSDP	0.00E+00	0.00E+00
	V**FT**K.DNLVGNSQGSFTF**GP**SLS**DcPAFK**$_{100}$DGILK.AY**HE**	DQCR.ILWK$_{184}$**GNG**K.SSDP	0.00E+00	2.79E–02
	PAFK.DGILK$_{105}$AY**HEY**K.ITSI	DQCR.ILWK$_{184}$**GNG**K.SSDP	2.79E–02	1.40E–02
	YVNK.FQI**TK**$_{155}$GGAK.TYQAR	DQCR.ILWK$_{184}$**GNG**K.SSDP	0.00E+00	2.62E–02
	ILWK.**GNG**K$_{188}$SSDPAGSFR.VTIR	DQCR.ILWK$_{184}$**GNG**K.SSDP	0.00E+00	0.00E+00
RTD-CP	DGVK.ISK$_{351}$LR.NDNT	DQCR.ILWK$_{184}$**GNG**K.SSDP	8.70E–04	0.00E+00
	TDGR.FFLV**GPA**IQK$_{405}$TAK.**YNY**T	PH**C**K.VSSLQSYVNK$_{150}$FQI**TK**.GGAK	8.77E–03	8.77E–03
	TDGR.FFLV**GPA**IQK$_{405}$TAK.**YNY**T	DQCR.ILWK$_{184}$**GNG**K.SSDP	1.70E–02	0.00E+00

Table A2.1: Cross-linked peptides derived from PLRV structural proteins.

[a]Type of cross-linked pair identified, unambiguous homodimer or inter-/intramolecular cross-link between CP-CP and RTD-CP.

[b]Amino acid sequence of viral peptides deduced from MS3 fragmentation and database searching with MASCOT and/or SEQUEST. The four amino acid residues before and after trypsin cleavage are given as a reference. The K residue number indicates position of cross-linker reactivity. Residues in boldface indicate positions in PLRV with known biological function. Modified cysteine residues are marked in lowercase.

[c]Representative sequence assignment false discovery rates (FDR) for the indicated peptides. All FDRs are <0.05.

For larger version, see: https://jvi.asm.org/content/90/4/1973

Host protein	Protein symbol	Biological process[b]	Cross-linked host peptide[c]	Viral protein[d]	Reactive K in viral peptide[e]
NbS00017260g0020.1+1	AGLU	Carbohydrate metabolism	M.K$_{3}$FVDK.LHQD	CP	K184
NbS00031448g0006.1+1	PRK	Carbohydrate metabolism	LRVR.LIMK$_{334}$ EGVK.NFNP	CP/RTP	K76;105;150;184;351
NbS00030497g0015.1	FBP	Carbohydrate metabolism	DDRL.K$_{282}$YIDHLK.ETGP	CP	K150
NbS00028148g0006.1	ACO3	Metabolism	AVPK.DAQEK$_{506}$VVK.FSFH	CP	K150
NbS00055792g0005.1	HLTT	Metabolism	LAGR.IIEGPNK$_{46}$K.LLVN	CP	K150
NbS00006351g0005.1	ENG1	Cell wall catabolism	LDYK.WDVKGK$_{203}$GK.LLML	CP	K150
NbS00010498g0007.1	PSBQ2	Photosynthesis	DEAR.DFGLPLK$_{114}$K.RFYL	CP	K150
NbS00018819g0113.1	PEX44	Oxidoreductase	SMDR.NLFAK$_{190}$LSR.TCAA	CP	K150
NbS00058832g0007.1+1	ATM1	Cell movement	SKLR.EVK$_{430}$ATMK.QLGH	CP	K150
NbS00029310g0009.1+1	DYM	Golgi organization	KYNK.LADIK$_{928}$NDK.MHVP	CP/RTP	K76;105;150;159;184;351
NbS00041061g0004.1	GOGC5	Golgi vesicle transport	EQNK.K$_{484}$SDAAALLK.EKDE	CP	K150
NbS00018319g0022.1	MSTO1	Mitochondrion distribution	MDSK.GRK$_{243}$QAISR.NLHD	CP	K150
NbS00003910g0002.1	VITH1	Iron transport	STQR.DIAK$_{97}$SIADNCR.SENE	CP	K150
NbS00032747g0004.1	NOP2	rRNA processing	MAGP**K**LGK$_{8}$K.AGSK	CP	K150
NbS00039676g0017.1	BIP1	Protein folding ER	VDEK.EK$_{500}$IETAVK.EALE	CP	K76
NbS00029684g0026.1+1	HSP70	Protein folding	DASK.FLNDK$_{200}$VSK.AVVT	CP	K155
NbS00013225g0002.1	TSF	Translation	RPAR.K$_{126}$SEMPPVK.NEDL	CP	K76
NbS00024032g0009.1	RPS23	Translation	KCAR.VQLMK$_{71}$NGK.KIAA	CP	K105
NbS00006630g0001.1+1	HTB1	Chromatin assembly	AGKK.LPK$_{71}$EGGAAGADK.KKKR	CP	K184
NbS00006307g0001.1+1	WNK5	Signaling	GRFK.EILGK$_{33}$GATK.IVYK	CP/RTP	K76;100;105;150;155;159;184;351
NbS00035343g0006.1	KEG	Signaling	KCIK.SK$_{588}$LTKDPK.NHQT	CP	K100;150;159
NbS00046587g0006.1	PNCBP	Signaling	SDEK.VK$_{854}$EADNVELQESHKSAAVDLHSVAR.DRKL	CP	K159
NbS00005411g0003.1	KED	Stress response	ITTR.EIK$_{490}$IGGGNK.LPVA	CP/RTP	K76;100;105;150;405
NbS00009361g0013.1	MYND	Transcription	AFGR.FQEQFGSGPGLGPGSGTNLMK$_{32}$IDGIAPPFIKSVYR.AAAA	CP	K159
NbS00016541g0014.1	ZF_PHD	Transcription	EGIR.AK$_{208}$AQSAYYPK.RVKV	CP	K150
NbS00038737g0015.1+1	CRF4	Transcription	DEEK.AGGEK$_{91}$SEQHGK.TCVK	CP	K150
NbS00056942g0009.1	TFB3	Transcription	EEER.IK$_{74}$LENDGK.DSKF	CP	K76;105;155;184
NbS00028345g0001.1		Transcription	DAPR.K$_{232}$PVNRFR.NIDK	CP	K76
NbS00014790g0110.1		Unknown	GYQK.LIK$_{108}$MLDGK.TISV	CP	K150
NbS00016817g0004.1		Unknown	SRGK.K$_{95}$TIGFYGK.CGVS	CP	K150
NbS00058297g0001.1		Unknown	HGDK.GKQVK$_{65}$DNK.KEAK	CP	K76;100;105;150
NbS00004956g0015.1	RBCL	Photosynthesis	RNIK.IPPAYVK$_{28}$TFQGPPHGIQVER.DKLN	P1	K426;K549
NbS00004956g0015.1	RBCL	Photosynthesis	IKPK.LGLSAK$_{65}$NYGR.AVYE	P1	K549

Table A2.2: PLRV-host interaction topologies identified using PIR technology[a]

[a]The gene accession number and protein symbols (columns 1 and 2) were manually curated from an in-house database of protein sequences from the *N. benthamiana* draft genome or from BLAST analysis. A +1 indicates the number of additional plant proteins sharing the same PIR peptide sequence in the *N. benthamiana* protein database.

[b]Biological process was manually curated using UniProt.

[c]Amino acid sequence of host peptide deduced from MS3 fragmentation and database searching with MASCOT and/or SEQUEST. The four amino acid residues before and after trypsin cleavage are given as a reference. K residue number indicates position of cross-linker reactivity and is based on host protein sequences derived from the *N. benthamiana* draft genome including the initial methionine. False discovery rates (FDRs) for host peptides were <0.05.

[d]Protein parent of viral peptide identified in cross-linked pair.

[e]Residue number of the cross-linked lysine(s) in the viral peptide based on the PLRV infectious clone CP/RTP sequence shown in Fig. S1 in the supplemental material and the PLRV P1 sequence in our in-house *Luteoviridae* protein database. FDRs for viral peptides were <0.05.

Larger version of table is available from: https://jvi.asm.org/content/90/4/1973

In WT PLRV samples, the majority of virus-virus cross-links identified were between residues in the CP domain, with only three unique cross-links identified between the CP and the N-terminal domain of the RTD (Table A2.1). These results most likely reflect the differential abundance of these two proteins within the virion, with the majority of subunits being CP and only a few subunits being readthrough protein (Brown et al., 1996; Gray et al., 2014). As expected, cross-links within or between the RTD C terminus were not identified in WT samples due to cleavage of this region during virus purification (Filichkin et al., 1994; Perry et al., 1998; Wang et al., 1995) (Fig. A2.1C). Interestingly, deletion of the entire or partial RTD in the mutants did not result in any new cross-links identified within the CP domain (data not shown), even though the two mutants showed distinct bands on Western blots after cross-linking (Fig. A2.1C). We also identified the viral replicase P1 polyprotein cross-linked to multiple sites in the host RuBisCO large subunit (RbcL) (Fig. A2.2) but not the PLRV structural proteins, data that are consistent with previous immunological studies that show P1 is enriched in membrane and cytosolic fractions from infected plants but not directly associated with virions (Prüfer et al., 1999).

Among the host-virus interactions identified, the CP interacted with 32 host proteins, some of which were observed with multiple cross-linked peptide pairs. Four of these proteins also formed cross-links with the RTD (Fig. A2.2). Orthologues of these PLRV-interacting plant proteins function in diverse biochemical pathways, including photosynthesis, carbon fixation, plant defense, protein folding, and trafficking (Table A2.2). Some have been shown to play important roles in the propagation and movement of other plant and animal viruses (53–57). Forming 104 unique intra- and intermolecular cross-links with 41 different plant proteins, RbcL was the most identified plant protein in our samples (Fig. A2.2 and see Data Set S1 in the supplemental material). However, we did not identify cross-links between RbcL and

the PLRV structural proteins, supporting the validity of the 32 CP/RTD-host cross-links as specific interactions and not an artifact of the purification or cross-linking. To the best of our knowledge, these are the first measurements of a host-viral protein interaction network that include topological features for every cross-linked site identified.

Comparison of PIR with affinity purification-mass spectrometry (AP-MS) data (DeBlasio et al., 2015a; DeBlasio et al., 2015b) revealed unique insights into the architecture of the PLRV-plant interaction network. By comparing the PIR results to an AP-MS data set generated using quantitative, affinity isolations of WT or ΔRTD PLRV from *N. benthamiana* (DeBlasio et al., 2015a; DeBlasio et al., 2015b) at the same time point during PLRV infection as our PIR experiments, 53 host proteins (or functional homologs) were found to be associated (directly or indirectly) with virus by both approaches. Of these 53 plant proteins, 10 were found directly cross-linked to the viral structural proteins by PIR, while the remaining 43 mapped onto the P1 interaction network (Fig. A2.2). Of the 53 proteins, 41, including P1, were equally enriched in AP-MS experiments with WT or ΔRTD PLRV; however, 12 host proteins (or functional homologs) in the PIR network were enriched in WT compared to ΔRTD (yellow nodes, Fig. A2.2). Five of these (AGLU, TSF, ACO3, HTB1, and PRK) were cross-linked to sites within the CP with one, phosphoribulokinase (PRK), forming an additional cross-link to the RTD (Table A2.1). Our data collectively show that these five host proteins directly interact with topologies created by the CP and RTD and that the strength of their association to the virion is dependent on the presence of the RTD. The remaining 65 host proteins detected in this study were unique to the PIR-derived PLRV-host interaction network and not detected in complex with virus by AP-MS. Among these, 22 were found cross-linked to the viral structural proteins (black nodes, Fig. A2.2, Table A2.2, and see Data Set S1 in the supplemental material). In

contrast, more than 1,000 host proteins were identified as enriched in PLRV affinity purifications that were not identified in the PIR experiments (DeBlasio et al., 2015a).

PLRV capsid possesses multifunctional hot spots of protein interaction

Sites of host-virus cross-linking and four unambiguous CP homodimer cross-links (Fig. A2.3A and Tables A2.1 and A2.2) were used to refine the topological surface features of the CP trimer, the oligomeric protein building block that comprises the protein lattice of the PLRV virion (Fig. A2.1A). Only one trimer structural model (Fig. A2.3B) predicted all seven of the CP lysine residues found in host-viral cross-links to be solvent exposed by Xwalk analysis (Kahraman et al., 2011) and therefore accessible to react with PIR molecules (data not shown). The additional virus cross-link sites identified in this study predicted a looser packing of the CP subunits compared to previous trimer model predictions (Chavez et al., 2012; Lee et al., 2005). Looser CP subunit packing would facilitate exposure of the CP N terminus on the surface of virions, a model supported by epitope mapping data that shows this region is partially solvent accessible in PLRV (Torrance, 1992) and the related *Barley yellow dwarf virus* (Rizzo and Gray, 1992).

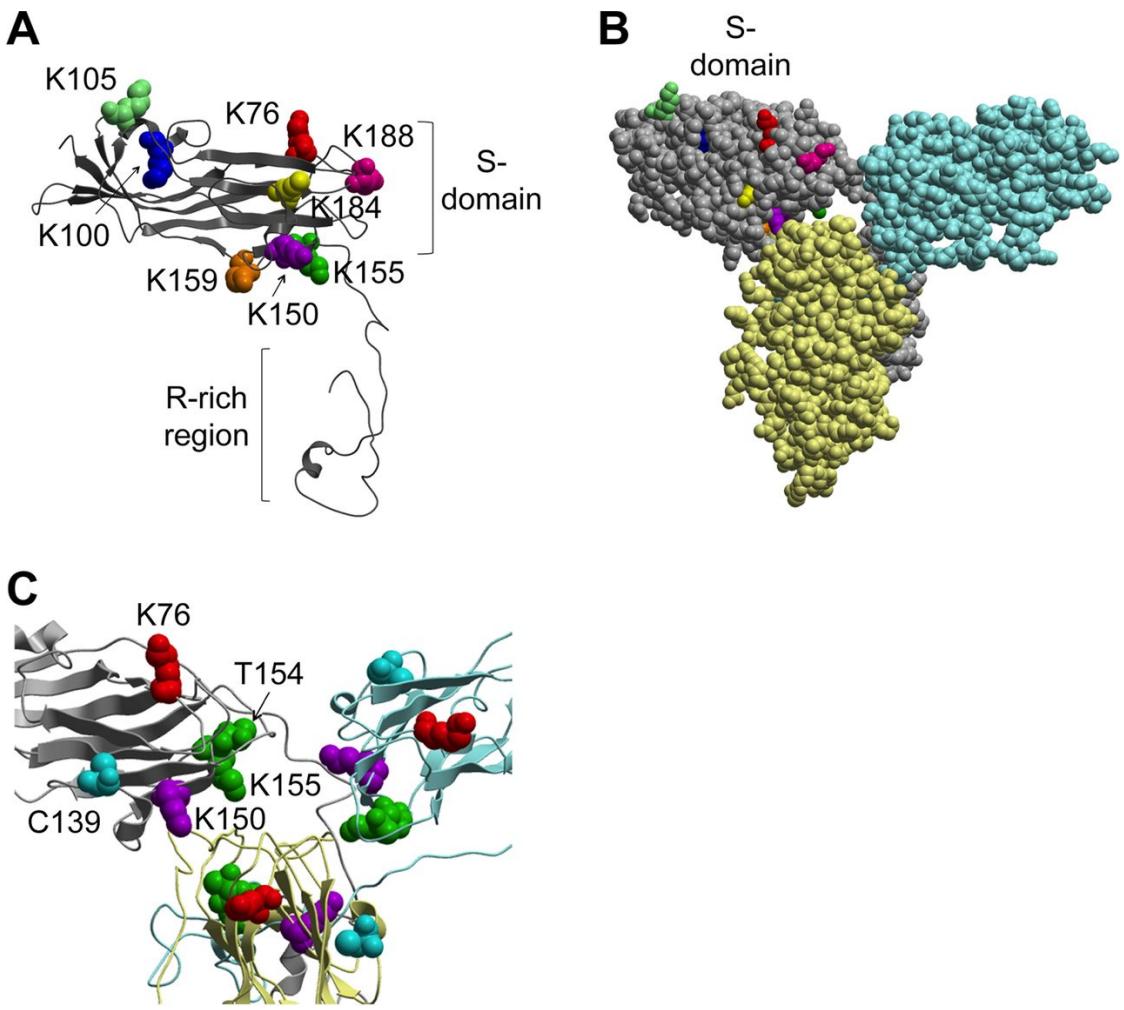

Figure A2.3: Protein interaction reporter data are useful for predicting PLRV capsid topology. (A) Shell (S) domain and arginine (R)-rich region of the CP monomer. (B) Top-view model of a CP trimer using the four unambiguous homodimers K_{150}, K_{155}, K_{159}, and K_{184} as distance constraints. Residues found cross-linked with plant proteins are highlighted as follows: K_{76} (red), K_{100}(blue), K_{105} (light green), K_{150} (purple), K_{155} (green), K_{159} (orange), and K_{184} (yellow). The K_{188}residue (pink) has previously been shown to be PIR reactive (16). (C) Ribbon model of the CP trimer interface. Substitutions of residues C_{139} (light blue) and TK_{155} (green) result in defects in the virus life cycle (Table A2.3) and are located near K_{150} (purple), a positional "hot spot" for virus-host protein interactions.

One reactive lysine site (K_{150}) located on the surface of the virus within the CP (purple, Fig. A2.3) was a "hot spot" for protein interactions. Residue K150 was detected in seven virus-virus (Table A2.1) and 22 host-virus cross-linked peptide pairs (Table A2.2). Reverse genetics confirms the importance of this topology for virion structure-function relationships (7). Mutation of C139 (light blue, Fig. A2.3C), near this highly reactive K_{150}, affects systemic virus movement within the host (Table A2.3). In contrast, mutations in residues TK_{155} (green, Fig. A2.3C), also in proximity to K_{150}, alter virion assembly and accumulation of the nonincorporated form of the RTP (Table A2.3). A previous study has shown that a TK_{155} deletion mutant could be partially rescued by an additional K-to-R substitution at residue K_{76}, a PIR-reactive CP site identified cross-linked to nine host proteins (Table A2.2). Together, these data support the idea that different virus-host protein interactions topologies may be functionally redundant *in planta*.

Viral peptide[a]	Mutation[b]	Virion assembly[c]	RTP[d]	Systemic infection[e]	Aphid transmission[f]	Residue characteristics[g]
GVPR.GRGSSETFV**FT**K$_{76}$DNLVGNSQGSFTF**GP**SLS**DcPAFK**.DGI**L**	FT	–	–	–	–	Conserved, epitope
V**FT**K.DNLVGNSQGSFTF**GP**SLS**DcPAFK**$_{100}$DGILK.AY**HE**	GP	–	–	–	–	Conserved
V**FT**K.DNLVGNSQGSFTF**GP**SLS**DcPAFK**$_{100}$DGILK.AY**HE**	DCPAFK	+	+	Defect	Defect	Surface
PAFK.DGI**L**K$_{105}$AY**HEY**K.ITSI	L-H	–	–	–	–	Conserved, acid patch
PAFK.DGI**L**K$_{105}$AY**HEY**K.ITSI	E	+	+	Defect	Defect	Conserved, acid patch
PH**C**K.VSSLQSYVNK$_{150}$FQI**TK**.GGAK	C	+	+	Defect	Defect	Surface, external
YVNK.FQI**TK**$_{155}$GGAK.TYQAR	TK	–	+	–	–	Conserved, internal
QI**TK**.GGAK$_{159}$TYQAR.MING						
DQCR.ILWK$_{184}$**GNG**K.SSDP	GNG	–	–	–	–	Conserved, surface
ILWK.**GNG**K$_{188}$SSDPAGSFR.VTIR						
TDGR.FFLV**GPA**IQK$_{405}$TAK.**YNY**T	GPA	+	Not incorporated	Not tested	Not tested	Conserved, NT-RTD
TDGR.FFLV**GPA**IQK$_{405}$TAK.**YNY**T	YNY	+	Not incorporated	Not tested	Not tested	Conserved, NT-RTD

Table A2.3: Protein interaction site neighbor residues in PLRV structural proteins that are critical for virion function

[a]Amino acid sequence of viral peptides found cross-linked to viral and/or host peptides. The four amino acid residues before and after trypsin cleavage are given as a reference. K residue number indicates position of cross-linker stump mass. Residues in boldface indicate positions in PLRV with a known biological function.

[b]Residues in CP/RTP found previously to play a role during the life cycle of PLRV (7–9).

[c]Effect of mutation on virion assembly. A − or + indicates virion dissociation or WT assembly, respectively.

[d]Effect of mutation on the detection of full-length RTP in host and incorporation in assembled virions.

[e]Efficiency of mutant to move systemically within the host. Complete loss of systemic infection is indicated by a minus sign (–).

[f]Ability of mutant virus to be transmitted by aphids.

[g]Structural or biological characteristics of residues based on epitope-mapping studies, predictive secondary structure models, or sequence alignments of known polerovirus sequences (7, 8). NT-RTD is the N terminus of the readthrough domain.

Larger version of table can be found at: https://jvi.asm.org/content/90/4/1973

Validating biological function of host-virus interactions using reverse genetics

To test the biological relevance of PLRV-interacting host proteins, we used virus-induced gene silencing (VIGS) (Lu, 2003) to knock down the expression of three plant proteins we identified cross-linked to the PLRV CP: luminal binding protein (BiP), cytosolic aconitase (ACO3), and oxygen-evolving enhancer protein (PsbQ2). These proteins were chosen for silencing on the basis that (i) full crystal structures existed for modeling with PLRV (see below), (ii) these proteins were also identified in complex with PLRV in our AP-MS experiments (Fig. A2.2) (DeBlasio et al., 2015a), and (iii) evidence existed in the literature of their involvement in regulating other known pathogens (Balasubramaniam et al., 2014; Buchkovich et al., 2009; Klessig et al., 2000).

After gene silencing was confirmed (Fig. A2.4A), we tested the effect on PLRV accumulation during local infection of N. benthamiana (Fig. A2.4B). Independent of PLRV infection, 75.6 and 76.5% silencing of BIP and ACO3, respectively (Fig. A2.4A), resulted in significant morphological defects that mimicked PLRV disease symptoms, including curled, distorted leaves in BIP-silenced plants and severe dwarfism and chlorosis in ACO3-silenced plants (Fig. A2.4C to F). Both the BIP and the ACO3-silenced plants also developed localized regions of cell death (Fig. A2.4Eand F, red arrows) in the absence of PLRV. The phenotypes observed in ACO3-silenced plants were previously reported when *ACO* expression was reduced using PVX-based VIGS (Moeder et al., 2007). Silencing of *PSBQ2* had no phenotypic effect on plant morphology. Silencing these three genes resulted in a decrease in PLRV titer early on during infection (Fig. A2.4B), while silencing of BIP led to an increase in PLRV titer at a later stage of infection (Fig. A2.5). The results are described further below.

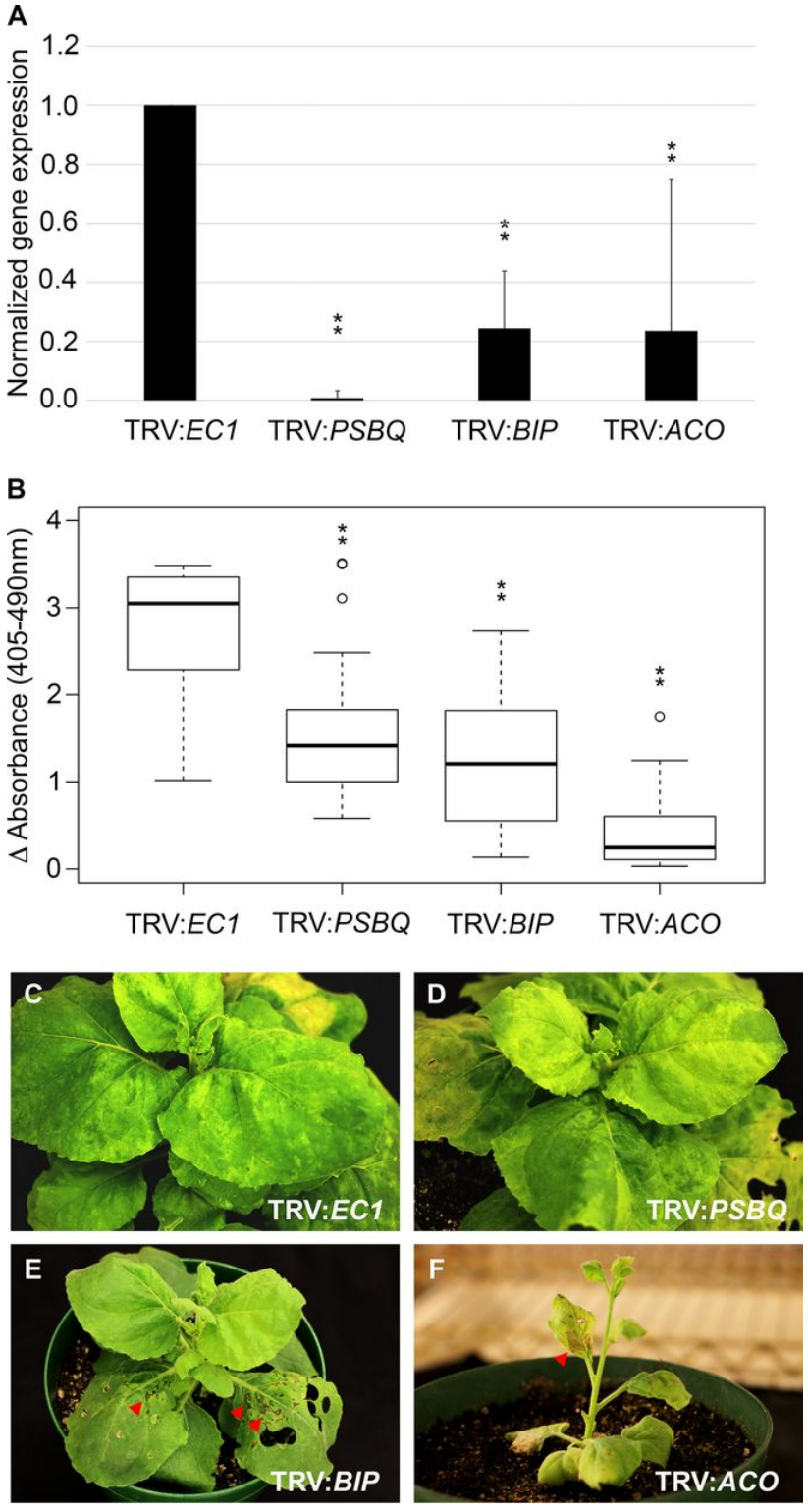
A
Normalized gene expression
1.2
1.0
0.8
0.6
0.4
0.2
0.0
TRV:EC1
TRV:PSBQ
TRV:BIP
TRV:ACO
B
Δ Absorbance (405-490nm)
4
3
2
1
0
TRV:EC1
TRV:PSBQ
TRV:BIP
TRV:ACO
C
TRV:EC1
D
TRV:PSBQ
E
TRV:BIP
F
TRV:ACO

Figure A2.4: Virus-induced gene silencing (VIGS) of PIR-derived host interaction partners reveals function in local accumulation of PLRV. (A) Average relative gene expression of PLRV interacting host proteins (BiP, ACO3, and PsbQ2), measured by RT-qPCR in TRV-infected plants on day zero of infiltration with PLRV (n = 7 to 8 plants). Normalizations were performed using REST 2009 (Pfaffl et al., 2002) with L23 as a reference gene. **, $P < 0.01$, as determined by a pairwise fixed-allocation randomization test (Pfaffl et al., 2002). Error bars represent standard errors of normalized expression calculated by REST 2009. (B) Box plots show the range and median change in Δ absorbance (405 to 490 nm) values for DAS-ELISA analysis of PLRV accumulation in VIGS-silenced *N. benthamiana* leaves at 3 dpi with an infectious PLRV cDNA (n = 8 to 10 plants, three leaf discs from a single leaf per plant). Circles indicate outlier absorbance readings. **, $P < 0.01$, as calculated by paired (TRV:*PSBQ*) or unpaired (TRV:*BIP* and TRV:*ACO*) Student t tests comparing a given treatment group to TRV:*EC1* controls. (C to F) Representative images of morphological phenotypes observed in silenced plants independent of PLRV infection. Red arrows indicate areas of spontaneous, localized cell death.

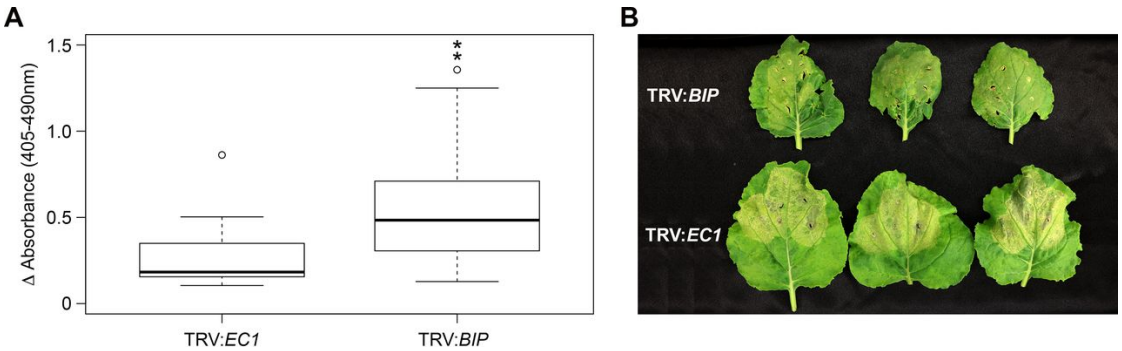

Figure A2.5: *BIP*-silenced leaves locally infected with PLRV show increased virus titer and decreased necrosis at a later stage during infection. (A) Box plots show the range and median Δ absorbance (405 to 490 nm) values for DAS-ELISA analysis of PLRV accumulation in *BIP*-silenced *N. benthamiana* leaves at 5 dpi with an infectious PLRV cDNA (n = 8 to 10 plants, three leaf discs from a single leaf per plant). Circles indicate outlier absorbance readings. **, $P< 0.01$, as calculated by an unpaired Student t test compared to TRV:*EC1* controls. (B) Representative images of TRV:*BIP* and TRV:*EC1* leaves at 5 dpi with PLRV.

Evidence that PLRV may use structural mimicry to interact with host luminal binding protein

Endogenously, BiPs are endoplasmic reticulum (ER)-localized, HSP70 chaperones that assist in protein folding via two highly conserved structural domains (Fig. A2.6A). Polypeptides bind within the BiP substrate-binding domain, which stimulates ATP hydrolysis in the N-terminal ATPase domain and promotes protein folding (Hendrick and Hartl, 1993). On average, BIP-silenced leaves showed a 55% decrease ($P < 0.01$) in virus titer at 3 days postinfiltration (dpi) with an infectious clone of PLRV compared to controls (Fig. A2.4B), indicating BiP is a positive regulator of PLRV infection. However, BiP may serve a dual regulatory role during infection. At 5 dpi, *BIP*-silenced leaves exhibited less severe PLRV-induced necrosis compared to TRV:*EC1* control leaves, and the average PLRV titer was 2-fold higher in these leaves (Fig.A2. 5, $P < 0.01$), despite variability in PLRV accumulation observed within leaves of control and all candidate target plants ($n = 8$ to 10 plants, three discs per single leaf) at both the 3- and the 5-day time points (Fig. A2.4B and A2.5A). Using the identified K_{500} (BiP) and K_{76} (virus) PIR cross-link as a distance constraint to model the interaction between PLRV CP and *N. benthamiana* BiP, we identified a 7-amino-acid motif in the arginine (R)-rich region of the CP N terminus docked within the substrate-binding domain of BiP (Fig. A2.6A and B). This CP domain, defined by neutral residues surrounded by a variable arginine-rich region, was conserved across 19 *Luteoviridae* species (Fig. A2.6C) and mimics the substrate-binding site of human BiPs, which also have strong affinity for seven-residue peptides, rich in neutral, hydrophobic amino acids.

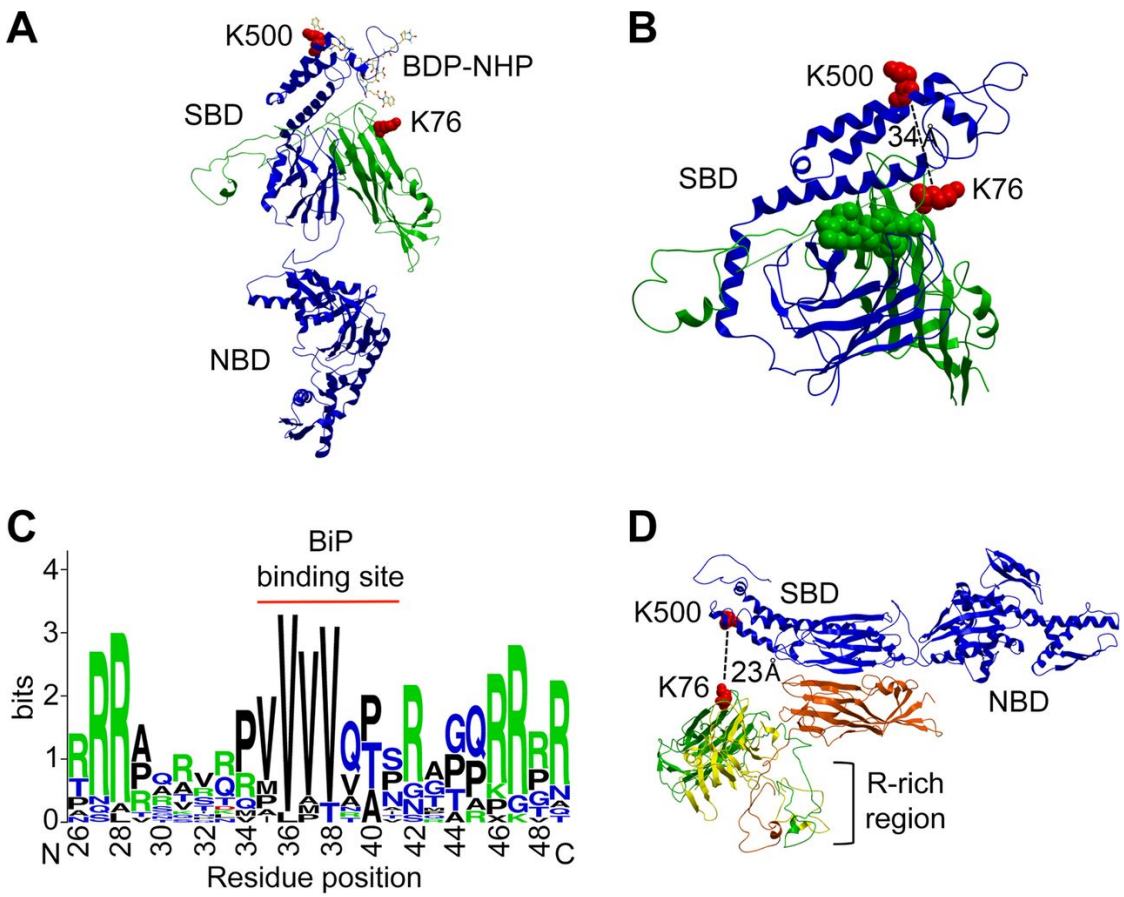

Figure A2.6: Visualization of BiP-virus interaction topologies reveals that structural mimicry may be a strategy for host manipulation. (A and B) The CP monomer (green) docks within the substrate-binding domain (SBD) of BiP (blue), with a predicted distance of 34 Å between the two PIR reactive lysines, K_{76} (virus) and K_{500} (host). (B) CP residues (green, space-filled) binding within the BiP SBD. (C) Weblogo alignment of the predicted BiP binding site (red line) within the CP sequence of 19 *Luteoviridae* species shows conservation of hydrophobic, neutral residues. (D) Alignment of jellyroll structures within the interaction site between a CP subunit within the trimer and a region adjacent to the BiP SBD. The nucleotide-binding domain (NBD) of BiP, the arginine (R)-rich region of the CP trimer of an individual CP monomer and the PIR cross-linker (BDP-NHP) are indicated. CP subunits in the trimer model are colored orange, green, and yellow.

Modeling of BiP with the CP trimer revealed a striking degree of structural similarity within the binding interface (Fig. A2.6D). This alternative BiP-CP interaction topology showed how the jellyroll structure of the CP S domain symmetrically stacked with the β-roll conformation of the BiP substrate-binding domain (residues 370 to 430) to partially block access to the BiP substrate-binding domain (Fig. A2.6D). Human BiP has been shown to adopt multiple conformations to control access to its substrate-binding domain where BiP oligomerizes via contacts spanning amino acids 392 to 636 within cells but dissociates into monomers when bound to nucleotide or polypeptides (Buchkovich et al., 2009). CP mimicry of BiP oligomerization could be an additional viral strategy for modulating BiP activity.

PLRV-host interaction topologies exhibit signatures of coevolution

In plants, ACO3 catalyzes the interconversion of citrate and isocitrate during cellular respiration (Moeder et al., 2007). *ACO3*-silenced plants showed an 86% decrease ($P < 0.01$) in PLRV titer at 3 dpi, indicating that ACO3 also functions as a positive regulator of PLRV (Fig. A2.4B). At 5 dpi, ACO3-silenced infiltrated leaves were completely necrotic (data not shown). These results are in line with a previous study, which showed that ACO in *N. benthamiana* functions to restrict pathogen-induced cell death to the site of infection (Moeder et al., 2007). However, it has also been shown that silencing of aconitase in *N. benthamiana* plants leads to increased accumulation of bacteria in early infection due to reduction in pathogen-induced cell death and greater resistance to oxidative stress (Moeder et al., 2007). We observed the opposite effect on PLRV accumulation, suggesting that poleroviruses may require the function of aconitase in a different manner.

As a protein that could be involved in general pathogen defense, we hypothesized ACO3 may be under diversifying selection, a hallmark molecular

signature of host-pathogen interactions. Periodic, alternating attempts at fitness maximization by each partner, host and virus, often result in recurring amino acid changes over time at sites of host-virus protein interaction.

Using Fast Unconstrained Bayesian AppRoximation (FUBAR) (Murrell et al., 2013), we identified six residues within the N terminus of *N. benthamiana* ACO3 under diversifying selection with a posterior probability > 0.9 (see Data Set S2 in the supplemental material). Modeling of ACO3 with the CP trimer using the PIR cross-link between K_{506} (ACO3) and K_{150} (virus) as a distance constraint predicts that five of these residues form direct contacts with the S domain of a CP subunit within the trimer (Fig. A2.7). The sixth ACO3 residue site under diversifying selection, V_{104}, is a residue that could potentially interact with the RTD of an incorporated RTP protruding from the virion (Fig. A2.7). In agreement, AP-MS results showed a severely weakened association of ACO3 with PLRV virions lacking the RTP (DeBlasio et al., 2015b). These data highlight how PIR and quantitative AP-MS experiments can be used in conjunction to define the topological features of a host-pathogen interaction.

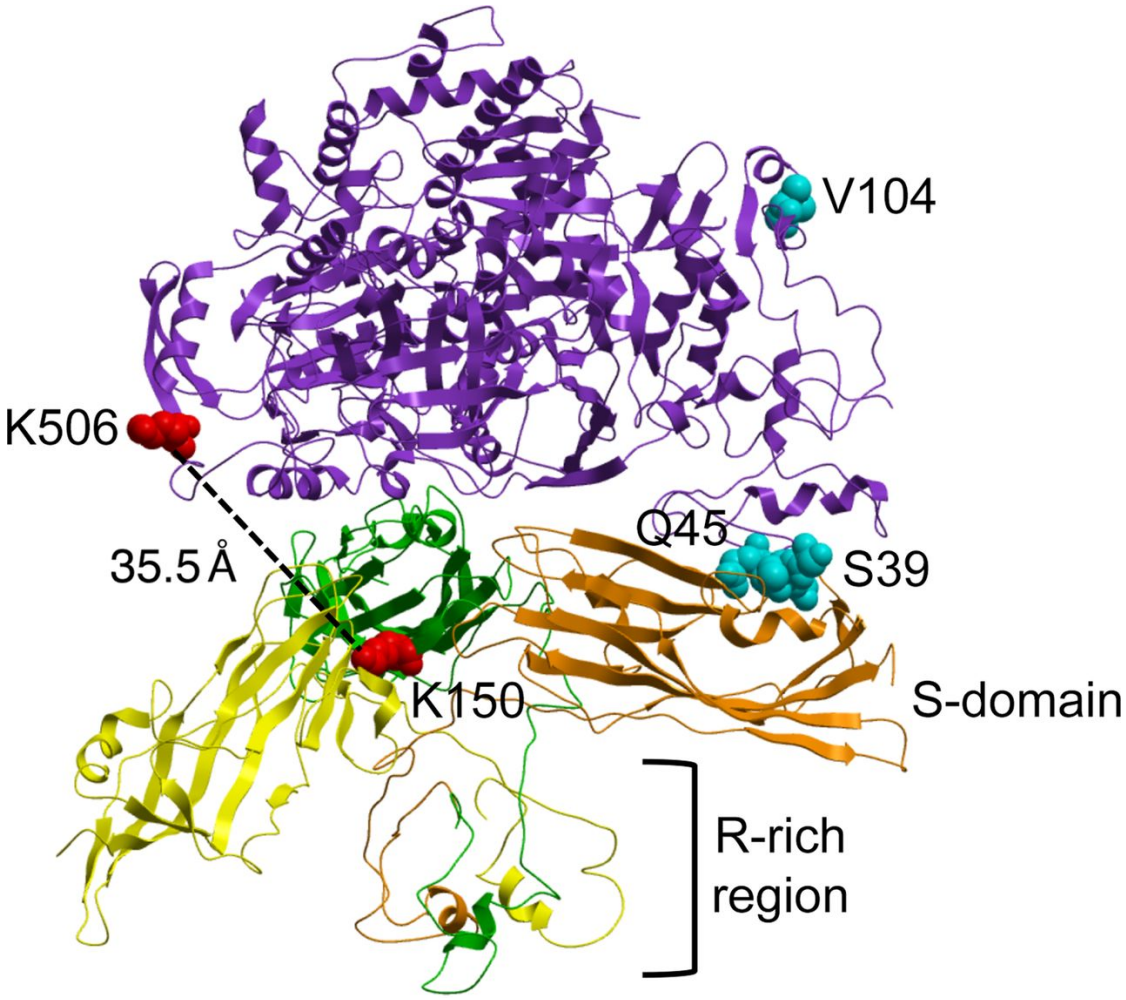

Figure A2.7: Protein interaction reporter enables visualization of ACO3-virus coevolutionary molecular signatures. Six residues (light blue) within the N terminus of ACO3 (purple) identified as being under diversifying selection by Fast Unconstrained Bayesian AppRoximation (FUBAR) analysis are predicted to interact with the CP trimer (orange, green, and yellow) in a Patchdock structural model generated using the PIR cross-link between K506 (host) and K150 (virus) as a distance constraint. Three of these ACO3 residues (S39, Q45, and V104) are labeled as sequence reference points.

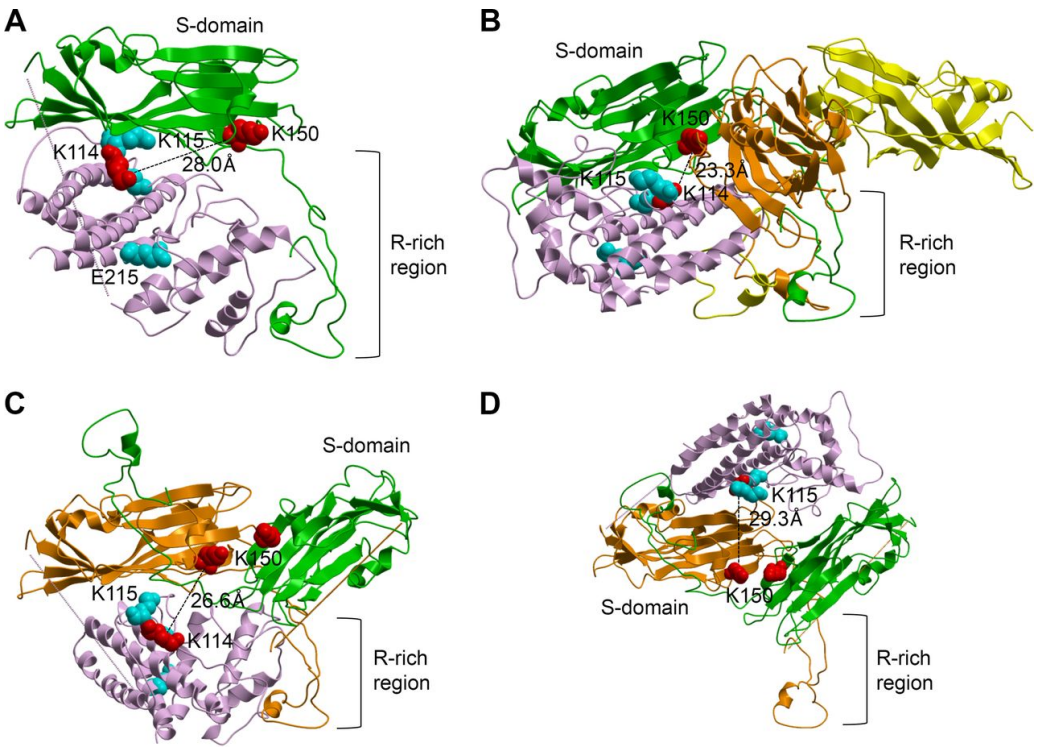

Figure A2.8: Protein interaction reporter enables visualization of PsbQ2-virus coevolutionary molecular signatures. Structural modeling of putative interactions between *N. benthamiana* PsbQ2 (pink) and PLRV CP (A) monomer, (B) trimer, and (C and D) dimer using Patchdock and XWALK analysis predicts PsbQ2 interacting with either the CP arginine (R)-rich region (A to C) or the dimer surface (D). Three residues (G_{110}, K_{115}, and E_{215}) within PsbQ2 were identified as being under diversifying selection by Fast Unconstrained Bayesian AppRoximation analysis (light blue). One, K_{115}, is predicted to be surface accessible and to interact with PLRV CP in all models. CP subunits are colored orange, green, and yellow. Models were generated using the PIR cross-link between K_{114} (host) and K_{150} (virus) as a distance constraint.

FUBAR analysis of *N. benthamiana* PsbQ2, a component of the oxygen evolving complex (Cady et al., 2008), also revealed three residues ($K_{110,115,215}$) under diversifying selection, one of which is located within the CP-PsbQ2 interaction site that was identified by PIR (Fig. A2.8; see also Data Set S3 in the supplemental material). In N. benthamiana, a 99.3% reduction in *PSBQ2* expression (Fig. A2.4A) resulted in a 43% decrease in PLRV titer at 3 dpi ($P < 0.01$). Interestingly, silencing of *PSBQ2* had no obvious effect on the morphology of the plant (Fig. A2.4D) despite being a key component involved in photosynthesis (Cady et al., 2008). These data indicate that PsbQ2 also acts as a positive regulator of local PLRV accumulation.

Structural modeling of the PsbQ2-CP monomer and trimer interactions using the PIR-identified cross-link K_{114} (PsbQ2) to K_{150} (virus) as a distance constraint predicted an association with the arginine-rich domain of the CP (Fig. A2.8A and B). However, studies have shown that the CP of *Alfalfa mosaic virus* (AMV), an icosahedral shaped *Alfamovirus*, interacts with PsbP, a binding partner of PsbQ, as a dimer (Balasubramaniam et al., 2014). Indeed, we did detect an α-PLRV-reactive protein corresponding to the molecular weight of a CP dimer in WT and RTP mutant PLRV samples that were reacted with PIR (Fig. A2.1C, red arrow) showing that PLRV CP also exists as a dimer. Assuming a symmetrical dimer, we used the four CP homodimer cross-links (Table A2.1) and one from a previous study (Chavez et al., 2012) to model the structural topology of a PLRV CP dimer. From the top models, only three displayed solvent accessible surface distances that fit within the PIR distance constraint (Weisbrod et al., 2013) for all five homodimer cross-links (data not shown). Only one model (Fig. A2.8C and D) predicted the N-terminal sequence of a CP monomer to be surface exposed, a model that is supported by epitope mapping (Torrance, 1992) and hypothesized to occur during virus disassembly (Taliansky et al., 2003). Visualization of the PsbQ2-CP dimer interface using this CP dimer model

predicts two general interaction topologies, one where PsbQ2 interacts with the internal CP arginine-rich domain (Fig. A2.8C) as seen with the CP monomer and trimer models (Fig. A2.8A and B), and the other where PsbQ2 interacts with the surface of the dimer (Fig. A2.8D). In all models, the surface accessible PsbQ2 K_{115} residue predicted to be under pervasive diversifying selection by FUBAR (light blue, Fig. A2.8; see also Data Set S3 in the supplemental material), flanked the PIR reactive PsbQ2 lysine, K_{114}, and was positioned within the PsbQ2-CP binding interface, showing that this interaction topology is also under positive selective pressure.

Discussion

In this study, the advanced capabilities of PIR technology enabled us to simultaneously identify plant proteins in complex with purified virus, to confidently assign binary connections to the PLRV-host interaction network, and to fine-map the precise residues involved in binding. Viral infection was induced in *N. benthamiana* mesophyll and vascular cells via *Agrobacterium*-mediated transformation (Haupt et al., 2005) with infectious clones of the PLRV genome. Virus-host protein complexes were isolated from this tissue at 3 dpi by sucrose-density purification and cross-linker applied. Thus, protein-protein interactions captured by application of the PIR cross-linker to these infectious particles most likely represent protein interactions formed during either viral replication/assembly, evasion of plant defense, intracellular trafficking, or early cell-to-cell movement events where virus moves from companion cells into sieve elements for viral dissemination.

Our results show PIR and AP-MS are two complementary approaches for virus-host protein interaction identification. By integrating molecular virology, AP-

MS and PIR, we showed several proteins interacting directly with the CP domain that depended upon interactions with the RTD for their binding affinity. Despite virus-host protein complexes being isolated at the same time point during infection, differences observed in the identity and the number of host proteins found associated with virus using each approach are most likely attributable to differences in lysis buffer conditions, rapidity of purification (1 h for AP-MS; 2 days for sucrose density purification), and truncation of the RTD C terminus during sucrose density purification, as well as differences in MS analysis (DeBlasio et al., 2015a). In addition, accessible surface residues and protein disorder could also be an important factor in the success of PIR due to cross-linker reactivity with solvent-exposed lysine residues that would serve to bias the identification of some protein interactions by PIR and not others (Bruce, 2012).

The absence of RTD-derived cross-links was the only observable difference among virus-derived cross-links in the RTP deletion mutants tested. Thus, it is likely that it is perturbations in host-viral protein interaction networks rather than changes in virion surface topologies that lead to the specific defects in plant and aphid tissue tropism that are observed for these RTP mutants, such as phloem-unloading, delay in systemic movement, and reduced symptom development (Peter et al., 2009). However, the low frequency at which host-viral cross-links were observed in this study precluded us from testing this hypothesis quantitatively.

Based on distance constraints gleaned from PIR technology, we generated the first structural models that visualize interactions between a phloem-limited pathogen and its interacting host proteins, as well as further refined the predicted structure of the polerovirus capsid. The R-rich domain in some CP subunits is predicted to interact with the viral RNA packaged within the interior of the virion (Weiss and Narayana,

1998). However, the PIR-derived CP trimer model defined in this study (Fig. A2.3B) supports epitope mapping data that shows the N terminus of the PLRV CP domain in some virus particles is partially surface accessible in virions purified from infected tissue (Torrance, 1992). Our host-virus interaction models predict both BiP and PsbQ2 interacting with this R-rich domain, while ACO3 is predicted to interact with the surface of the virion (Fig. A2.6 to 8). Alternatively, these data may represent interactions with virions at different stages of assembly that copurified with intact virions (Taliansky et al., 2003; Torrance, 1992) or even multimeric forms of the structural proteins (DeBlasio et al., 2015a) that could act in *trans* to regulate PLRV infection. It is known that viral proteins can be a part of many different host protein complexes that are dynamically regulated throughout the course of an infection (Brizard et al., 2006; Wang, 2015). Indeed, Western blot analyses showed evidence supporting several distinct multimers containing PLRV CP/RTD after cross-linker application, including a CP dimer not previously observed in PLRV purified from infected tissue (Fig. A2.1C). In addition, we identified cross-links between the P1 viral replicase of PLRV to multiple sites within RuBisCO but no direct association of the structural proteins with either P1 or RuBisCO, indicating the presence of multiple viral-host protein complexes within our samples. Although we used known structural information gathered from X-ray crystallography in combination with the distance constraints defined by the identified PIR cross-links to generate models that best fit all the observed host-virus and virus-virus interactions, it is also possible that the identified cross-links could represent single connections within several different protein complexes whose topological features change over time or in the presence of posttranslational modification (Bruce, 2012). Due to rapid hydrolysis of the cross-linker, PIR application in cells or to infectious particles captures protein complexes during a single moment in time and thus represents a “snap-shot” of all the possible

protein-protein interactions that can occur. PIR cross-linking studies using mutational analysis to target viral and host residues predicted by our models to be within the site of protein binding, as well as infection time course studies, would help to further pinpoint the most accurate models and the functions of these interactions.

Silencing of *ACO3*, *BIP*, and *PSBQ2* demonstrates that PLRV-binding plant proteins have functional roles in either limiting or promoting PLRV infection at different time points during infection, with downregulation of *ACO3* and *BIP* leading to physiological and developmental changes in the plant that mimic severe PLRV disease symptoms such as chlorosis, stunting, and leaf distortion. These results support a model whereby binding of these two proteins by PLRV inhibits their endogenous function leading to symptom development. However, it is difficult to separate whether the effect on PLRV titer in these silenced plants is direct or is a consequence of other host changes connected to the observed morphology. It is well known that plant and animal pathogens target proteins that act as pathway hubs as a means to control many different proteins at once, maximizing the impact on host protein interaction networks for their own benefit (Rodrigo et al., 2012). This may also be the case for poleroviruses. Silencing of *PSBQ2* had no morphological phenotype (Fig. A2.4D) but still showed significant effect on PLRV titer. In addition, all host-virus interaction topologies modeled exhibit characteristic molecular signatures (i.e., binding promiscuity, structural mimicry, and positive selection) that are known to manifest as a result of the evolutionary interplay that exists between pathogen and host (Daugherty and Malik, 2012; Elde et al., 2009; Franzosa and Xia, 2011). Analysis of PIR data also revealed an example of conservation of structure in both virus and host binding domains, a finding suggestive of convergent evolution of virus-host interactions across broad taxa. The animal MYND-domain zinc binding protein BS69 and *Caenorhabditis elegans* Bra-1 and Bra-2 proteins bind a conserved PXLXP motif

in proteins from viruses in the *Herpesviridae* and *Adenoviridae* (Ansieau and Leutz, 2002). The peptide from the *N. benthamiana* MYND protein found cross-linked to the PLRV CP contained a PXLXP motif flanking the PIR-reactive lysine residue (Table A2.2), showing that this motif could be a topological feature used by viruses in diverse families for protein interactions.

The PIR-defined interaction between the substrate binding domain of the ER chaperone BiP and the arginine-rich region of PLRV CP monomer uncovered a highly conserved CP peptide domain rich in hydrophobic, neutral residues that was not identified as a putative functional domain in previous predication studies that were based on epitope mapping and sequence alignments with distantly related, icosahedron-shaped viruses (Brault et al., 2003; Dolja and Koonin, 1991; Kaplan et al., 2007; Lee et al., 2005; Torrance, 1992). The high degree of conservation of this BiP binding site among the *Luteoviridae* CP sequences supports the conclusion that the interaction of CP with BiP is beneficial to the virus. Indeed, the VIGS functional data indicate that BiP is a positive regulator of PLRV during early infection. One hypothesis is that CP-BiP interactions *in planta* act to reduce ER cytotoxicity caused by high levels of viral protein synthesis. BiPs act as sensors of ER stress in plants by inducing the unfolded protein response (UPR). Suppression of the UPR in plants by the virus may have collateral benefits for virus transmission: circulative transmission of PLRV by aphids, which require prolonged feeding on healthy phloem (Gray et al., 2014). HSP70 family members, including BiP, are known targets of viruses during host infection (Buchkovich et al., 2009; Hafren et al., 2010; Ye et al., 2011). For example, depletion of BiP in fibroblast cells inhibited human cytomegalovirus (HCMV) virion formation and cytosolic egress, although viral protein synthesis was unaffected (Buchkovich et al., 2009). Upon infection with HCMV, BiP becomes relocalized from the ER to cytoplasmic structures that act as assembly compartments

for the virus (Buchkovich et al., 2009). It is possible that a similar mechanism occurs in plant cells infected with poleroviruses, which also replicate in the cytoplasm. Transmission electron micrographs of PLRV-infected phloem cells show the formation of virus-induced vesicles within the cytoplasm, the protein composition and function of which still remains unknown (Shepardson et al., 1980).

Comparative analysis of "omic" data sets across different plant pathosystems has revealed photosynthesis and related pathways, such as glycolysis and respiration, as main targets of pathogen infection (Di Carli et al., 2012; Rodrigo et al., 2012). Downregulation or inhibition of these pathways during the course of an infection appears to be the common trend, with the outcome being the manifestation of symptoms such as chlorosis (Balasubramaniam et al., 2014; Hodgson et al., 1989; Kong et al., 2014; Reinero and Beachy, 1989; Takahashi and Ehara, 1992). In this study, we identified several plant proteins involved in these pathways as directly interacting with either the PLRV structural proteins or the viral replication protein P1. Two of them, PsbQ2 (photosynthesis) and ACO3 (respiration), regulate virus accumulation via these interactions. Unlike viruses such as *Tobacco mosaic virus*, which is known to replicate within chloroplasts (Reinero and Beachy, 1989), replication and assembly of *Luteoviridae* species is generally believed to be cytoplasmic (Gill and Chong, 1979). Our data (DeBlasio et al., 2015a; DeBlasio et al., 2015b) and previously published microscopic analyses that show interaction with organelle-localized proteins and membranes (Esau and Hoefert, 1972; Peter et al., 2009; Shepardson et al., 1980) call that dogma into question. For example, virions of the wild type, as well as the ΔRTD mutant form, of PLRV have been shown to associate with chloroplast membranes in phloem companion cells and mesophyll, respectively (Peter et al., 2009; Shepardson et al., 1980). RNA viruses that replicate in the cytosol, such as AMV and *Rice stripe virus*, affect photosynthesis by binding and

inhibiting the transport of PsbP, a binding partner of PsbQ, from the nucleus to the chloroplast (Balasubramaniam et al., 2014; Kong et al., 2014; Takahashi and Ehara, 1992). However, the latter interactions negatively regulate replication and virus accumulation in plant cells (Balasubramaniam et al., 2014; Kong et al., 2014). These observations are in contrast to what we observed for PsbQ2 and PLRV, which may represent a unique mode of action for PsbQ-PsbP during polerovirus infection or a role for PsbQ2 in viral infection independent of PsbP.

Collectively, our data show that selection has favored viruses such as PLRV to structurally mimic the endogenous interaction topologies of some host proteins and that these interactions regulate virus accumulation during infection. These results illuminate the functional diversity of the PLRV-host protein interaction network and demonstrate the application of PIR as a tool to allow precision mapping of functional host-pathogen protein interaction topologies. Our host-PLRV interaction models have uncovered new sites within virus and host that can be targeted either through mutation or molecular inhibition to eliminate infection without sacrificing endogenous host function. The data underscore that PIR and other MS-compatible cross-linking technologies will be indispensable tools for future exploration of the interface between other plant viruses and their hosts.

Supplementary Materials

Supplemental material for this article may be found at http://dx.doi.org/10.1128/JVI.01706-15.

Acknowledgments

We acknowledge Tom Hammond (retired, Cornell), Katherine Parks, and Rogerio Santos (Boyce Thompson Institute [BTI]) for care of plants and Marc Fuchs (Cornell) and Gary Blissard (BTI) for reviews of the manuscript. We especially want to thank Greg Martin (BTI) for supplying VIGS cloning plasmids.

Funding was provided by an Association of Independent Plant Research Institutes Research Award (to M.C.), NSF-IOS grant 1354309 (to M.C. and J.E.B.), USDA NIFA grant 1907-22000-021-20 (to M.C. and S.M.G.), and NIH grants 1U19AI 107775 and 5R01GM086688 (to J.E.B.).

REFERENCES

2006. Solutions for preparing resolving gels for Tris-glycine SDS-polyacrylamide gel electrophoresis. Cold Spring Harbor Protocols 2006.

Ansieau, S., Leutz, A., 2002. The conserved Mynd domain of BS69 binds cellular and oncoviral proteins through a common PXLXP motif. J Biol Chem 277, 4906-4910.

Bahner, I., Lamb, J., Mayo, M.A., Hay, R.T., 1990. Expression of the genome of *Potato leafroll virus*: Readthrough of the coat protein termination codon in vivo. Journal of General Virology 71 (Pt 10), 2251-2256.

Balasubramaniam, M., Kim, B.-S., Hutchens-Williams, H.M., Loesch-Fries, L.S., 2014. The photosystem II oxygen-evolving complex protein PsbP interacts with the coat protein of *Alfalfa mosaic virus* and inhibits virus replication. Mol Plant Microbe Interact 27, 1107-1118.

Boissinot, S., Erdinger, M., Monsion, B., Ziegler-Graff, V., Brault, V., 2014. Both structural and non-structural forms of the readthrough protein of *Cucurbit aphid-borne yellows virus* are essential for efficient systemic infection of plants. PLoS One 9, e93448.

Bombarely, A., Rosli, H.G., Vrebalov, J., Moffett, P., Mueller, L.A., Martin, G.B., 2012. A draft genome sequence of *Nicotiana benthamiana* to enhance molecular plant-microbe biology research. Mol Plant Microbe Interact 25, 1523-1530.

Bortolamiol, D., Pazhouhandeh, M., Marrocco, K., Genschik, P., Ziegler-Graff, V., 2007. The polerovirus F box protein P0 targets ARGONAUTE1 to suppress RNA silencing. Curr Biol 17, 1615-1621.

Brault, V., Bergdoll, M., Mutterer, J., Prasad, V., Pfeffer, S., Erdinger, M., Richards, K.E., Ziegler-Graff, V., 2003. Effects of point mutations in the major capsid protein of *Beet western yellows virus* on capsid formation, virus accumulation, and aphid transmission. Journal of Virology 77, 3247-3256.

Brault, V., Mutterer, J., Scheidecker, D., Simonis, M.T., Herrbach, E., Richards, K., Ziegler-Graff, V., 2000. Effects of point mutations in the readthrough domain of the *Beet western yellows virus* minor capsid protein on virus accumulation *in planta* and on transmission by aphids. J Virol 74, 1140-1148.

Brault, V., Perigon, S., Reinbold, C., Erdinger, M., Scheidecker, D., Herrbach, E., Richards, K., Ziegler-Graff, V., 2005. The polerovirus minor capsid protein determines vector specificity and intestinal tropism in the aphid. J Virol 79, 9685-9693.

Brault, V., van den Heuvel, J.F.J.M., Verbeek, M., Ziegler-Graff, V., Reutenauer, a., Herrbach, E., Garaud, J.C., Guilley, H., Richards, K., Jonard, G., 1995. Aphid transmission of *Beet western yellows luteovirus* requires the minor capsid read-through protein P74. The EMBO Journal 14, 650-659.

Brizard, J.P., Carapito, C., Delalande, F., Van Dorsselaer, A., Brugidou, C., 2006. Proteome analysis of plant-virus interactome: Comprehensive data for virus multiplication inside their hosts. Mol Cell Proteomics 5, 2279-2297.

Brown, C.M., Dinesh-Kumar, S.P., Miller, W.A., 1996. Local and distant sequences are required for efficient readthrough of the *Barley yellow dwarf virus* PAV coat protein gene stop codon. J Virol 70, 5884-5892.

Bruce, J.E., 2012. *In vivo* protein complex topologies: Sights through a cross-linking lens. Proteomics 12, 1565-1575.

Buchkovich, N.J., Maguire, T.G., Paton, A.W., Paton, J.C., Alwine, J.C., 2009. The endoplasmic reticulum chaperone BiP/GRP78 is important in the structure and function of the human cytomegalovirus assembly compartment. J Virol 83, 11421-11428.

Cady, C.W., Crabtree, R.H., Brudvig, G.W., 2008. Functional models for the oxygen-evolving complex of photosystem II. Coord Chem Rev 252, 444-455.

Chavez, J.D., Cilia, M., Weisbrod, C.R., Ju, H.J., Eng, J.K., Gray, S.M., Bruce, J.E., 2012. Cross-linking measurements of the *Potato leafroll virus* reveal protein interaction topologies required for virion stability, aphid transmission, and virus-plant interactions. J Proteome Res 11, 2968-2981.

Chavez, J.D., Liu, N.L., Bruce, J.E., 2011. Quantification of protein-protein interactions with chemical cross-linking and mass spectrometry. J Proteome Res 10, 1528-1537.

Chavez, J.D., Schweppe, D.K., Eng, J.K., Zheng, C., Taipale, A., Zhang, Y., Takara, K., Bruce, J.E., 2015. Quantitative interactome analysis reveals a chemoresistant edgotype. Nat Commun 6, 7928.

Chavez, J.D., Weisbrod, C.R., Zheng, C., Eng, J.K., Bruce, J.E., 2013. Protein interactions, post-translational modifications and topologies in human cells. Mol Cell Proteomics 12, 1451-1467.

Cilia, M., Peter, K.A., Bereman, M.S., Howe, K., Fish, T., Smith, D., Gildow, F., MacCoss, M.J., Thannhauser, T.W., Gray, S.M., 2012. Discovery and targeted LC-MS/MS of purified polerovirus reveals differences in the virus-host interactome associated with altered aphid transmission. PLoS One 7, e48177.

Daugherty, M.D., Malik, H.S., 2012. Rules of engagement: Molecular insights from host-virus arms races. Annu Rev Genet 46, 677-700.

DeBlasio, S.L., Johnson, R., Mahoney, J., Karasev, A., Gray, S.M., MacCoss, M.J., Cilia, M., 2015a. Insights into the polerovirus-plant interactome revealed by co-immunoprecipitation and mass spectrometry. Mol Plant Microbe Interact 28, 467-481.

DeBlasio, S.L., Johnson, R., Sweeney, M.M., Karasev, A., Gray, S.M., MacCoss, M.J., Cilia, M., 2015b. *Potato leafroll virus* structural proteins manipulate overlapping, yet distinct protein interaction networks during infection. Proteomics 15, 2098-2112.

Di Carli, M., Benvenuto, E., Donini, M., 2012. Recent insights into plant-virus interactions through proteomic analysis. J Proteome Res 11, 4765-4780.

Dolja, V.V., Koonin, E.V., 1991. Phylogeny of capsid proteins of small icosahedral RNA plant viruses. J Gen Virol 72 (Pt 7), 1481-1486.

Dupuy, J., Volbeda, A., Carpentier, P., Darnault, C., Moulis, J.M., Fontecilla-Camps, J.C., 2006. Crystal structure of human iron regulatory protein 1 as cytosolic aconitase. Structure 14, 129-139.

Elde, N.C., Child, S.J., Geballe, A.P., Malik, H.S., 2009. Protein kinase R reveals an evolutionary model for defeating viral mimicry. Nature 457, 485-489.

Eng, J.K., Fischer, B., Grossmann, J., Maccoss, M.J., 2008. A fast SEQUEST cross correlation algorithm. J Proteome Res 7, 4598-4602.

Eng, J.K., McCormack, A.L., Yates, J.R., 1994. An approach to correlate tandem mass spectral data of peptides with amino acid sequences in a protein database. Journal of the American Society for Mass Spectrometry 5, 976-989.

Esau, K., Hoefert, L.L., 1972. Ultrastructure of sugarbeet leaves infected with *Beet western yellows virus*. Journal of Ultrastructure Research 40, 556-571.

Filichkin, S.A., Lister, R.M., McGrath, P.F., Young, M.J., 1994. *In vivo* expression and mutational analysis of the *Barley yellow dwarf virus* readthrough gene. Virology 205, 290-299.

Franco-Lara, L.F., McGeachy, K.D., Commandeur, U., Martin, R.R., Mayo, M.A., Barker, H., 1999. Transformation of tobacco and potato with cDNA encoding the full-length genome of *Potato leafroll virus*: Evidence for a novel virus distribution and host effects on virus multiplication. J Gen Virol 80 (Pt 11), 2813-2822.

Franzosa, E.A., Xia, Y., 2011. Structural principles within the human-virus protein-protein interaction network. Proc Natl Acad Sci U S A 108, 10538-10543.

Gill, C.C., Chong, J., 1979. Cytopathological evidence for the division of *Barley yellow dwarf virus* isolates into two subgroups. Virology 95, 59-69.

Gray, S., Cilia, M., Ghanim, M., 2014. Circulative, "nonpropagative" virus transmission: An orchestra of virus-, insect-, and plant-derived instruments. Adv Virus Res 89, 141-199.

Hafren, A., Hofius, D., Ronnholm, G., Sonnewald, U., Makinen, K., 2010. HSP70 and its co-chaperone CPIP promote potyvirus infection in *Nicotiana benthamiana* by regulating viral coat protein functions. Plant Cell 22, 523-535.

Haupt, S., Stroganova, T., Ryabov, E., Kim, S.H., Fraser, G., Duncan, G., Mayo, M.A., Barker, H., Taliansky, M., 2005. Nucleolar localization of *Potato leafroll virus* capsid proteins. J Gen Virol 86, 2891-2896.

Hendrick, J.P., Hartl, F.U., 1993. Molecular chaperone functions of heat-shock proteins. Annu Rev Biochem 62, 349-384.

Hodgson, R.A.J., Beachy, R.N., Pakrasi, H.B., 1989. Selective inhibition of photosystem II in spinach by *Tobacco mosaic virus*: An effect of the viral coat protein. FEBS Letters 245, 267-270.

Kahraman, A., Malmstrom, L., Aebersold, R., 2011. Xwalk: computing and visualizing distances in cross-linking experiments. Bioinformatics 27, 2163-2164.

Kaplan, I.B., Lee, L., Ripoll, D.R., Palukaitis, P., Gildow, F., Gray, S.M., 2007. Point mutations in the *Potato leafroll virus* major capsid protein alter virion stability and aphid transmission. J Gen Virol 88, 1821-1830.

Kelley, L.A., Sternberg, M.J.E., 2009. Protein structure prediction on the Web: A case study using the Phyre server. Nature protocols 4, 363-371.

Kessner, D., Chambers, M., Burke, R., Agus, D., Mallick, P., 2008. ProteoWizard: Open source software for rapid proteomics tools development. Bioinformatics 24, 2534-2536.

Klessig, D.F., Durner, J., Noad, R., Navarre, D.a., Wendehenne, D., Kumar, D., Zhou, J.M., Shah, J., Zhang, S., Kachroo, P., Trifa, Y., Pontier, D., Lam, E., Silva, H., 2000. Nitric oxide and salicylic acid signaling in plant defense. Proceedings of the National Academy of Sciences 97, 8849-8855.

Kong, L., Wu, J., Lu, L., Xu, Y., Zhou, X., 2014. Interaction between *Rice stripe virus* disease-specific protein and host PsbP enhances virus symptoms. Mol Plant 7, 691-708.

Lee, L., Kaplan, I.B., Ripoll, D.R., Liang, D., Palukaitis, P., Gray, S.M., 2005. A surface loop of the *Potato leafroll virus* coat protein is involved in virion assembly,

systemic movement, and aphid transmission. J Virol 79, 1207-1214.

Liu, D., Shi, L., Han, C., Yu, J., Li, D., Zhang, Y., 2012. Validation of reference genes for gene expression studies in virus-infected *Nicotiana benthamiana* using quantitative real-time PCR. PLoS One 7, e46451.

Liu, Y., Schiff, M., Dinesh-Kumar, S.P., 2002. Virus-induced gene silencing in tomato. The Plant Journal 31, 777-786.

Lu, R., 2003. Virus-induced gene silencing in plants. Methods 30, 296-303.

Moeder, W., Del Pozo, O., Navarre, D.A., Martin, G.B., Klessig, D.F., 2007. Aconitase plays a role in regulating resistance to oxidative stress and cell death in *Arabidopsis* and *Nicotiana benthamiana*. Plant Mol Biol 63, 273-287.

Murrell, B., Moola, S., Mabona, A., Weighill, T., Sheward, D., Kosakovsky Pond, S.L., Scheffler, K., 2013. FUBAR: a fast, unconstrained bayesian approximation for inferring selection. Mol Biol Evol 30, 1196-1205.

Nagy, P.D., 2008. Yeast as a model host to explore plant virus-host interactions. Annu Rev Phytopathol 46, 217-242.

Navare, A.T., Chavez, J.D., Zheng, C., Weisbrod, C.R., Eng, J.K., Siehnel, R., Singh, P.K., Manoil, C., Bruce, J.E., 2015. Probing the protein interaction network of *Pseudomonas aeruginosa* cells by chemical cross-linking mass spectrometry. Structure 23, 762-773.

Pazhouhandeh, M., Dieterle, M., Marrocco, K., Lechner, E., Berry, B., Brault, V., Hemmer, O., Kretsch, T., Richards, K.E., Genschik, P., Ziegler-Graff, V., 2006. F-box-like domain in the polerovirus protein P0 is required for silencing suppressor function. Proc Natl Acad Sci U S A 103, 1994-1999.

Perkins, D.N., Pappin, D.J., Creasy, D.M., Cottrell, J.S., 1999. Probability-based protein identification by searching sequence databases using mass spectrometry data. Electrophoresis 20, 3551-3567.

Perry, K.L., Miller, J., Lister, R.M., Mayo, M.A., 1998. Luteovirus isolation and RNA extraction. Methods Mol Biol 81, 231-239.

Peter, K.A., Gildow, F., Palukaitis, P., Gray, S.M., 2009. The C terminus of the polerovirus P5 readthrough domain limits virus infection to the phloem. J Virol 83, 5419-5429.

Peter, K.A., Liang, D., Palukaitis, P., Gray, S.M., 2008. Small deletions in the *Potato leafroll virus* readthrough protein affect particle morphology, aphid transmission, virus movement and accumulation. J Gen Virol 89, 2037-2045.

Pfaffl, M.W., Horgan, G.W., Dempfle, L., 2002. Relative expression software tool (REST) for group-wise comparison and statistical analysis of relative expression results in real-time PCR. Nucleic acids research 30, e36-e36.

Prüfer, D., Kawchuk, L., Monecke, M., Nowok, S., Fischer, R., Rohde, W., 1999. Immunological analysis of *Potato leafroll luteovirus* (PLRV) P1 expression identifies a 25 kDa RNA-binding protein derived via P1 processing. Nucleic Acids Research 27, 421-425.

Reinbold, C., Lacombe, S., Ziegler-Graff, V., Scheidecker, D., Wiss, L., Beuve, M., Caranta, C., Brault, V., 2013. Closely related poleroviruses depend on distinct translation initiation factors to infect *Arabidopsis thaliana*. Mol Plant Microbe Interact 26, 257-265.

Reinero, A., Beachy, R.N., 1989. Reduced photosystem II activity and accumulation of viral coat protein in chloroplasts of leaves infected with *Tobacco mosaic virus*. Plant Physiology 89, 111-116.

Rizzo, T.M., Gray, S.M., 1992. Localization of a surface domain of the capsid protein of *Barley yellow dwarf virus*. Virology 186, 300-302.

Rodrigo, G., Carrera, J., Ruiz-Ferrer, V., del Toro, F.J., Llave, C., Voinnet, O., Elena, S.F., 2012. A meta-analysis reveals the commonalities and differences in *Arabidopsis thaliana* response to different viral pathogens. PLoS One 7, e40526.

Rosli, H.G., Zheng, Y., Pombo, M.a., Zhong, S., Bombarely, A., Fei, Z., Collmer, A., Martin, G.B., 2013. Transcriptomics-based screen for genes induced by flagellin and repressed by pathogen effectors identifies a cell wall-associated kinase involved in plant immunity. Genome Biology 14, R139-R139.

Schneidman-Duhovny, D., Inbar, Y., Nussinov, R., Wolfson, H.J., 2005. PatchDock and SymmDock: Servers for rigid and symmetric docking. Nucleic Acids Res 33, W363-367.

Schweppe, D.K., Harding, C., Chavez, J.D., Wu, X., Ramage, E., Singh, P.K., Manoil, C., Bruce, J.E., 2015. Host-microbe protein interactions during bacterial infection. Chem Biol 22, 1521-1530.

Shannon, P., Markiel, A., Ozier, O., Baliga, N.S., Wang, J.T., Ramage, D., Amin, N., Schwikowski, B., Ideker, T., 2003. Cytoscape: A software environment for integrated models of biomolecular interaction networks. Genome Res 13, 2498-2504.

Shepardson, S., Esau, K., McCrum, R., 1980. Ultrastructure of potato leaf phloem infected with *Potato leafroll virus*. Virology 105, 379-392.

Stewart, L.R., Ding, B., Falk, B.W., 2012. Viroids and phloem-limited viruses: Unique molecular probes of phloem biology, Phloem, pp. 271-292.

Takahashi, H., Ehara, Y., 1992. Changes in the activity and the polypeptide composition of the oxygen-evolving complex in photosystem II of tobacco leaves infected with *Cucumber mosaic virus* strain Y. Mol Plant Microbe Interact 5, 269-272.

Taliansky, M., Mayo, M.A., Barker, H., 2003. *Potato leafroll virus*: a classic pathogen shows some new tricks. Molecular Plant Pathology 4, 81-89.

Torrance, L., 1992. Analysis of epitopes on *Potato leafroll virus* capsid protein. Virology 191, 485-489.

Velasquez, A.C., Chakravarthy, S., Martin, G.B., 2009. Virus-induced gene silencing (VIGS) in *Nicotiana benthamiana* and tomato. J Vis Exp.

Wang, A., 2015. Dissecting the molecular network of virus-plant interactions: the complex roles of host factors. Annu Rev Phytopathol 53, 45-66.

Wang, J.Y., Chay, C., Gildow, F.E., Gray, S.M., 1995. Readthrough protein associated with virions of *Barley yellow dwarf luteovirus* and its potential role in regulating the efficiency of aphid transmission. Virology 206, 954-962.

Weisbrod, C.R., Chavez, J.D., Eng, J.K., Yang, L., Zheng, C., Bruce, J.E., 2013. *In vivo* protein interaction network identified with a novel real-time cross-linked peptide identification strategy. J Proteome Res 12, 1569-1579.

Weiss, M.A., Narayana, N., 1998. RNA recognition by arginine-rich peptide motifs. Biopolymers 48, 167-180.

Ye, C., Dickman, M.B., Whitham, S.A., Payton, M., Verchot, J., 2011. The unfolded protein response is triggered by a plant viral movement protein. Plant Physiol 156, 741-755.